

**Variability in the Nicola/Takla Group basalts and implications for
alkalic Cu-Au porphyry prospectivity in the Quesnel terrane,
British Columbia, Canada**

by

Santiago Vaca

Eng., Hons., Escuela Politécnica Nacional, Quito, 2005

A THESIS SUBMITTED IN PARTIAL FULFILLMENT OF THE
REQUIREMENTS FOR THE DEGREE OF

MASTER OF SCIENCE

in

The Faculty of Graduate Studies
(Geological Sciences)

THE UNIVERSITY OF BRITISH COLUMBIA
(Vancouver)

September, 2012
© Santiago Vaca 2012

Abstract

The Late Triassic – Early Jurassic Quesnel terrane located in the interior of British Columbia in Canada, is largely composed of rocks of the Nicola Group and equivalents, which are mostly represented by black to dark-green, clinopyroxene±plagioclase porphyritic basalts with variable Fe-Ti oxide content, and locally presenting analcime phenocrysts, interpreted as a volcano oceanic-arc sequence with calc-alkalic and alkalic signatures. The Quesnel terrane hosts most alkalic Cu-Au porphyry deposits of British Columbia.

Petrography, whole rock and mineral chemistry of basaltic rocks, together with their physical properties (magnetic susceptibility and density), in context with regional geological and geophysical (gravity and magnetic) maps, allow to delineate prospective arc segments for comagmatic Cu-Au porphyry development within the Quesnel terrane.

Incompatible element variations from whole rock geochemistry exhibit heterogeneities along the arc. For instance Ce/Yb ratios from 6.6 to 24.5 suggest that slight regional and local tectonic changes controlled the degree of partial melting in distinct portions of the mantle wedge, where the higher values represent a relatively compressive setting, resulting in volcanic products with high alkalinity, whereas the lower values denote extension and relatively low alkalinity.

Primary Fe-Ti oxide inclusions in clinopyroxene within basalts showing Cr and higher Fe²⁺ contents, whole-rock Fe³⁺/Fe²⁺ ratios from 0.13 to 0.60 and magnetic susceptibilities <1.30x10⁻³SI units, indicate that basalts were produced from reduced source magmas; Fe-Ti oxides showing higher Fe³⁺ contents, Fe³⁺/Fe²⁺ ratios between 0.60 and ~3.50, and magnetic susceptibilities of 10.00 to 111.00x10⁻³SI units denote oxidized magmas; whereas Fe-Ti oxides with higher Fe³⁺ contents, Fe³⁺/Fe²⁺ ratios between ~3.50 and 7.10 together with magnetic susceptibilities <1.55x10⁻³SI units show secondary oxidation of Fe-rich minerals within rocks. Primary oxidized magmas are related to the formation of Cu-Au porphyry mineralization.

Carbon and oxygen isotopic composition of secondary carbonate minerals within the low temperature alteration assemblage of the rocks, allow classifying basalts in oxidized and reduced as described above. Secondary carbonate minerals from primary oxidized basalts exhibit δ¹⁸O_{SMOW} of +12.3 to +20.5‰, and δ¹³C_{PDB} between -5.6 and +2.2‰ compared to the relatively reduced ones, which show δ¹⁸O from +10.6 to 14.2‰ and δ¹³C between -9.2 and -6.4‰.

Table of Contents

Abstract.....	ii
Table of Contents.....	iii
List of Tables.....	v
List of Figures.....	vi
List of Abbreviations.....	xii
Acknowledgements	xiv
Dedication.....	xv
CHAPTER 1: OVERVIEW.....	1
1.1 INTRODUCTION.....	1
1.2 THESIS ORGANIZATION.....	3
1.3 PROJECT SUPPORT AND STUDY METHODOLOGY.....	4
CHAPTER 2: THE QUESNEL TERRANE - REGIONAL SETTING.....	5
2.1 INTRODUCTION.....	5
2.2 BASEMENT.....	7
2.3 STRATIGRAPHY, ROCK TYPES AND METALLOGENY.....	10
2.4 METAMORPHISM.....	15
2.5 TECTONIC MODEL.....	15
CHAPTER 3: PETROGRAPHY AND PHYSICAL PROPERTIES OF BASALTS IN THE QUESNEL TERRANE.....	21
3.1 INTRODUCTION.....	21
3.2 SAMPLES.....	22
3.3 ANALYTICAL PROCEDURES.....	24
3.4 LIMITATIONS AND FIELD OBSERVATIONS.....	25
3.5 PETROGRAPHY.....	30
3.5.1 Mount Polley.....	30
3.5.1.1 LTNpv Unit.....	30
3.5.1.2 LTNav Unit.....	30
3.5.1.3 LTNpt Unit.....	31
3.5.2 Mount Milligan.....	31
3.5.3 Woodjam.....	31
3.5.4 Copper Mountain.....	32
3.5.5 Lac la Hache.....	32
3.5.6 Bridge Lake.....	32
3.5.7 South of Merritt.....	33
3.6 GEOLOGY, PHYSICAL PROPERTIES AND REGIONAL MAGNETIC AND GRAVITY SURVEYS	36
3.6.1 Mount Polley.....	36
3.6.1.1 LTNpv Unit.....	36
3.6.1.2 LTNav Unit.....	36

3.6.1.3	LTNpt Unit.....	37
3.6.2	Mount Milligan.....	38
3.6.3	Woodjam.....	39
3.6.4	Copper Mountain.....	41
3.6.5	Lac la Hache.....	43
3.6.6	Bridge Lake.....	45
3.6.7	South of Merritt.....	47
3.7	DISCUSSION.....	49
CHAPTER 4:	GEOCHEMISTRY.....	56
4.1	INTRODUCTION.....	56
4.2	ANALYTICAL PROCEDURES.....	57
4.3	WHOLE ROCK GEOCHEMISTRY.....	58
4.3.1	Major Elements Chemistry.....	58
4.3.2	Incompatible Elements Chemistry.....	61
4.4	OXIDATION STATE OF BASALTS.....	63
4.5	MINERAL CHEMISTRY.....	64
4.5.1	Scanning Electron Microscopy and Electron Microprobe Analyses	64
4.5.1.1	Clinopyroxene.....	64
4.5.1.2	Fe-Ti Oxide Minerals.....	70
4.5.1.3	Apatite.....	72
4.6	DISCUSSION AND CONCLUSIONS.....	73
CHAPTER 5:	CARBON AND OXYGEN ISOTOPIC COMPOSITIONS OF SECONDARY CARBONATE MINERALS, IMPLICATIONS FOR POST-EXTRUSION PROCESSES AFFECTING THE NICOLA GROUP BASALTS	82
5.1	INTRODUCTION.....	82
5.2	ANALYTICAL PROCEDURES.....	82
5.3	CARBON AND OXYGEN ISOTOPES.....	83
5.4	DISCUSSION.....	84
CHAPTER 6:	SUMMARY AND CONCLUSIONS.....	87
REFERENCES.....		93
APPENDICES.....		110

List of Tables

Table 4.1	Standards, analysis lines and crystals used for pyroxene, Fe-Ti–oxide and apatite analyses.....	57
Table A1.	List of samples showing the amounts of the most important phenocryst phases and the occurrence of Fe-Ti oxides and hematite within the basalts. All of the samples contain (5 – 10 %) of epidote, chlorite, calcite and clays as alteration minerals. Rocks with (*) in the sample ID show aphanitic texture, then, the mineral amount of those samples represents the content within the whole rock.....	110
Table B1.	Major elements package ME-ICP06, indicating lower and upper limits.....	113
Table B2.	Trace elements package ME-MS81, indicating lower and upper limits.....	114
Table B3.	Ferrous iron package Fe-VOL05, indicating lower and upper limits.....	115
Table B4.	Whole rock geochemistry in rock samples collected in different localities along the Nicola Group.....	116
Table B5.	Quality assurance/Quality control (QA/QC) of whole rock and trace elements chemistry. Comparison of standards used in this thesis with a compilation of results using the same standard (BAS-1) and the same geochemical methods and laboratory (ALS).....	126
Table B6.	Electron microprobe analyses of clinopyroxene from different localities along the Nicola Group.....	128
Table B7.	Electron microprobe analyses of Fe-Ti oxide inclusions in clinopyroxene from different localities along the Nicola Group.....	139
Table B8.	Electron microprobe analyses of apatite inclusions in clinopyroxene from different rocks units within the Mount Polley area	146
Table C1.	$\delta^{13}\text{C}_{\text{PDB}}$ (‰) and $\delta^{13}\text{C}_{\text{PDB}}$ (‰) isotopic compositions of carbonates within basalts from different arc segments along the Nicola Group.....	147

List of Figures

Figure 1.1.	Global distribution of porphyry deposits. Orange areas cover major Porphyry Cu provinces (from Titley and Beane, 1981). The red spots refer to alkalic porphyry deposits, whereas yellow spots indicate alkali epithermal systems. World bathymetry map from the General Bathymetric Chart of the Oceans (www.gebco.net)2
Figure 2.1.	Morphogeological belts of the Canadian Cordillera (Gabrielse et al., 1991).....5
Figure 2.2.	Terranes of the Canadian- Cordillera in British Columbia (modified from Nelson and Colpron, 2007).....6
Figure 2.3.	Map of the southern Canadian Cordillera. The shaded line shows the approximate location of the Lithoprobe transect across the southern Canadian Cordillera. CC - Cache Creek terrane; CD – Cadwallader terrane; KO, Kootenay terrane; OC, Core of the Olympic Mountains; SH – Shuksan terrane, and exposed part of the accreted wedge; QN – Quesnel terrane; ST, Stikine terrane; WR, Wrangellia terrane, (modified from http://www.lithoprobe.ca/media/poster/panels/2.asp)8
Figure 2.4.	Interpreted lithospheric cross section of the Lithoprobe transect across southern Canadian Cordillera (Modified from Clowes and Hammer, 2000).....8
Figure 2.5.	Western part of the litoprobe snorcle transect in northwestern BC in the Canadian Cordillera (http://www.litho.ucalgary.ca/atlas/snorcle/snorcle_menu.html).....9
Figure 2.6.	Interpreted cross section of the western part of the Snorcle transect showed in Figure 2.5 (Hammer and Clowes, 2007)9
Figure 2.7.	Simplified stratigraphic columns in three different locations of the Quesnel terrane, including: Southern BC, considering the stratigraphy of the central and eastern belt between Merritt and Princeton areas described by Preto (1979), Mortimer (1987) and Preto et al. (2004); central BC, representing the stratigraphy described in the Mount Polley area by Jackson (2008; after Bailey, 1978; Panteleyev, et al., 1996; Logan and Mihaliynuk, 2004; Logan and Bath, 2005 and Logan et al., 2007). Note: the abbreviations LTNpv, LTNav and LTNav are referred to geological map units of Logan et al. (2007) for the Nicola Group sampled in this research); northern BC, represented by the stratigraphy in the Mount Milligan area from Nelson and Bellefontaine (1996).....11
Figure 2.8.	Simplified geologic map of the Nicola Group in southern BC, showing the spatial distribution of the three different volcanic belts (Mortimer, 1987).....13
Figure 2.9.	Triassic to Middle Jurassic magmatic belts and deposits in the Quesnel terrane of the Canadian Cordillera (modified from Nelson and Colpron, 2007).....14
Figure 2.10.	Jurassic paleobiogeography of western North America. Left, Late Pliensbachian ammonite faunas of the Canadian terranes prior to amalgamation with the mainland. Right, Suggested restoration of latitudinal displacements (modified from Gabrielse et al.,1991).....16
Figure 2.11.	Tectonic model for the Quesnel terrane during the Late Triassic (modified from Gabrielse et al., 1991).17
Figure 2.12.	Kinematic model of the escape hypothesis for Stikine terrane during Late

	Jurassic-Early Jurassic (modified from Wernike and Klepacki (1988). QN= Quesnel terrane, ST= Stikine terrane, T= Melange with tethyan fauna (Cache Creek terrane).....	18
Figure 2.13.	Staged evolution of the Cache Creek enclosure (enclosure hypothesis) and the amalgamation of the Intermontane superterrane (Mihalynuk et al, 1994).....	19
Figure 3.1.	Major alkalic porphyry Cu-Au deposits in the Quesnel terrane, showing sample locations for this research. The outlined Quesnel terrane is modified from Goodfellow (2007).....	22
Figure 3.2.	Schematic W-E cross section showing lateral facies change of the Nicola Group in Central British Columbia (modified from Schiarizza, 2009).....	26
Figure 3.3.	Structures and textures found along the Nicola Group. A) Volcaniclastic rocks presenting vertical bedding at Mount Milligan; B) Volcaniclastic rocks presenting sub-vertical bedding in the South of Merritt area; C) Pillow basalt from the Bridge Lake area (sample BTB057); D) Polimictic breccia containing pyroxene-phyric basalt fragments, from the Bridge Lake area (sample BTB056); E) Peperite from Mount Milligan; F) Peperite at Woodjam, close to sample WTB083; G) Peperite at Woodjam sample WTB087; H) Gray, porphyritic, clinopyroxene bearing basalt from Mount Polley (sample PSV022); I) Gray-reddish, porphyritic, clinopyroxene bearing basalt, note the presence of hematite masses (after olivine?) within the rock (sample PSV001); J) Reddish, porphyritic-trachytic, clinopyroxene- plagioclase-analcime basalt (sample PSV002); K) Gray-reddish, porphyritic, clinopyroxene- -analcime basalt (sample SSV128); D) Reddish, highly vesiculated basalt, calcite (Cc) filling vesicles (sample PSV036); M) Gray porphyritic-trachytic plagioclase bearing andesite from Woodjam (sample WTB087); N) Possible pillow basalt affected by chlorite-epidote alteration from Lac la Hache (sample LTB071).....	29
Figure 3.4.	Representative porphyritic basalts from the Nicola Group, showing typical phenocryst and alteration minerals. A) Cpx±Plg basalt, note the presence of Fe-Ti oxides as inclusions in Cpx and within the matrix. Dark matrix is related to the hematite content (sample LTB073 – Lac la Hache area). B) Cpx±Plg±Anl basalt, observe the euhedral phenocryst of Anl (sample PSV002 – LTNav unit, Mount Polley area). C) Cpx±Plg basalt, note the amygdales of Chl-Cc-Ep (sample BTB053 – Bridge Lake area). D) Cpx±Plg basalt, Fe-Ti oxides within the matrix, amygdales of Cc-Chl-Ep, dark matrix due to hematite content (sample LTB058 – Lac la Hache area). E) Cpx±Plg basalt, presenting vesicles of Zeo (sample PSV047 – LTNav unit, Mount Polley area). F) Cpx basalt, note the amygdales of Zeo-Chl-Ep and absence of Fe-Ti oxides (sample MTB030 – Mount Milligan area). G) Basalt showing Anl as phenocryst, filling fractures and partially replacing Cpx (sample PSV039 – LTNav unit, Mount Polley area). Abbreviations: An, analcime; Cc, calcite; Chl, chlorite; Cpx, clinopyroxene; Ep, epidote; Plag, plagioclase; Zeo, zeolite.....	35
Figure 3.5.	Geology, gravity and magnetic maps, showing the sample location of the Mount Polley area; dashed pink lines, within the maps, outlines intrusive bodies. A) Geology of the Mount Polley area (Modified from Logan et al.,	

	2007). B) Gravity Bouguer Corrected map, Quest project (Geoscience BC., 2009). C) Magnetics Total Field map, Quest project (Geoscience BC., 2009). Red dots, in the three maps, indicate sample locations.....	37
Figure 3.6.	Geology, gravity and magnetic maps, showing the sample location of the Mount Milligan area; dashed brown lines in the gravity and dashed pink lines in the magnetic maps, outlines intrusive bodies. A) Geology of the Mount Milligan area (Modified from Logan et al., 2010). B) Bouguer Corrected Gravity map, Quest project (Geoscience BC., 2009). C) Magnetics Total Field map, Quest project (Geoscience BC., 2009). Red dots, in the three maps, indicate sample locations.....	38
Figure 3.7.	Geology, gravity and magnetic maps, showing the sample location of the Woodjam area; dashed pink lines within the maps, outlines intrusive bodies. A) Geology of the Woodjam area (Modified from Massey et al., 2005). A') Detailed geological map from the Woodjam area (modified from Blackwell et al., 2010). B) Gravity Bouguer Corrected map, Quest south project (Geoscience BC., 2010). C) Magnetics Total Field map, Quest south project (Geoscience BC., 2010). Red dots, in the three maps, indicate sample locations.....	40
Figure 3.8.	Geology, gravity and magnetic maps, showing the sample location of the Copper Mountain area; dashed pink lines within the maps, outlines intrusive bodies. A) Geology of the Copper Mountain area (Modified from Massey et al., 2005). B) Gravity Bouguer Corrected map, Quest south project (Geoscience BC., 2010). C) Magnetics Total Field map, Quest south project (Geoscience BC., 2010). Red dots, in the three maps, indicate sample locations.....	41
Figure 3.9.	Geology, gravity and magnetic maps, showing the sample location of the Lac la Hache area; dashed pink lines within the maps, outlines intrusive bodies. A) Geology of the Lac la Hache area (Modified from Massey et al., 2005). B) Gravity Bouguer Corrected map, Quest south project (Geoscience BC., 2010). C) Magnetics Total Field map, Quest south project (Geoscience BC., 2010). Red dots, in the three maps, indicate sample locations.....	43
Figure 3.10.	Geology, gravity and magnetic maps, showing the sample location of the Bridge Lake area; dashed pink lines within the maps, outlines intrusive bodies. A) Geology of the Bridge Lake area (Modified from Massey et al., 2005). B) Gravity Bouguer Corrected map scale 1:500,000, Quest south project (Geoscience BC., 2010). C) Magnetics Total Field map, Quest south project (Geoscience BC., 2010). Red dots, in the three maps, indicate sample locations.....	45
Figure 3.11.	Geology, gravity and magnetic maps, showing the sample location of the South of Merritt area; dashed pink lines within the maps, outlines intrusive bodies. A) Geology of the South of Merritt area (Modified from Massey et al., 2005). B) Gravity Bouguer Corrected map, Quest south project (Geoscience BC., 2010). C) Magnetics Total Field map, Quest south project (Geoscience BC., 2010). Red dots, in the three maps, indicate sample locations.....	47
Figure 3.12.	Histograms showing variation in density between basalts of the Nicola Group. A) Density of the three map units of the Mount Polley area.	

	B) Density of the different areas in this study, except Mount Polley.....	50
Figure 3.13.	Regional airborne gravity Bouguer corrected map of the Quest and Quest-south areas (Geoscience BC., 2009 and Geoscience BC., 2010, respectively). Black semi-circles delineate the areas considered in this research. The gray-dashed line indicates a deflection within the arc, and from there to the south the gravity decreases	51
Figure 3.14.	Histograms showing variation in the magnetic susceptibility reading between basalts of the Nicola Group. A) Magnetic susceptibilities of the three map units of Mount Polley. B) Magnetic susceptibilities of rocks from all other areas in this study.	53
Figure 3.15.	Regional airborne total magnetic field map of the Quest and Quest-south areas (Geoscience BC., 2009 and Geoscience BC., 2010, respectively). Black semi-circles delineate the areas considered in this research. The white-dashed line indicates a deflection within the arc.....	54
Figure 4.1.	Bivariant plot SiO ₂ vs Na ₂ O+K ₂ O of Irvine and Baragar (1971). A) Showing the alkaline nature of the basalts from Mount Polley, note that most rocks from the LTNav unit have more alkalic signature. B) Comparing the alkalinity of the basalts from different localities of the Nicola Group with the Mount Polley area. Basalts from Bridge Lake and a sample from Mount Milligan display a less alkaline signature.....	59
Figure 4.2.	Harker plots, evidencing some geochemical variations on basalts from the Nicola Group. A-1, B-1 and C-1) Indicate variations of Na ₂ O, K ₂ O and MgO for basalts from Mount Polley. A-2, B-2 and C-2) Show a comparison of basalts of different areas along the Nicola Group with rock from Mount Polley.	60
Figure 4.3.	Geochemical index (Fe ₂ O ₃ t+MgO) vs Al ₂ O ₃ , as an indicator of differentiation for rocks from the Nicola Group. A) Exhibit changes in the differentiation between the three map units of Mount Polley. B) Comparison of differentiation of rocks from different localities within the Nicola Group with basalts from Mount Polley.	61
Figure 4.4.	Ternary Th-Zr/117-Nb/16 diagram of Wood (1980), denoting the tectonic environment for basalts from the Nicola Group. A) Showing that all rocks from Mount Polley belong to the arc magmatic tectonic setting. B) Evidencing that all rocks from different localities along the arc fall within the arc-basalt setting.....	62
Figure 4.5.	Ce/Yb vs Th/Nb ratios, indicating variations of the different magma sources, and also suggesting changes in the tectonic setting during volcanism. A) Showing variation in Ce/Yb ratios, and relatively homogeneous. B)Th/Nb ratios between the three map units of Mount Polley. C) Exhibiting changes in both, Ce/Yb and Th/Nb ratios of rocks from different localities within the Nicola Group with basalts from Mount Polley.....	63
Figure 4.6.	Bivariant plot of Fe ³⁺ /Fe ²⁺ versus magnetic susceptibility of rocks from the Nicola Group, indicating similarities between rocks of Mount Milligan, Bridge Lake and Copper Mountain, and between Mount Polley, Lac la Hache and South of Merritt basalts. Note that samples from Woodjam and some from South of Merritt and Lac la Hache form a separate group.....	64

Figure 4.7.	Representative backscattered electron images of clinopyroxene, electron microprobe (EMP) analysis spots are shown in yellow: A) clinopyroxene showing concentric zonation and Fe-Ti-oxide inclusions (bright gray); B) Zoned clinopyroxene evidencing a sharp transition between the core/interior (dark gray) and rim (light gray), note the absence of Fe-Ti oxide inclusions.....	65
Figure 4.8.	The pyroxene quadrilateral of Morimoto (1988), showing clinopyroxene compositions of basalts from the Nicola Group. A) Basalts from three map units of Mount Polley, the circled field corresponds to some clinopyroxene from core and interiors (no rims). B) Basalts from different areas along the Nicola Group compared with rocks from Mount Polley, the circled field corresponds to pyroxene from core to rim of the Woodjam sample, and some spots from cores and interiors (no rims) of clinopyroxene crystals from Bridge Lake and Mount Polley areas (group B).....	66
Figure 4.9.	Chemical distribution based on the content of SiO ₂ and Mg# from electron microprobe (EMP) analyses of clinopyroxene crystals in basalts of the Nicola Group. High Mg# is indicative for primitive melts. A) Clinopyroxene analyses from three map units from the Mount Polley area, dashed brown line outlines some pyroxene analyses from core and interior (no rims). B) Clinopyroxene analyses from different localities along the Nicola Group compared with analyses from Mount Polley. Dashed brown line outlines pyroxene analyses from Woodjam, with some core and interior analyses from Bridge Lake and Mount Polley (group B).....	68
Figure 4.10.	Cation relationships for clinopyroxenes from samples of Nicola Group basalts: A) direct relationship between Al ^{IV} and Fe ³⁺ cpfu in pyroxene composition from core to rim from three map units of Mount Polley brown line outlines some core and interior (no rims) pyroxene analyses; B) Comparison of clinopyroxene compositions from different localities along the arc with clinopyroxene from Mount Polley. Dashed brown line outlines pyroxene analyses from Woodjam, with some core and interior analyses from Bridge Lake and Mount Polley (group B).....	69
Figure 4.11.	Representative backscattered electron images of Fe-Ti-oxide minerals from Mount Polley; electron microprobe (EMP) analytical spots are shown in red-orange dots: A) magnetite with lamellae of titanomagnetite, maghemite at the border of the grain (right side of the crystal); B) magnetite composition in the core (dark gray) and titanomagnetite composition at the border (light gray) of the crystal; C) Ferropseudobrookite lamellae (dark gray) within titanomagnetite grain (light gray).....	70
Figure 4.12.	The Fe ³⁺ -Ti-Fe ²⁺ relative amounts of Fe-Ti-oxide minerals as inclusions in clinopyroxene crystals of the Nicola Group, plotted in FeO-Fe ₂ O ₃ -TiO ₂ space after the method of Taylor (1964). A) Fe-Ti oxide composition from three map units of Mount Polley. B) Fe-Ti oxide composition of different localities along the arc, compared with Mount Polley.....	71
Figure 4.13.	Amounts of SiO ₂ , CaO and oxide-totals of Fe-Ti oxide inclusions in clinopyroxene from rocks from the Nicola Group. A) Plot showing anomalous SiO ₂ and CaO contents within most of the Fe-Ti oxides in the	

	LTNpt and LTNav units from Mount Polley. B) Graph denoting the low oxide-totals content of the Fe-Ti oxides from different localities along the arc.	72
Figure 4.14.	Representative backscattered electron image of a clinopyroxene crystal, showing apatite inclusions; electron microprobe (EMP) analysis spots are indicated with red numbers.	73
Figure 4.15.	Chlorine and fluorine compositions of apatite crystals included in pyroxenes from basalts of the LTNav and LTNav units from Mount Polley.	73
Figure 4.16.	The $(\text{Fe}_2\text{O}_3+\text{MgO})$ index showing variation in the differentiation of rocks along and across the Nicola Group. A) North to south variations of differentiation between basalts along the belt. B) East to west changes in differentiation in the central-south part of the Nicola arc.	74
Figure 4.17.	Incompatible element ratios of rocks along the Nicola Group. A) North to south variations of Th/Nb ratios along the belt. B) North to south variations of Ce/Yb ratios along the arc.	76
Figure 5.1.	Plot showing the $\delta^{18}\text{O}_{\text{SMOW}}$ (‰) and $\delta^{13}\text{C}_{\text{PDB}}$ (‰) mineral compositions of carbonate from altered basalts along the Nicola Group; fields for Triassic marine carbonate rocks (Veizer et al., 1999), and magmatic hydrothermal carbonate cooling curve (Pass, 2010), are shown for comparison.	84
Figure 6.1.	Geology, gravity and magnetic maps of the QUEST and QUEST-South areas, dashed polygons showing the location of the studied areas in this research; Simplified geologic map (Modified from Massey et al., 2005). Gravity Bouguer Corrected map, QUEST and QUEST-South projects (Geoscience BC., 2009; Geoscience BC., 2010). Magnetics Total Field map, QUEST and QUEST-South projects (Geoscience BC., 2009; Geoscience BC., 2010).	91
Figure D1.	Molar element ratio plots documenting the level of Ca, K, and Na mobility in the Nicola Group rocks. A) The basaltic to andesitic rocks all plot to the right of the albite-K-feldspar-kaolinite triangle in the diagram. The most primitive rocks (e.g. Bridge Lake) plot to the right, reflecting their high anorthite content, whereas the andesitic rocks of Woodjam plot furthest to the left. Note that with the possible exception of two Mount Polley samples (PSV036 and PSV049 from the LTNav unit, red-dashed line) no addition of K is evident. B) Loss on Ignition (LOI) versus $(2*\text{Ca}+\text{Na}+\text{K})/\text{Al}$. There is no correlation of LOI with Ca-Na-K content in the rock, again with the possible exception of samples PSV001, PSV036 and PSV049 from the LTNav unit (red-dashed line). The spread of LOI in the sample set is interpreted as the effect of variable amounts of secondary carbonate formation and hydration of the rock during seafloor alteration or low grade metamorphism but secondary carbonate formed with Ca already present in the rock and did not require addition of Ca to the rock.	148

List of Abbreviations

apfu	:	Anion Per Formula Unit
BC	:	British Columbia
CC	:	Cache Creek terrane
CD	:	Cadwallader terrane
Chl	:	Chlorite
CIM	:	Canadian Institute of Mining, Metallurgy and Petroleum
CODES	:	Centre for Excellence in Ore Deposit Research
cpfu	:	Cation Per Formula Unit
EMP	:	Electron Microprobe
ICP-MS	:	Inductively coupled plasma mass spectrometry
ID	:	Identification
IV	:	Tetrahedral
KO	:	Kootenay terrane
LGR	:	Los Gatos Research
LIF	:	Lithium fluoride
LOI	:	Lost on Ignition
LTN	:	Late Triassic Nicola
m	:	Methamorphic belt
M _D	:	mass of the dry sample
MDRU	:	Mineral Deposit Research Unit
Mg#	:	Magnesium Number
MS	:	Magnetic Susceptibility
M _w	:	mass of the sample submerged in H ₂ O
n	:	number of samples
NRCan	:	Natural Resources Canada
ND	:	Not detectable
OC	:	Core of the Olympic Mountains
PC1	:	Pseudo crystal, multilayered W/Si
PDB	:	Peedee Belemnite
PET	:	Pentaerythritol
PGE	:	Platinum Group Element
QA	:	Quality Assurance
QC	:	Quality Control
QN	:	Quesnel terrane
QUEST	:	Quesnellia Exploration Strategy
R	:	Rim
SEM	:	Scanning Electron Microscope
SH	:	Shuksan terrane
SI	:	Système International d'unités (International System of Units)
SM	:	Slide Mountain terrane
SMOV	:	Standard Mean Ocean Water

SNORCLE : Slave-Northern Cordillera Lithospheric Evolution
ST : Stikine terrane
TAP : Thallium acid phthalate
UBC : University of British Columbia
USA : United States of America
UTM : Universal Transverse Mercator
VI : Hexahedral
WR : Wrangellia terrane
 ρ : density
 ρ_{H_2O} : water density
 ρ_s : density of sample

Mineral Abbreviations

Anl : Analcime
Cc : Calcite
Cpx : Clinopyroxene
Ep : Epidote
Hem : Hematite
Plg : Plagioclase
Zeo : Zeolite

ACKNOWLEDGMENTS

Many thanks to my supervisors Thomas Bissig and Craig Hart who provided guidance, discussions and valuable criticism during the length of this project until its completion. Special thanks go out to Jim Mortensen for his critical comments which help to enrich this manuscript.

I would like to express my gratitude to Geoscience BC for the financial support to this project, and also for honouring me with a scholarship which facilitated my time here in Canada.

I acknowledge Mati Raupsepp, Edith Czech and Jenny Lai for their help in the SEM-EMP laboratory at UBC during sample preparation and data acquisition. I appreciate the constructive comments and suggestions from Mitch Mihalynuk, Kelly Russell and Shaun Barker. I also appreciate the help received from Arne Toma (MDRU resource centre coordinator), Manjit Dosanjh and Karie Smith (MDRU accountants).

Many thanks go out to Christa Sluggett and Fion Ma at Geoscience BC for all the technical support received during these years.

My gratitude to Jacqueline Blackwell at Gold Fields Canada Exploration for providing me with her knowledge of the Woodjam property.

I am very grateful with my friends: Razique, Ayesha A., Ben H., Bernardo P., Betsy F., Esther B., Jack M., Karen R., Jaime P., Jessica N., Leanne S., Leif B., Lindsay M, Moira C., Pablo S., Shawn H., Tatiana A., Tim W., Will L., who make my time in Vancouver enjoyable.

My deep gratitude and friendship go to Alfonso Rodriguez, Alejandra Medina and Peter Macdonald who always extended a helping hand when needed.

Thank you very much Diana for your encouragement, understanding, and patience.

To the memory of my Father

CHAPTER 1: OVERVIEW

1.1 INTRODUCTION

Porphyry deposits account for about 50 to 70% of Cu, one-fifth of Au and more than 95% of Mo production in the world (Sinclair, 2007; Sillitoe, 2010). In Canada, porphyry deposits are responsible for more than 40% of Cu, about 10% of Au and virtually all the Mo production, and are mostly hosted in the Canadian Cordillera and to lesser extent in eastern Canada (Sinclair, 2007).

Porphyry deposits can be classified in calc-alkalic and alkalic types, based on the chemical composition of the source intrusion. Porphyries can also be discriminated on the basis of their metal content, mainly Cu, Au and Mo (Kirkham and Sinclair, 1995). Alkalic porphyries tend to have high Au content, typically between 0.2 and 2.0 g/t, 0.15 to 0.7 wt% Cu but only negligible amounts of Mo (Sinclair, 2007). Calc-alkalic Cu-porphyry deposits can contain from 0.005 to 0.15% Mo, and typically from none to 0.35 g/t Au (Sillitoe, 1980; Sinclair, 2007). Alkalic porphyry deposits typically form clusters, where mineralization is hosted in pipes or dyke swarms (<200m diameter), or in large intrusive complexes; individual deposits typically not exceeding a few 100's of metres across (Holliday and Cooke, 2007). In contrast, calc-alkalic deposits can form individual ore bodies measuring hundreds up to thousands of metres across, and also occur as clusters. The Canadian Cordillera hosts both calc-alkalic and alkalic porphyry deposits (McMillan and Panteleyev, 1995).

The Canadian Cordillera contains the largest concentration of alkalic Cu-Au porphyry deposits and prospects in the world (Tosdal et al., 2009). These porphyries are scattered over a 1500 km strike length, hosted by Late Triassic marine arc rocks of the Quesnel and Stikine terranes, and were emplaced between 210 and 178 Ma (Mortensen et al., 1995; Bath et al., in press).

Besides the Canadian Cordillera, alkalic deposits have also been reported in the Ordovician and Early Silurian Lachlan Fold Belt in New South Wales in eastern Australia (Cooke et al., 2007), the Early Oligocene continental arc in the Chalkidiki Peninsula, Greece (Kroll et al., 2002), the Late Oligocene to Early Miocene Didipio region, North Luzon in the Philippines (Wolfe, 2001) and in the Late Oligocene alkalic volcanic rocks in Colorado Front Range in USA (Jensen and Barton, 2000; Fig. 1.1).



Figure 1.1. Global distribution of porphyry deposits. Orange areas cover major porphyry Cu provinces (from Titley and Beane, 1981). The red spots refer to alkalic porphyry deposits, whereas yellow spots indicate alkalic epithermal systems. World bathymetry map from the General Bathymetric Chart of the Oceans (www.gebco.net).

Lang et al. (1995a) discriminates the host intrusions of the alkalic porphyry deposits in British Columbia into silica saturated (e.g., Mount Milligan and Copper Mountain) and silica undersaturated (e.g., Mount Polley and Lorraine). These two types of alkalic porphyries are associated with Cu-Au mineralization and also have potential for economic by-products such as platinum group elements (PGEs; Lang et al., 1995b; Thompson et al., 2001; Nixon et al., 2004).

The relationship between alkalic volcanism, plutonism and related mineralization in the Canadian Cordillera has been discussed first in the paper of Barr et al. (1976). However, detailed research on alkalic porphyry deposits was presented in the publication “Porphyry Deposits of the Northwestern Cordillera of North America”, CIM Special Volume 46 (Schroeter, 1995). Recent studies on different alkalic porphyry deposits within the Cordillera carried out by the Mineral Deposit Research Unit (MDRU) at the University of British Columbia (UBC) and the Centre for Excellence in Ore Deposit Research (CODES) at the University of Tasmania, have increased the knowledge on the alkalic porphyries themselves (e.g., Jago, 2008 on Mount Milligan; Jackson, 2008 and Pass, 2010 on Mount Polley; Byrne, 2009 and Micko, 2010 on Galore Creek; Norris, 2012 on Red Chris). In contrast to the deposit scale studies, little work aimed at the regional setting of alkalic porphyry deposits has been carried out. However, a better understanding of the tectonic and volcanic setting on a regional scale is crucial to investigate the unique factors that led to the anomalous concentration of alkalic porphyry deposits in BC (cf., Tosdal et al., 2009).

This project is a regional study focused on host volcanic rocks of the Quesnel terrane, which occur over extensive but poorly exposed areas with unknown potential for alkalic porphyry mineralization.

A better understanding of the chemical and physical distinctions of basaltic volcanic rocks in areas hosting Cu-Au porphyry mineralization and regions apparently devoid of that kind of mineralization was accomplished by petrography, physical properties in relation to regional scale geophysical data, together with whole rock and mineral chemistry, and isotopic-traces compositions with the aim to delineate prospective arc segments to focus exploration for Cu-Au alkalic porphyries along the Quesnel terrane.

1.2 THESIS ORGANIZATION

This thesis is arranged in five chapters (Chapters 2 to 6), underlining the geology, as well as the physical and chemical characteristics of the Quesnel terrane:

Chapter 2 provides background information by means of a literature review of the tectonic setting of the Canadian Cordillera, particularly the Quesnel terrane and describes the regional geological history and metallogeny of this terrane.

Chapter 3 presents the results of petrographic description and physical property measurements of host rocks in different arc-segments along the Quesnel terrane, as well as, interpretation of regional geophysical surveys with respect to the relationship between host rocks and alkalic Cu-Au porphyry deposits.

Chapter 4 addresses the characteristics of different arc-segments along the Quesnel terrane, on the basis of whole rock and mineral chemistry of coherent basaltic rocks, in view of their association with alkalic Cu-Au porphyry deposits.

Chapter 5 presents C-O isotopic data on trace carbonate-minerals within the alteration mineral assemblage of rocks, interpreting the nature of this alteration for different arc segments along the terrane.

Chapter 6 concludes with a compilation and discussion of the main points addressed in previous chapters.

1.3 PROJECT SUPPORT AND STUDY METHODOLOGY

This project was proposed and supervised by the Mineral Deposit Research Unit (MDRU) at the University of British Columbia (UBC) and supported through Geoscience BC funding. Three papers have been published by Geoscience BC in the 2010, 2011 and 2012 Summary of Activities Reports (Bissig et al., 2010; Vaca et al., 2011 and Vaca et al., 2012); these articles summarized the project progress at that time.

Rock sampling and magnetic susceptibility measurements were conducted by Thomas Bissig and the author during the 2009 and 2010 summer seasons. Laboratory analyses were done at UBC, including rock-density, thin-section petrographic description, scanning electron microscope (SEM) and electron microprobe (EMP) analyses. Oxygen and carbon isotopic analysis were done using the instrument (Los Gatos Research (LGR), model 908-0021) at the UBC facilities by Shaun Barker. Whole rock geochemistry was performed at ALS-Chemex Laboratories, North Vancouver, Canada.

CHAPTER 2: THE QUESNEL TERRANE - REGIONAL SETTING

2.1 INTRODUCTION

The Canadian Cordillera is composed of five main geomorphological belts (Monger et al., 1972), from west to east these are the Insular, Coast, Intermontane, Omineca and Foreland (Figure 2.1), which in British Columbia vary in width from less than 20 to ~350 km and are northwest trending.

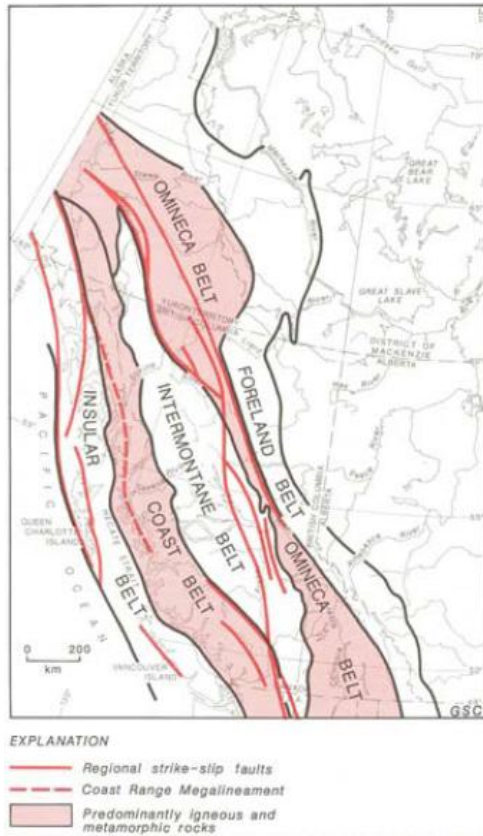


Figure 2.1. Morphogeological belts of the Canadian Cordillera (Gabrielse et al., 1991).

These belts are underlain by several terranes¹ with a distinctive geologic history, such as volcanic arcs, oceanic crust, shelf and slope deposits, basins, as well as intrusive and metamorphic complexes, ranging in age from Middle Proterozoic to Cenozoic.

The Cordillera orogen includes accreted terranes of oceanic origin and terranes of the zone of deformed rocks along the western margin of the North American craton (Laurentia; Gabrielse et al., 1991).

Each of the geomorphological belts is underlain by several terranes (Figure 2.2). Terranes vary in age, lithology, metamorphism, physical properties,

paleomagnetic record and metallogeny (Gabrielse et al., 1991).

The Intermontane belt largely represents the Intermontane superterrane², comprising the Quesnel and Stikine island-arc terranes, as well as the Cache Creek oceanic terrane. This superterrane is thought to have been amalgamated offshore prior to its accretion to North America around the Early–Middle Jurassic (Monger et al., 1982).

¹ *Terrane*. Fault-bounded geologic entity of regional extent characterized generally by a coherent stratigraphic sequence in which depositional continuity can be established (Coney, 1980; Coney, 1989).

² *Superterrane*. An aggregate of terranes that is interpreted to share either a similar stratigraphic kindred or affinity, or a common geologic history after accretion (Moore, 1992).

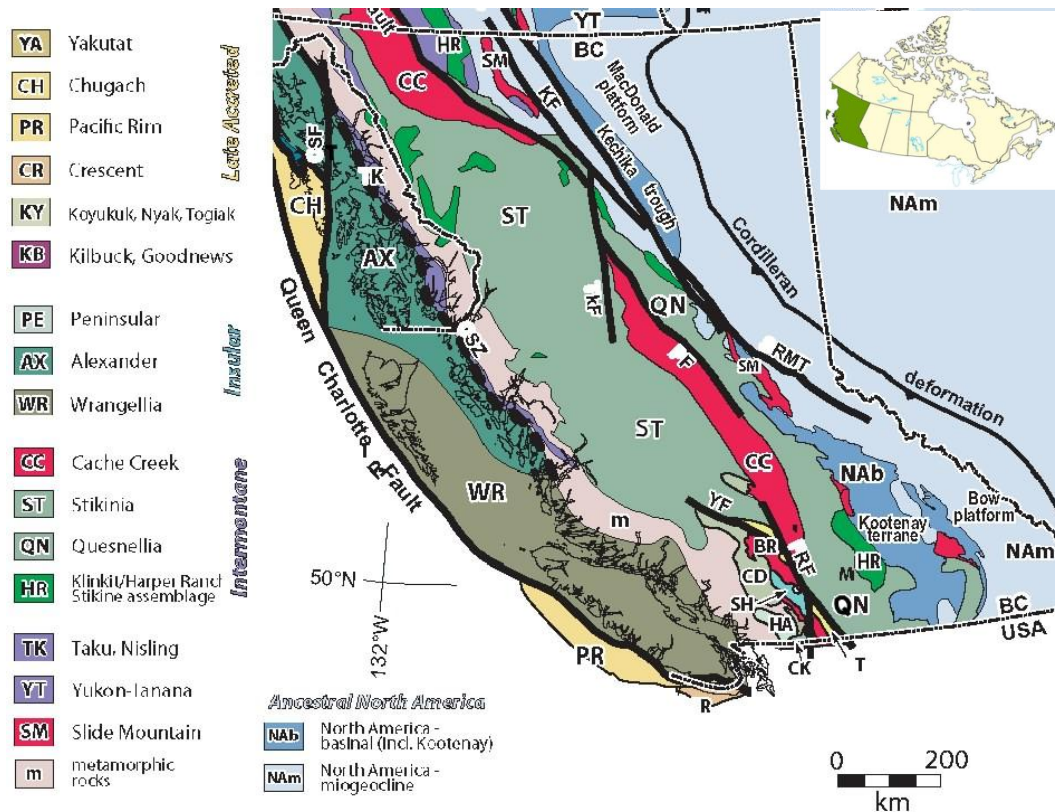


Figure 2.2. Terranes of the Canadian- Cordillera in British Columbia (modified from Nelson and Colpron, 2007).

The Quesnel terrane underlies part of the eastern Intermontane belt (Figure 2.2), and comprises upper Paleozoic and lower Mesozoic volcanic and associated intrusive bodies and sedimentary rocks. The Quesnel terrane extends into the Yukon as a narrow region lying between the Slide Mountain terrane to the east and the Cache Creek terrane to the west (Gabrielse et al., 1991). The Quesnel terrane stratigraphically and structurally overlies Slide Mountain, Cassiar and Kootenay terranes on its east side. To the west, the contact with the Cache Creek terrane is defined by major zones of strike-slip faulting or locally, thrust faults which place the Cache Creek terrane eastward over Quesnel (Coney, 1989). In central BC, the Quesnel terrane presents a faulted contact to the west with the Stikine terrane (Figure 2.2).

In southern BC, Upper Paleozoic rocks of the Quesnel terrane comprise two distinctive lithotectonic assemblages³ that have been subdivided into the Harper Ranch and Okanagan

³ *Lithotectonic assemblage*. A distinctive succession of stratified rocks, mainly bounded by unconformities or faults, deposited in specific tectonic environments during particular intervals of time (Wheeler and McFeely, 1991).

subterrane⁴ (Monger, 1975, 1977b; Peatfield, 1978), which are characterized by sedimentary and volcanic rocks associated with marginal basins (Smith, 1979; Monger, 1977b; Peatfield, 1978; Milford, 1984). The northern equivalent of the Harper Ranch is the Lay Range assemblage (Nelson and Bellefontaine, 1996).

The most characteristic and extensive assemblage in the Quesnel terrane is the Upper Triassic - Lower Jurassic island arc volcano-sedimentary sequence and related intrusions, represented by the Nicola Group in the south of the province (Schau, 1968) and the Takla Group at north (Armstrong, 1948; Armstrong, 1965). However, Nicola Group is currently the accepted name for all the Triassic-Jurassic volcanic arc and related rocks in the Quesnel terrane (Gabrielse and Yorath, 1991; Panteleyev et al., 1996). In this regard, the equivalent Upper Triassic Takla and Nicola groups hereafter will be referred to as Nicola Group.

The youngest lithological unit that comprises the Quesnel terrane is the Early-Middle Jurassic Ashcroft Formation, located in southern BC. It ranges from Late Sinemurian to Callovian, and consist largely of clastic rocks with minor carbonate members (Crickmay, 1930; Travers, 1982).

2.2 BASEMENT

The relationship between the terranes and the North American craton has been studied using seismic reflection surveys. The Lithoprobe program in the “Southern Canadian Cordillera” and “Slave-Northern Cordillera Lithospheric Evolution (SNORCLE)” transects comprised sections across the Intermontane belt, which help understanding the relationship between the Quesnel terrane and its basement.

The terranes comprising the Intermontane superterrane (Cache Creek, Stikine and Quesnel) are interpreted to have been transported eastwards over the cratonic basement of western North America. The southern Canadian Cordillera seismic section (Figure 2.3), interpreted by Clowes and Hammer (2000), shows that the crystalline basement extends as far west as the Fraser fault (Figure 2.4).

⁴ *Subterrane*. A fault-bounded unit within a terrane that exhibit similar, but not identical geologic history relative to another fault bounded unit in the same terrane (Nokleberg et al. 2005).

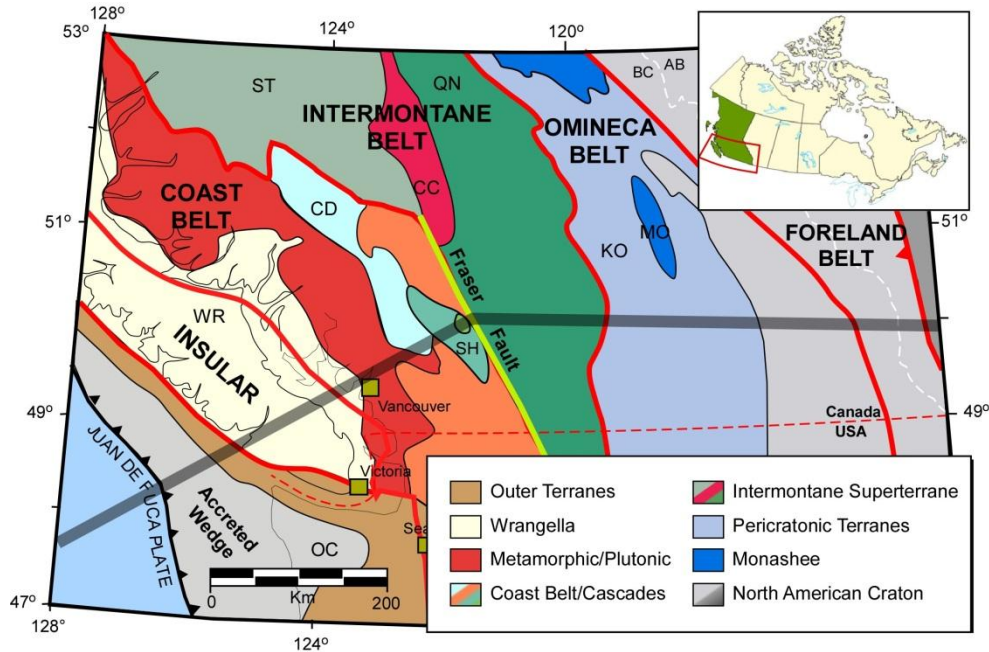


Figure 2.3. Map of the southern Canadian Cordillera. The shaded line shows the approximate location of the Lithoprobe transect across the southern Canadian Cordillera. CC - Cache Creek terrane; CD - Cadwallader terrane; KO, Kootenay terrane; OC, Core of the Olympic Mountains; SH - Shuksan terrane, and exposed part of the accreted wedge; QN - Quesnel terrane; ST, Stikine terrane; WR, Wrangellia terrane.

(Modified from <http://www.lithoprobe.ca/media/poster/panels/2.asp>).

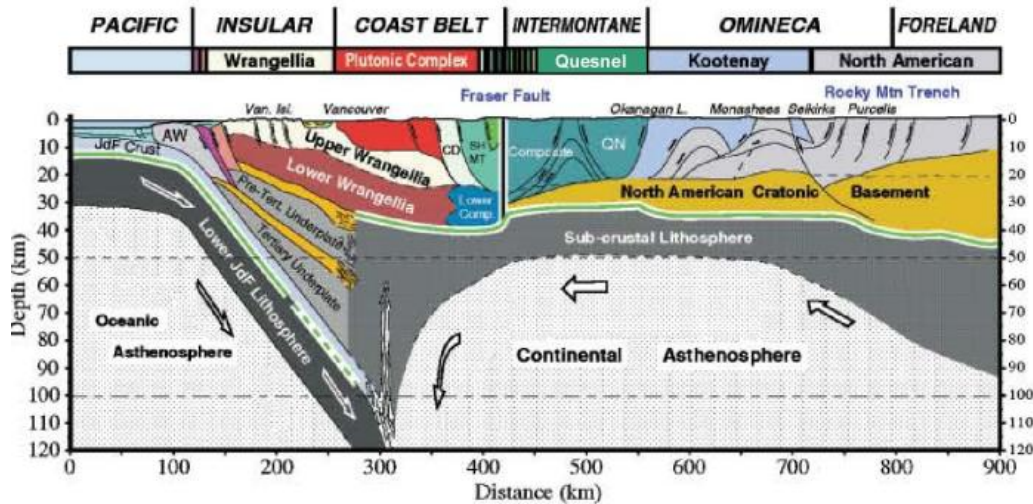


Figure 2.4. Interpreted lithospheric cross section of the Lithoprobe transect across southern Canadian Cordillera (Modified from Clowes and Hammer, 2000).

In the western part of the transect across the northern Canadian Cordillera (SNORCLE; Figure 2.5), the basement of the accreted terranes is formed by Proterozoic sedimentary rocks (Hammer

and Clowes, 2007; Figure 2.6). These rocks were deposited along the west passive margin of Ancestral North America.

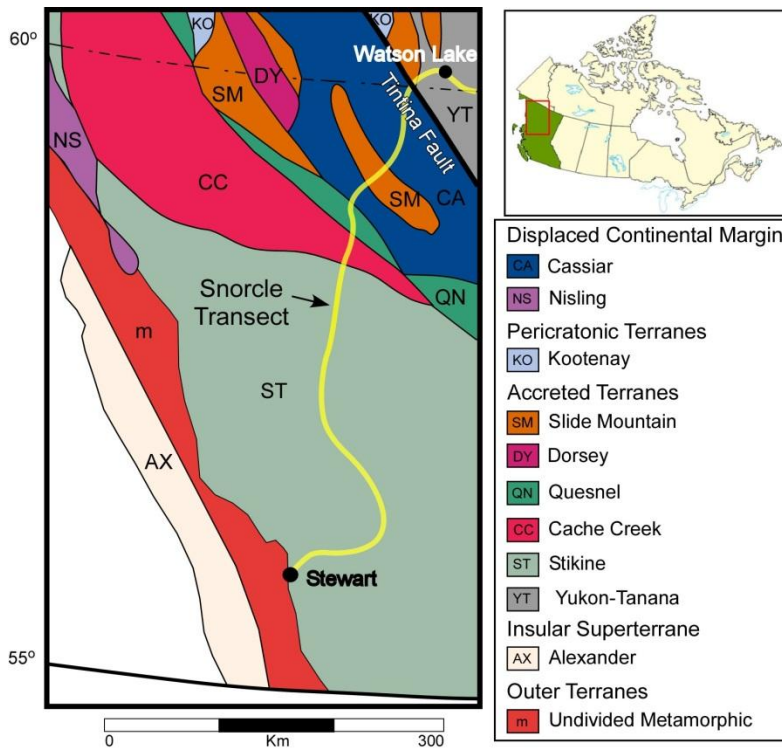


Figure 2.5. Western part of the litoprobe snorcle transect in northwestern BC in the Canadian Cordillera (http://www.litho.ucalgary.ca/atlas/snorcle/snorcle_menu.html).

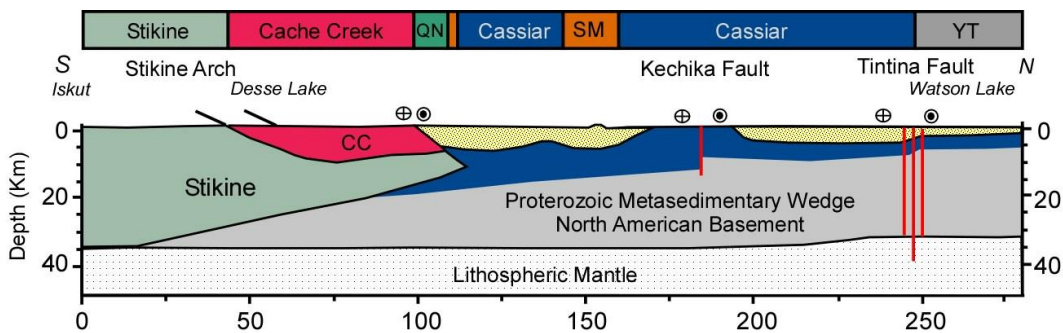


Figure 2.6. Interpreted cross section of the western part of the Snorcle transect showed in Figure 2.5 (Hammer and Clowes, 2007).

Based on the information provided above, it is possible to note that the cratonic basement extends farther west in southern than in northern British Columbia.

An additional observation from the seismic transects is that, while some terrane boundaries are vertical (faults?), others are subhorizontal. These subhorizontal boundaries indicate that the

accreted terranes comprise stacks of terranes (nappes), which have been thrust from the west over different basement (crystalline craton or metasediments) to their actual position.

2.3 STRATIGRAPHY, ROCK TYPES AND METALLOGENY

The stratigraphy of the Nicola Group is summarized as follows (Figure 2.7): In southern BC, Ordovician to Late Permian rocks from the Okanagan subterrane (or Apex Mountain Complex), comprise lithologies such as chert, argillite, basalt (greenstone), minor limestone and serpentinized ultramafic rocks, which were emplaced in a marginal oceanic basin (Monger, 1977b; Peatfield, 1978; Milford, 1984). However, Mortensen et al. (2011) presented U-Pb dates in detrital zircons from a siltstone to fine grained sandstone from the Apex Mountain Complex, which yield a range of Late Archean to Proterozoic ages, suggesting an affiliation with a NW Laurentian source. The Late Devonian to Late Permian Harper Ranch subterrane, consists of argillite, chert, limestone, clastic and volcanoclastic rocks, including sandstone and conglomerate, which were deposited in a basin adjacent to an island-arc (Smith, 1979).

In central BC, at Mount Polley area, Paleozoic rocks of the Quesnel terrane do not crop out; but, the Paleozoic is represented by amphibolites from the Slide Mountain terrane (Bloodgood, 1988).

In northern BC, the Pennsylvanian to Permian Lay Range assemblage is represented by lapilli tuff, volcanic and mixed-source sandstone, siltstone, argillite, siliceous tuff, chert and carbonate rocks (Ferri et al., 1993a, b). This assemblage is equivalent to the Harper Ranch rocks farther south (Nelson and Bellefontaine, 1996). The Slide Mountain terrane is also present in this area represented by pillow basalts, basalt, chert and argillites of the Nina Creek Group.

The most representative assemblage within the Quesnel terrane is the Late Triassic - Early Jurassic Nicola Group (Dawson, 1879; Preto, 1979; Mortimer, 1987; Nelson and Bellefontaine, 1996). This group unconformably overlies the Late Paleozoic rocks, and consists of submarine, lesser subaerial arc volcanic sequence dominated by pyroxene \pm plagioclase (locally analcime) phyric, dominantly basaltic to andesitic lavas and associated volcanoclastics, interbedded with sedimentary rocks.

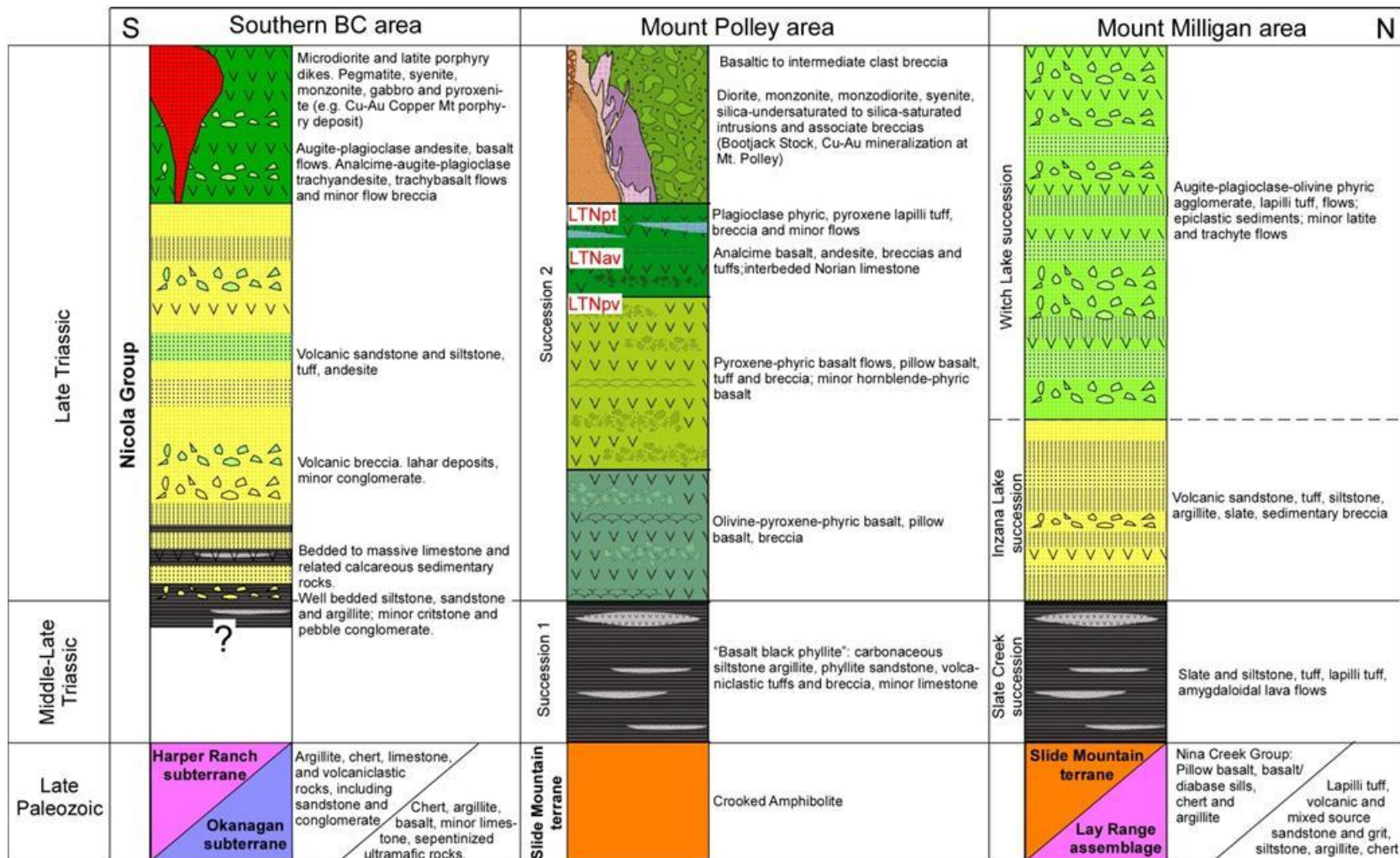


Figure 2.7. Simplified stratigraphic columns in three different locations of the Quesnel terrane, including: Southern BC, considering the stratigraphy of the central and eastern belt between Merritt and Princeton areas described by Preto (1979), Mortimer (1987) and Preto et al. (2004); central BC, representing the stratigraphy described in the Mount Polley area by Jackson (2008; after Bailey, 1978; Panteleyev, et al., 1996; Logan and Mihalynuk, 2004; Logan and Bath, 2006 and Logan et al., 2007). Note: the abbreviations LTNpv, LTNav and LTNpt refer to geological map units of Logan et al. (2007) for the Nicola Group sampled in this research); northern BC, represented by the stratigraphy in the Mount Milligan area from Nelson and Bellefontaine (1996).

The basal part of the Nicola Group in southern BC is composed by massive to graded-bedded siltstone, sandstone and pebble conglomerates, and interbedded limestone and tuffs (Preto, 1979). In central BC (Mount Polley area), the lower part of the Nicola Group is comprised of argillite, siltstone, minor limestone, sandstone and greywacke, and volcanoclastic rocks in the upper part (succession 1, Figure 2.7), whereas in northern BC (Mount Milligan area), the lowest part of the Nicola Group consists of slate, argillite, tuff and minor lava flows (Slate Creek succession; Nelson and Bellefontaine, 1996). The volcanic rocks mark the initial stage of arc activity and fringing reef construction.

Volcanic breccias, laharitic deposits and minor conglomerate overlie the basal sediments in southern BC (Figure 2.7, Preto, 1979). In central BC, olivine-pyroxene-phyric basalt, followed by pyroxene-phyric basalt, analcime-bearing basalt and basaltic-andesite, lie on top of the basal package (succession 2, Figure 2.7; Panteleyev et al., 1996). Whereas, the Inzana Lake succession in the Mount Milligan area represented by volcanic sandstone, tuff, siltstone, argillite, slate and sedimentary breccia, stratigraphically overlies the Slate Creek succession, followed by the Witch Lake succession, which consists of olivine-augite-plagioclase phyric agglomerate, lapilli tuff, flows, epiclastic sediments, minor latite and trachyte flows (Nelson and Bellefontaine, 1996). The upper Nicola Group represents a mature arc, denoting an increase in differentiation upwards in the stratigraphy.

Preto (1979) and Mortimer (1987) showed a west – east chemical variation within the Nicola Group in southern BC that define three major belts (Figure 2.8): the western belt comprises augite-plagioclase phyric basalt and andesite with a calc-alkalic signature. The central and eastern belts are petrographically similar to each other, consisting mainly of augite-phyric basalt, locally analcime bearing, and heterogeneous andesite and basalt. The central belt is characterized by variably tholeiitic to alkalic basalts, whereas the eastern belt is predominantly alkalic (shoshonitic). Paleontological data suggest that the eastern belt is younger (Late Norian, ca. ~203 Ma) than the western belt (Late Carnian – Early Norian, ca. ~216 Ma) (Carter et al., 1991).

Basaltic augite-plagioclase phyric rocks with shoshonitic affinity and locally containing analcime phenocrysts have also been reported in central BC (Quesnel Trough; Panteleyev et al., 1996; Logan and Bath, 2006).

In southern Quesnel terrane, shoshonites are restricted to the east belt (Mortimer, 1987), while in the central and northern part of the Quesnel terrane, shoshonites occur across the width of the terrane (Panteleyev et al., 1996; Nelson and Bellefontaine, 1996). Thus, the suggestion of Mortimer (1987) that an easterly increase of potassium in the Nicola Group corresponds to increasing depth to the paleo-Benioff zone, does not apply north of 51°N (Nelson and Bellefontaine, 1996), where the Nicola Group has not been subdivided into different volcanic belts as in the south.

The Quesnel volcanic arc produced a variety of plutons at the end of its volcanic activity, ranging from dikes and sills to major batholiths. These intermediate to shallow depth intrusions, which vary from gabbro to granodiorite and from alkaline to calc-alkaline in composition, have proven potential for porphyry and other epigenetic types of mineralization. The Late Triassic to Early Jurassic Cu-Au and Cu-Mo porphyry deposits of the Quesnel terrane represent an important group of ore deposits in British Columbia.

The calc-alkaline porphyry Cu-Mo deposits such as Highland Valley, Brenda and Gibraltar (Figure 2.9) are ~ 215 to 210 Ma (Mortensen et al., 1995) and typically hosted in quartz-diorite to granodiorite intrusions, whereas the alkalic porphyry Cu-Au deposits are younger, and commonly hosted in monzonite, monzodiorite and syenite (Woodsworth et al., 1991), and formed during two temporal events. The first episode includes Mount Polley, Copper Mountain

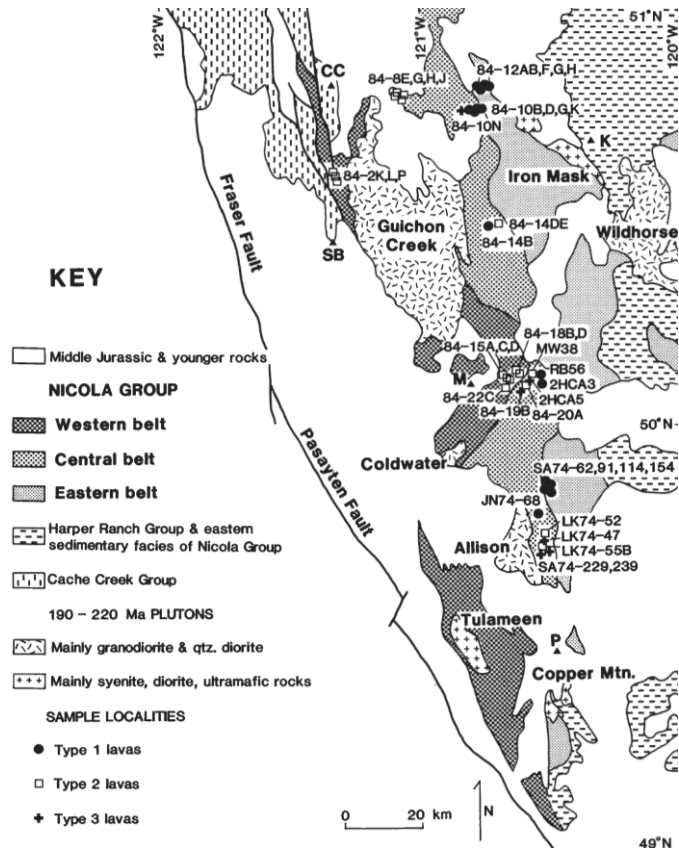


Figure 2.8. Simplified geologic map of the Nicola Group in southern BC, showing the spatial distribution of the three different volcanic belts (Mortimer, 1987).

and deposits around the Iron Mask batholith (e.g., Afton/Ajax, Figure 2.9), formed between 210 and 200 Ma (Mortensen et al., 1995; Logan et al., 2007). The second event includes Mount Milligan and Lorraine, which range in age from 178 to 183 Ma (Mortensen et al., 1995; Bath et al., in press).

Other magmatic-related deposit types found in the Quesnel terrane include the Au-skarn at Hedley and the Au-Ag epithermal deposits of the Toodoggone district (Figure 2.9), as well as several Middle Triassic to Early Jurassic Alaskan-type zoned ultramafic bodies, related to Platinum Group Element (PGE) mineralization (Nixon et al., 1997).

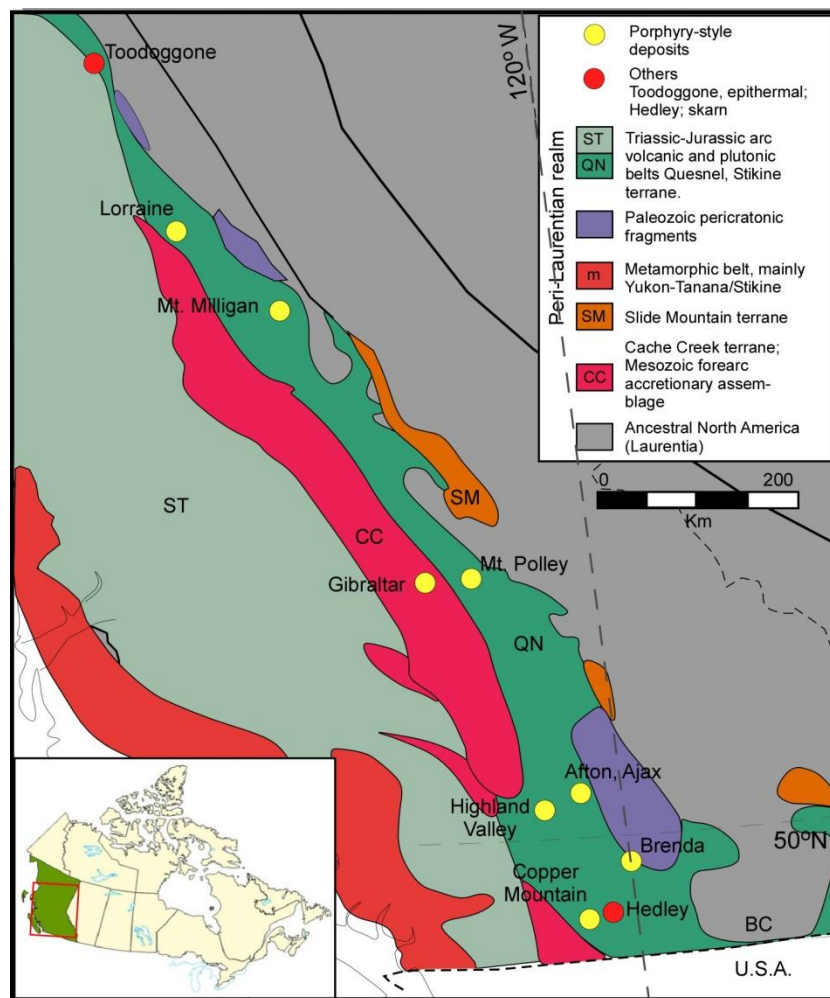


Figure 2.9. Triassic to Middle Jurassic magmatic belts and deposits in the Quesnel terrane of the Canadian Cordillera (modified from Nelson and Colpron, 2007).

The presence of porphyry and related mineralization types in Quesnel make this terrane a remarkable metallogenic province in the Canadian Cordillera.

2.4 METAMORPHISM

In south-central British Columbia, rocks of the Nicola Group present a low grade metamorphism (Schau, 1968; Lefebure, 1976; Preto, 1979) of the prehnite-pumpellyite and locally zeolite facies (Shannon, 1982). In north-central British Columbia, the Nicola Group volcanics are mainly in the prehnite-pumpellyite facies (Meade, 1977; Ferri and Melville, 1988 and 1989; Nelson and Bellefontaine 1996). Nevertheless, in southern BC along the eastern edge of the Eagle Plutonic Complex and surrounding the intrusive bodies in the Nicola horst, which is interpreted as a window into the middle crust and perhaps below the base of the Nicola Group (Moore, 2000), rocks have passed through the garnet zone into the low-grade amphibolite facies (Greig, 1989; Moore and Pettipas, 1990).

In general, the Quesnel terrane falls in the prehnite-pumpellyite and zeolite metamorphic facies (Read et al., 1991), which took place from Late Triassic to Paleogene (Greenwood et al., 1991). However, volcanoclastic rocks from the Harper Ranch Group southern BC, present somewhat higher-grade metamorphism than the Nicola Group, ranging up to greenschist facies. These rocks include phyllite and chlorite-schist (Smith, 1979), suggesting that the southern Paleozoic rocks were affected by an additional Permo-Triassic metamorphic event pre-dating the volcanic rocks of the Nicola Group.

2.5 TECTONIC MODEL

Terranes of the Canadian Cordillera have a high diversity of Tethyan faunas in the southern regions and mixed Boreal/Tethyan faunas in the north. This is based on the presence of two different Jurassic ammonite species, one that belongs to Boreal latitudes (autochthonous to North America) and another to Tethyan latitudes south of North America (Carter et al., 1991; Figure 2.10). In fact, the Quesnel terrane is considered to be allochthonous, having travelled approximately 500 km northward to its actual position, after the Pliensbachian (Carter et al., 1991).

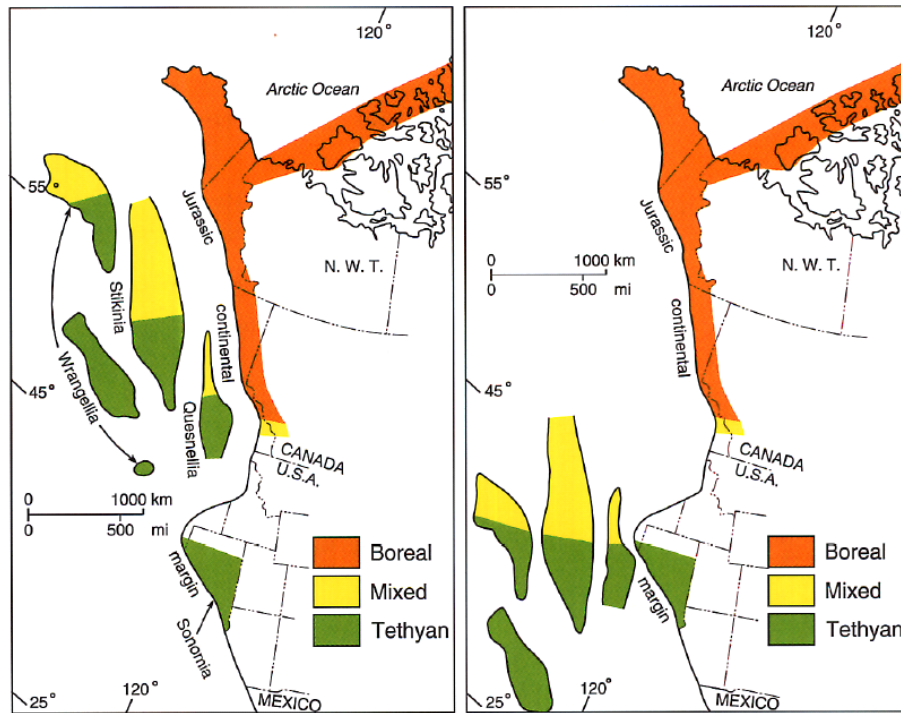


Figure 2.10. Jurassic paleobiogeography of western North America. Left, Late Pliensbachian ammonite faunas of the Canadian terranes prior to amalgamation with the mainland. Right, Suggested restoration of latitudinal displacements (modified from Gabrielse et al., 1991).

Paleomagnetic studies have been used to determine displacements and rotations on the terranes of the Canadian Cordillera. Paleopoles from the Nicola Group, Guichon Creek batholith and Copper Mountain intrusions located in southern BC, imply displacements from the south of at least 4° (Irving and Wynne, 1991). In addition, data available from north-central BC in the Stikine terrane, indicates rotations from 19° clockwise to 116° counter clockwise (Vandall, 1990, and Irving and Wynne, 1990 *in* Mihalynuk et al., 2004).

Gabrielse et al. (1991) proposed a tectonic model for the Quesnel terrane during the Late Paleozoic, which consists of a west-facing island arc that developed offshore of the western margin of Ancestral North America (Figure 2.11). The back-arc basin is represented by the Slide Mountain terrane, and the fore arc by the Cache Creek terrane, which represents an accretionary prism complex. The Quesnel terrane was accreted to Laurentia in the Middle Jurassic (Monger et al., 1982). This collision is evidenced by the presence of obducted blueschist-facies sheets of the same age in a number of localities in the Slide Mountain and Cache Creek terranes (Gabrielse and Yorath, 1991; Mihalynuk et al., 1994).

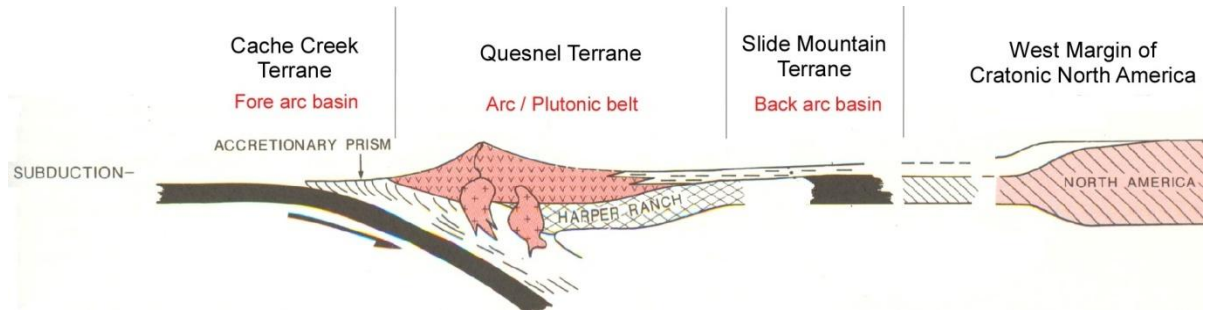


Figure 2.11. Tectonic model for the Quesnel terrane during the Late Triassic (modified from Gabrielse et al., 1991).

The amalgamation process which formed the Intermontane superterrane prior to its accretion to the continent is problematic. The Stikine and Quesnel island-arc terranes are similar in terms of age, petrography, paleotectonic setting, paleofauna, and metallogeny (Gabrielse et al., 1991); however, these terranes are separated from each other by the oceanic plateau with sedimentary fringing rocks that comprise the Cache Creek terrane (Johnston and Borel, 2007).

Two models have been proposed to explain the presence of the Cache Creek terrane between the Stikine terrane to the west and the Quesnel terrane to the east.

Wernicke and Klepacki (1988) proposed the “Escape” hypothesis (Figure 2.12), where the Stikine terrane is considered to be a southern continuation of the Quesnel terrane. These two terranes are interpreted to be a marginal arc tied to North America. The Stikine terrane moved northward along dextral strike-slip faults during Late Jurassic and Early Cretaceous, triggered by the collision of the Wrangellia superterrane over the inboard Intermontane superterrane. Product of this collision, Stikine ended up at its current position, west of the Cache Creek terrane. This model implies a single west facing arc. However, the faults required to move the Stikine terrane have not been identified yet.

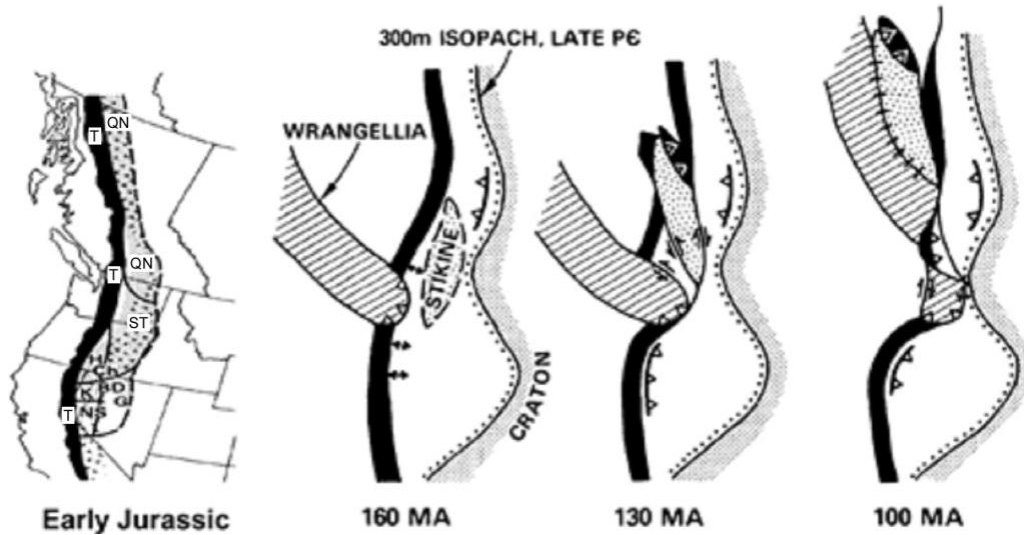


Figure 2.12. Kinematic model of the scape hypothesis for Stikine terrane during Late Jurassic-Early Jurassic (modified from Wernicke and Klepacki (1988)). QN= The Quesnel terrane, ST= Stikine terrane, T= Melange with tethyan fauna (Cache Creek terrane).

The other alternative is the “Enclosure” hypothesis (Nelson and Mihalynuk, 1993; Mihalynuk et al., 1994; Nelson and Colpron, 2007; Figure 2.13). This hypothesis suggests the Stikine terrane was originally a northern extension of the Quesnel terrane, that rotated anticlockwise (oroclinal bending) by $\sim 180^\circ$ (scissor closure) around the intervening Cache Creek terrane, amalgamating the Intermontane superterrane prior to its emplacement to the North American craton in the Middle Jurassic (ca. 175 Ma; Nelson and Colpron, 2007) .

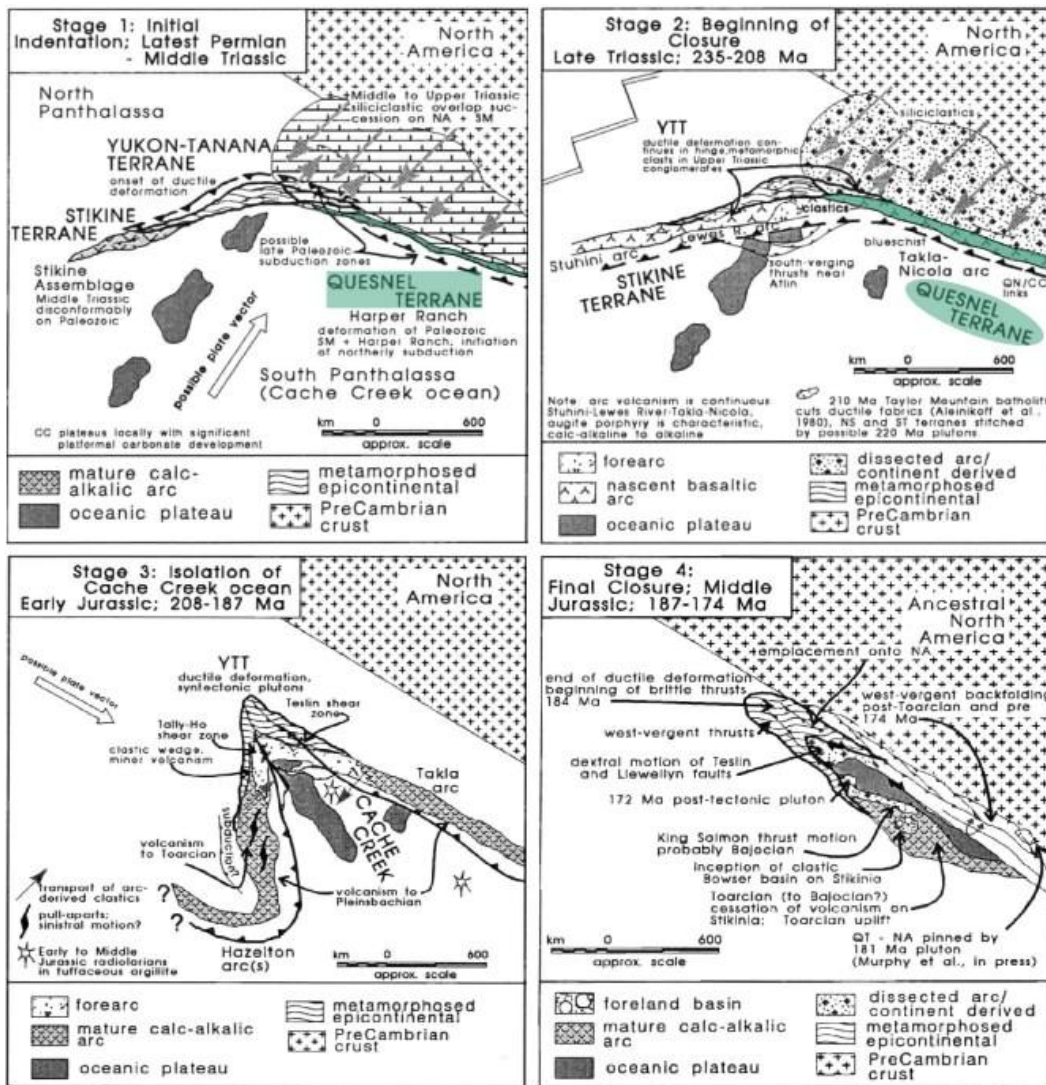


Figure 2.13. Staged evolution of the Cache Creek enclosure (enclosure hypothesis) and the amalgamation of the Intermontane superterrane (Mihalynuk et al., 1994).

The “Enclosure” hypothesis implies the formation of at least two subduction zones, one dipping east and the other dipping west, trapping the Cache Creek accretionary prism and remaining Cache Creek ocean floor between the Stikine and Quesnel volcanic arcs during the Early Jurassic (Nelson and Mihalynuk, 1993; Mihalynuk et al. 1994).

Any of the two models exposed above are possible. However, currently the “Enclosure” hypothesis has been widely ratified by the scientific community.

The modern analogue for the Mesozoic island volcanic arcs in western North America, is considered to be the Philippine basin (Nelson and Mihalynuk, 1993; Mihalynuk et al., 1994;

Nelson and Bellefontaine, 1996; Nelson and Colpron, 2007; Figure 2.13), taking in account the type of magmatism, the multiplicity of subducting slabs and the amalgamation of juvenile island-arc crustal blocks occurring currently.

CHAPTER 3: PETROGRAPHY AND PHYSICAL PROPERTIES OF BASALTS IN THE QUESNEL TERRANE

3.1 INTRODUCTION

The Late Triassic – Early Jurassic Quesnel terrane is a volcano-sedimentary intra-oceanic-arc sequence. The Upper Triassic Nicola Group, which mostly defines the Quesnel terrane, is composed largely of alkalic and lesser calc-alkalic basalts, derivative volcanic products and associated marginal basin sedimentary strata (Preto, 1979; Mortimer, 1987; Panteleyev et al., 1996; Nelson and Bellefontaine, 1996). Paleontological and paleomagnetic data show that this volcanic belt may have originated more than 1000 km south of its present location (Irving et al., 1980), and was accreted to the western margin of North America by pre-Middle Jurassic (Monger et al., 1982).

The Quesnel terrane hosts the majority of the alkalic porphyry Cu–Au deposits in British Columbia, including from north to south: Lorraine, Mount Milligan, Mount Polley, Afton/Ajax and Copper Mountain (Figure 3.1).

Much of the area underlain by the Quesnel terrane is densely vegetated and extensively covered by younger glacial and volcanic products, making mineral exploration challenging.

Basalts from seven areas along the Quesnel terrane were chosen for this study. Five of those are spatially related to Cu porphyry style mineralization. These are, Mount Milligan, Mount Polley, Woodjam, Lac la Hache and Copper Mountain (Figure 3.1). The other two areas represent arc segments without operating Cu-Au mines or advanced exploration projects, including Bridge Lake and South of Merritt (Figure 3.1).

The main objective of this chapter is to identify regional variations in the arc and the relationships between alkalic porphyry mineralization and the basaltic host rocks, with the aim of generating a regional understanding of arc segments potentially prospective for porphyry exploration. This chapter presents the results of detailed petrographic description, magnetic susceptibility and density measurements of basalts. These observations are also presented in the context of regional geological, total magnetic field and gravity Bouguer corrected maps.

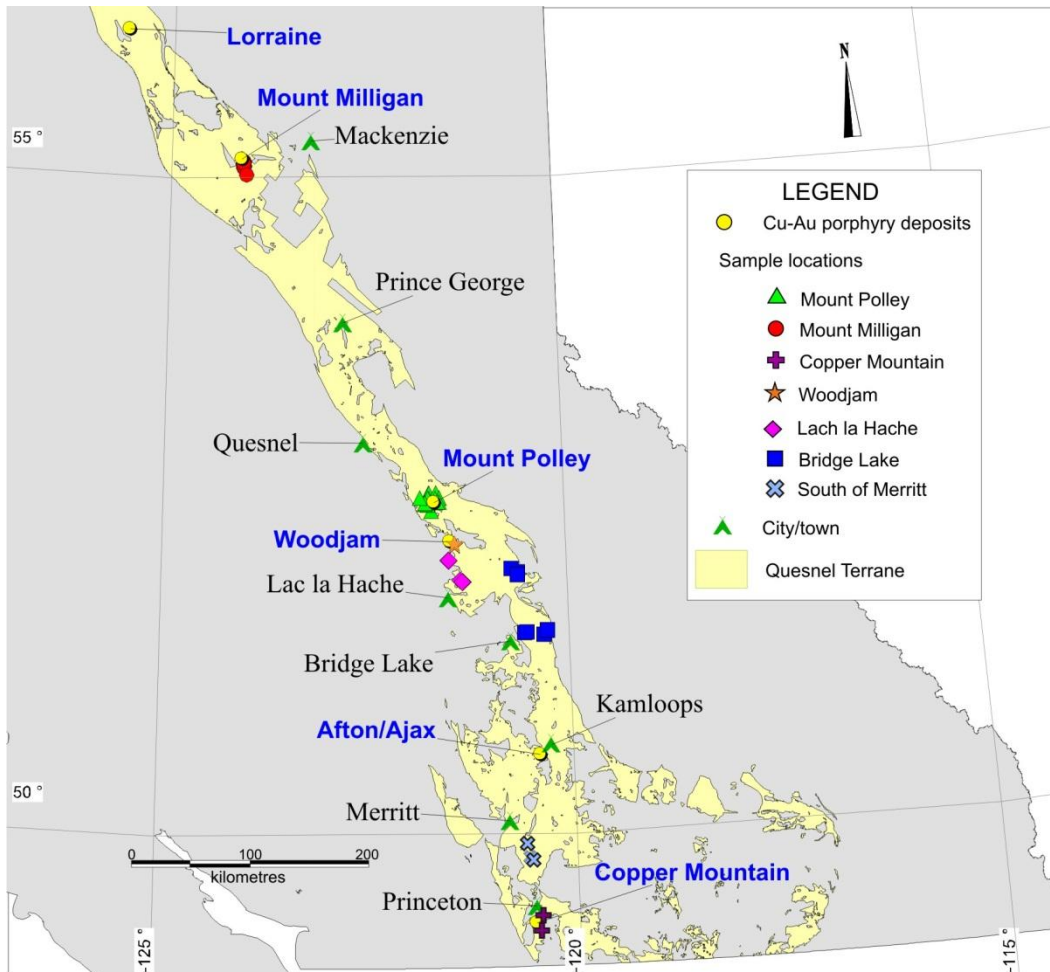


Figure 3.1. Major alkalic porphyry Cu-Au deposits in the Quesnel terrane, showing sample locations for this research. The outlined Quesnel terrane is modified from Goodfellow (2007).

Basalts around Mount Polley were studied in more detail, with the aim of investigating the relationships between three different volcanic map units in this area (Logan et al., 2007), since previous researchers have interpreted these rocks to be temporally and genetically related to porphyry Cu-Au mineralization (Bailey and Hodgson, 1979; Logan and Bath, 2006).

3.2 SAMPLES

Sampling was conducted during the 2009 and 2010 summer seasons, and was focused on coherent volcanic rocks or large volcanic clasts in volcanoclastic breccias from different localities along the Quesnel terrane (Figure 3.1).

The areas studied in this research, include:

- Mount Polley, where host volcanic rocks are interpreted to be broadly coeval with the mineralization. Intrusive rocks, mainly monzonites, monzodiorites, diorites and syenites range in age between 201.7 and 203.4 Ma (Mortensen et al., 1995), and conodonts contained in limestone lenses interbedded in the Upper Nicola volcanics are Norian, 216.5 – 203.6 Ma (H.W. Tipper *in* Panteleyev et al., 1996). Field relationships, such as the presence of laharic breccias containing fragments of propylitically altered volcanic rocks, and intrusive rocks similar to those which form the Polley stock, suggest that volcanism, plutonism and ore deposition were synchronous in this area (Bailey and Hodgson., 1979; Logan and Bath., 2006). Three different map units of volcanic host rocks around this silica undersaturated alkalic Cu-Au porphyry deposit were sampled.
- Mount Milligan, where volcanic host rocks are cut by silica saturated quartz-monzonite to monzodiorite intrusions (Barrie, 1993; Lang, 1992, and Lang et al., 1995), these are related to alkalic porphyry Cu-Au mineralization. The age of the intrusive bodies range from 182.5 to 183 Ma (Mortensen et al., 1995), while host volcanic rocks of the Witch Lake succession, sampled in this study, are interpreted to be Norian, 216.5 – 203.6 Ma (Nelson and Bellefontaine., 1996), at least ~ 20 Ma older than the intrusions.
- Woodjam prospect, where monzonite and quartz-monzonite intrusions feature silica saturated porphyry Cu-Au-Mo mineralization. Recent detailed mapping in the area by Blackwell et al. (2010) revealed that a rock unit previously mapped as a plagioclase porphyry stock (Schiarizza et al., 2009) is actually a plagioclase-phyric-andesite conformable with the volcanic succession. This unit has been dated at 203.9 ± 0.4 Ma (Schiarizza unpublished U/Pb zircon age *in* Logan et al., 2011), while the age of the intrusion from the South-east-zone prospect of Woodjam is 196.84 ± 0.22 Ma (Schiarizza unpublished U/Pb zircon age *in* Logan et al., 2011). Also, a similar age of 196.9 ± 0.9 Ma (Logan et al., 2011) was obtained from Re-Os dating in molybdenite in the same area. Thus, volcanic rocks here are ~ 7 Ma older than the fertile intrusions.
- Copper Mountain, where silica saturated alkalic Cu-Au porphyry deposits (Lang et al., 1995) related to diorite, monzonite and syenite intrusions (Preto, 1972; Preto, 1979) are

interpreted to be coeval with the volcanic host rocks. Paleontological data of the south-east part of the Nicola Group indicate a Late Norian age of ca. 203 Ma, whereas intrusive bodies in the Copper Mountain complex were dated at ~ 200 - 205 Ma (Carter et al., 1991; Mortensen et al., 1995; Mihalynuk et al., 2010). However, K-Ar biotite determinations on the Copper Mountain stock and mineralized veins yield a mean age of 193 ± 7 Ma (Sinclair and White, 1968).

- Lac la Hache prospect, where Cu-Au mineralization is interpreted to be related with diorite, monzodiorite and quartz-monzodiorite alkalic intrusions (Schiarizza et al., 2008); both host rock and mineralization ages are unknown.
- Exposures around Bridge Lake and South of Merritt representing arc segments where no alkalic porphyry Cu-Au deposits or advanced prospects are present (Figure 3.1).

3.3 ANALYTICAL PROCEDURES

Physical properties (magnetic susceptibility and density) and petrographic description were done on the rock samples, as follows:

Magnetic susceptibility was measured in the field using a KT-9 Kappameter handheld instrument. The values reported are the average of 10 readings over the outcrop (Appendix A). This device automatically displays the true measured susceptibility of the sample in SI units, having a sensitivity of 1×10^{-5} SI units.

Density was determined in selected samples (Appendix A), using the wet/dry method, also known as the hydrostatic weighing, which is derived from the Buoyancy law. The bulk density of the sample (ρ_S) was determined using the following equation:

$$\rho_S = M_D * \rho_{H_2O} / (M_D - M_W)$$

where:

ρ_{H_2O} is the density of the water (dependent upon temperature)

M_D is the mass (g) of the dry sample

M_w is the mass (g) of the sample submerged in H_2O

Each sample measurement was replicated 3 times. After the dry mass is determined, all samples were soaked for 24 hours to allow water to fill any pore spaces within the sample. A calibration experiment of a pyrex glass standard (known $\rho = 2.23 \text{ g/cm}^3$) was done every 15 samples.

Rock samples from the different map units in the study area were sent to Vancouver Petrographics Ltd. to obtain thin sections and polished thin sections made for petrography. Density measurements and petrographic study were done at the laboratories of the University of British Columbia.

Regional geological maps of the British Columbia Province (Massey et al., 2005 and Logan et al., 2010), as well as, Geology, Total Magnetic Field and Bouguer Corrected Gravity maps, from the Quest and Quest South projects (Geoscience BC., 2009 and Geoscience BC., 2010), were used to interpret the relationships between geology and physical properties in the selected areas.

3.4 LIMITATIONS AND FIELD OBSERVATIONS

One of the limitations to correlate basalts of the Nicola Group is the imprecise age constraints along and across the arc. Basalts within the Quesnel terrane do not contain any datable mineral to obtain absolute ages; therefore, the available relative ages come from fossils found in sedimentary rocks, which are interpreted to be located stratigraphically above or below the volcanic rocks sampled.

The wide time span obtained from fossil-dating (e.g., Norian goes from 216.5 ± 2.0 to 203.6 ± 1.5 , Ogg et al., 2010) increase the uncertainty of the age of basalts, and if periods of erosion and/or non-deposition are taken into account, the age ambiguity may be larger. Then basalts of the Nicola Group erupted during the Late Triassic, but it would not be possible to document age differences between basalts from the different areas studied.

Another problem within the Nicola Group is the lack of outcrop continuity. This impedes collecting samples systematically.

To visualize the interrelationship of the different volcanic products and sediments, Schiarizza (2009) presented an interpreted stratigraphy across a W-E cross-section of the Quesnel terrane (Figure 3.2), around the latitude of 52°N where the Takomkane batholith is now located. This section can be considered representative of the entire arc. Basaltic flows, monomictic and polymictic breccias, and sediments are interfingered across the terrane. Note that towards the east side of the arc, sediment deposition played a more important role (back-arc basin), while to the west proximal-volcanic products are more commonly found (Figure 3.2). The focus of magmatism is tentatively interpreted to have migrated to the west with time (Schiarizza et al., 2009).

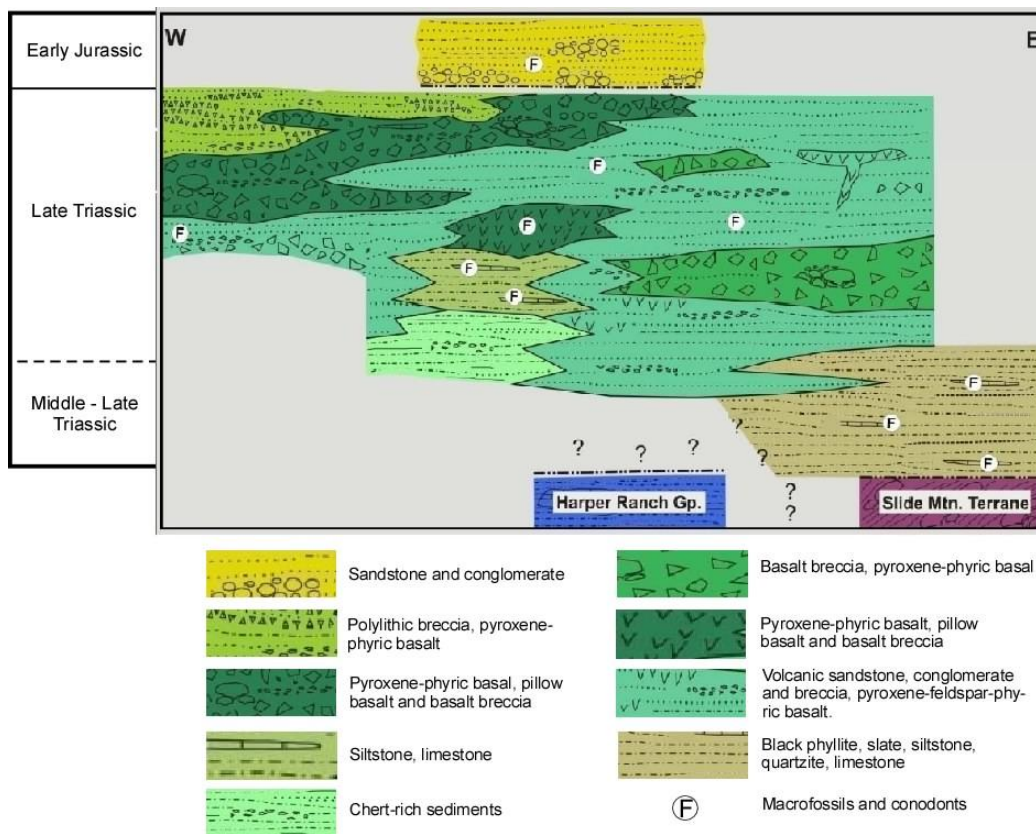
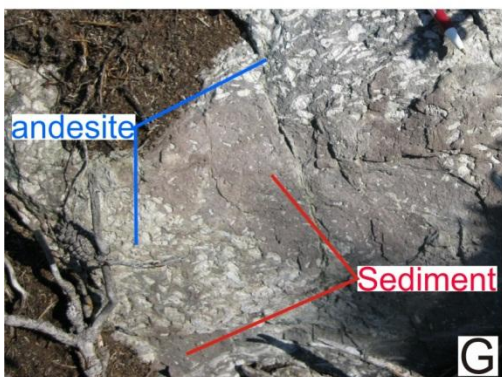
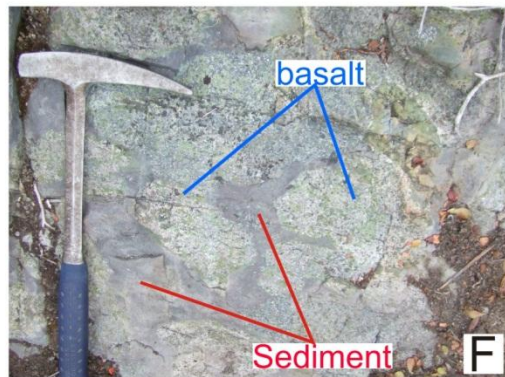
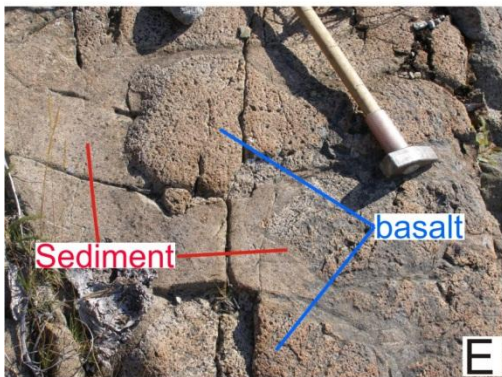
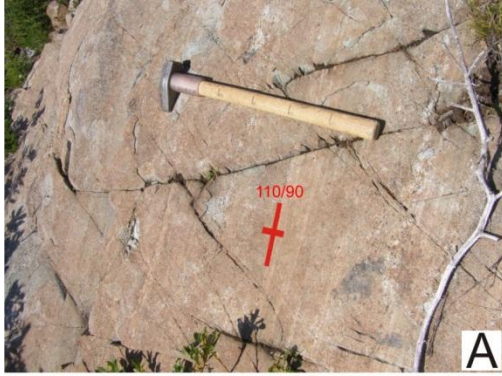


Figure 3.2. Schematic W-E cross section showing lateral facies change of the Nicola Group in Central British Columbia (modified from Schiarizza, 2009).

Rocks from the Quesnel terrane underwent some deformation, and most the porphyry deposits hosted by the Nicola Group are tilted from as little at 20° to as much as perhaps 60° (Tosdal et al., 2008). Field observations show that rocks within the Nicola Group may be tilted as much as 90°, as shown in the Mount Milligan area ~80 metres SE of sample site MTB032 (Figure 3.3A) and in southern BC in the South of Merritt area [UTM: 671521E, 5530322N] (Figure 3.3B).

The subaqueous volcanism of the arc is evidenced by the presence of pillow basalts (Figure 3.3C), which can be found along the entire arc. Monomictic and polymictic breccias (Figure 3.3D) containing basalt fragments are also widespread within the terrane. Interaction between wet-sediments and volcanism is also suggested by the occurrence of peperites at Mount Milligan (~47 metres NE of sample site MTB032) (Figure 3.3E), and Woodjam in different places within the stratigraphic sequence sampled (Figure 3.3F and 3.3G). At Woodjam, peperites were identified and mapped by Blackwell et al. (2010).

The most typical coherent basaltic rock within the Nicola Group is gray pyroxene-phyric basalt (Figure 3.3H); hematite masses (after olivine?) within basalts are a common feature along the arc (Figure 3.3I). It is also possible to find basalt flows containing analcime phenocrysts. Analcime bearing basalts were found at Mount Polley and South of Merritt (Figure 3.3J and 3.3K). Basalts show different amount of vesicles, which are normally filled with alteration minerals (Figure 3.3L). Reddish basalts due to hematite content in the rock are locally abundant along the volcanic belt (e.g., Mount Polley, Figure 3.3J), hematite could be an indication of a subaerial environment of deposition as suggested by Panteleyev et al. (1996) and Logan and Bath (2006). At Woodjam, the coherent volcanic rocks are represented by basaltic-andesite to andesite flows (Figure 3.3M). The whole volcano-sedimentary package of the Quesnel terrane underwent low grade metamorphism, represented by the presence of a chlorite-epidote-calcite assemblage (Figure 3.3N).



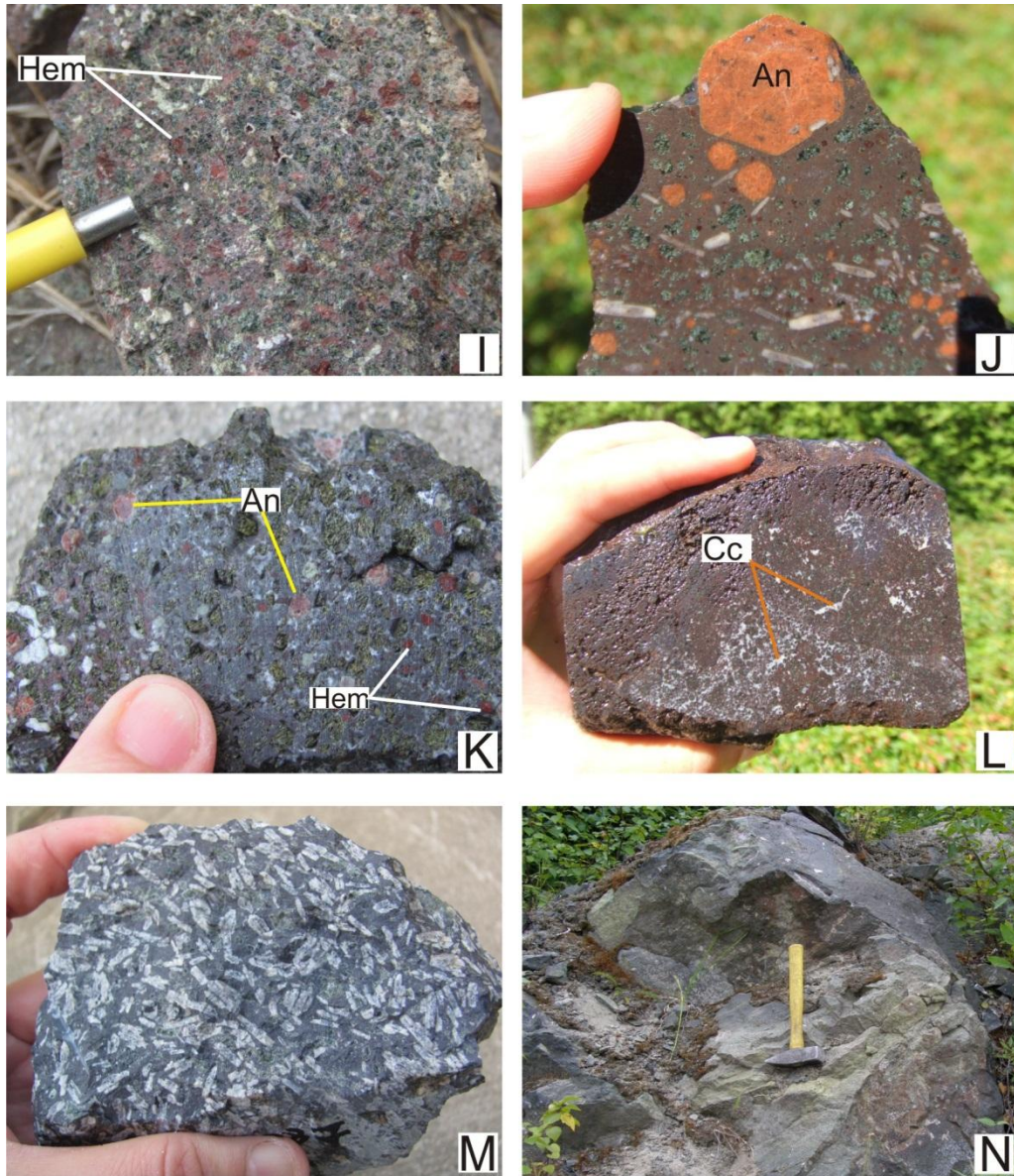


Figure 3.3. Structures and textures found along the Nicola Group. A) Volcaniclastic rocks presenting vertical bedding at Mount Milligan; B) Volcaniclastic rocks presenting sub-vertical bedding in the South of Merritt area; C) Pillow basalt from the Bridge Lake area (sample BTB057); D) Polymictic breccia containing pyroxene-phyric basalt fragments, from the Bridge Lake area (sample BTB056); E) Peperite from Mount Milligan; F) Peperite at Woodjam, close to sample WTB083; G) Peperite at Woodjam sample WTB087; H) Gray, porphyritic, clinopyroxene bearing basalt from Mount Polley (sample PSV022); I) Gray-reddish, porphyritic, clinopyroxene bearing basalt, note the presence of hematite masses (after olivine?) within the rock (sample PSV001); J) Reddish, porphyritic-trachytic, clinopyroxene-plagioclase-analcime basalt (sample PSV002); K) Gray-reddish, porphyritic, clinopyroxene- -analcime basalt (sample SSV128); L) Reddish, highly vesiculated basalt, calcite (Cc) filling vesicles (sample PSV036); M) Gray porphyritic-trachytic plagioclase bearing andesite from Woodjam (sample WTB087); N) Possible pillow basalt affected by chlorite-epidote alteration from Lac la Hache (sample LTB071).

3.5 PETROGRAPHY

The following petrographic description is based on detailed thin section observations under petrographic microscope.

3.5.1 **Mount Polley.** Three Late Triassic Nicola (LTN) map units, which contain basalts, were chosen in this study area. These units were described by Logan et al. (2007), and are interpreted to lay stratigraphically one on top of the other: the LTNpv unit lies at the bottom, followed by the LTN_{av}, and the LTN_{pt} unit on top.

3.5.1.1 **LTN_{pv} Unit:** Basalts in this unit are generally dark gray-green (reddish when hematite is present), showing porphyritic and occasionally aphanitic (sample PSV046) and brecciated (sample PSV017) texture, containing 7-30% colorless – pale green, 1.0-5.0mm euhedral to subhedral, typically zoned, slightly chloritized and fractured clinopyroxene, which contains Fe-Ti oxide and apatite inclusions; from none to 60% colorless-pink-brownish, 0.5-6.0mm euhedral to subhedral, elongated and fractured plagioclase, which is moderately altered to clay minerals and epidote; occasionally up to 7%, <2.0mm euhedral – subhedral and fractured pink-whitish analcime phenocryst (sample PSV017); 5-10% amygdales containing chlorite-calcite-epidote. Some fractures containing this same mineral assemblage are found as well. 30-60% groundmass consists of fine grained plagioclase (commonly difficult to recognize due to alteration), pyroxene, Fe-Ti oxides and recrystallized glass. Alteration minerals are chlorite, calcite, epidote, hematite, clays and occasionally zeolite (sample PSV047). These alteration minerals are filling cavities, fractures and affecting the groundmass and phenocrysts.

3.5.1.2 **LTN_{av} Unit:** Basalts in this unit are reddish or dark gray-green, showing porphyritic to trachytic texture, containing 8-35% colorless-pale green, ≤4.0mm euhedral to subhedral zoned pyroxene crystals, which are fractured and contain Fe-Ti oxide and apatite inclusions; 5-25% colorless-pink to brownish, ≤6.0mm euhedral to subhedral, elongated and fractured plagioclase which is moderately altered to clay minerals; also 2-30% pink whitish, ≤6.0mm euhedral to anhedral and fractured analcime could be found; 5-15% amygdales of

chlorite-calcite-epidote; 30-50% groundmass consisting of fine grained plagioclase, pyroxene, analcime, Fe-Ti oxides and recrystallized glass. Alteration minerals are hematite, chlorite, calcite, epidote, and clays, which are filling cavities, fractures and affecting the groundmass and phenocrysts. Locally analcime is filling cavities as well.

3.5.1.3 LTNpt Unit: Basalts in this unit are dark gray-green, showing porphyritic to trachytic texture, containing 10-25% colorless, ≤ 3.5 mm euhedral to subhedral pyroxene, which are fractured and contain Fe-Ti oxide inclusions; 30-50% colorless-pink brownish, 0.3-2.0mm euhedral to subhedral, fractured plagioclase phenocrysts, moderately altered to clay minerals; 5% amygdales of chlorite-calcite-epidote; 30-35% groundmass consisting of fine grained plagioclase, pyroxene and Fe-Ti oxides. Analcime is absent in this unit. Alteration minerals are chlorite, calcite, epidote and clays, which are filling cavities, fractures and affecting the groundmass and phenocrysts.

3.5.2 Mount Milligan.- Basalts around Mount Milligan are typically dark gray-green, showing porphyritic to trachytic texture, containing 7-27% colorless – pale green, ≤ 5.0 mm euhedral to subhedral pyroxene phenocrysts, these are fractured, rarely zoned and contain few to none Fe-Ti oxide inclusions; 7-30% colorless – pink – brownish, ≤ 4.0 mm euhedral to subhedral, tabular and fractured plagioclase which is moderately altered to clay minerals (Appendix A-Table A1); 5-7% amygdales containing chlorite-calcite-epidote, locally zeolite is present (sample MTB030); 30-75% groundmass consisting of fine grained plagioclase, pyroxene, rare Fe-Ti oxides and recrystallized glass. Alteration minerals are chlorite, calcite, epidote, clays and occasionally zeolite, which are filling cavities, fractures and affecting the groundmass and phenocrysts. Fine grained Fe-Ti oxides (~1%) within the alteration assemblage were noted in samples MTB019 and MTB041 (Appendix A-Table A1).

3.5.3 Woodjam.- Basaltic andesites around the Woodjam area are typically dark gray-green-reddish, showing porphyritic, trachytic and occasionally aphanitic (sample WTB084) textures, containing from none to 20% colorless to green-brownish, ≤ 5.0 mm euhedral to subhedral pyroxene phenocrysts, which are rarely zoned, fractured and containinig few to none Fe-Ti oxide inclusions; 20-30% colorless - brownish, ≤ 4.0 mm euhedral to subhedral, tabular, fractured plagioclase which is moderately altered to clay minerals (Appendix A); 3-5% amygdales filled

with chlorite-epidote; 45-65% groundmass consisting of fine grained plagioclase, pyroxene, Fe-Ti oxides and recrystallized glass. Alteration minerals are chlorite, epidote, hematite and clays which are filling cavities, fractures and affecting the groundmass and phenocrysts.

3.5.4 Copper Mountain.- Basalts here are generally dark gray-green, showing porphyritic texture, containing 15-30% colorless – pale green, ≤ 3.5 mm euhedral to subhedral, occasionally zoned, slightly chloritized and fractured clinopyroxene, which rarely contains Fe-Ti oxides inclusions; from none to 20% colorless-pink-brownish, 0.5-1.8mm euhedral to subhedral, elongated and fractured plagioclase which is moderately altered to clay minerals and epidote (Appendix A); ~5% amygdales of chlorite-calcite-epidote; some fractures with the same mineral assemblage are found as well; 30-60% groundmass consisting of fine grained plagioclase, pyroxene, Fe-Ti oxides and recrystallized glass. Alteration minerals are chlorite, calcite, epidote and clays, which are filling cavities, fractures and affecting the groundmass.

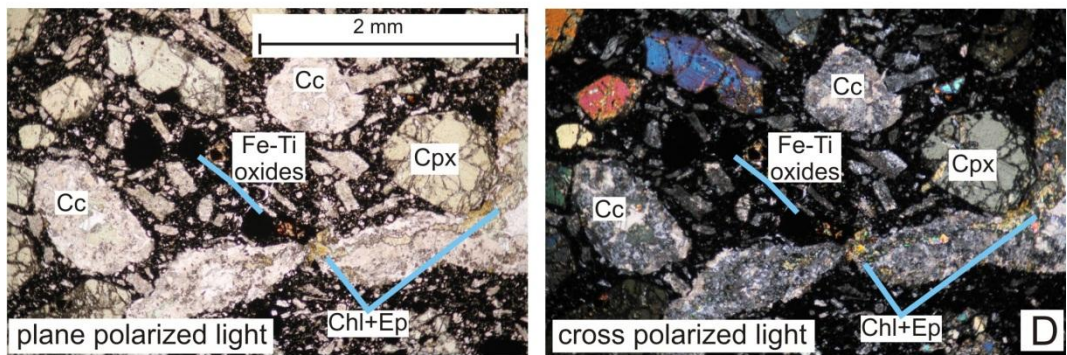
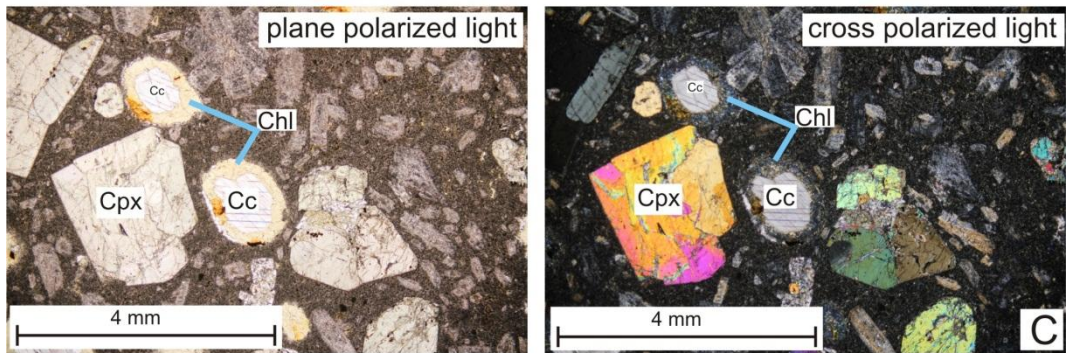
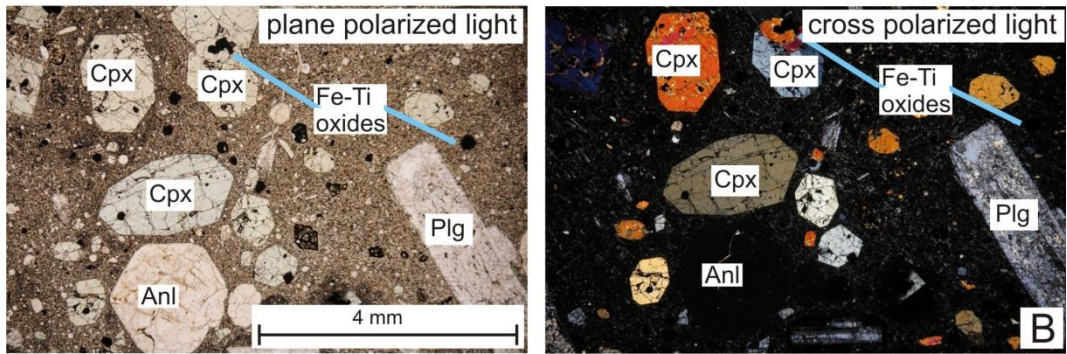
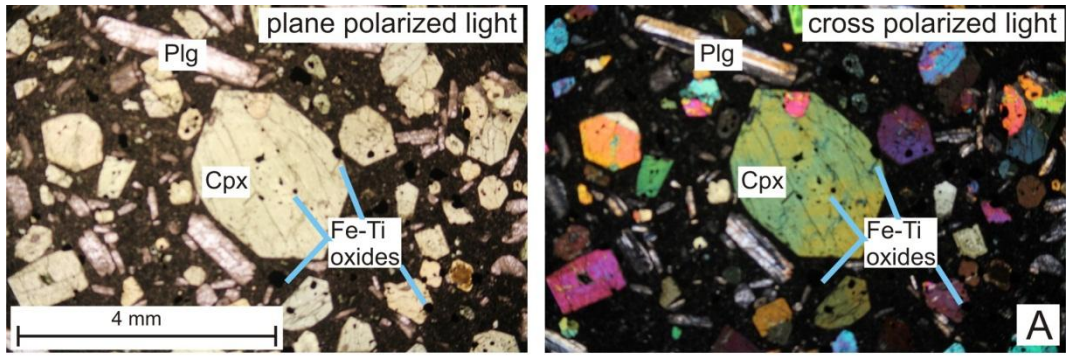
3.5.5 Lac la Hache.- Basalts within this area are generally dark gray-green to reddish, showing porphyritic texture, containing 10-35% colorless to pale green, ≤ 4.0 mm euhedral to subhedral pyroxene phenocrysts, some crystals display zonation, they are fractured and contain Fe-Ti oxide inclusions; 13-30% colorless-brownish, ≤ 4.0 mm, elongated euhedral to subhedral, fractured plagioclase which is moderately altered to clay minerals and epidote (Appendix A); 3-10% amygdales filled with chlorite-epidote; 35-75% groundmass consisting of fine grained plagioclase, pyroxene, Fe-Ti oxides and recrystallized glass. Alteration minerals are hematite, chlorite, calcite, epidote, and clays, which are filling cavities, fractures and affecting the groundmass. Hematite is present within the matrix.

3.5.6 Bridge Lake.- Basalts around this area are generally dark gray-green, showing porphyritic texture, containing 13-37% colorless to pale green, ≤ 7.0 mm euhedral to subhedral pyroxene phenocrysts, some crystals display zonation, they are fractured and rarely contain Fe-Ti oxide inclusions; 5-10% colorless-brownish, ≤ 2.0 mm, elongated euhedral to subhedral, fractured plagioclase which is moderately altered to clay minerals and epidote (Appendix A); 3-10% amygdales containing chlorite-epidote; 35-75% groundmass consisting of fine grained plagioclase, pyroxene, Fe-Ti oxides and recrystallized glass. Alteration minerals are chlorite,

calcite, epidote and clays which are filling cavities, fractures and affecting the groundmass and phenocrysts.

3.5.7 South of Merritt.- Basalts here are generally gray-reddish, showing porphyritic texture, containing 7-30% pale green, ≤ 4.3 mm euhedral to subhedral pyroxene phenocrysts, some crystals display zonation, they are fractured and rarely contain Fe-Ti oxide inclusions; 7-12% colorless-brownish, ≤ 2.0 mm, elongated euhedral to subhedral, fractured plagioclase which is intensely altered to clay minerals and epidote; none to 10% pink whitish, ≤ 1.0 mm euhedral to anhedral and fractured analcime is present in sample SSV128 (Appendix A); 5-10% amygdales of chlorite-epidote; 45-70% groundmass consisting of fine grained plagioclase, pyroxene, Fe-Ti oxides and recrystallized glass. Alteration minerals are chlorite, calcite, epidote and clays which are filling cavities, fractures and affecting the groundmass and phenocrysts. Analcime is also occasionally filling cavities (sample SSV127).

The most representative textures, phenocryst and alteration minerals found in thin sections from samples along and across the Nicola Group, are illustrated below (Figure. 3.4.):



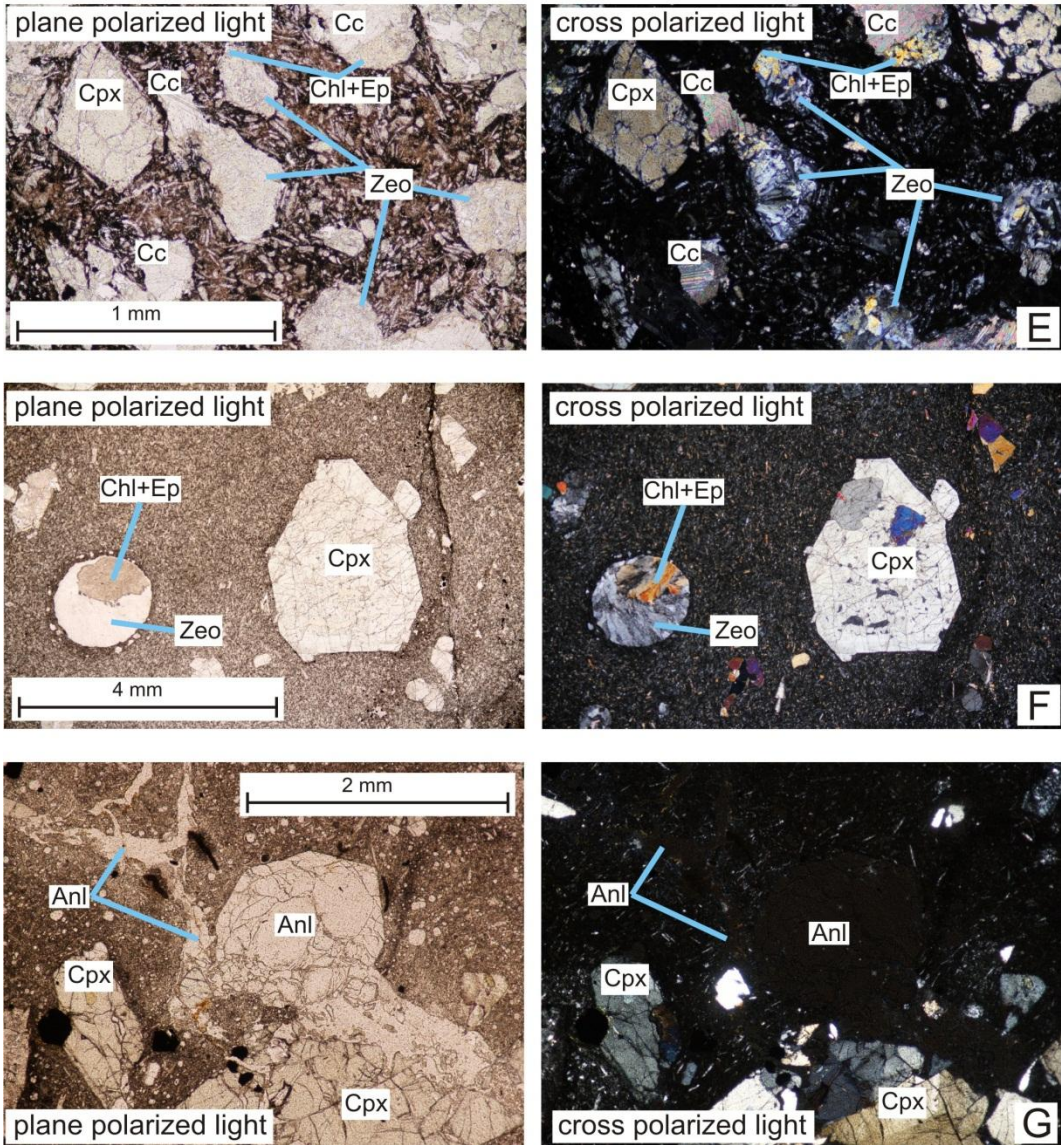


Figure 3.4. Representative porphyritic basalts from the Nicola Group, showing typical phenocryst and alteration minerals. A) Cpx±Plg basalt, note the presence of Fe-Ti oxides as inclusions in Cpx and within the matrix. Dark matrix is related to the hematite content (sample LTB073 – Lac la Hache area). B) Cpx±Plg±Anl basalt, observe the euhedral phenocryst of Anl (sample PSV002 – LTNav unit, Mount Polley area). C) Cpx±Plg basalt, note the amygdales of Chl-Cc-Ep (sample BTB053 – Bridge Lake area). D) Cpx±Plg basalt, Fe-Ti oxides within the matrix, amygdales of Cc-Chl-Ep, dark matrix due to hematite content (sample LTB058 – Lac la Hache area). E) Cpx±Plg basalt, presenting vesicles of Zeo (sample PSV047 – LTNav unit, Mount Polley area). F) Cpx basalt, note the amygdales of Zeo-Chl-Ep and absence of Fe-Ti oxides (sample MTB030 – Mount Milligan area). G) Basalt showing Anl as phenocryst, filling fractures and partially replacing Cpx (sample PSV039 – LTNav unit, Mount Polley area).
Abbreviations: An, analcime; Cc, calcite; Chl, chlorite; Cpx, clinopyroxene; Ep, epidote; Plg, plagioclase; Zeo, zeolite.

3.6 GEOLOGY, PHYSICAL PROPERTIES AND REGIONAL MAGNETIC AND GRAVITY SURVEYS

Geological maps of the studied areas (Figures 3.5A, 3.6A, 3.7A, 3.8A, 3.9A, 3.10A and 3.11A, modified from Massey et al., 2005, Logan et al., 2007 and Logan et al., 2010) show the spatial relationship between volcanic rocks and intrusive bodies within the Quesnel terrane.

Magnetic susceptibilities and density measurements on basalts were used to compare with the regional total magnetic field and Bouguer corrected gravity maps, produced by Geoscience BC for the Quesnellia Exploration Strategy (QUEST) and QUEST South ongoing projects (Geoscience BC., 2009 and Geoscience BC., 2010, respectively). Both gravity and magnetic surveys are airborne, flown in east-west lines with 2km line spacing for gravity and 800m for magnetics. The aeromagnetic data is from Natural Resources Canada (NRCan; Canadian aeromagnetic data base, 2005) and has been cartographically prepared by Geoscience BC as part of a suite of maps for the QUEST and QUEST-South projects.

The results of the physical properties tested are present below:

3.6.1 Mount Polley.- This area is represented by coherent and volcanoclastic rocks of different units of the Late Triassic Nicola Group. The volcanic sequence is cut by monzonites, syenites, diorites and breccias (central map area) of broadly the same age. Most of the area is covered by Quaternary deposits (Figure 3.5A).

3.6.1.1 LTN_{pv} Unit.- Basalts in this unit present magnetic susceptibility readings typically from 44.90×10^{-3} to 70.00×10^{-3} SI units (n=9), with the exception of samples PSV016, PSV017, and PSV047, which have values from 1.20×10^{-3} to 23.70×10^{-3} SI units, these rocks contain hematite. Density measurements vary from 2.83 to 3.00g/cm^3 (Appendix A).

3.6.1.2 LTN_{av} Unit.- Basalts display magnetic susceptibility values between 21.50×10^3 and 86.10×10^3 SI units (n=7), with the exception of sample PSV001 which present a magnetic susceptibility value of 1.41×10^3 SI units. Most of samples within this unit contain hematite, but samples without hematite display the higher magnetic susceptibility numbers. Density measurements vary from 2.65 to 2.91g/cm^3 (Appendix A).

3.6.1.3 **LTNpt Unit.**- Magnetic susceptibility numbers in basalts from this unit have values of 70.1×10^{-3} to 111×10^{-3} SI units (n=2). Rocks in this unit do not present hematite. Density measurements vary from 2.78 to 2.87 g/cm^3 (Appendix A).

Rocks around Mount Polley show gravity values between -115 to -100 milligals (mGal) (Figure 3.5B) and magnetic values from 400 to >1000 nanoteslas (nT) (Figure 3.5C). Late Triassic alkalic intrusive bodies show slight contrast in density and in magnetic values with the volcanic host rocks. (Figure 3.5A, 3.5B and 3.5C).

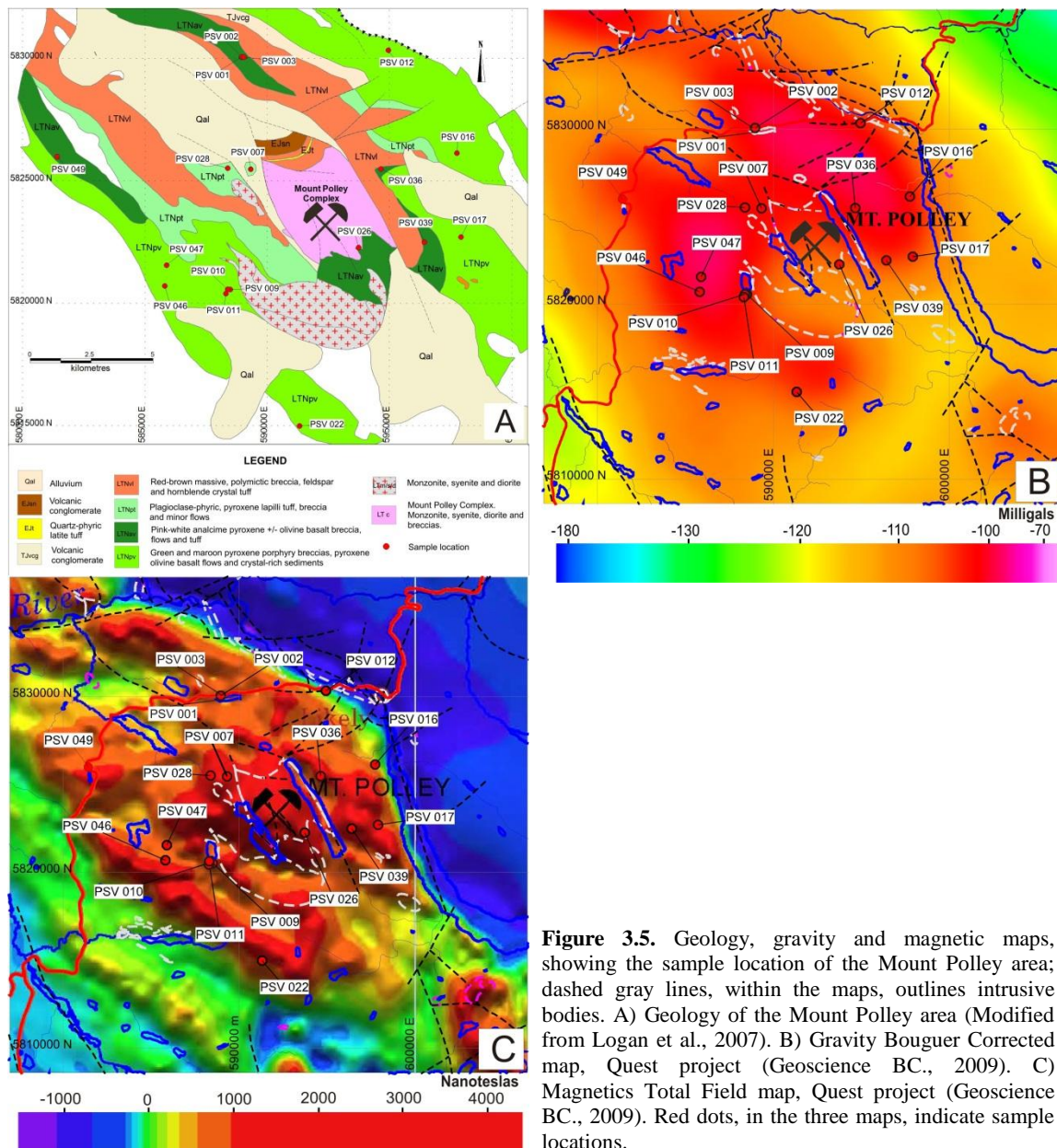


Figure 3.5. Geology, gravity and magnetic maps, showing the sample location of the Mount Polley area; dashed gray lines, within the maps, outlines intrusive bodies. A) Geology of the Mount Polley area (Modified from Logan et al., 2007). B) Gravity Bouguer Corrected map, Quest project (Geoscience BC., 2009). C) Magnetics Total Field map, Quest project (Geoscience BC., 2009). Red dots, in the three maps, indicate sample locations.

3.6.2 Mount Milligan.- The geology of this area is characterized by coherent and

volcaniclastic rocks from the Late Triassic Witch Lake succession (Nelson and Bellefontaine, 1996) of the Nicola arc. This volcanic sequence is cut by Early Jurassic syenitic intrusion (north-central part of the map). In the north-east side of the map, lies a Late Proterozoic to Late Paleozoic paragneiss unit. The area is extensively covered by Quaternary deposits (Figure 3.6 A).

Basalts from Mount Milligan show magnetic susceptibilities typically from 0.50×10^{-3} to 0.96×10^{-3} SI units (n=11), with the exception of samples MTB041, MTB027, and MTB019,

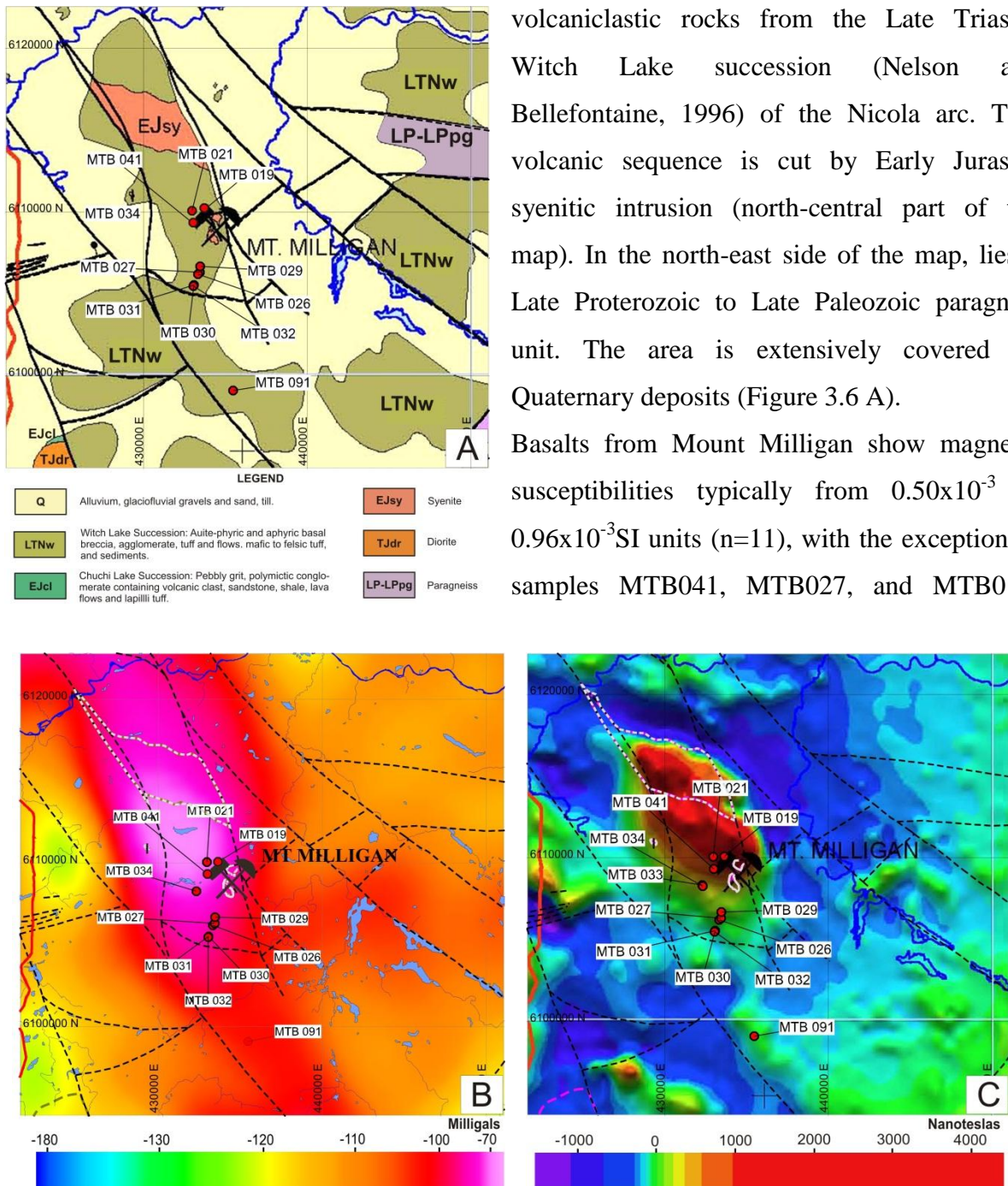


Figure 3.6. Geology, gravity and magnetic maps, showing the sample location of the Mount Milligan area; dashed gray lines in the gravity and dashed pink lines in the magnetic maps, outlines intrusive bodies. A) Geology of the Mount Milligan area (Modified from Logan et al., 2010). B) Bouguer Corrected Gravity map, Quest project (Geoscience BC., 2009). C) Magnetics Total Field map, Quest project (Geoscience BC., 2009). Red dots, in the three maps, indicate sample locations.

which have values from 14.00×10^{-3} to 38.80×10^{-3} SI units, these rocks may contain secondary Fe-Ti oxides. Density values vary from 2.83 to 2.97 g/cm^3 (Appendix A-TableA1).

Rocks around the Mount Milligan area show gravity readings between -105 and -90 mGal (Figure 3.6B) and magnetic values from 0 to >1000 nT (Figure 3.6C). Intrusive bodies do not show any contrast with the volcanic host rocks in the gravity map, however, there is an evident positive magnetic anomaly which includes the alkalic intrusions (Figure 3.6A, 3.6B, 3.6C).

3.6.3 Woodjam.- This area is underlain by a Late Triassic volcanic succession of the Nicola group (north and west sides of the map). These rocks host the Late Triassic-Jurassic Takomkane batholith, which occupies most of the map area. Volcanic rocks of the Paleogene Kamloops and Neogene Chilcotin Groups cover partially the central-east and west-north parts of the area, respectively (Figure 3.7A). A detailed map from Blackwell et al. (2010) shows part of the Nicola volcanic sequence from where samples were collected (Figure 3.7A').

Basaltic andesites in the Woodjam area display magnetic susceptibility readings $< 1.55 \times 10^{-3}$ SI units (n=5). Density of rocks varies from 2.72 to 2.92 g/cm^3 (Appendix A-TableA1). Sample WTB087 displays the lowest density value in this area; here, plagioclase is the main phenocryst phase within the rock.

The area around the collected samples shows gravity values ~ -115 mGal (Figure 3.7B) and magnetic intensities from 400 to 800 nT (Figure 3.7C). Intrusive bodies, mainly calc-alkalic (e.g. Takomkane batholith) show a variety of density readings, presenting values from -140 to -100 mGal, the western border of the batholith displays the highest gravity values. Magnetic readings vary from -400 to 1000 nT. High magnetic values tend to be related to the borders of the batholith (See figures 3.7A, 3.7B and 3.7C).

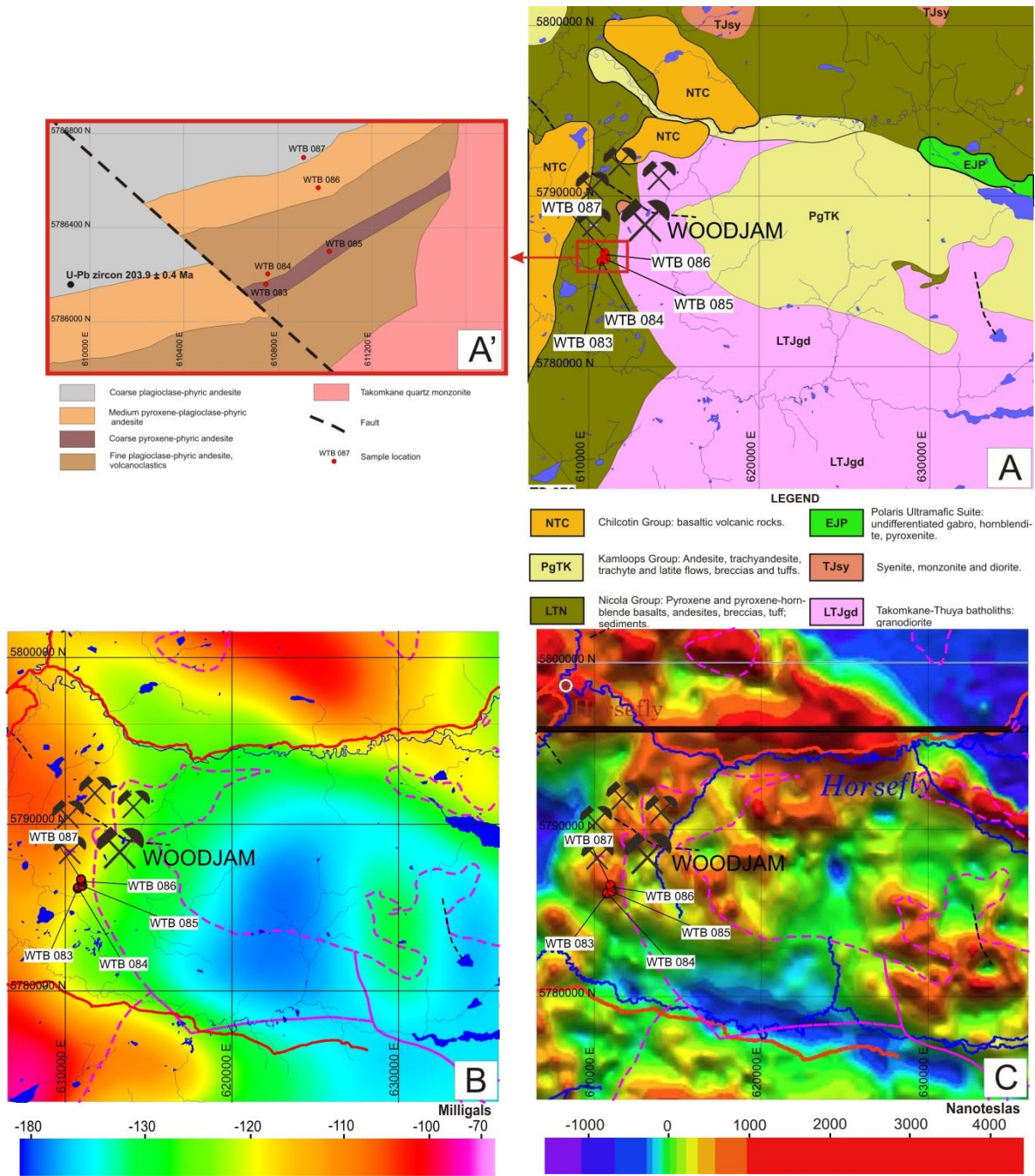
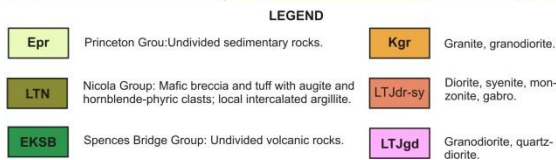
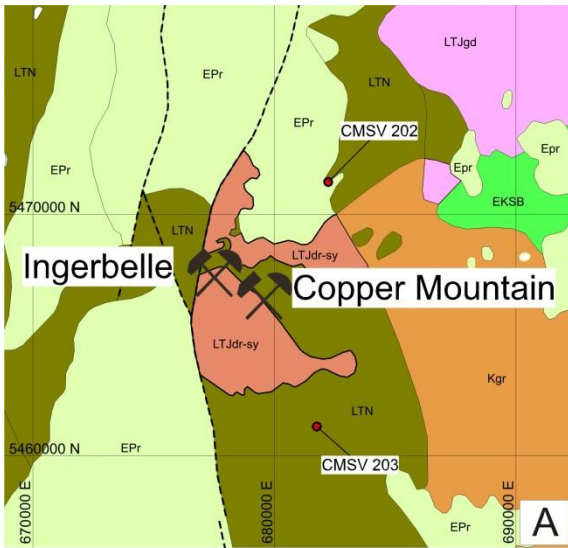


Figure 3.7. Geology, gravity and magnetic maps, showing the sample location of the Woodjam area; dashed pink lines within the maps, outlines intrusive bodies. A) Geology of the Woodjam area (Modified from Massey et al., 2005). A') Detailed geological map from the Woodjam area (modified from Blackwell et al., 2010). B) Gravity Bouguer Corrected map, Quest south project (Geoscience BC., 2010). C) Magnetics Total Field map, Quest south project (Geoscience BC., 2010). Red dots, in the three maps, indicate sample locations.

3.6.4 **Copper Mountain.-** This area is characterized by volcanic rocks of the Late Triassic



Nicola Group, hosting Late Triassic-Jurassic diorite to syenite of the Copper Mountain Stock (central part of the map) and granodiorite intrusions (north east corner). To the east, Cretaceous volcanic rocks of the Spences Bridges Group and granite - granodiorite bodies of the same age are present. Eocene sediments corresponding to the Princeton Group partially cover the area (Figure 3.8A).

Magnetic susceptibility readings are $<1.00 \times 10^{-3}$ SI units (n=2). Density measurements are 2.88 and 2.99 g/cm^3 (Appendix A-TableA1).

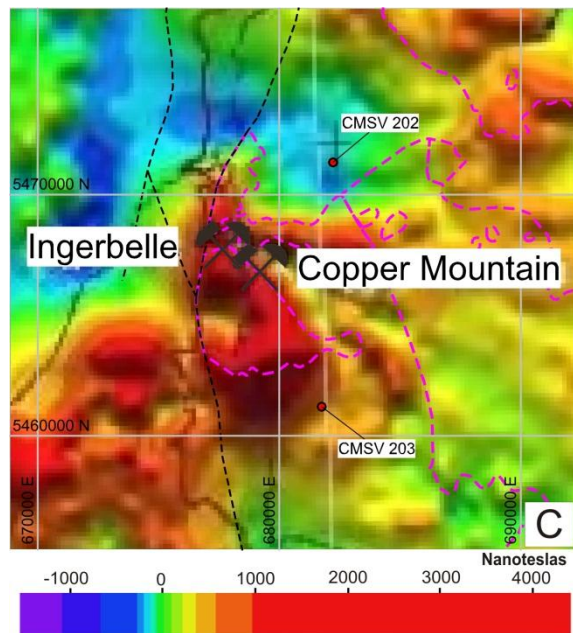
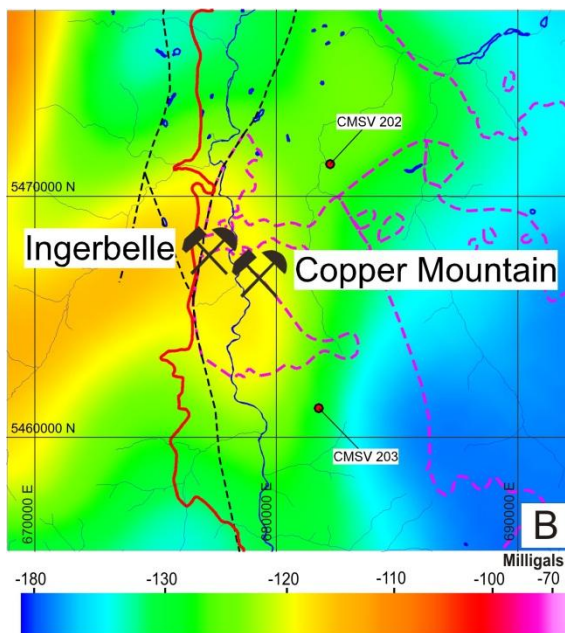


Figure 3.8. Geology, gravity and magnetic maps, showing the sample location of the Copper Mountain area; dashed pink lines within the maps, outlines intrusive bodies. A) Geology of the Copper Mountain area (Modified from Massey et al., 2005). B) Gravity Bouguer Corrected map, Quest south project (Geoscience BC., 2010). C) Magnetics Total Field map, Quest south project (Geoscience BC., 2010). Red dots, in the three maps, indicate sample locations.

Rocks around Copper Mountain show gravity values between -125 and -120mGal (Figure 3.8B) and magnetic values from -200 to 800nT (Figure 3.8C). Late Triassic – Early Jurassic intrusive bodies close to the mineralization (Figure 3.8A), show only a slight contrast in gravity with the volcanic host rocks (Figure 3.8B), while intrusions to the east and north east present lower gravity values than the latter. Magnetic values >1000nT in the intrusion close to the mineralization show a strong contrast with the host volcanics (Figure 3.8A and 3.8C).

3.6.5 **Lac la Hache.-** The geology of the area consists of volcanic rocks of the Late Triassic

Nicola Group crosscut by Triassic-Jurassic syenite – diorite intrusions. To the east, the Late Triassic-Jurassic Takomkane Batholith is present. The Paleogene Kamloops and Neogene Chilcotin volcanics overlap the older rocks in the west-central part of the map (Figure 3.9A).

Magnetic susceptibility values on basalts in this area vary from 25.40×10^{-3} to 115.00×10^{-3} SI units ($n=7$); samples LTB068 and LTB081 show magnetic susceptibility numbers of 1.62×10^{-3} SI units and 0.59×10^{-3} SI units, respectively. These values coincide with high hematite content within the rock.

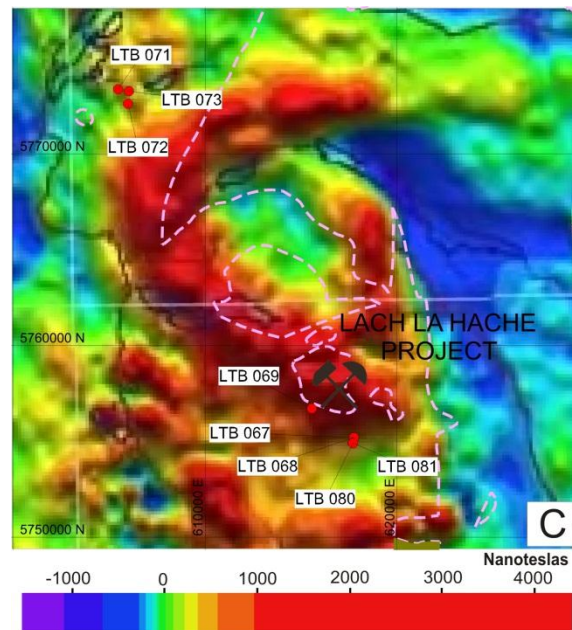
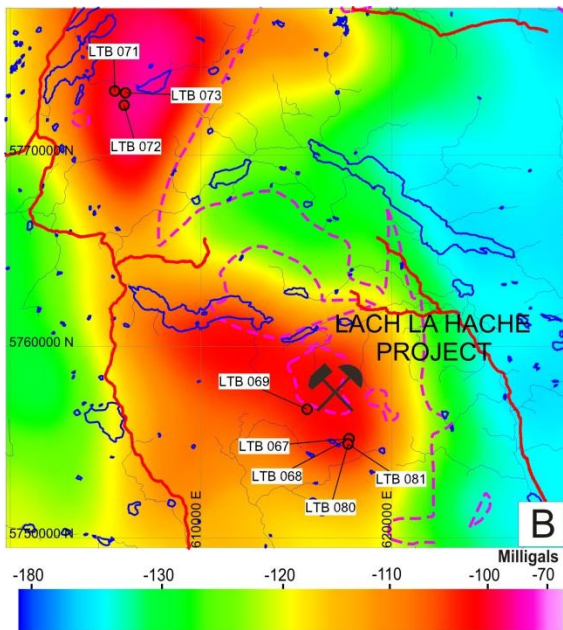
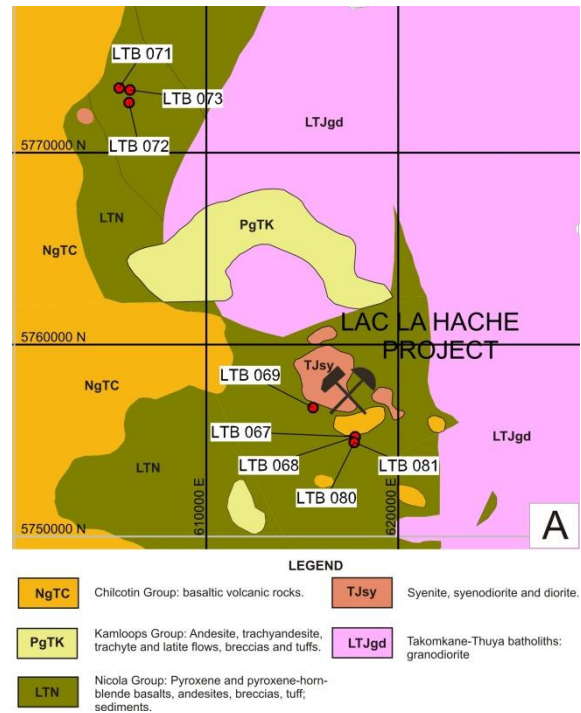
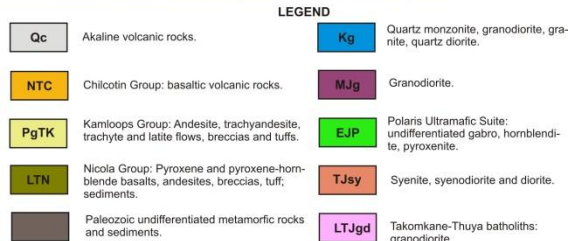
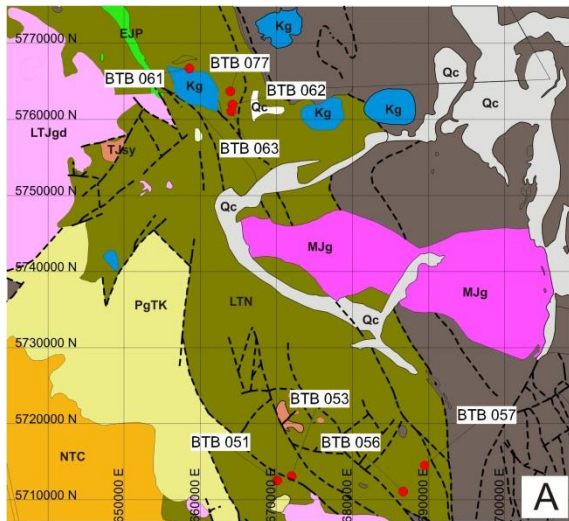


Figure 3.9. Geology, gravity and magnetic maps, showing the sample location of the Lac la Hache area; dashed pink lines within the maps, outlines intrusive bodies. A) Geology of the Lac la Hache area (Modified from Massey et al., 2005). B) Gravity Bouguer Corrected map, Quest south project (Geoscience BC., 2010). C) Magnetics Total Field map, Quest south project (Geoscience BC., 2010). Red dots, in the three maps, indicate sample locations.

Density measurements vary from 2.86 to 2.98g/cm³ (Appendix A-TableA1). Rocks in the sampled area show gravity values from -105 to -100mGal (Figure 3.9B) and magnetic values from 400 to >1000nT (Figure 3.9C). Intrusive bodies (e.g., Takomkane batholith; Figure 3.9A) contrast with the volcanic host rocks in density, exhibiting gravity values from -140 to -130mGal, and magnetic values vary from -800 to >1000nT. The borders of the batholith tend to have higher magnetic values. Although the alkalic intrusions closer to the mineralization present similar to slightly less gravity values than the volcanic hosts, magnetic values of the intrusions closer to the mineralization are high >1000nT (Figure 3.9A, 3.9B and 3.9C).

3.6.6 Bridge Lake.- Geology here comprises Paleozoic metamorphic rocks to the east of the



map, Late Triassic Nicola volcanics intruded by small Triassic-Jurassic syenite – diorite in the central part and the Late Triassic-Jurassic Takomkane Batholith is present to the north-west. Middle Jurassic granodiorite and Cretaceous quartz-monzonite to quartz-diorite intrusions cut the sequence in the central and northern part, respectively. Paleogene Kamloops, Neogene Chilcotin and Quaternary volcanics partially cover the area (Figure 3.10A).

Basalts in this area show magnetic susceptibility readings varying from 0.61×10^{-3} to 1.85×10^{-3} SI units (n=8), with the exception of samples

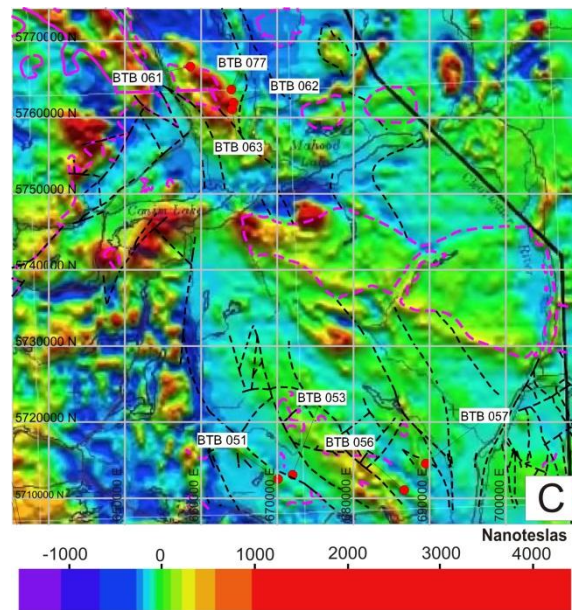
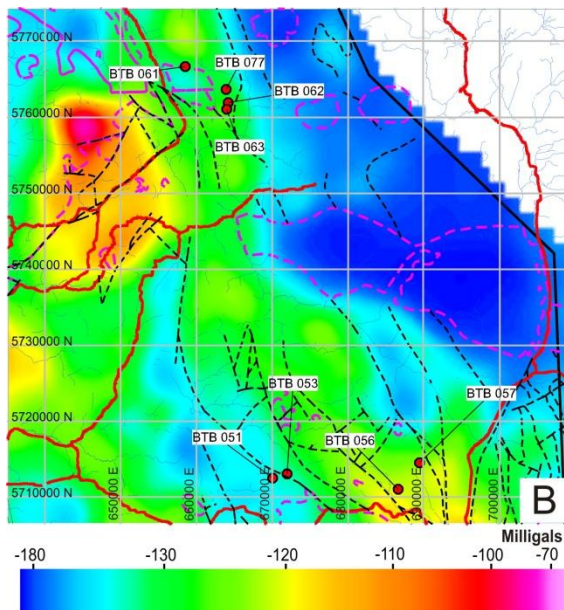
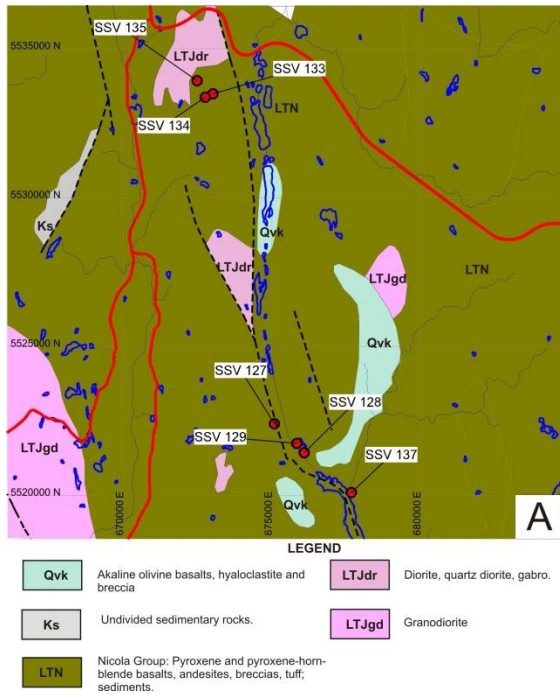


Figure 3.10. Geology, gravity and magnetic maps, showing the sample location of the Bridge Lake area; dashed pink lines within the maps, outlines intrusive bodies. A) Geology of the Bridge Lake area (Modified from Massey et al., 2005). B) Gravity Bouguer Corrected map scale 1:500,000, Quest south project (Geoscience BC., 2010). C) Magnetics Total Field map, Quest south project (Geoscience BC., 2010). Red dots, in the three maps, indicate sample locations.

BTB056 and BTB077, which show magnetic susceptibility numbers of 52.10×10^{-3} and 44.50×10^{-3} SI units, respectively. Density measurements vary from 2.95 to 3.01 g/cm^3 (Appendix A-TableA1).

Rocks around the sampled area show gravity values between -125 and -120mGal (Figure 3.10B). However, the area around samples sites BTB051 and BTB053 show gravity values $< -130 \text{ mGal}$, these samples are close to a regional fault (Figure 3.10B). Magnetic values vary from -200 to 0nT (Figure 3.10C), volcanic rocks which have a nearby intrusive body, go up to $\sim 800 \text{ nT}$ (Figure 3.10C). The east border of the Takomkane batholith shows contrast in the gravity response with the volcanic host rocks, presenting gravity values varying from -140 to -100mGal, and magnetic values from -400 to $> 1000 \text{ nT}$ (Figure 3.10A, 3.10B and 3.10C).

3.6.7 **South of Merritt.** The area is underlain by Late Triassic volcanic rocks of the Nicola



Group cross-cut by scattered Late Triassic-Jurassic granodiorite, diorite and gabbro intrusions. Small areas are covered by Cretaceous sedimentary and Quaternary volcanic rocks (Figure 3.11A).

Basalts present magnetic susceptibility readings from 0.40×10^{-3} to 63.10×10^{-3} SI units ($n=7$); sample SSV137 shows the highest magnetic susceptibility value, and this sample does not contain hematite. Density measurements vary from 2.96 to 3.03 g/cm^3 (Appendix A-TableA1).

Rocks in the South of Merritt area show gravity

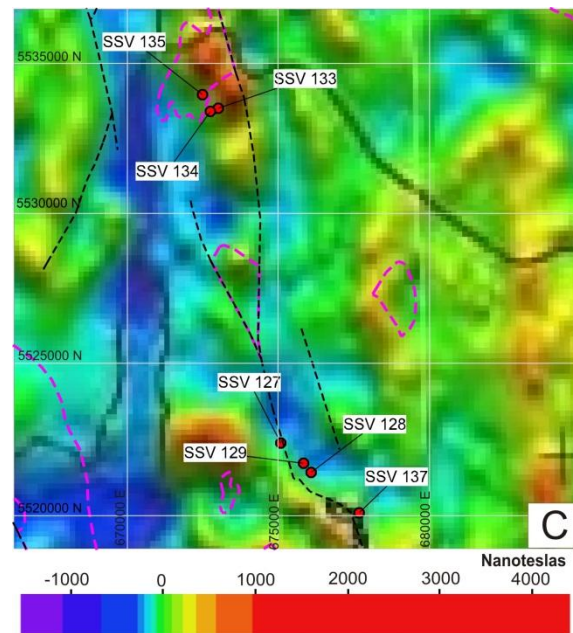
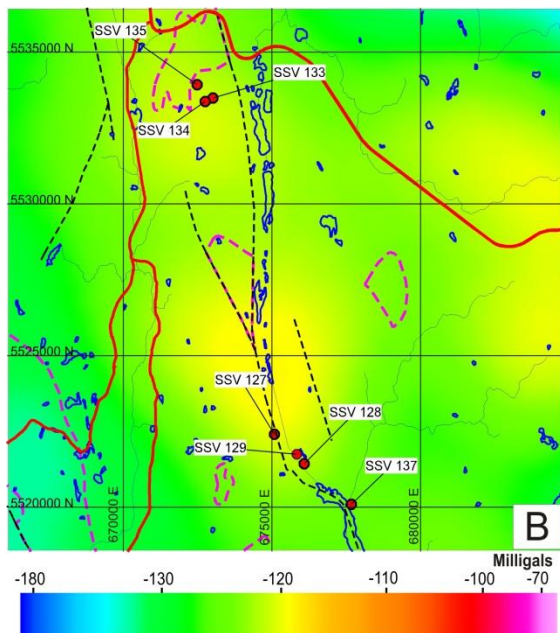


Figure 3.11. Geology, gravity and magnetic maps, showing the sample location of the South of Merritt area; dashed pink lines within the maps, outlines intrusive bodies. A) Geology of the South of Merritt area (Modified from Massey et al., 2005). B) Gravity Bouguer Corrected map, Quest south project (Geoscience BC., 2010). C) Magnetics Total Field map, Quest south project (Geoscience BC., 2010). Red dots, in the three maps, indicate sample locations.

values between -125 and 120mGal (Figure 3.11B) and magnetic values from -200 to 0nT. Areas underlain by volcanic rocks recorded readings as high as 600nT when intrusive bodies are close

to (Figure 3.11C). Late Triassic intrusive bodies (granodiorites) (Figure 3.11A), show slightly difference in the gravity response, presenting a small negative contrast (left bottom) with the host volcanics $\sim -130\text{mGal}$, and small intrusions in the center of the map (diorite to gabbro) show gravity values from -120 to -110mGal , this bodies are indistinguishable from the volcanic rocks in the gravity map (Figure 3.11C); magnetic values of intrusives vary from -800 to 0nT (map-left bottom), and $\sim 800\text{nT}$ for the intrusives in the centre-north and centre-south of the map.

3.7 DISCUSSION

Detailed petrographic description, magnetic susceptibility and density measurements in basalts from the Quesnel terrane compared with regional corrected bouguer gravity and total magnetic field maps, allows discriminating these rocks into different groups, albeit on the basis of relatively subtle variations.

Rocks in this research are Late Triassic and petrographically similar in the different studied areas, and are generally black to dark-green, clinopyroxene±plagioclase porphyritic basalts with variable Fe-Ti oxide content. Olivine crystals were not identified but patches and subhedral masses of hematite, which are probably pseudomorphous after olivine, are present in some areas. The overall petrographic similarity implies regional relatively uniform subduction parameters in the Late Triassic giving rise to the intra oceanic arc assemblage.

The whole volcanic belt of the Quesnel terrane underwent a similar degree of regional low grade metamorphism, which took place from Late Triassic to Paleogene (Greenwood et al., 1991). Metamorphic assemblages include chlorite, epidote, calcite, clays, hematite and occasionally zeolites, however, prehnite and/or pumpellyite have been reported in central, southern and northern BC by Morton (1976), Preto (1979) and Nelson and Bellefontaine (1996), respectively. The presence of all these minerals correspond to the regional zeolite to prehnite-pumpellyite metamorphic facies reported by Read et al. (1991) for the Quesnel terrane.

The presence of analcime within the Nicola volcanics as a primary or secondary mineral has been causing a long-standing debate. Coates (1960), Morton (1976), Preto (1977) and Bailey (1978) favour a primary origin; however, studies carried out on primary analcime stability presented by Roux and Hamilton (1976) and Gottardi and Galli (1985) led Mortimer (1987) to suggest that the Nicola Group analcimes could be pseudomorphs after igneous leucite. Karlsson and Clayton (1991) studied the analcime bearing volcanics from the Crowsnest Formation in Alberta and favoured a secondary origin, considering among other arguments the lack of hydrous igneous minerals in the rocks from Crowsnest, evidencing relatively dry source magma. Basalts from the Nicola Group do not contain any hydrous phase as phenocrysts. Therefore, the leucite replacement hypothesis seems a more viable explanation than the igneous origin for analcime in

the Nicola Group. Nevertheless, the problem of the analcime origin in the Nicola volcanics is still unresolved.

Some basalts of the LTNpv and LTNav units (Mount Polley), around Woodjam, Lac la Hache and South of Merritt present a reddish color, due to the hematite content in the groundmass. Hematite is more stable than other Fe-oxides under weathered conditions, however, it may be produced by alteration and/or weathering of Fe-Ti oxides or mafic minerals. Alteration and/or weathering could be produced as result of seafloor alteration (Irving, 1970), or by the interaction of basalts with surficial waters. This changes the physical properties of basalts, since the break-down of minerals such as Fe-Ti oxides modify their magnetic properties (e.g., Irving, 1970). Therefore basalts which currently contain secondary hematite could present lower magnetic susceptibility values than expected in fresh specimens. Hematite can also be added or form by hydrothermal fluids, in this case there is an addition of Fe to the rocks from an external source (e.g., nearby intrusive body).

Density of basalts in the study areas generally lies between 2.75 and 3.05g/cm³ (Figures 3.12A and 3.12B; Appendix A), with an average of 2.9g/cm³, these density values are basically controlled by the amount of mafic versus felsic minerals in the rock (Appendix A-Table A1), as well as by the porosity of rocks, which is related to the amount of vesicularity and/or fracturing. Also, the presence of high density minerals such as Fe-Ti oxides within the rock, do not influence the density of basalts to a significant degree, considering their low content, typically <2% (Appendix A-TableA1).

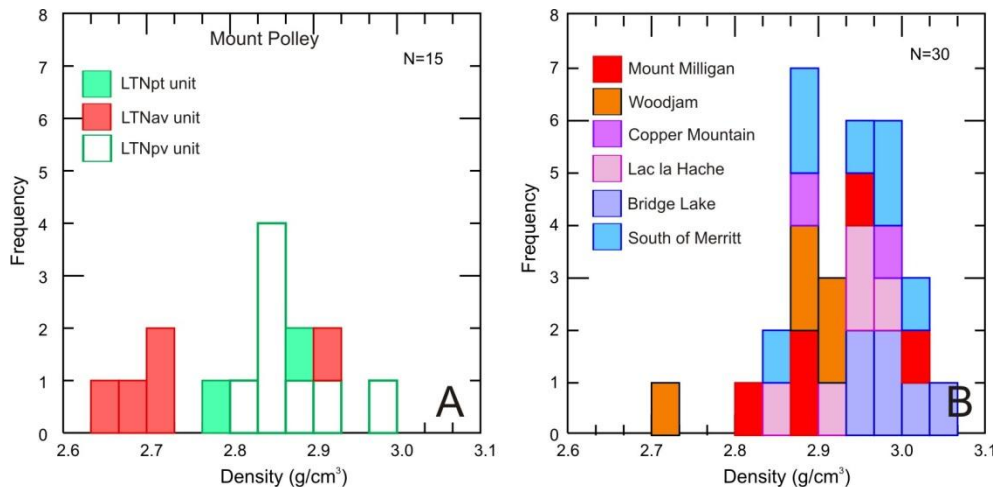


Figure 3.12. Histograms showing variation in density between basalts of the Nicola Group. A) Density of the three map units of the Mount Polley area. B) Density of the different areas in this study, except Mount Polley.

Most samples from the LTNav unit of Mount Polley tend to have relatively lower densities, from 2.65 to 2.73g/cm³ (Figure 3.12A). These samples contain between 15 and 45% felsic minerals (Appendix A-Table A1), with the exception of samples PSV003 and PSV036 which show a relatively high porosity (Figure 3.3L). Sample WTB087 from Woodjam falls into the same low density range (Figure 3.12B), containing 30% phenocrystic plagioclase (Figure 3.3M, Appendix A). These anomalous densities can be explained by igneous differentiation, which increases the content of felsic minerals (e.g., plagioclase and/or analcime) within the basalts, thus decreasing their density. Plagioclase precipitation instead of mafic minerals suggests a more evolved magmatic chamber, and the presence of analcime in basalts implies an alkalic and silica under-saturated environment. Moreover, weathering and/or alteration could also play a role in the low-density samples cited above.

The regional Bouguer gravity values in areas where the Nicola volcanics are mapped on surface, range from -115 to 90mGal in the central-north part of the arc, including Mount Polley, Mount Milligan, Woodjam and Lac la Hache (Figure 3.5B, 3.6B, 3.7B and 3.9B), suggesting relatively similar lithospheric composition and thickness for these arc segments. However, the arc segments in central-south Quesnel, comprised by Copper Mountain, Bridge Lake and South of Merritt show a range between -125 and -120mGal (Figure 3.8B, 3.10B and 3.11B). These relatively low gravity values, compared to the northern areas, may imply variations in the lithospheric composition and thickness. Possible reasons to explain this variation could be:

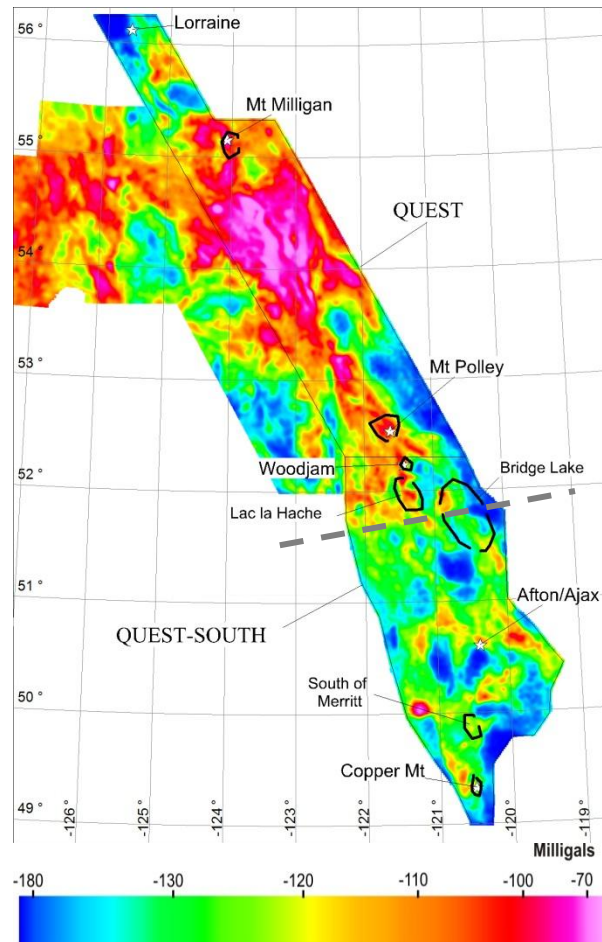


Figure 3.13. Regional airborne gravity bouguer corrected map of the Quest and Quest-south areas (Geoscience BC., 2009 and Geoscience BC., 2010, respectively). Black semi-circles delineate the areas considered in this research. The gray-dashed line indicates a deflection within the arc, and from there to the south the gravity decreases

- The difference in the basement between northern and southern BC, as has been suggested by the Lithoprobe seismic program (see Chapter 2).
- Gough (1986) reported that the southern Intermontane belt overlies a region of upper mantle upwelling, known as the Canadian Cordillera Regional conductor. This is characterized by high temperatures in the upper mantle and lower crust, which potentially could decrease the gravity values.
- The Bridge Lake area is located in the eastern part of the belt, where the Nicola volcanics overlaid Paleozoic metamorphic rocks (Figure 3.10A); thus, this area could represent a thickening of the crust, implying lower gravity values.

Another feature noticed in the regional gravity map (Figure 3.13), is a deflection of the terrane around the latitude of 51.5- 52°N (the same area of the previously cited variation in gravity measurements). The trend of the terrane changes from north to south, from ~30°NW in the northern part to ~10°NW in the south.

The regional Bouguer gravity along the Quesnel terrane displays a complex pattern of positive and negative anomalies. Much of the steep changes in gravity are due to the presence of Early Jurassic to Cretaceous intrusive bodies. Late Triassic alkalic intrusions, mainly monzonites and syenites related to Cu-Au porphyry mineralization, are geographically related to mafic intrusive bodies (diorite - gabbro) (Figure 3.5A, 3.6A, 3.8A and 3.9A). These intrusions are indistinguishable of the host volcanic rocks in the regional gravity maps in Mount Polley, Mount Milligan, Copper Mountain and Lac la Hache (Figure 3.5B, 3.6B, 3.8B and 3.9B). This suggests that differentiated alkalic-magmas (monzonite and syenite) were probably fractionated from dense, mafic-alkalic and larger magmatic chambers present at depth, producing gravity signatures similar to the host rocks. However, the small size (<2Km in diameter, which is the aero-gravity line spacing) of the monzonite-syenite intrusions could be another reason why these bodies are not detected in the regional gravity maps.

Late Triassic or younger calc-alkalic intrusives, mainly granodiorite (e.g., Takomkane batholith), have a low gravity signature on regional maps when compared to surrounding volcanic dominated areas. This is evident at Woodjam, Copper Mountain, Lac la Hache, Bridge Lake and

South of Merritt (Figure 3.7A, 3.8A, 3.9A and 3.11A). Nevertheless, calc-alkalic intrusions are not directly related to any alkalic porphyry Cu-Au mineralization in BC.

Magnetic susceptibility readings change from one location to another; this is directly related to the content of magnetic minerals (i.e., Fe-Ti oxides) within the basalts. Mount Polley shows a wide range of magnetic susceptibilities from 1.16×10^{-3} to 111.00×10^{-3} SI units (Figure 3.14A), but most readings are at values above 14.00×10^{-3} SI units. The highest magnetic susceptibility was recorded where the sample PSV028 from the LTNpt unit was taken. Relatively high magnetic susceptibilities also characterize a few samples from Mount Milligan, Lac la Hache, Bridge Lake and South of Merritt (Figure 3.14B). However, basalts from Mount Milligan, Copper Mountain, Woodjam and Bridge Lake, display mostly low magnetic susceptibility numbers of $< 10.00 \times 10^{-3}$ SI units (Figure 3.14B).

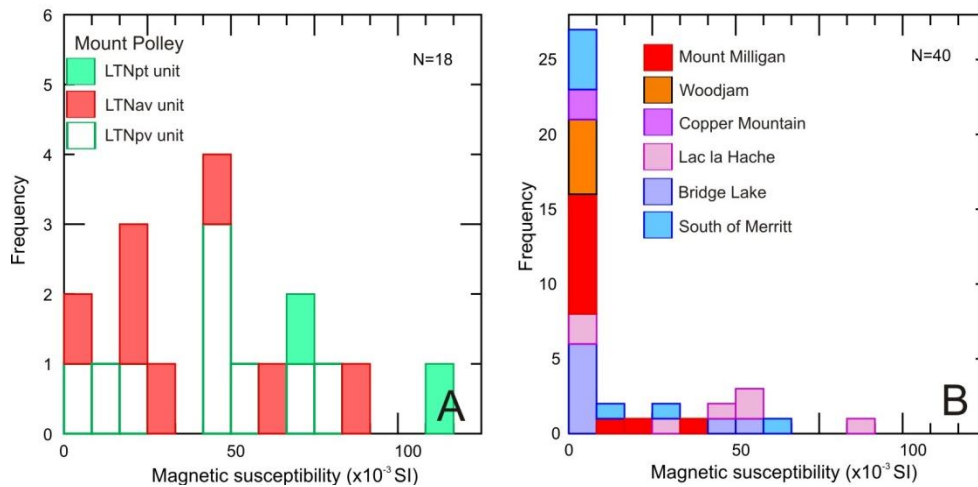


Figure 3.14. Histograms showing variation in the magnetic susceptibility reading between basalts of the Nicola Group. A) Magnetic susceptibilities of the three map units of Mount Polley. B) Magnetic susceptibilities of rocks from all other areas in this study.

The regional total magnetic field maps indicate some differences between the volcanic host rocks in the study areas. Mount Polley, Woodjam and Lac la Hache show magnetic highs (Figure 3.5C, 3.7C and 3.9C). Conversely, Mount Milligan, Copper Mountain, Bridge Lake and South of Merritt present average to magnetic lows correlated to the host volcanics (Figure 3.6C, 3.8C, 3.10C and 3.11C).

Positive magnetic anomalies in the volcanic rocks could be considered partially false, due to the influence of nearby intrusions. However, magnetic susceptibility recorded in basalts (Appendix A-Table A1) helped to interpret regional magnetics.

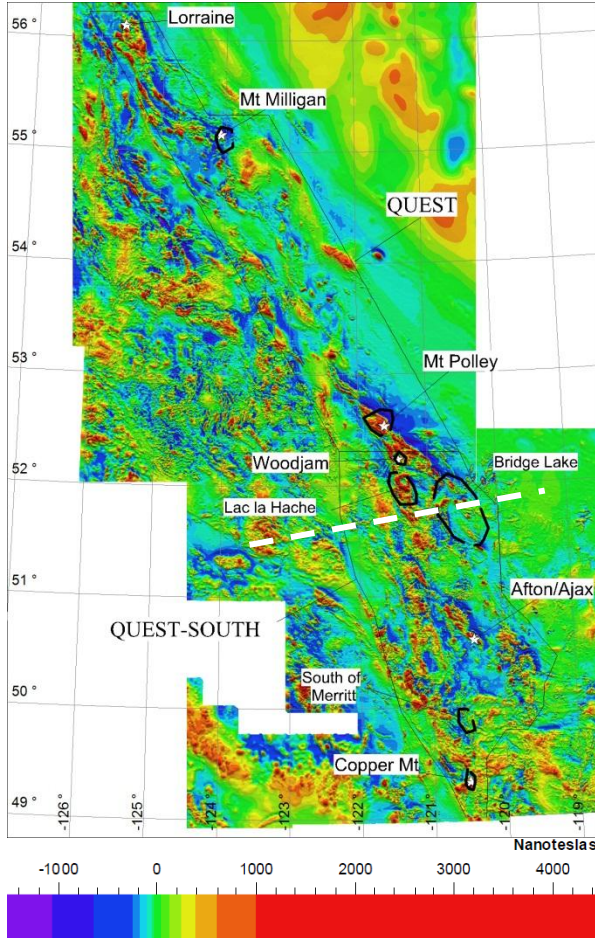


Figure 3.15. Regional airborne total magnetic field map of the Quest and Quest-south areas (Geoscience BC., 2009 and Geoscience BC., 2010, respectively). Black semi-circles delineate the areas considered in this research. The white-dashed line indicates a deflection within the arc.

non-prospective arc segment for coeval fertile intrusions, where volcanic rocks were developed from a relatively reduced magma chamber.

Considering Mount Polley and Mount Milligan as end members, the areas studied can potentially be grouped as prospective and non-prospective for coeval for Cu-Au alkalic porphyry mineralization, as well as arc segments with uncertain level of prospectivity, as follows:

Regionally, the total magnetic field map can help identifying arc segments showing different magnetic characteristics. This is the case for the area delineated by Mount Polley, Woodjam and Lac la Hache (Figure 3.15) which could be described as magnetic high zones. The deflection noticed around the latitude of 51.5-52°N in the gravity map (Figure 3.13), is also identified here (Figure 3.15).

The presence of primary Fe-Ti oxides in basalts suggests a source with a relatively high oxidation state. This oxidized magmatic chamber would have also produced oxidized intrusive facies, which could be related to porphyry Cu-Au mineralization (e.g., Seedorff et al., 2005; Chamberlain et al., 2007).

In this scenario, Mount Polley may represent an example of a prospective arc segment for coeval Cu-Au alkalic porphyry mineralization.

In contrast, Mount Milligan could represent a

- Group 1. Mount Polley, Lac la Hache, and South of Merritt, representing prospective arc segments.
- Group 2. Mount Milligan and Bridge Lake, representing non-prospective for coeval mineralization, and,
- Group 3. Copper Mountain and Woodjam can be grouped as uncertain arc segments, since the contradictory information obtained from the regional magnetic map and the magnetic susceptibility recorded on basalts are inconclusive. The presence of widespread secondary hematite in Woodjam may have obscured the original magnetic susceptibilities of rocks in this area.

Note that porphyry mineralization significantly post-dating the volcanic rocks, could potentially be present anywhere in the arc, as exemplified by Mount Milligan.

Petrography and physical properties of the basalts in Copper Mountain and Woodjam do not provide the necessary constrains to classify them into prospective or non-prospective arc segments.

Although there is no major porphyry Cu-Au mineralization reported in South of Merritt, the occurrence of mafic intrusive bodies with positive magnetic anomalies (Figure 3.11 A and 3.11C), and the presence of analcime within basalts (Section 3.5.7, Appendix A-TableA1) are comparable to the Mount Polley area, and may serve as indicators for a region potentially prospective for porphyry Cu-Au mineralization.

CHAPTER 4: GEOCHEMISTRY

4.1 INTRODUCTION

Basalts from three map units (Logan et al., 2007) around the Mount Polley Cu-Au porphyry deposit were selected for whole-rock and mineral chemistry. Results were compared with six other localities along strike within the arc, including four areas which are spatially related to porphyry Cu style mineralization (Mount Milligan, Woodjam, Copper Mountain and Lac la Hache). The other two areas represent arc segments without any significant reported mineralization, including Bridge Lake and South of Merritt (for details, see Chapter 3).

Major and minor elements chemistry was used to discriminate basalts from different localities along the Nicola Group. In this regard, the geochemical index ($\text{Fe}_2\text{O}_3\text{t}+\text{MgO}$ vs Al_2O_3) was used to show variations in differentiation along and across the arc. Incompatible elements such as Zr, Yb, Nb and Th help to find differences in the magma sources between the study areas. The Ce/Yb ratios were used as an indicator of tectonic changes in the lithosphere during volcanism (e.g., Ellam, 1992; Hawkesworth et al., 1992; Hawkesworth et al., 1993; Doe, 2002).

Variation in $\text{Fe}^{2+}/\text{Fe}^{3+}$ ratios obtained from whole-rock geochemistry and magnetic susceptibility values recorded on basalts along the belt show that the volcanic arc can be subdivided on the basis of variation in oxidation state and magnetic susceptibility. However, magnetic susceptibility and Fe^{3+} content may be influenced by alteration processes. Thus, in this chapter an alternate way to estimate oxidation state and alkalinity of magmas using the chemistry of effectively unaltered phenocrysts is also presented.

Scanning electron microscopy (SEM) and electron microprobe (EMP) analyses were performed to obtain qualitative and quantitative analyses of the chemical variations within and among clinopyroxene crystals. In addition, the compositions of Fe-Ti oxide and few apatite inclusions within clinopyroxene were determined. Pyroxene and Fe-Ti oxide chemistry records the alkalinity and oxidation state of parent magma (Kushiro, 1960; LeBas, 1962; Taylor, 1964). High oxidation state is an important characteristic of igneous rocks related to porphyry Cu-Au mineralization (e.g., Seedorff et al., 2005; Chamberlain et al., 2007). Studying chemical variations of minerals within basalts will lead to a more complete understanding of the magmatic evolution of the arc.

4.2 ANALYTICAL PROCEDURES

Detailed petrographic observations were made using transmitted and reflected light microscopy. Basalt samples were analyzed at the ALS laboratory, North Vancouver, by the major and trace element whole rock package ME-MS81d. This is a combination of whole rock package by method ME-ICP06, plus rare earth and trace elements from method ME-MS81. Ferrous iron was measured on thirty-nine selected samples by the Fe-VOL05 package to obtain Fe^{3+}/Fe^{2+} ratios. Full description about the geochemical methods cited above and all analytical data are presented in the appendix B.

Polished thin sections were carbon coated in an Edwards Auto 306 carbon coater instrument. The SEM analyses were done with a PhilipsTM XL-30 scanning electron microscope/Bruker QuantaTM 200 energy-dispersion X-ray microanalysis system. Chemical compositions of pyroxene and Fe-Ti oxides were determined using a fully automated CAMECATM SX-50 electron microprobe. Pyroxene and Fe-Ti-oxide compositions were measured with the following operating conditions: excitation voltage: 15kV; beam current: 20nA; peak count-time: 20s; background count-time: 10s; spot diameter: 5 μ m. Apatite compositions were acquired with the operating conditions of excitation voltage: 15kV; beam current: 5nA; peak count time: 20s (except S: 40s); background count-time: 10s (except S: 20s); spot diameter: 5 μ m. Standards for pyroxene, Fe-Ti-oxide and apatite analyses are indicated in Table 4.1.

Table 4.1. Standards, analysis lines and crystals used for pyroxene, Fe-Ti-oxide and apatite analyses.

Pyroxene	Fe-Ti Oxides	Apatite
albite, NaKa, TAP	synthetic spinel, AlKa, TAP	apatite, PK α , PET
kyanite, AlKa, TAP	synthetic magnesiochromite, MgKa, TAP	apatite, CaK α , PET
diopside, MgKa, TAP	diopside, SiKa, TAP	barite, SK α , PET
diopside, SiKa, TAP	diopside, CaKa, PET	scapolite, ClK α , PET
diopside, CaKa, PET	rutile, TiKa, PET	topaz, FK α , PC1
rutile, TiKa, PET	synthetic magnesiochromite, CrKa, LIF	
synthetic magnesiochromite, CrKa, LIF	synthetic rhodonite, MnKa, LIF	
synthetic rhodonite, MnKa, LIF	synthetic fayalite, FeKa, LIF	
synthetic fayalite, FeKa, LIF	synthetic Ni ₂ SiO ₄ , NiKa, LIF	
synthetic Ni ₂ SiO ₄ , NiKa, LIF	vanadium metal, VKa, PET	

TAP =Thallium acid phthalate; LIF=Lithium fluoride; PET= Pentaerythritol; PC1= Pseudo crystal, multilayered W/Si.

Data reduction was done using the 'PAP' $\phi(\rho Z)$ method (Pouchou and Pichoir, 1985). The structural formulas of pyroxene were calculated on the basis of 6 O; for Fe-Ti oxide, structural formulas were calculated on the basis of 32 O; and for apatite, ion calculation was done on the basis of 26 O-Cl-F-OH. The Fe^{3+} content was calculated using the method proposed by Droop (1987).

4.3 WHOLE ROCK GEOCHEMISTRY

Rocks of the Nicola Group commonly present alteration minerals (e.g. epidote, chlorite, calcite and clays; see Chapter 3), these minerals are the evidence of chemical changes underwent by the rock. Molar element ratios and loss on ignition values were used to test major elements mobility (e.g. Ca, Na, and K; Appendix D, Figure D1), neither significant addition nor subtraction of Ca, Na or K was detected. Thus, secondary minerals present in the rocks are interpreted to be the product of isochemical alteration.

4.3.1 Major Elements Chemistry

Whole rock chemical compositions show that basalts from the different map units around Mount Polley fall in the alkaline-field, using the major elements Si, Na and K (expressed as oxides) in the bivariate diagram of Irving and Baragar (1971) (Figure 4.1 A). Basalts from the unit LTNav tend to have higher alkali contents than basalts from the other two map units.

Plotting the samples collected from the other areas along the Nicola arc in the same diagram (Figure 4.1 B), it is observed that most basalts plot in the alkaline field and partly overlap with those from Mount Polley although the LTNav unit extends to slightly higher alkali content than the other basalts. Only few samples from Bridge Lake and one from Mount Milligan, just cross the border into the sub-alkaline space.

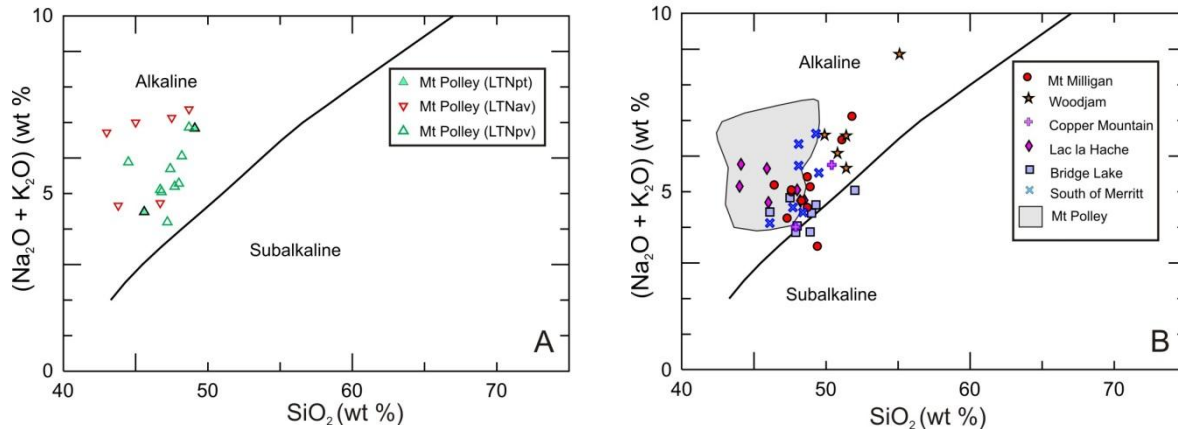


Figure 4.1 Bivariate plot SiO_2 vs $\text{Na}_2\text{O} + \text{K}_2\text{O}$ of Irvine and Baragar (1971). A) Showing the alkaline nature of the basalts from Mount Polley, note that most rocks from the LTNav unit have more alkalic signature. B) Comparing the alkalinity of the basalts from different localities of the Nicola Group with the Mount Polley area. Basalts from Bridge Lake and a sample from Mount Milligan display a less alkaline signature.

Geochemical variations between the different Mount Polley units are subtle; nevertheless, samples from LTNav tend to be more depleted in SiO_2 (38.90-48.70wt%) (Figure 4.2), but exhibit a wide range in Na_2O from 1.50 to 6.42wt%, and K_2O between 0.66 to 5.22wt% (Figure 4.2B-1 and 4.2C-1), as well as, generally low MgO contents, from 4.33 to 5.63wt%, although one sample has 9.82wt% MgO. Units LTNpv and LTNpt in comparison show higher SiO_2 (44.50-49.10wt%), but do not extend to Na_2O and K_2O values above 3.25 and 3.61wt%, respectively (Figure 4.2A-1, 4.2B-1). The Mount Polley samples overall display MgO contents between 4.10 and 10.00wt% (Figure 4.2C-1).

Basalts from the other sampled areas generally display SiO_2 values (<52.00wt%), with the exception of Woodjam which is relatively enriched in SiO_2 (≤ 55.00 wt%) (Figure 4.2A-2, 4.2B-2 and 4.2C-2). Nonetheless, Lac la Hache contains the lowest SiO_2 values (44.00-48.50wt%), presenting similar composition to Mount Polley samples. All the other areas sampled tend to be slightly less alkaline, having lower Na_2O and K_2O concentrations at given silica content, compared to Mount Polley (Figure 4.2B-2 and 4.2C-2). However, at Woodjam samples show Na_2O content up to 5.14wt%, while in the other areas the amount of Na_2O varies from 1.37 to 3.50wt% (Figure 4.2A-2); the K_2O content ranges between 0.81 to 3.40wt%, with the exception of some samples from Mount Milligan, Woodjam and South of Merritt which present values between 3.60 and 4.30wt% (Figure 4.2B-2). The MgO content is similar between Mount Polley

and the other localities, with the exception of Woodjam which presents a lower MgO content ranging from 2.20 to 6.80wt% (Figure 4.2C-2).

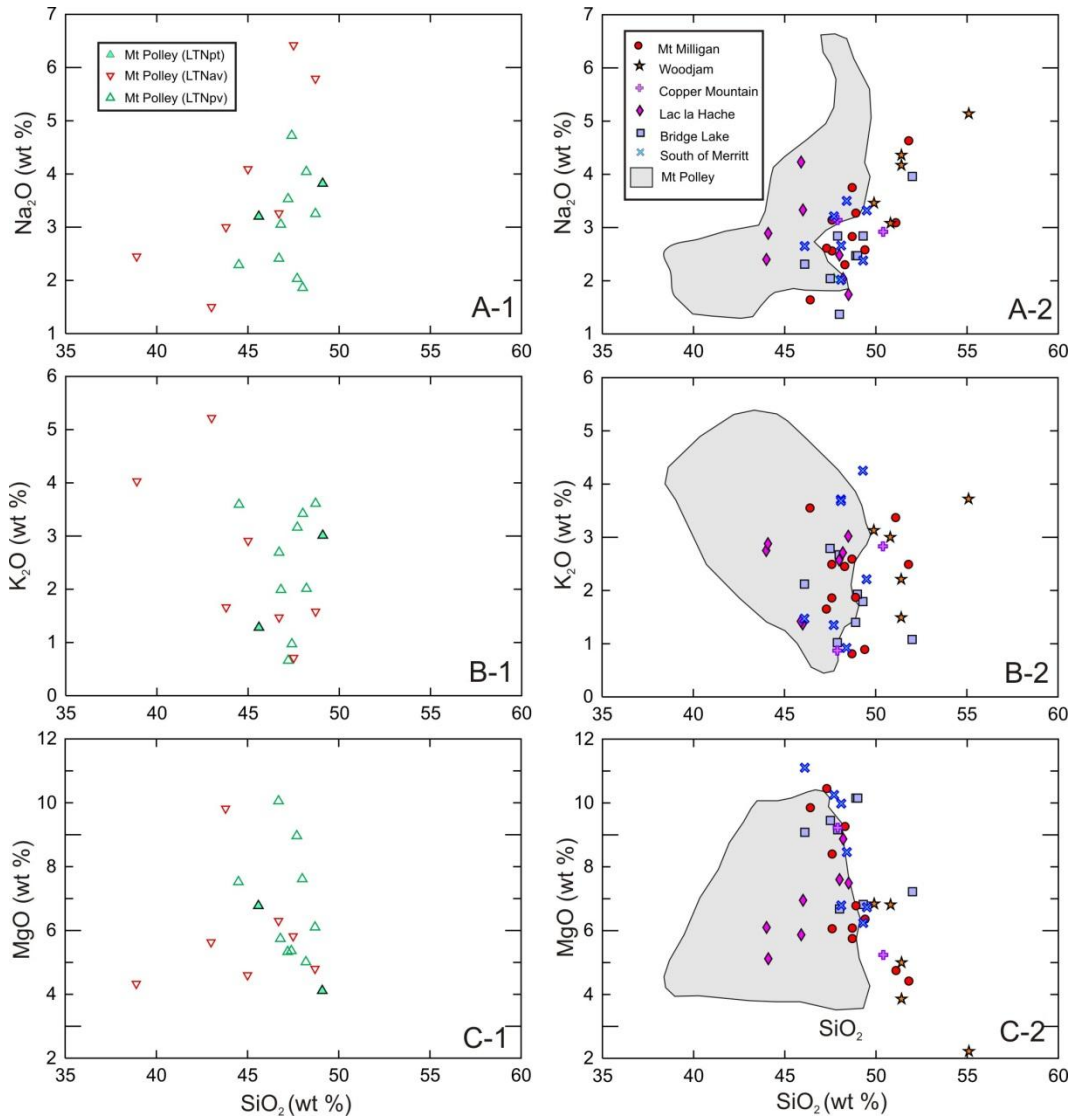


Figure 4.2. Harker plots, evidencing some geochemical variations on basalts from the Nicola Group. A-1, B-1 and C-1). Indicate variations of Na₂O, K₂O and MgO for basalts from Mount Polley. A-2, B-2 and C-2). Show a comparison of basalts of different areas along the Nicola Group with rock from Mount Polley.

The degree of differentiation was tested in basalts from the areas studied along the Nicola Group, plotting the geochemical index (Fe₂O₃(t)+MgO)wt% versus Al₂O₃wt% (Figure 4.3). Differentiation is indicated by the decrease in Fe₂O₃(t)+MgO content and the increase of Al₂O₃ amount.

Mount Polley exhibits $\text{Fe}_2\text{O}_3(\text{t})+\text{MgO}$ (13.40-21.22wt%) and Al_2O_3 (10.00-16.65wt%), denoting an overlap between the three units. However, some samples from LTNav present slightly lower $\text{Fe}_2\text{O}_3(\text{t})+\text{MgO}$ values for a given Al_2O_3 content (Figure 4.3A).

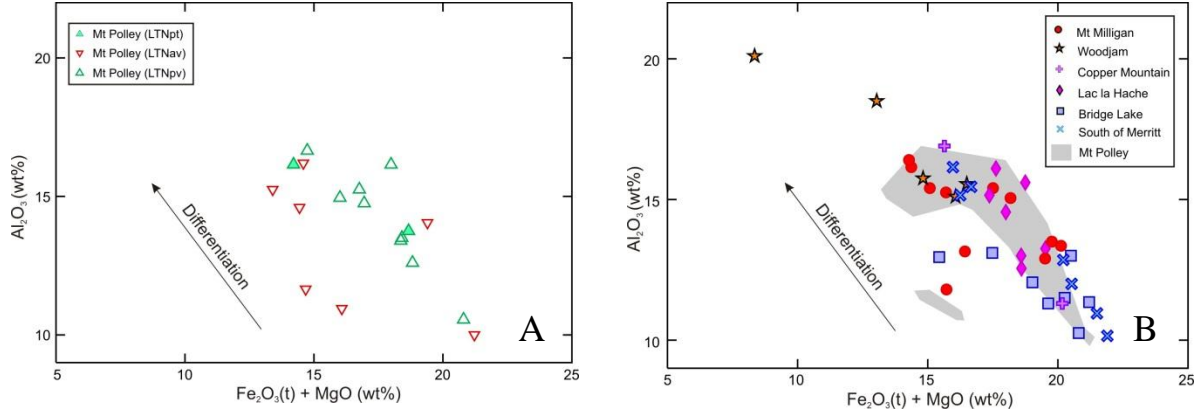


Figure 4.3. Geochemical index ($\text{Fe}_2\text{O}_3+\text{MgO}$) vs Al_2O_3 , as an indicator of differentiation for rocks from the Nicola Group. A) Exhibit changes in the differentiation between the three map units of Mount Polley. B) Comparison of differentiation of rocks from different localities within the Nicola Group with basalts from Mount Polley.

Woodjam presents $\text{Fe}_2\text{O}_3(\text{t})+\text{MgO}$ (8.35-16.50%) and Al_2O_3 (15.55-20.10%) (Figure 4.3B), showing the highest degree of differentiation, as expected from petrographic observations (basaltic-andesite; see Chapter 3); whereas, Bridge Lake basalts have high $\text{Fe}_2\text{O}_3(\text{t})+\text{MgO}$ of 15.44 to 21.2wt% and low Al_2O_3 contents of 10.25 to 13.10wt%, being the least differentiated rocks (Figure 4.3B). Mount Milligan, Copper Mountain, Lac la Hache and south of Merritt fall on a similar differentiation trend as Mount Polley, with $\text{Fe}_2\text{O}_3(\text{t})+\text{MgO}$ from 14.30 to 21.90wt% and Al_2O_3 from 10.10 to 16.90wt%, although Lac la Hache occupies a narrow variation in $\text{Fe}_2\text{O}_3(\text{t})+\text{MgO}$ between 17.37 and 19.52wt% (Figure 4.3B).

4.3.2 Incompatible Elements Chemistry

Rocks from Mount Polley fall within the arc-basalt field in the triangular Th-Zr/117-Nb/16 plot of Wood (1980) (Figure. 4.4A). All samples from the LTNav unit have relatively high Th concentrations, some samples from LTNpv overlap with LTNav basalts, while others present higher Zr content. Basalts from LTNpt have the highest Zr concentrations. Rocks from the three different units of Mount Polley show relatively uniform Nb values (Figure 4.4A).

Rocks from the other localities fall in the arc-basalt setting, overlapping the Mount Polley samples (Figure 4.4B), and displaying limited variations with respect to Th, Zr and Nb. However, basalts from Mount Milligan have slightly higher Nb compared to the others (Figure 4.4B).

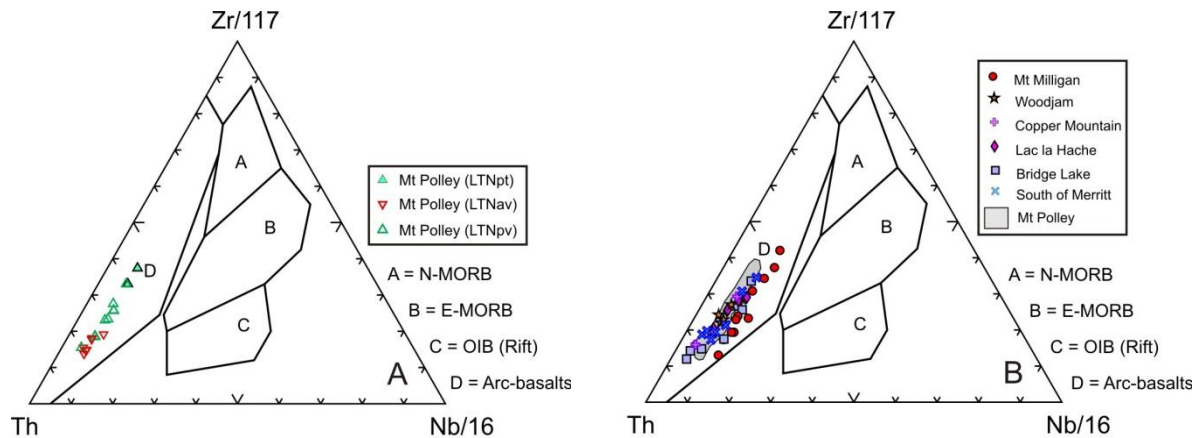


Figure 4.4. Ternary Th-Zr/117-Nb/16 diagram of Wood (1980), denoting the tectonic environment for basalts from the Nicola Group. A) Showing that all rocks from Mount Polley belong to the arc magmatic tectonic setting. B) Evidencing that all rocks from different localities along the arc fall within the arc-basalt setting.

To discriminate between the different sources of magmatism in the studied areas along the arc, the Ce/Yb and Th/Nb ratios were used.

Mount Polley exhibits a relatively narrow range in Th/Nb ratios (0.40-1.20) for the three map units, whereas the Ce/Yb ratio displays distinct ranges. The LTNpv unit presents the widest range (7.40-16.90), and the LTNv unit has a narrow range but relatively high values (17.60-24.50), contrasting with the LTNpt unit which has the lowest Ce/Yb ratios (6.60-6.70) (Figure 4.5A).

The other areas display some differences in the Th/Nb ratios. Mount Milligan has consistently lower Th/Nb ratios (0.26-0.45); Woodjam shows a relatively narrow variation from 0.63 to 0.81, Copper Mountain, Lac la Hache, Bridge Lake and South of Merritt show some overlap in Th/Nb ratios, presenting values of 0.54 to 1.26, 0.40 to 0.62, 0.40 to 1.40, and 0.40 to 1.16, respectively (Figure 4.5B). Ce/Yb ratios are relatively similar between the different areas. Mount Milligan (6.00-16.70), Woodjam (8.00-17.00), Copper Mountain (10.30-14.00), Lac la Hache (9.13-12.60) showing the narrowest range. Bridge Lake varies from 6.30 to 15.30 and South of Merritt between 7.58 and 13.70 (Figure 4.5B).

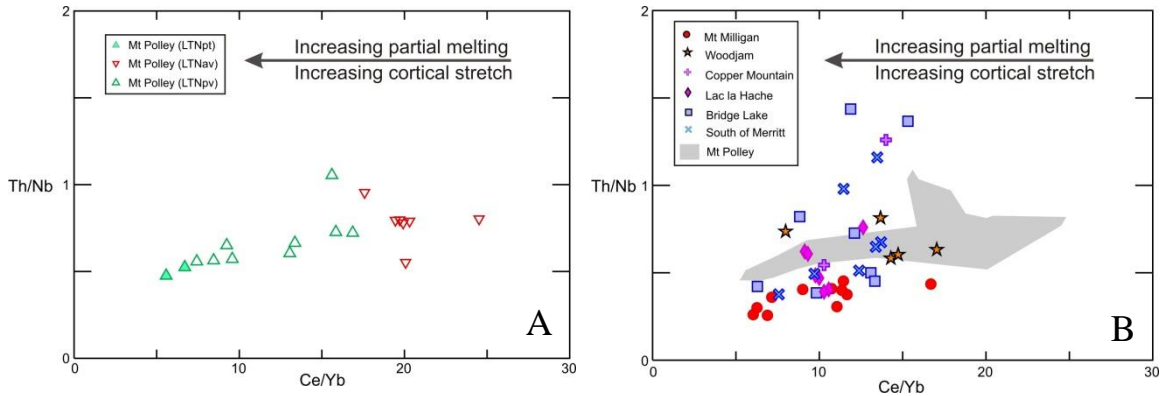


Figure 4.5. Ce/Yb vs Th/Nb ratios, indicating variations of the different magma sources, and also suggesting changes in the tectonic setting during volcanism. A) Showing variation in Ce/Yb ratios, and relatively homogeneous Th/Nb ratios between the three map units of Mount Polley. B) Exhibiting changes in both, Ce/Yb and Th/Nb ratios of rocks from different localities within the Nicola Group with basalts from Mount Polley.

4.4 OXIDATION STATE OF BASALTS

The Fe^{3+}/Fe^{2+} ratio was used to evaluate the variation in the oxidation state, as well as secondary oxidation of Fe-rich minerals in selected samples (Appendix B, Table B4). The results were plotted versus the magnetic susceptibility of the respective rocks (Figure 4.6). The three units from Mount Polley display narrow variations in Fe^{3+}/Fe^{2+} ratios (0.96-2.81), and show a wide range of magnetic susceptibilities (21.50×10^{-3} - 111.00×10^{-3} SI units), with the exception of sample PSV017 from the LTNpv unit which displays the highest Fe^{3+}/Fe^{2+} ratio of 4.97 and a lower magnetic susceptibility of 1.16×10^{-3} SI units (Appendix A, Table A1).

For the rest of the arc, Fe^{3+}/Fe^{2+} ratios and magnetic susceptibilities shows the following: Mount Milligan presents low Fe^{3+}/Fe^{2+} ratios (0.20-0.52) and magnetic susceptibilities $<14.00 \times 10^{-3}$ SI units; Woodjam shows consistently high Fe^{3+}/Fe^{2+} ratios of 5.05 to 7.10 and magnetic susceptibilities $<1.55 \times 10^{-3}$ SI units. Copper Mountain displays Fe^{3+}/Fe^{2+} ratios between 0.21 and 0.38, and low magnetic susceptibilities $<1.20 \times 10^{-3}$ SI units; Lac la Hache has moderate Fe^{3+}/Fe^{2+} ratios ranging from 0.63 to 2.29 and a wide range of magnetic susceptibility readings from 0.59×10^{-3} to 83.50×10^{-3} SI units; Bridge Lake presents relatively low Fe^{3+}/Fe^{2+} ratios (0.13-0.61), and also low magnetic susceptibilities $<1.30 \times 10^{-3}$ SI units; and South of Merritt shows relatively high Fe^{3+}/Fe^{2+} ratios of 0.83 to 5.13 and magnetic susceptibilities varying between 0.40×10^{-3} and 63.10×10^{-3} SI units (Figure 4.6). Note that both low and high Fe^{3+}/Fe^{2+} ratios coincide to low magnetic susceptibility values.

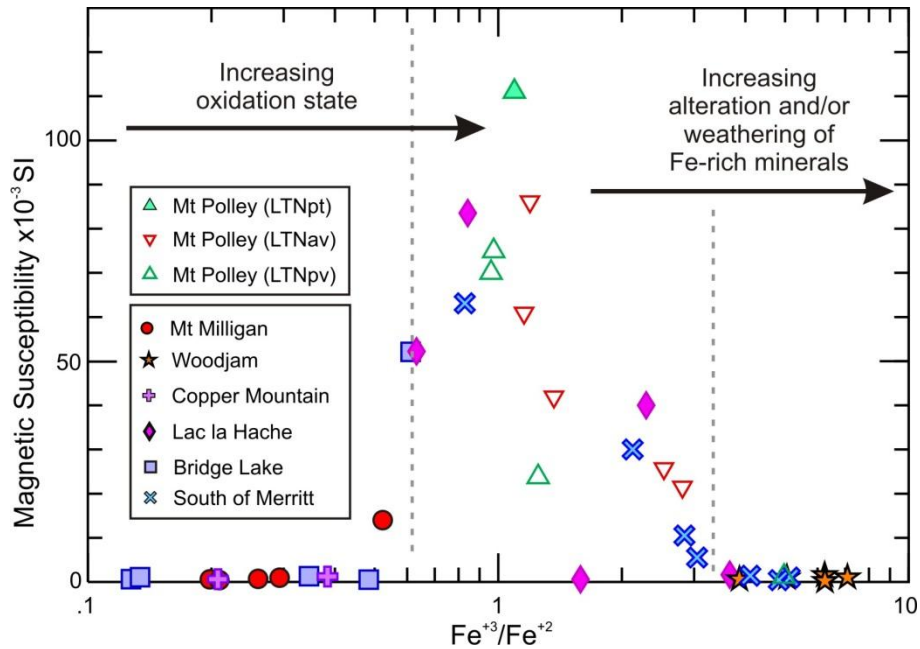


Figure 4.6. Bivariate plot of Fe^{3+}/Fe^{2+} versus magnetic susceptibility of rocks from the Nicola Group, indicating similarities between rocks of Mount Milligan, Bridge Lake and Copper Mountain, and between Mount Polley, Lac la Hache and South of Merritt basalts. Note that samples from Woodjam and some from South of Merritt and Lac la Hache form a separate group.

4.5 MINERAL CHEMISTRY

4.5.1 Scanning Electron Microscopy and Electron Microprobe Analyses

4.5.1.1 Clinopyroxene

Thin section observations show that pyroxene is the main phenocryst phase within basalts in the study areas. Clinopyroxene is colourless to pale green in transmitted light, ≤ 4.0 mm, from euhedral to subhedral, and typically displays concentric zonation. Pyroxene crystals are variably fractured and locally chloritized. Only unaltered spots within crystals were analyzed by the electron microprobe in this study. Primary Fe-Ti oxide is commonly present as inclusions within clinopyroxene (Figure 4.7), inclusions of apatite were also found.

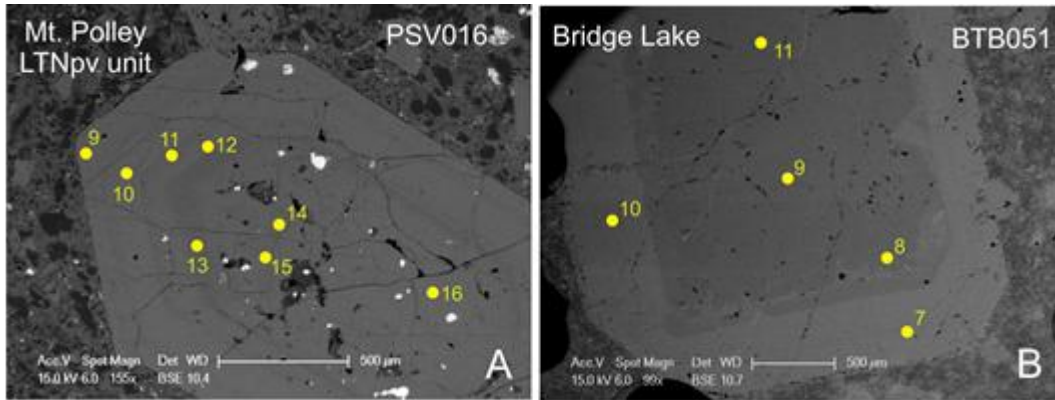


Figure 4.7. Representative backscattered electron images of clinopyroxene, electron microprobe (EMP) analysis spots are shown in yellow: A) clinopyroxene showing concentric zonation and Fe-Ti-oxide inclusions (bright gray); B) Zoned clinopyroxene evidencing a sharp transition between the core/interior (dark gray) and rim (light gray), note the absence of Fe-Ti oxide inclusions.

Results of electron microprobe analyses show that, at Mount Polley, clinopyroxene composition exhibits some chemical variations from core to rim; spot analyses are separated into two main groups, using the pyroxene quadrilateral (Figure 4.8A).

The more populated group (group A) (Figure 4.8A right) ranges between 10 and 20mol%Fe content and corresponds to analyses done from core to interior to rim in crystals from the three map units. The average clinopyroxene composition in this group is $(\text{Ca}_{0.892}, \text{Fe}^{2+}_{0.085}, \text{Na}_{0.034})(\text{Al}^{\text{VI}}_{0.034}, \text{Fe}^{3+}_{0.143}, \text{Fe}^{2+}_{0.04}, \text{Ti}_{0.018}, \text{Mg}_{0.757}, \text{Mn}_{0.008})(\text{Si}_{1.831}, \text{Al}^{\text{IV}}_{0.169})\text{O}_6$, falling in the diopside field, except for some analyses from the LTNpv and LTNpt units, which straddle the border into the augite field (Figure 4.8A bottom right). Basalts from the LTNav unit present a slightly higher Ca and lower Si content with respect to the other two units (Appendix B, Table B5).

The other group (group B) (Figure 4.8A left, circled by brown dashed line) lies within 0-10mol%Fe content, and includes some spots from cores and interiors only (no rims) of the samples PSV016 and PSV017 (LTNpv unit), PSV026 and PSV039 (LTNav unit), and PSV007 (LTNpt unit). The average clinopyroxene composition for this group is $(\text{Ca}_{0.928}, \text{Fe}^{2+}_{0.04}, \text{Na}_{0.016})(\text{Fe}^{3+}_{0.055}, \text{Fe}^{2+}_{0.013}, \text{Ti}_{0.005}, \text{Mg}_{0.924}, \text{Mn}_{0.003})(\text{Si}_{1.936}, \text{Al}^{\text{IV}}_{0.064})\text{O}_6$, plotting in the diopside field.

For the other studied areas along the Nicola Group, clinopyroxene compositions fall into the same two compositional groups described above for Mount Polley. Analyses from core to interior to rim of Mount Milligan, Copper Mountain, Lac la Hache and most analyses from Bridge Lake, fall within the group A in the pyroxene quadrilateral (Figure 4.8B right), plotting in

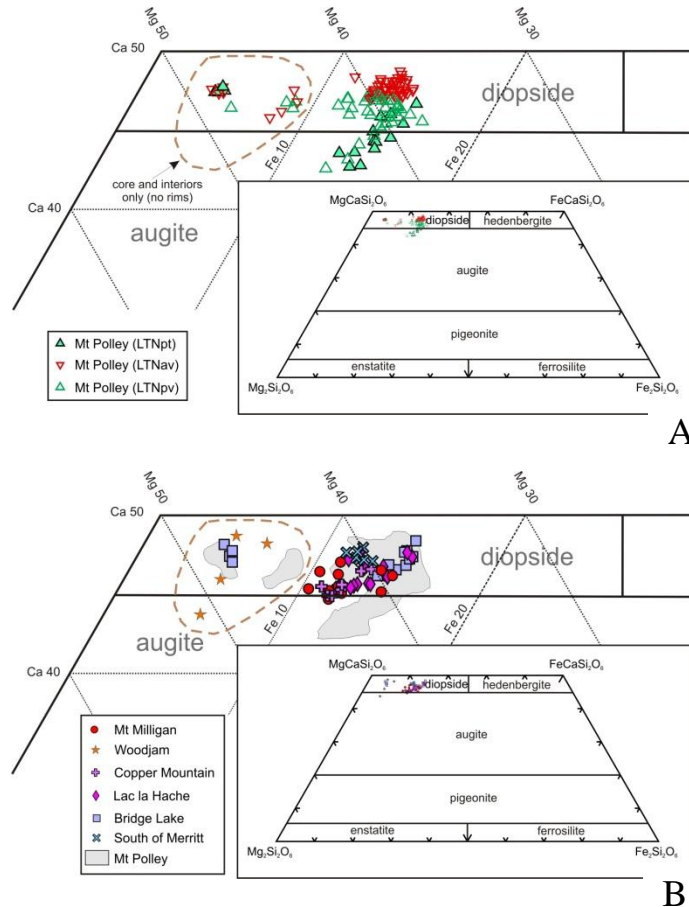


Figure 4.8. The pyroxene quadrilateral of Morimoto (1988), showing clinopyroxene compositions of basalts from the Nicola Group. A) Basalts from three map units of Mount Polley, the circled field corresponds to some clinopyroxene from core and interiors (no rims). B) Basalts from different areas along the Nicola Group compared with rocks from Mount Polley, the circled field corresponds to pyroxene from core to rim of the Woodjam sample, and some spots from cores and interiors (no rims) of clinopyroxene crystals from Bridge Lake and Mount Polley areas (group B).

the diopside field. Similarly, all analyses from Woodjam and some spots from cores and interiors (no rims) of the Bridge Lake sample yield within the group B (Figure 4.8B left, circled by brown dashed line), belonging to the diopside field, with the exception of one spot from Woodjam, which plots as augite.

The same two groups defined above were identified in the bivariate plot SiO_2 versus Mg\# ($\text{Mg\#} = 100 * \text{Mg}^{2+} / (\text{Mg}^{2+} + \text{Fe}^{2+})$). At Mount Polley, the more populated group (Figure 4.9A left) displays some differences between the map units. The LTNav unit exhibits Mg\# (83.46-91.82) and SiO_2 (46.59-50.35%); and the LTNpt unit presents Mg\# (80.86-85.51) and SiO_2 (47.39-52.76%). These two units are clearly separated around Mg\# of 85; most of the analyses from LTNav plot above, while most of the analyses from LTNpt fall below this value (Figure 4.9A left). Similarly, the LTNav unit has a rough correlation of increasing Mg\# with decreasing $\text{SiO}_2\%$, presenting the lowest $\text{SiO}_2\%$ content. The unit LTNpv presents Mg\# (79.32-91.80) and SiO_2 (47.81-51.88%)

overlapping the other two units (Figure 4.9A left). This group approximately contains the same analytical spots as group A shown in the pyroxene quadrilateral (Figure 4.8A right).

The other group of spots (Figure 4.9A top right, dashed brown line) show higher Mg# (85.56–98.12) and SiO₂ (51.03–53.86 %) corresponding to core and interiors of some pyroxene analyses from Mount Polley. This group contains almost the same analytical spots as group B of the pyroxene quadrilateral (Figure 4.8A left).

Most of the clinopyroxene analyses from the other localities investigated in this study, except Woodjam, fall close to or within group A (Figure 4.9B left). Analyses from Copper Mountain have Mg# of 87.60 to 92.60 and SiO₂ of 47.30 to 50.12%. Pyroxenes from South of Merritt presents Mg# between 90.54 and 94.10 and SiO₂ between 47.60 and 48.50%, both overlapping the compositions of the LTNav unit of Mount Polley, which has Mg# above of 85 (Figure 4.9B left). Clinopyroxene spots from Mount Milligan show Mg# from 81.70 to 86.80 and SiO₂ between 48.20 and 51.10%, and most analyses from Bridge Lake display Mg# of 80.60 to 85.90 and SiO₂ from 47.70 to 49.20% overlapping the compositional field of the LTNpt unit of Mount Polley, falling mostly below Mg# of 85 (Figure 4.9B left). Analyses from Lac la Hache, exhibit Mg# of 48.10 to 50.10 and SiO₂ between 79.90 and 89.10% matching with the LTNpv unit, plotting above and below of Mg# value of 85 (Figure 4.9B left).

Spot analyses from Woodjam present Mg# from 91.90 to 95.80 and SiO₂ between 52.10 and 54.00% and some core and interiors analyses from Bridge Lake display Mg# of 93.10 to 95.80 and SiO₂ from 53.20 to 53.60% (Figure 4.9B top right). This group corresponds to group B.

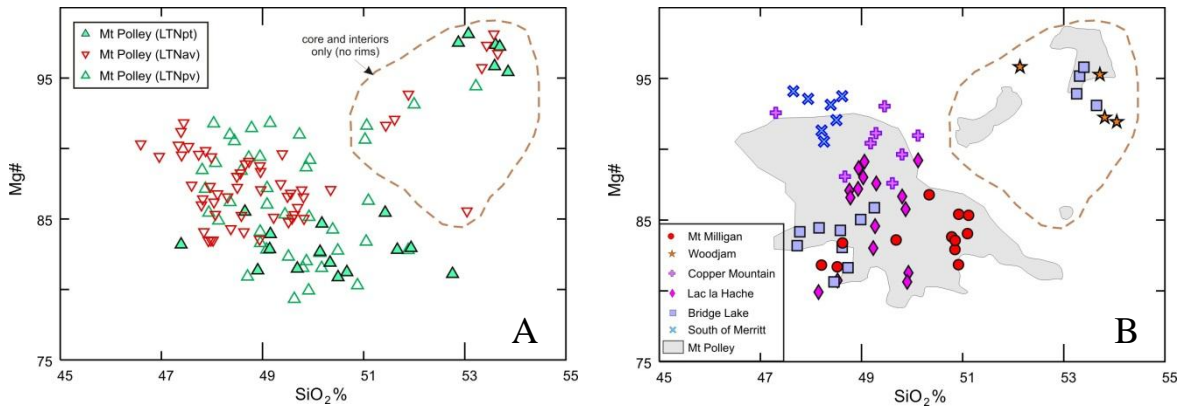


Figure 4.9. Chemical distribution based on the content of SiO_2 and Mg# from electron microprobe (EMP) analyses of clinopyroxene crystals in basalts of the Nicola Group. High Mg# is indicative for primitive melts . A) Clinopyroxene analyses from tree map units from the Mount Polley area, dashed brown line outlines some pyroxene analyses from core and interior (no rims). B) Clinopyroxene analyses from different localities along the Nicola Group compared with analyses from Mount Polley. Dashed brown line outlines pyroxene analyses from Woodjam, with some core and interior analyses from Bridge Lake and Mount Polley (group B).

At Mount Polley, overall calculated Fe^{3+} within clinopyroxene presents values from 0.04 to 0.19cpfu and Al^{IV} ranging between 0.036 and 0.25cpfu (Figure 4.10A). Overlap among the units is common, but, some trends in the data can be recognized. Pyroxene from LTNv has consistently higher calculated Fe^{3+} (~0.11-0.19cpfu) and Al^{IV} (~0.14–0.25cpfu) content, compared to Fe^{3+} (0.04–0.13cpfu) and Al^{IV} (0.006–0.15cpfu) from LTNpt. While LTNpv, show Fe^{3+} (0.079-0.181cpfu) and Al^{IV} (0.077-0.213cpfu) contents overlapping the other two units (Figure 4.10A).

Variations in clinopyroxene composition for the other studied areas show that, Copper Mountain displays Fe^{3+} contents from 0.11 to 0.19cpfu and Al^{IV} between 0.14 and 0.22cpfu, Lac la Hache Fe^{3+} from 0.09 to 0.14cpfu and Al^{IV} from 0.13 to 0.18cpfu, Bridge Lake has Fe^{3+} values of 0.12 to 0.15cpfu and Al^{IV} between 0.16 and 0.2cpfu, and South of Merritt Fe^{3+} from 0.15 to 0.17cpfu and Al^{IV} of 0.18 to 0.20cpfu. All of these overlap with most of the LTNv analyses from Mount Polley (Figure 4.10B).

Clinopyroxene analyses from Woodjam display $\text{Fe}^{3+} < 0.08\text{cpfu}$ and Al^{IV} between 0.006 and 0.06cpfu. Some analyses (core and interiors) from Bridge Lake and Mount Polley present similarly low Fe^{3+} and Al^{IV} contents (Figure 4.10B left bottom). These analyses mostly correspond to group B.

Clinopyroxene analyses from Mount Milligan present Fe^{3+} from 0.06 to 0.10cpfu and Al^{IV} from 0.10 to 0.20cpfu, and do not fit in any of the two groups described above, but most of the analyses lie closer to group B than to group A (Figure 4.10B).

Pyroxene crystals contain sufficient Si and Al to fill the tetrahedral site (Al^{IV}), except for few core and interior analyses from Mount Polley and Bridge Lake samples (Appendix B, Table B5), which require addition of Fe^{3+} (0.003–0.018 cpfu). These analyses form part of the group B in Figure 4.8 (top left) and Figure 4.9 (top right).

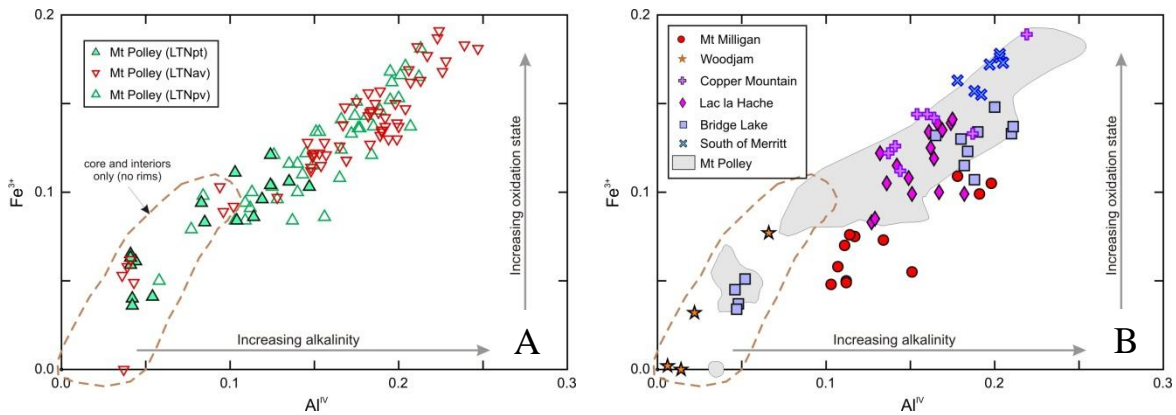


Figure 4.10. Cation relationships for clinopyroxenes from samples of Nicola Group basalts: A) direct relationship between Al^{IV} and Fe^{3+} cpfu in pyroxene composition from core to rim from three map units of Mount Polley brown line outlines some core and interior (no rims) pyroxene analyses; B) Comparison of clinopyroxene compositions from different localities along the arc with clinopyroxene from Mount Polley. Dashed brown line outlines pyroxene analyses from Woodjam, with some core and interior analyses from Bridge Lake and Mount Polley (group B).

4.5.1.2 Fe-Ti Oxide Minerals

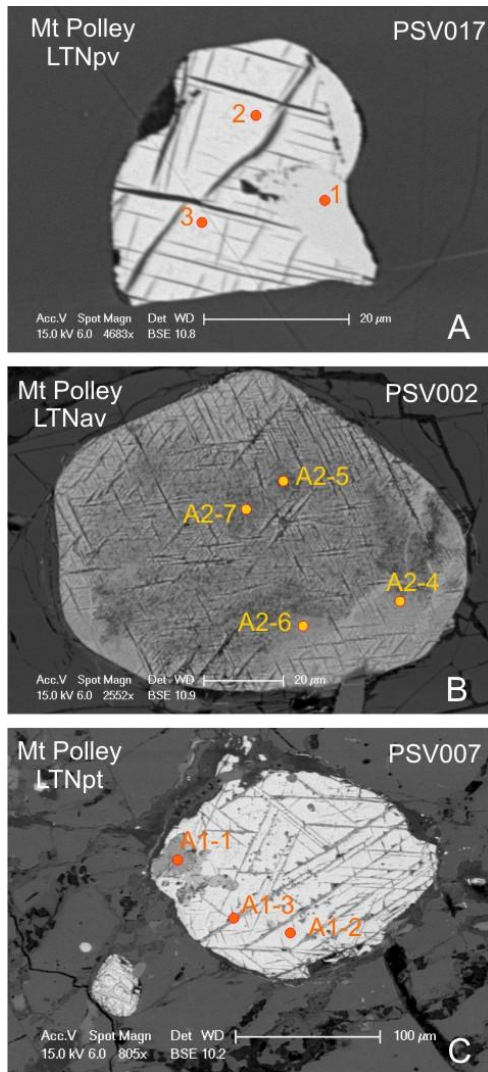


Figure 4.11. Representative backscattered electron images of Fe-Ti-oxide minerals from Mount Polley; electron microprobe (EMP) analytical spots are shown in red-orange dots: A) magnetite with lamellae of titanomagnetite, maghemite at the border of the grain (right side of the crystal); B) magnetite composition in the core (dark gray) and titanomagnetite composition at the border (light gray) of the crystal; C) Ferropseudobrookite lamellae (dark gray) within titanomagnetite grain (light gray).

Different spots within Fe-Ti oxide minerals were analyzed in this study (e.g. Figure 4.11), analyses are presented in the Appendix B-Table B6. Opaque inclusions (Fe-Ti oxide) in clinopyroxene are consistently present in the three map units of Mount Polley. However, Fe-Ti oxide inclusions do not have a uniform distribution in the different arc segments sampled along the Quesnel terrane. Mount Polley, Woodjam, Copper Mountain, Lac La Hache and South of Merritt have a consistent presence of Fe-Ti oxides (e.g. Figure 4.7A) while in Mount Milligan and Bridge Lake, Fe-Ti oxide inclusions in pyroxene are normally absent (e.g. Figure 4.7B).

These oxides exhibit subsolidus exsolution features, and distinctive compositions and textures (Figure 4.11). At Mount Polley, representative analyses of primary Fe-Ti oxides show variable Fe^{2+} , Fe^{3+} and Ti contents (Figure 4.12A). Most of the analyzed Fe-Ti oxide minerals from LTNpv, LTNav and some from LTNpt have high ferric iron values plotting as magnetite and maghemite (cation-deficient spinel) (Banerjee, 1991), resulting from oxidation of magnetite and titanomagnetite. Some analyses from LTNav and LTNpt units show a composition of titanomagnetite (Figure 4.12A). Two analyses in exsolution lamellae within a crystal from the LTNpt unit are depleted in Fe^{3+} and relatively enriched in Ti and Fe^{2+} , plotting around the ferropseudobrookite field (Figure 4.11C and 4.12A).

The Fe-Ti oxides from Mount Milligan plot as a relatively Fe²⁺-enriched magnetite. While crystals analyzed from samples of Woodjam, Copper Mountain, Lac la Hache, Bridge Lake and South of Merritt tend to increase the ferric iron content, falling in the titanomagnetite, magnetite and maghemite fields (Figure 4.12B), coinciding with most of the analyses from Mount Polley.

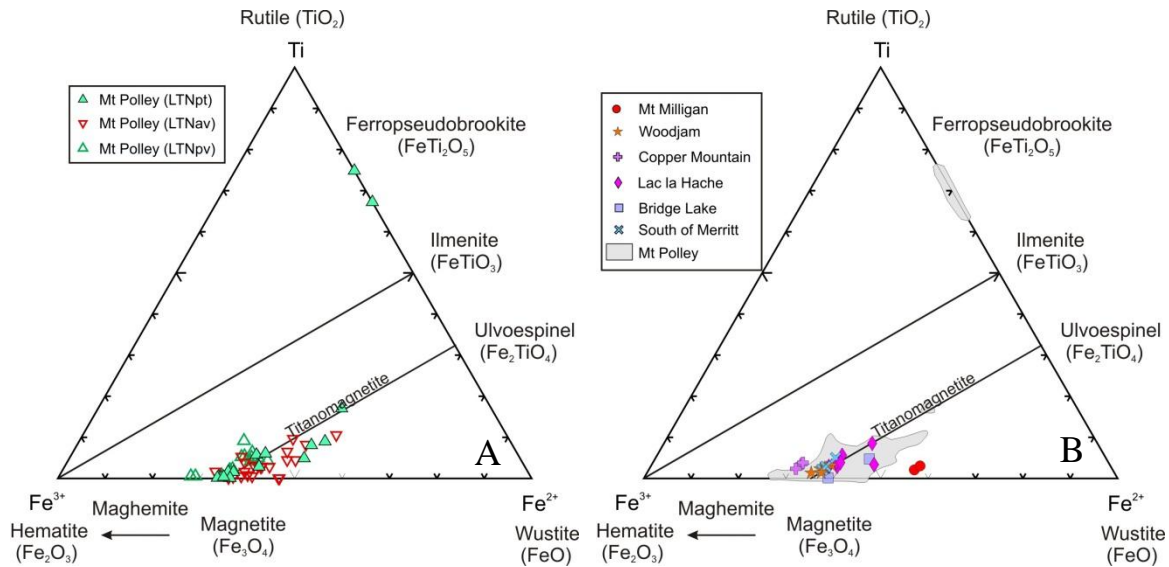


Figure 4.12. The Fe³⁺-Ti-Fe²⁺ relative amounts of Fe-Ti-oxide minerals as inclusions in clinopyroxene crystals of the Nicola Group, plotted in FeO-Fe₂O₃-TiO₂ space after the method of Taylor (1964). A) Fe-Ti oxide composition from three map units of Mount Polley. B) Fe-Ti oxide composition of different localities along the arc, compared with Mount Polley.

Cr content within Fe-Ti oxides is relatively low in almost all areas (≤ 0.6 cpfu) (Appendix B-Table B6), nevertheless, at Mount Milligan and Bridge Lake, Cr shows higher numbers of (1.3-3.2cpfu) and ~ 5.0 cpfu, respectively.

Most of Fe-Ti oxide compositions from LTNav and LTNpt units, (Appendix B, Table B6) exhibit an unusually high SiO₂ and CaO content, showing values reaching up to 10.8 and 6.83%, respectively. Most of the high SiO₂ values are directly proportional to the CaO content (Figure 4.13A). Analyses from the LTNpv unit are generally depleted in SiO₂ and CaO.

Fe-Ti oxides from Mount Milligan, Woodjam, Copper Mountain, Lac la Hache, Bridge Lake and South of Merritt present low SiO₂ and CaO concentrations (<1.50 and <1.00% respectively), with the exception of two analyses, one from Lac la Hache and the other from Bridge Lake, which display higher values (Figure 4.13A).

At Mount Polley, oxide totals are low, most of the samples contain between ~90.5 and ~93.5wt% (Figure 4.13B, Appendix B-Table B6), showing overlap between the three units. The totals do not correlate with the SiO₂ content in Fe-Ti oxide (Figure 4.13B). Mount Milligan, Copper Mountain, Lac la Hache and Bridge Lake exhibit total oxide values comparable with those of Mount Polley. While Fe-Ti oxides from Woodjam and South of Merritt present lower total oxide numbers from ~89 to ~91.50wt% (Figure 4.13B).

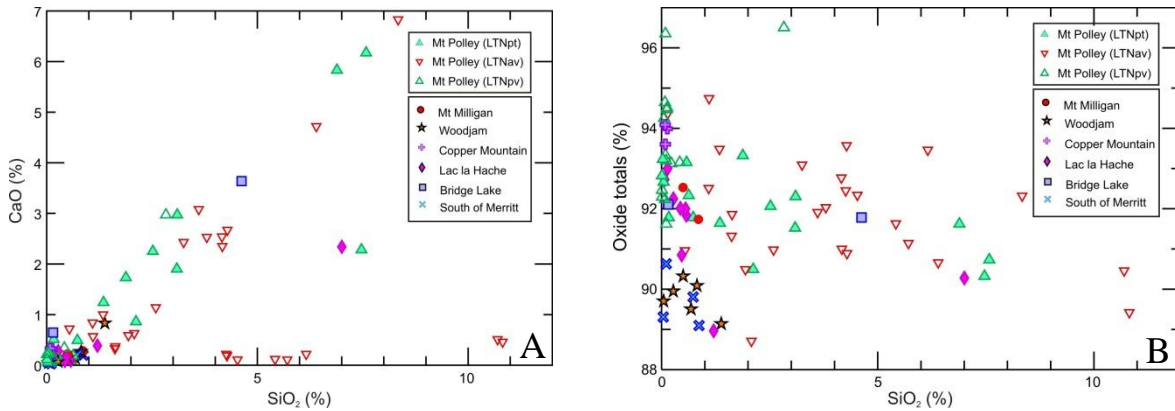


Figure 4.13. Amounts of SiO₂, CaO and oxide-totals of Fe-Ti oxide inclusions in clinopyroxene from rocks from the Nicola Group. A) Plot showing anomalous SiO₂ and CaO contents within most of the Fe-Ti oxides in the LTNpt and LTNNav units from Mount Polley. B) Graph denoting the low oxide-totals content of the Fe-Ti oxides from different localities along the arc.

4.5.1.3 Apatite

At Mount Polley, apatite is a relatively abundant accessory mineral with grain sizes of ≤ 5 to 250 μm , which occurs as inclusions in clinopyroxene within basalts (Figure 4.14). Chemical composition of apatite crystals of the LTNpv and LTNNav units are presented in Appendix B-Table B7. Apatite grains of the LTNpt unit could be not analyzed because they were too small ($< 5\mu\text{m}$).

LTNpv presents average elemental values of chlorine (0.33apfu) and fluorine (0.73apfu), while in the unit LTNNav the average values are 0.07 and 1.45apfu, respectively (Figure 4.15; Appendix B-Table B7). Apatite of the two studied units has sulfur contents below detection limit. Hydroxyl was calculated by stoichiometry from fluorine and chlorine (Appendix B-Table B7) assuming that it, along with measured fluorine and chlorine, fills the halogen site and that there are no vacancies or other significant anion substitutions. LTNpv is relatively chlorine-rich and fluorine-poor compared to LTNNav. The average composition of apatite crystals for LTNpv is Ca_{9.9}(P_{5.96}

O_{24}) ($OH_{0.95} F_{0.73} Cl_{0.33}$), and for LTNav is $Ca_{9.72} (P_{5.9} O_{24}) (OH_{0.48} F_{1.45} Cl_{0.07})$. Apatite from the two units described above fall in the fluorapatite group (Klein and Hurlbut, 1993).

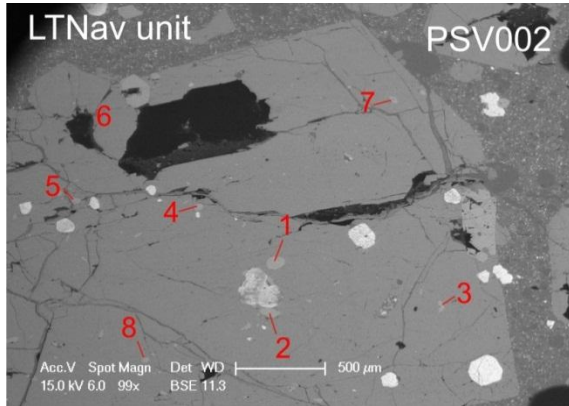


Figure 4.14. Representative backscattered electron image of a clinopyroxene crystal, showing apatite inclusions; electron microprobe (EMP) analysis spots are indicated with red numbers.

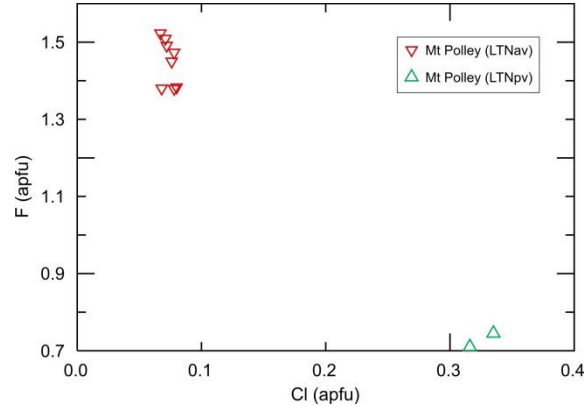


Figure 4.15. Chlorine and fluorine compositions of apatite crystals included in pyroxenes from basalts of the LTNpv and LTNNav units from Mount Polley

Considering the results presented above (low S and Cl contents), apatite analyses from basalts within the Mount Polley area, no further apatite crystals were analyzed from other arc segments.

4.6 DISCUSSION AND CONCLUSIONS

All basalts from Mount Polley present similar chemical characteristics, being alkalic and depleted in SiO_2 . Nevertheless, the unit LTNav shows some differences, presenting more depletion in SiO_2 , higher alkali and lower MgO contents, as well as a slightly higher degree of differentiation when using the geochemical index $Fe_2O_3(t)+MgO$ versus Al_2O_3 , when compared to the LTNpv and LTNpt units (Figure. 4.1A, 4.2A and 4.3A).

Most rocks from the other areas studied along the Nicola arc (Mount Milligan, Copper Mountain, Lac la Hache, Bridge Lake and South of Merritt), fall in the alkalic suite, are to some extent depleted in SiO_2 , and contain less alkalis and similar MgO concentrations when compared to rocks from Mount Polley (Figure. 4.1B and 4.2B). Basalts from these areas show a similar degree of differentiation as Mount Polley, except those from Bridge Lake which have a more primitive signature.

Basaltic andesites from Woodjam show relatively high SiO₂ and alkali content, and lower MgO values (Figure 4.1B and 4.2B). This arc segment is more differentiated than basalts from the other localities along the belt (Figure 4.3B).

Plotting the differentiation index with respect to the latitude and longitude (Figure 4.16), it is possible to observe some variations in the degree of differentiation in basalts from the central part of the Nicola Group, Woodjam, having the most differentiated rocks. However, variations within sample suites from particular localities were noted, as well. For instance, at Lac la Hache, basalts from the northern-part are slightly more primitive than basalts from the south (Figure 4.16A). Also, basalts from the northern part of South of Merritt are more differentiated than basalts from the south (Figure 4.16A).

East-west variations in differentiation in south-central BC (Figure 4.16B) show that basalts from the eastern side of the belt (Bridge Lake) are generally more primitive than rocks from the west side (Mount Polley). This evidences a tendency of increasing differentiation toward the west. Differentiation could be directly related to lithospheric thickness, and basalts from the western side of south-central Nicola Group could be produced from a mantle wedge overlain by a relatively thick lithosphere. The relative location of the eruptive centers with respect to the arc and back-arc settings may have influenced in the degree of differentiation as well.

All basalts from Mount Polley show relatively uniform Nb values (Figure 4.1A and 4.2A). The unit LTN_{av} contains higher Th content than the other two units (Figure 4.3A1, 4.3B1). Samples from LTN_{pt} are relatively enriched in Zr (Figure 4.2A). Basalts from the other areas along the Nicola Group (Mount Milligan, Woodjam, Copper Mountain, Lac la Hache, Bridge Lake and

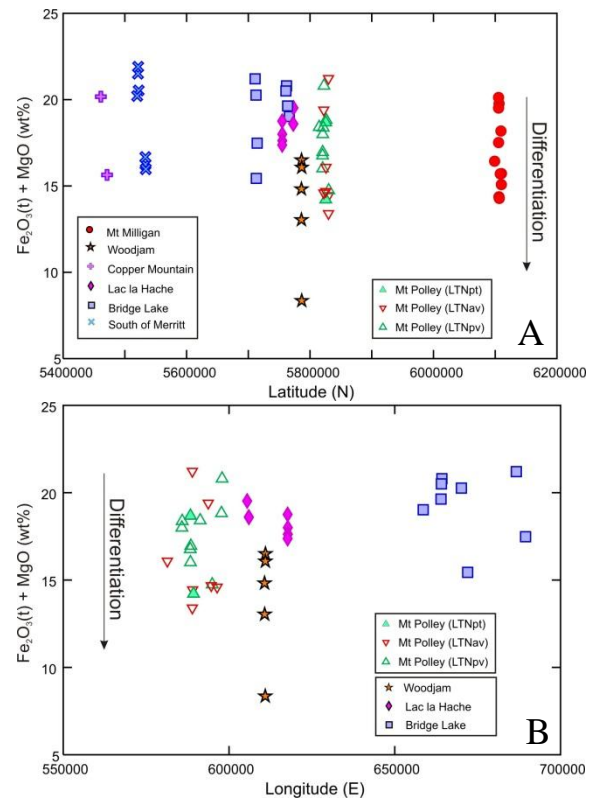


Figure 4.16. The (Fe₂O_{3t}+MgO) index showing variation in the differentiation of rocks along and across the Nicola Group. A) North to south variations of differentiation between basalts along the belt. B) East to west changes in differentiation in the central-south part of the Nicola arc.

South of Merritt) display narrow variations between themselves with respect to Th, Zr and Nb (Figure 4.1B and 4.2B); however, basalts from Mount Milligan are relatively enriched in Nb.

Variation in incompatible elements shows different sources of magma, and degree of partial melting. In this regard, lower abundances of Zr, Yb and Nb in island-arc basalts represent a greater degree of partial melting (Rollinson, 1993). The degree of partial melting in arcs varies with crustal thickness, and hence with the length of the melting column (i.e., thickness of mechanical lithosphere); this column varies from ca. 15 km to over 50 km beneath different arcs (Plank and Langmuir, 1988; Davies and Bickle, 1991; Hawkesworth et al., 1992). Thorium content is controlled by the alkalinity of the rock, so that the more alkaline rocks will become more Th enriched (Gabelman, 1977 and Boyle, 1982 *in* Mernagh and Miezitis, 2008). The increase in alkalinity correlates with greater depths and lower percentages of partial melting (Winter, 2010).

At Mount Polley, the relatively high Zr and Th values suggest low degrees of partial melting. The LTNav unit contains the highest Th concentrations, in agreement with its more alkalic nature compared to the other two units, it is also evidenced by major elements chemistry (Figure 4.1A and 4.2A).

Mount Polley exhibits relatively similar values in Th/Nb ratios for the three map units, while Ce/Yb ratios are distinct between these units. LTNav shows the highest Ce/Yb values, LTNpt the lowest and LTNpv displays intermediate values (Figure 4.5A). The other areas studied along the arc display a wider range of Th/Nb ratios with respect to Mount Polley. However, Mount Milligan presents consistently lower Th/Nb ratios. The Ce/Yb ratios are relatively similar between the different areas, falling within the LTNpv and LTNpt ranges (Figure 4.5B).

North to south variation of Th/Nb and Ce/Yb ratios on rocks from the different localities studied along the arc (Figure 4.17), evidences that Mount Milligan is depleted in Th/Nb ratios (Figure 4.17A), while LTNav of Mount Polley show the highest Ce/Yb ratios (Figure 4.17B).

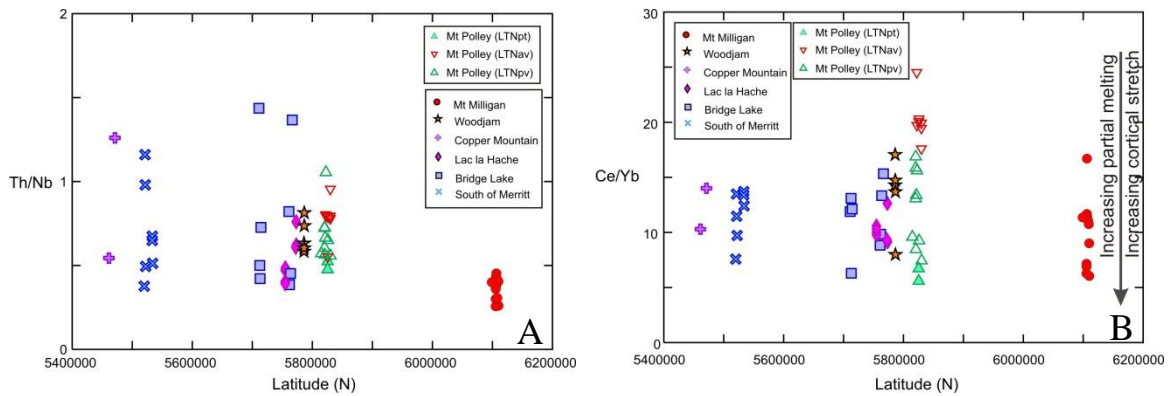


Figure 4.17. Incompatible element ratios of rocks along the Nicola Group. A) North to south variations of Th/Nb ratios along the belt. B) North to south variations of Ce/Yb ratios along the arc.

The Ce/Yb ratios offer a sensitive indicator of tectonic changes in the lithosphere. This can be applied to basalts because they will not be radically affected by crystal fractionation (Ellam, 1992). Low Ce/Yb ratios imply a thinner lithosphere, suggesting relatively high degree of partial melting (Hawkesworth et al., 1993) during lithospheric extension (Ellam, 1992). High Ce/Yb ratios suggest lower degrees of partial melting related to a thicker lithosphere during eruption (Ellam, 1992; Hawkesworth et al., 1993; Doe, 2002).

Considering the Mount Polley units chronologically, it is possible to suggest the following: The LTNpv basalts, which present intermediate to low Ce/Yb ratios were produced in an extensional tectonic setting. This period was followed by slightly less extensional tectonics, where the amount of lithospheric extension was more modest, probably producing lower degrees of partial melting in a deeper portion of the mantle-wedge, generating the more-alkalic LTNv basalts, which show the highest Ce/Yb ratios. Then, the area underwent a period of stretching, probably producing a slight thinning of the lithosphere, and a subsequent asthenospheric upwelling, which suffered higher degrees of partial melting, forming the LTNpt basalts, exhibiting the lowest Ce/Yb ratios.

Basalts from Mount Milligan are discriminated from the other areas by their lower Th/Nb ratios (Figure 4.17A), resulting from melting of a different portion of mantle wedge characterized by an incompatible element signature different from other areas along the arc. The basalts here probably originated in a relatively extensional environment, presenting only subtle variations in the degree of extension, considering that most of the samples display low Ce/Yb ratios (Figure 4.17B).

Copper Mountain, Bridge Lake and South of Merritt share similar Th/Nb ratios showing an overall wider range than basalts from Mount Polley (Figure 4.17A). Basalts from these areas, probably originated from sources with similar proportions of incompatible elements and degrees of partial melting, and were produced in a moderately extensional tectonic setting, resembling those from the LTNpv unit of Mount Polley (Figure 4.17B). Basaltic andesites from Woodjam exhibit a narrower range in Th/Nb ratios than rocks from the other areas (Figure 4.17B), suggesting that they may have originated from a geochemically distinctive portion of the mantle wedge, and from a discrete extensive tectonics, like the LTNpv unit of Mount Polley, in view of its Ce/Yb ratios (Figure 4.17B). Basalts from Lac la Hache, show relatively low Th/Nb ratios, and a narrow variation of Ce/Yb ratios, indicating that the magma was produced in a moderately extensional environment, fitting within the range of rocks from the LTNpv unit of Mount Polley (Figure 4.17).

Variations in $\text{Fe}^{3+}/\text{Fe}^{2+}$ ratios and magnetic susceptibility readings were used to discriminate the arc segments into three different groups. Group 1 includes basalts from Mount Milligan, Copper Mountain and Bridge Lake. This group is characterized by relatively low oxidation state (low $\text{Fe}^{3+}/\text{Fe}^{2+}$ ratios <0.60 and generally low magnetic susceptibility $<1.30 \times 10^{-3}$ SI units; Figure 4.6), with the exception of two samples, one from Mount Milligan and another from Bridge Lake, which display higher magnetic susceptibilities. Group 2 comprises most samples from the Mount Polley, Lac La Hache and South of Merritt areas. Here basalts are relatively oxidized (moderate $\text{Fe}^{3+}/\text{Fe}^{2+}$ ratios ranging between 0.60 and 3.00, and a wide range of magnetic susceptibilities from 0.40×10^{-3} to 111.00×10^{-3} SI units (Figure 4.6). And, Group 3 comprises basaltic-andesites from Woodjam, and some basalts from other localities, including, the LTNpv unit of Mount Polley (1 sample), Lac la Hache (1 sample) and 3 samples from South of Merritt, showing high oxidation state (high $\text{Fe}^{3+}/\text{Fe}^{2+}$ ratios >3 and low magnetic susceptibility $<1.62 \times 10^{-3}$ SI units). Rocks in this group are interpreted to have suffered a secondary-oxidation process due to alteration and/or weathering of their Fe-rich minerals (e.g., Fe-Ti oxides), which is also evidenced by the widespread presence of hematite in the rock (see Chapter 3).

Some of the EMP analyses from core and interiors in clinopyroxene from Mount Polley, assigned to group B, present 0-10mol%Fe, high Mg# and $\text{SiO}_2\%$, as well as, low Fe^{+3} and Al^{IV} cpdf values (Figure 4.8A, 4.9A and 4.10A) contrasting with most of the analyses that includes

core, interiors and rims, included in group A. Some core and interiors spot analyses from Bridge Lake and all the analyses from Woodjam also fall into group B (Figure 4.9B).

Chemical variation from core to interior to rim in Mount Polley and Bridge Lake indicates a pyroxene-fractionation trend, evidenced by the presence of spot analyses within groups A and B. In group B, cores are richer in Mg and Si, and, poorer in Fe, Ti and Al, than rims, suggesting a rapid change in the temperature-pressure-composition (T-P-X) parameters during crystallization. Thus, a few samples from Mount Polley and one sample from Bridge Lake suggest a transition from a primitive, relatively reduced and less alkaline magma (group B), to a less primitive, relatively oxidized and more alkaline one (group A). Clinopyroxene from the Woodjam area denotes a relatively homogeneous, primitive and reduced magma chamber (group B). This contradicts results from petrography and whole-rock chemistry, where basaltic-andesites from Woodjam are the most evolved and less primitive than rocks from the other areas along the arc. The clinopyroxene analyzed from Woodjam may represent an inherited phenocryst from a primitive cumulate and is not necessarily representative for the bulk rock.

The Al^{IV} and Fe^{3+} contents in pyroxene are indicators of alkalinity and oxygen fugacity of magma (Kushiro, 1960; LeBas, 1962), respectively. Pyroxene from LTNav and LTNpv units from Mount Polley, Copper Mountain, Lac la Hache, Bridge Lake, and South of Merritt, is more alkaline, and crystallized at higher oxygen fugacity, than the pyroxene crystals around LTNpt unit from Mount Polley, Mount Milligan, and Woodjam areas (Figure 4.10A and 4.10B).

Chemistry of Fe-Ti oxide inclusions in pyroxene can be grouped into two populations. The first one corresponds to crystals relatively rich in Fe^{3+} , such as magnetite from LTNpv and LTNav units at Mount Polley, Woodjam, Copper Mountain, Lac la Hache, and South of Merritt (Figure 4.12 and Appendix B-Table B7). The second group corresponds to grains relatively rich in Ti and Fe^{2+} , typically titanomagnetite showing locally subsolidus exsolution lamellae of ferropseudobrookite (Figure 4.11C), denoting relatively less oxidized conditions of formation for the LTNpt unit at Mount Polley (Figure 4.12). Mount Milligan and Bridge Lake are included in the latter group due to the slightly elevated Cr content in their Fe-Ti oxides (Appendix B-Table B7). The presence of maghemite within the Fe-Ti oxides along the arc (Figure 4.11A) can be explained by alteration and/or weathering of rocks.

Fe-Ti oxides from LTN_{av} and LTN_{pt} from Mount Polley show an unusual high SiO₂ and CaO content (Figure 4.13A), probably related to an alteration event. It is worth noting that, there is no evidence of silicon and/or calcium-rich mineral inclusions within the studied Fe-Ti oxide crystals and that fractures within or close the analyzed grain spots were not detected in the SEM and EMP devices (e.g., Figure 4.11). The high Si and Ca contents remain unexplained.

The low total oxide (wt%) of Fe-Ti oxide crystals may be explained by the fact that during microprobe data reduction, the oxygen is fixed by stoichiometry; thus, the Fe:O ratio is set to a default of 1:1. However, some iron is ferric (Fe:O 2:3), which introduces some undercounting. Lower total oxide (wt%) could also be explained by the presence of small amounts of trace elements, which were not analyzed in this study.

This research shows that the oxidation state predicted from Fe-Ti oxide chemistry is not proportional to the magnetic susceptibility of the rock (Figure 4.6). The Fe-Ti oxide minerals have variable magnetic susceptibility values (Hunt et al., 1995; Peters and Dekkers, 2003), and magnetic susceptibility of rocks depends on the abundance, as well as, type of Fe-Ti oxide minerals. Irving (1970) noted that low temperature seafloor alteration can cause maghematization of FeTi oxides within basalts, this decreases the magnetic susceptibility of rocks, thus, the magnetic susceptibility lectures collected on basalts along the Quesnel terrane represent only the minimum magnetic response of the rock, due to the presence of maghemite, and considering the widespread low grade metamorphism the entire terrane underwent (Read et al., 1991; see Chapter 3).

Halogen and sulfur data obtained from apatite in the LTN_{pv} and LTN_{av} units of Mount Polley is considered to represent a minimum amount of the composition of the source magma, since halogens are lost via degassing in volcanic rocks. Cl is typically degassed from magmas because it is highly soluble in fluids, whereas most magmatic F is retained due to its high solubility in melts (Aiuppa et al., 2009). This can partially explain the relative chlorine depletion and fluorine enrichment in the LTN_{av} unit (Figure 4.15). However, sulfur content is not detectable in the two map units studied by means of apatite analysis. Analytical problems with respect to halogen content in apatite (e.g., Stormer et al., 1993; Piccoli and Candella, 1994; Raudsepp, 1995) were not considered in this research, since the values obtained are homogeneous themselves

(Appendix B-Table B7). The results obtained from apatite chemistry show a slight difference in the source magma of the two studied units.

The results presented above show some systematic differences among the basalts, based on the chemistry of whole rock, clinopyroxene, Fe-Ti oxide and apatite. It implies that basalts along the Nicola Group were originated from a heterogeneous mantle wedge, and that basalt chemistry reflects regional, as well as, local tectonic variations in the lithosphere.

Chemical variations on basalts along the arc indicate that basalts from the LTNav unit of Mount Polley represent an anomaly within the studied areas. It is the most alkaline, differentiated, oxidized basalt and likely erupted in a relatively compressive tectonic setting.

In summary, it can be concluded that the LTNav and LTNpv units from Mount Polley, Copper Mountain, Lac la Hache, and South of Merritt were generated in a tectonic setting transitional between subtle to moderate extension. The magma-generating conditions were relatively similar within that group of basalts, which are likely oxidized and relatively alkaline. Such rocks are found in spatial and temporal proximity to porphyry style mineralization at Mount Polley and Copper Mountain; Lac la Hache may be part of this group; nevertheless, the age of the mineralization is unknown. Based on this empiric relationship, the source of the volcanic rocks around South of Merritt may also have had the potential to develop comagmatic porphyry-style mineralization.

The Bridge Lake area might represent a transition between reduced and oxidized magma, Mount Milligan may be indicative of a reduced magma-generating environment, all produced in a relatively extensional tectonic setting. The sources of these lavas had probably less potential to evolve into fertile intrusions, and the source-magma of the basaltic-andesites at Woodjam can not be classified as neither reduced nor oxidized due to the presence of probably inherited clinopyroxene phenocrysts and by the relatively high degree of alteration the Fe-rich minerals underwent.

Chemical changes found at Mount Polley, suggest that magmatism is extensively controlled by local changes in the tectonic setting. Periods of stretching and shortening could occur in relatively short periods of time. These changes imply a relatively active and continuous

magmatic system, which could be the key in the formation and evolution of fertile magmatic chambers.

This research is based on the mineral chemistry of basalt. To produce porphyry mineralization, a change in the tectonic setting that results in intrusive rather than extrusive magmatism is necessary. However, this work suggests that indications for a favourable magma-generating environment could be also recorded in the precursor volcanic rocks in prospective arc segments.

CHAPTER 5: CARBON AND OXYGEN ISOTOPIC COMPOSITIONS OF SECONDARY CARBONATE MINERALS, IMPLICATIONS FOR POST-EXTRUSION PROCESSES AFFECTING THE NICOLA GROUP BASALTS

5.1 INTRODUCTION

Basalts within the Nicola Group are affected by widespread low grade metamorphism, presenting chlorite, epidote, calcite, clays, and occasionally hematite and zeolites, which correspond to the zeolite to prehnite-pumpellyite metamorphic facies (Read et al., 1991). However, the calcite-chlorite-epidote assemblage is also widespread in propylitic halos around porphyry deposits and may extent as far as 1 km into the surrounding wall rock (Sillitoe, 2010), although, alkalic porphyry deposits display narrower alteration footprint (e.g., Jensen and Barton, 2000).

The nature of secondary carbonate minerals, which form part of the alteration mineral assemblage of basalts in the Nicola Group, was investigated in areas hosting porphyry style mineralization, such as Mount Polley, Mount Milligan, and Lac la Hache. The Bridge Lake and South of Merritt areas, representing apparently barren parts of the arc with respect to porphyry mineralization, were also considered.

The aim of this chapter is to distinguish propylitic porphyry-related alteration from regional seafloor alteration (low grade metamorphism), as well as to discriminate different parts of the arc. For these, carbon $\delta^{13}\text{C}_{\text{PDB mineral}} (\text{‰})$, and oxygen $\delta^{18}\text{O}_{\text{SMOW mineral}} (\text{‰})$ isotopic compositions of carbonate minerals within altered basalts were utilized.

5.2 ANALYTICAL PROCEDURES

Twenty eight pulps from rocks were analyzed for stable carbon $\delta^{13}\text{C}_{\text{PDB}} (\text{‰})$ and oxygen $\delta^{18}\text{O}_{\text{SMOW}} (\text{‰})$ isotopes using the spectroscopic instrument LGR DLT-100, model 908-0021 (Barker et al., 2011) at the University of British Columbia (UBC). This instrument analyzes CO_2 gas extracted from carbonates after rock powder has been exposed to 100% phosphoric acid at ambient temperature for 2 hours. The UBC-standards LM4 and BN13 (Barker et al., 2011) were analyzed every 12 samples.

5.3 CARBON AND OXYGEN ISOTOPES

Carbonate-minerals are filling vesicles and fractures within the volcanic rocks used in this study; these minerals were identified in hand specimens using 10% HCl solution and also in petrographic thin sections analyses. However, due to their small size and quantity (1-2% within the rock) was not possible to identify the specific mineral carbonate specie(s) present in the rocks.

The $\delta^{13}\text{C}_{\text{PDB mineral}} (\text{‰})$ and $\delta^{18}\text{O}_{\text{SMOW mineral}} (\text{‰})$ isotopic compositions of carbonate-minerals within basalts (Appendix C - Table C1) are shown in Figure 5.1. Two groups can be distinguished, the first group includes rocks from Mount Polley, Lac la Hache and South of Merritt, displaying $\delta^{13}\text{C}$ values between -5.6 and +2.2‰ and $\delta^{18}\text{O}$ from +12.3 to +20.5‰, with the exception of carbonate minerals from one basalt from South of Merritt (sample SSV137) which present a significantly lower $\delta^{18}\text{O}$ value of +5.1‰. The other group includes basalts from Mount Milligan and Bridge Lake, presenting lower $\delta^{13}\text{C}$ and $\delta^{18}\text{O}$ values compared to the former group, showing $\delta^{13}\text{C}$ values between -9.2 and -6.4‰ and $\delta^{18}\text{O}$ numbers from +10.6 to +14.2‰, with the exception of two samples, one from Mount Milligan (sample MTB030), displaying a lower $\delta^{13}\text{C}$ value of 16.1‰ and higher $\delta^{18}\text{O}$ value of +19.4‰ and another one from Bridge Lake (sample BTB053), exhibiting $\delta^{13}\text{C}$ of 15.4‰, and $\delta^{18}\text{O}$ of +8.3‰.

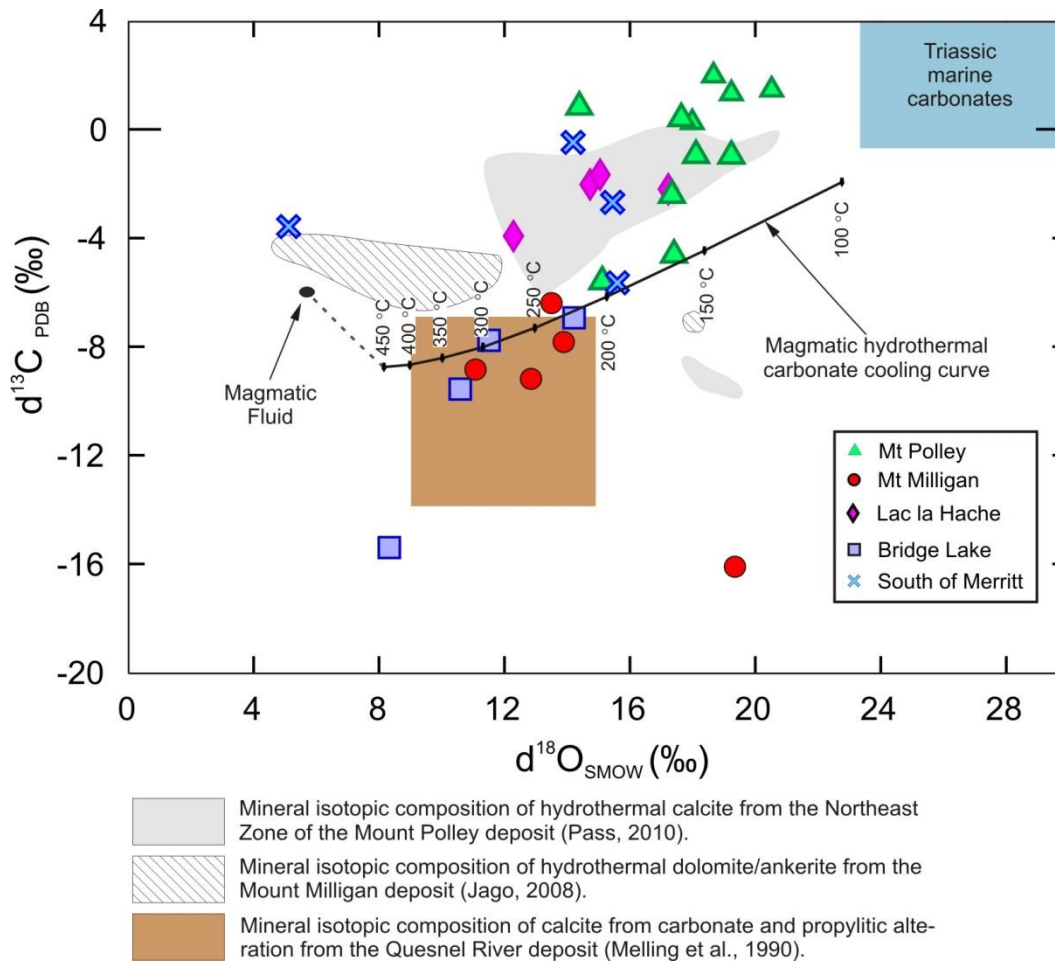


Figure 5.1. Plot showing the $\delta^{18}\text{O}_{\text{SMOW}}$ (‰) and $\delta^{13}\text{C}_{\text{PDB}}$ (‰) mineral compositions of carbonate from altered basalts along the Nicola Group; fields for Triassic marine carbonate rocks (Veizer et al., 1999), and magmatic hydrothermal carbonate cooling curve (Pass, 2010), are shown for comparison.

5.4 DISCUSSION

Studies on seafloor alteration indicate that carbonate minerals can form to depths of at least 550 metres into the oceanic basement (Staudigel et al., 1981), and that the water/rock ratios and extent of exchange between circulating seawater and recently formed crust, influence the rate of heat-loss and the chemical evolution of the hydrothermal fluid and rock (Staudigel and Hart, 1983). On this basis, the generally high values in $\delta^{18}\text{O}$ of secondary carbonate minerals within altered basalts from Mount Polley, Lac la Hache and South of Merritt, may be related to lower

water/rock ratios than carbonate minerals in basalts from Mount Milligan and Bridge Lake. The former could have formed in a system with restricted fluid circulation, being relatively depleted in $\delta^{18}\text{O}$. The decrease of $\delta^{18}\text{O}$ in carbonate-minerals can be attributed to formation conditions of progressively higher water/rock ratios (Sverjensky, 1981). However, Böhlke et al. (1981) suggests that the oxidation of titanomagnetite in oceanic basalts produce an increase in whole-rock $\delta^{18}\text{O}$ values of 1 to 2‰ relative to unaltered basalts. Considering the abundant hematite and the consistent maghematization of Fe-Ti oxides of basalts from Mount Polley, Lac la Hache and South of Merritt (see Chapter 3 and Chapter 4), the secondary carbonate minerals within these areas may underwent a change in their isotopic composition, increasing their $\delta^{18}\text{O}$ values.

The sources of C in the ocean floor are seawater HCO_3 -ion and magmatic CO_2 (Stakes and O'Neil, 1982). Triassic marine carbonates precipitated from seawater have $\delta^{13}\text{C}$ values generally around -1 to +5‰ (Veizer et al., 1999; Figure 5.1). Whereas, mantle-derived carbon found in carbonatites (Taylor et al., 1967), in CO_2 inclusions in oceanic basalt (Pineau et al., 1976), and dissolved in waters from submarine hot springs at the Galapagos hydrothermal vents (Craig et al., 1980), typically have $\delta^{13}\text{C}$ values of -5 to -8‰. Thus, carbonates from most basalts from Mount Polley, Lac la Hache and South of Merritt suggest seawater HCO_3 -ion as the predominant source of C, showing $\delta^{13}\text{C}$ values similar to Triassic marine carbonates (Figure 5.1) related to seafloor alteration. However, some samples exhibit $\delta^{13}\text{C}$ values similar to those from a magmatic source, plotting near to the magmatic hydrothermal carbonate cooling curve (Figure 5.1); this suggests the interaction of those basalts with hotter fluids during carbonate minerals precipitation.

Secondary carbonate minerals from Mount Milligan and Bridge Lake are interpreted to have formed at moderately high temperatures from predominantly magmatic carbon, reflected in their relatively low $\delta^{13}\text{C}$ values and their proximity to the magmatic hydrothermal carbonate cooling curve (Figure 5.1). For comparison the Quesnel River intrusion-related propylite-type gold deposit (Panteleyev et al., 1996) was considered. This deposit is hosted in the Nicola arc, and associated with a Late Triassic alkalic stock (Melling et al., 1990). The deposit presents carbonate-altered and propylitically-altered rocks, where the latter are associated with gold. Calcite from both alteration types has $\delta^{13}\text{C}$ values from -14 to -7‰ and $\delta^{18}\text{O}$ varying from +9 to +15 ‰ (Melling et al., 1990), overlapping with most of the rocks from Mount Milligan and

Bridge Lake (Figure 5.1). The isotopic composition of dolomite/ankerite from the Mount Milligan deposit shows $\delta^{18}\text{O}$ values between +4.39 and +17.98‰ and $\delta^{13}\text{C}$ numbers from -3.84 to -7.14‰ (Figure 5.1), interpreted to represent a combination between magmatic and meteoric fluids (Jago, 2008).

The samples with the lowest $\delta^{13}\text{C}$ value \sim -16‰ from Mount Milligan and Bridge Lake (Figure 5.1), suggest that C from organic-matter source has been important (e.g. Schidlowski, 1988). The sample from South of Merritt, which shows an anomalous $\delta^{18}\text{O}$ value \sim +5‰, is consistent with later interaction with meteoric water (e.g. Craig, 1961), plotting close to the samples from the Mount Milligan deposit.

The isotopic data presented above imply that the environment of secondary carbonate minerals formation was variable between different areas of the arc. Thus, Mount Polley, Lac la Hache and South of Merritt basalts are interpreted to be extruded and sealed from the overlying water column, producing low water/rock ratios, and alteration was produced at low temperatures. In contrast, basalts from Mount Milligan and Bridge Lake may have been exposed to higher water/rock ratios, and potentially elevated fluid temperatures during seafloor alteration.

Calcite from the Northeast Zone of the Mount Polley deposit (Figure 5.1) has values $\delta^{18}\text{O}$ of +4.0 to +20.9‰ and $\delta^{13}\text{C}$ from -0.2 to -10.5‰, which is interpreted to have originated from the interaction between magmatic-hydrothermal fluids and limestone lenses (Pass, 2010). These isotopic compositions are similar to most samples from Mount Polley, Lac la Hache and South of Merritt. However, the source of the fluid which produces carbonates within the alteration assemblage in those basalts, has a magmatic or seawater origin, is not clear.

Stable isotope data presented here show that secondary carbonates within altered basalts along the Quesnel terrane can be discriminated considering the nature of their host rocks, thus, basalts from Mount Polley, Lac la Hache and South Merritt, formed from magmas with relatively high oxidation state (see Chapter 2 and Chapter 3), exhibit higher $\delta^{18}\text{O}$ and $\delta^{13}\text{C}$ values, compared to the relatively reduced basalts from Mount Milligan and Bridge Lake.

CHAPTER 6: SUMMARY AND CONCLUSIONS

Rocks in this study are Late Triassic and petrographically similar in the different studied areas, and are generally black to dark-green, clinopyroxene±plagioclase porphyritic basalts with variable Fe-Ti oxide content, patches and subhedral masses of hematite after olivine(?) are present in some areas; analcime phenocrysts are also locally present. Additionally, the rocks have secondary minerals such as chlorite, epidote, calcite, clays, and occasionally hematite and zeolites.

Whole rock chemistry shows that basaltic rocks studied in this research along the Nicola arc fall within the alkalic suite (Figure 4.1 B). However, a few samples from Bridge Lake and one from Mount Milligan, just cross the border into the sub-alkaline field.

The Al^{IV} and Fe^{3+} contents from clinopyroxene chemistry, used as indicators of alkalinity and oxygen fugacity of magma (Kushiro, 1960; LeBas, 1962), helped to discriminate the studied areas in two groups. The first one, containing rocks from the LTNav and LTNpv units from Mount Polley, Copper Mountain, Lac la Hache, Bridge Lake, and South of Merritt, is more alkaline, and crystallized at higher oxygen fugacity (Figure 4.10), than the pyroxene crystals of the second group, represented by the LTNpt unit from Mount Polley, Mount Milligan, and Woodjam areas (Figure 4.10).

The differentiation index $Fe_2O_3(t)+MgO$ in rocks from the south-central part of BC, shows that the eastern side of the belt (Bridge Lake) are generally more primitive than rocks from the west side (Mount Polley, Lac la Hache and Woodjam; Figure 4.16B), evidencing a tendency of increasing differentiation toward the west, in accordance with the observations by Schiarizza et al. (2009) in central BC, who suggested that magmatism in the Nicola Group had migrated towards the west with time.

Variation in the amount of incompatible elements such as Zr, Yb, Nb, and Th/Nb ratios within rocks indicates chemical heterogeneities of the mantle wedge along the arc. Variations in the Ce/Yb ratios suggest that volcanism during the Late Triassic corresponds to slight regional and local differences in the tectonic setting, which controlled the degree of partial melting in distinct portions of the mantle wedge (i.e., different depths). These local changes are particularly evident in the Mount Polley area, where the three different map units studied (LTNpv, LTNav and

LTNpt) show chemical distinctions (Figure 4.4, 4.5 and 4.17). These minor lithospheric tectonic changes occurred prior or during eruption, then extensional tectonics are represented by rocks from the LTNpt unit of Mount Polley and Mount Milligan; moderate extensional regime by rocks from the LTNpv unit of Mount Polley, Woodjam, Lac la Hache, Copper Mountain, Bridge Lake and South of Merritt; and relatively compressional setting by the LTNav unit of Mount Polley, indicating that the less extensional tectonics the more alkaline rocks were produced.

The amount and chemistry of primary Fe-Ti oxide inclusions in clinopyroxene phenocryst of basalts, suggest variations in the oxidation state of the source magmas along the arc. In this regard, volcanic rocks showing absence or relative low content of Fe-Ti oxides ($\ll 1\%$), and Fe-Ti oxide compositions with relatively high Fe^{+2} (low Fe^{+3}) and/or Cr contents (3-5 cpdf), are considered to come from a relatively reduced source magma (LTNpt unit Mount Polley, Mount Milligan and Bridge Lake), basalts from these areas show low $\text{Fe}^{3+}/\text{Fe}^{2+}$ ratios and low magnetic susceptibility values (Figure 4.6). The consistent presence of Fe-Ti oxides (1-2%) within the rock, presenting low Fe^{+2} (high Fe^{+3}) contents denote a relatively oxidized magma (Mount Polley, Lac la Hache and South of Merritt), basalts from these areas show intermediate $\text{Fe}^{3+}/\text{Fe}^{2+}$ ratios, and high magnetic susceptibility values (Figure 4.6). However, basaltic rocks showing Fe-Ti oxides with elevated Fe^{+3} contents (e.g., hematite), come presumably from an primary oxidized magma source, which had undergone secondary oxidation via alteration and/or weathering (Woodjam, and some basalts from Mount Polley, Lac la Hache and South of Merritt), basalts from these areas show high $\text{Fe}^{3+}/\text{Fe}^{2+}$ ratios, but low magnetic susceptibilities (Figure 4.6).

Carbon and oxygen isotopic composition on secondary carbonate minerals, which form part of the alteration mineral assemblage of basaltic rocks in the Nicola Group, allow classifying basalts on the basis of the chemical characteristics describe above. Secondary carbonate minerals from the relatively primary oxidized basalts from Mount Polley, Lac la Hache and South Merritt exhibit higher $\delta^{18}\text{O}$ and $\delta^{13}\text{C}$ values, compared to secondary carbonate minerals from relatively reduced basalts from Mount Milligan and Bridge Lake.

Magnetic susceptibility is directly related to the content of magnetic minerals (i.e., Fe-Ti oxides) in volcanic rocks. Intrusions related to Cu-Au alkalic mineralization show high magnetic susceptibilities (e.g., Mount Milligan; Mitchinson, 2010). Magnetic susceptibility measurements on rocks have an analogous response in geophysical maps (i.e., magnetic; Mitchinson, 2010). In the studied areas, the regional total magnetic field map show magnetic highs in areas delineated by Cu-Au alkalic porphyries (e.g., Mount Polley, Mount Milligan and Copper Mountain; Figure 3.5C, 3.6C and 3.8C).

The regional Bouguer gravity along the Quesnel terrane, displays a complex pattern of positive and negative anomalies. Much of the steep changes in gravity are due to the presence of Early Jurassic to Cretaceous intermediate to felsic intrusive bodies (low gravity signature; e.g., Takomkane batholith; Figure 3.7B). Late Triassic alkalic intrusions, mainly monzonites and syenites related to Cu-Au porphyry mineralization, are geographically related to mafic intrusive bodies (diorite - gabbro) (Figure 3.5A, 3.6A, 3.8A and 3.9A). These intrusions are indistinguishable from the host volcanic rocks in the regional gravity maps in Mount Polley, Mount Milligan, Copper Mountain and Lac la Hache (Figure 3.5B, 3.6B, 3.8B and 3.9B).

Based on the above, it is suggested that mafic, alkalic and oxidized magmas, which generated basalts, can be accumulated in magma chambers, which after differentiation could form oxidized fertile intrusions (e.g., Cu-Au alkalic porphyries; Seedorff et al., 2005; Chamberlain et al., 2007). In this regard, basalts from different areas of the Quesnel terrane are grouped as prospective and non-prospective arc segments for comagmatic Cu-Au alkalic porphyry mineralization, as follows:

Group 1: Mount Polley, Lac la Hache and South of Merritt, representing prospective arc segments.

Group 2: Mount Milligan and Bridge Lake, representing non-prospective arc segment for comagmatic mineralization, and,

Group 3: Copper Mountain and Woodjam can be grouped as uncertain arc segments, considering they do not provide the necessary constraints to classify them into any of the former groups.

Chemical variations in the Mount Polley area suggest that magmatism is largely controlled by local changes in the tectonic setting. Alternating periods of stretching and shortening may have occurred over relatively short periods of time. At Mount Polley, the period of relative compression is related to the generation of the more alkaline basalts in the area (LTNav unit). A compressional tectonic setting is required for the generation and evolution of intrusions (e.g., porphyry development). Identifying alkaline volcanic products (e.g., silica undersaturated) formed during periods of shortening could be the key in the identification of potential areas where fertile magmatic chambers were formed (e.g., Mount Polley Complex).

This work suggests that indications of a favourable magma-generating environment for Cu-Au porphyry mineralization could also be recorded in the precursor volcanic rocks in prospective arc segments.

Additionally, the analysis of regional geological and geophysical maps (Figure 6.1), allow separating the Quesnel terrane into four major arc segments, limited by potential regional discontinuities, from north to south:

I: This segment comprises the area covering the Lorraine and Mount Milligan deposits. The area consists of intrusive, volcanic and sedimentary rocks, showing high and low gravity values and in general a low magnetic background with a NW high magnetic trend (intrusions). This segment ends toward the south where a big high gravity anomaly starts.

II: This arc segment is represented by volcanic and sedimentary rocks (no intrusive rocks at surface). The area is characterized by particularly high gravity values and low to moderate magnetism.

III: This area presents intrusive, volcanic and sedimentary rocks, and includes Mount Polley, Woodjam and Lac la Hache areas. This arc segment exhibits moderate to high gravity and relatively high magnetic values, and ends toward the south in a deflection, where the Quesnel terrane changes its strike from $\sim 30^\circ\text{NW}$ to $\sim 10^\circ\text{NW}$.

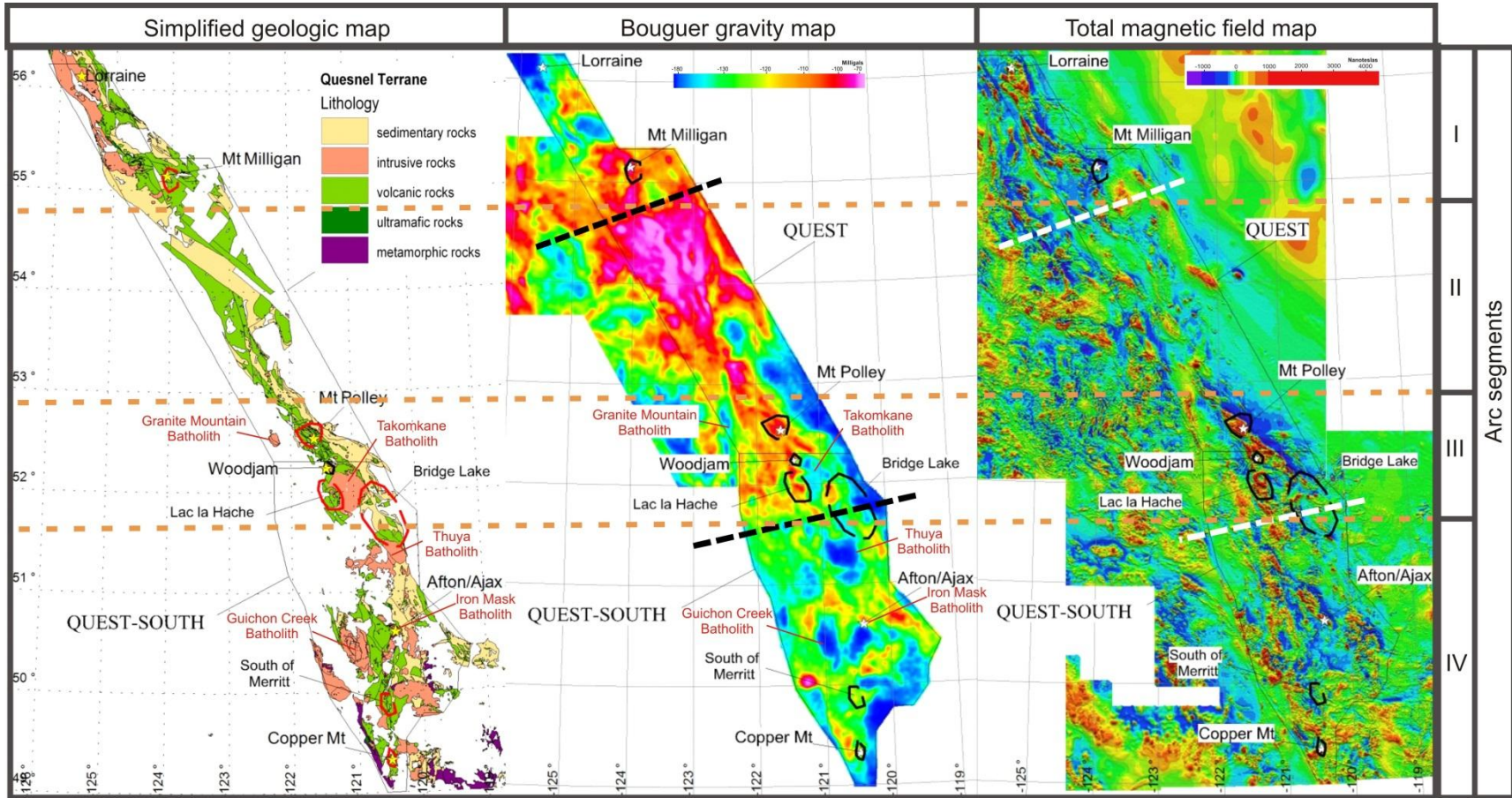


Figure 6.1. Geology, gravity and magnetic maps of the QUEST and QUEST-South areas, dashed polygons showing the location of the studied areas in this research; Simplified geologic map (Modified from Massey et al., 2005). Gravity Bouguer Corrected map, QUEST and QUEST-South projects (Geoscience BC., 2009; Geoscience BC., 2010). Magnetics Total Field map, QUEST and QUEST-South projects (Geoscience BC., 2009; Geoscience BC., 2010).

IV: This arc segment is represented by intrusive, volcanic and sedimentary rocks, which previously have been subdivided into three belts from west (calc-alkalic) to east (alkalic; Preto, 1979; Mortimer, 1987; see Chapter 2). This area is characterized by relatively lower gravity compared to rocks in the northern areas, and a collage of high and low magnetic values.

Intrusive bodies with calc-alkalic affinity are related to Cu-Mo porphyry-style mineralization (e.g., Guichon Creek batholith hosting the Highland Valley deposit, and Granite Mountain batholith hosting the Gibraltar deposit; Figure 6.1) and present low gravity values. Whereas, the areas surrounding Cu-Au porphyry mineralization exhibit relatively high gravity values (e.g., Afton-Ajax deposits hosted in the Iron Mask Batholith; Figure 6.1; see Chapter 3), which are interpreted to be related to deeper mafic comagmatic intrusions.

Typically, high magnetic anomalies have been used as a tool to explore porphyry mineralization, however, here is showed that gravity anomalies can also be used for delineating areas for Cu-Mo and Cu-Au porphyry exploration.

REFERENCES

- Aiuppa, A., Baker, D.R., Webster, J.D., (2009): Halogens in volcanic systems. *Chemical Geology*, 263 (1-4), 1-18.
- Anderson, T. F. (1980): Stable-isotope evidence for the origin of secondary carbonate veins in Deep Sea Drilling Project Leg 58 basalts. In Klein, G. deV., Kobayashi, K., et al., *Init. Repts.DSDP, 58: Washington (U.S. Govt. Printing Office)*, 905-911.
- Armstrong, J.E. (1948): Fort St. James; Geological Survey of Canada, Map 907A. 1:380,160.
- Armstrong, J.E. (1965): Fort St James Map-area, Cassiar and Coast Districts. British Columbia; Geological Survey of Canada, Memoir 252, 210 pages.
- Armstrong, R.L. (1988): Mesozoic and Cenozoic magmatic evolution of the Canadian Cordillera, *in* Clark, S.P., Burchfiel, B.C. and Suppe, J., eds., *Processes in Continental Lithospheric Deformation: Geological Society of America Special Paper 218*, p. 55-91.
- Bailey, D.G. (1978): The Geology of the Morehead Lake Area: unpublished Ph.D. thesis, Queen's University, 198 p.
- Bailey, D.G. and Hodgson C, J. (1979): Transported altered wall rock in laharic breccias at the Cariboo-Bell Cu-Au porphyry deposit, British Columbia; *Economic Geology*, v 74, p. 125–12. <http://econgeol.geoscienceworld.org/cgi/reprint/74/1/125.pdf> [November 2011].
- Banerjee, S.K., (1991): Magnetic properties of Fe-Ti oxides. In Lindsley, D.H. (Ed.), *Oxide Minerals: Petrologic and Magnetic Significance: Rev. Mineral.*, 25:107–128.
- Barker, S., Dipple, G., Dong, F. and Baer, D. (2011): The use of laser spectroscopy to measure the stable carbon and oxygen isotope composition of carbonate minerals, *Analytical Chemistry*, 83, 2220–2226 p.
- Barr, D. A., Fox, P. E., Northcote, K. E., and Preto, V. A., (1976): The Alkaline Suite Porphyry Deposits - A Summary, in Brown, A. S., ed., *Porphyry Deposits Of The Canadian Cordillera*, CIM Special Volume 15: Ste. Anne de Bellevue, Harpell's Press Cooperative, p. 359-367.

- Barrie, C.T. (1993): Petrochemistry of shoshonitic rocks associated with porphyry copper-gold deposits of central Quesnellia, British Columbia, Canada: *Journal of geochemical exploration*, v. 48, p. 225-258.
- Bath, A.B., Cooke, D.R., Friedman, R.M., Faure, K., Kamenetsky, V.S., Tosdal, R.M., and Berry, R.F. (in press): Mineralization, U-Pb geochronology and stable isotope geochemistry of the Lower Main zone of the Lorraine deposit, north-central British Columbia: a replacement-style alkalic Cu-Au porphyry: *Economic Geology*.
- Bissig, T., Vaca, S., Schiarizza, P. and Hart, C. (2010): Geo chemical and physical variations in the Late Triassic Nicola Arc and metallogenic implications, central British Columbia (NTS 092P, 093A, N): preliminary results; *in* *Geoscience BC Summary of Activities 2009*, Geoscience BC, Report 2010-1, p. 49–52.
- Blackwell, J., Lesage, G., Skinner, T., Eckfeldt, M., Hamilton, J., Hertel, J., Laird, B., Madsen, J., Rainbow, A., Sherlock, R., Sepp, M., (2010): Woodjam Property Mapping 2010 Interpretation, Geology of the Woodjam Property Core Area. Unpublished internal report, Gold Fields Canada Exploration.
- Bloodgood, M. A. (1988): Geology of the Quesnel Terrane in the Spanish Lake Area, Central British Columbia, *Geological Fieldwork 1987*, Paper 1988-1, B.C. Ministry of Energy, Mines and Petroleum Resources, p. 139-145.
- Böhlke, J. K., Honnorez, J., Honnorez-Guersteini, B. M., Muehlenbachs, and Petersen, N. (1981): Heterogeneous Alteration of the Upper Oceanic Crust: Correlation of Rock Chemistry, Magnetic Properties, and O Isotope Ratios With Alteration Patterns in Basalts From Site 396B, DSDP. *Journal of Geophysical Research*, vol. 86, No. B9, p. 7935-7950.
- Breitsprecher, K. (2010): Tectonic and metallogeny of Cordilleran porphyries. Earth and Ocean Science Department, the University of British Columbia, Vancouver, EOS-539 course, power point presentation.
- Byrne, K. (2009): The Southwest Zone breccia-centered silica-undersaturated alkalic porphyry Cu-Au deposit, Galore Creek, B.C: Magmatic-hydrothermal evolution and zonation, and a hydrothermal biotite perspective: Unpublished MSc thesis, University of British Columbia, 170 p.

- Canadian Aeromagnetic Data Base (2005): Regional Geophysics Section, GSC - Central Canada Division, Geological Survey of Canada, Earth Sciences Sector, Natural Resources Canada. www.gdcinfo.aggr.nrcan.gc.ca
- Carter, E. S., Orchard, M. J., Ross, C. A., Ross, J. R. P., Smith, P. L., and Tipper, H. W. (1991): Part B. Paleontological signatures of terranes; in Chapter 2 of *Geology of the Cordillera Orogen in Canada*, H. Gabrielse and C. J. Yorath (ed.); Geological Survey of Canada, *Geology of Canada*, no. 4, p. 28-38 (also *Geological Society of America, The Geology of North America*, v. G-2).
- Chamberlain, C.M., Jackson, M., Jago, C.P., Pass, H.E., Simpson, K.A., Cooke, D.R. and Tosdal, R.M. (2007): Toward an integrated model for alkalic porphyry copper deposits in British Columbia (NTS 093A, N; 104G); in *Geoscience BC Summary of Activities 2006, Report 2007-1*, p. 259–274, <http://www.empr.gov.bc.ca/Mining/Geoscience/PublicationsCatalogue/Fieldwork/Documents/26-Chamberlain.pdf> [November 2011].
- Clowes, R.M., and Hammer, P.T.C., (2000): Comparison of Lithospheric Structures Across the Alaskan and Canadian Cordillera, *GeoCanada 2000, Technical Session 18, Abstract #529* (on CD).
- Coates J.A. (1960): Analcite Bearing Volcanic Rocks of the Quesnel River Group, Cariboo District, British Columbia; unpublished B.Sc thesis, The University of British Columbia, 56 p.
- Craig, H. B. (1961): Isotopic variations in meteoric waters. *Science*, 133(3465), p. 1702-1703.
- Craig H., Welhan J.A., Kim K., Poreda R. and Lupton J.E. (1980): Geochemical studies of the 21°N EPR hydrothermal fluids, *Eos, Transactions, American Geophysical Union*, 61, 46, 992.
- Crickmay, C.H. (1930): The Jurassic rocks of Ashcroft, British Columbia; *University of California Publications in Geological Sciences*, v. 19(2), p. 23-74.
- Coney, P.J., Jones, D.L. and Monger, J.W.H., (1980): Cordilleran suspect terranes: *Nature*, v. 288, p. 329-333.

- Cooke, D. R., Wilson, A. J., House, M. J., Wolfe, R. C., Walshe, J. L., Lickfold, V., and Crawford, A. J. (2007): Alkalic porphyry Au-Cu and associated mineral deposits of the Ordovician to Early Silurian Macquarie Arc, NSW: *Australian Journal of Earth Science*, v. 54, p. 445-463.
- Dalton, J., and D. C. Presnall (1998): The continuums of primary carbonatitic-kimberlitic melt compositions in equilibrium with lherzolites: Data from the system CMAS-CO at 6 GPa, *Journal of Petrology*, 39, p. 1953–1964.
- Davies, J. H., Bickle, M. J. (1991): A physical model for the volume and composition of melt produce by hydrous fluxing above subduction zones. Special Publication, The Royal Society of London, vol 335: 355-64.
- Doe, B. R. (2002): Further Considerations of the Ce/Yb vs. Ba/Ce Plot in Volcanology and Tectonics, *International Geology Review*, 44:10, 877-912
- Droop, G.T.R. (1987): A general equation for estimating Fe³⁺ concentrations in ferromagnesian silicates and oxides from microprobe analyses, using stoichiometric criteria; *Mineralogical Magazine*, v. 51, p 431–435.
- Dawson, G.M. (1879): Preliminary report on the physical and geological features of the southern portion of the interior of British Columbia, 1877; Geological Survey of Canada, Progress Report, p. 1877-8, 1879.
- Ellam, R. M. (1992): Lithospheric thickness as a control on basalt geochemistry. *Geology*, v. 20, no. 2, p. 153-156.
- Ferri, F. and Melville, D.M. (1988): Manson Creek mapping project; British Columbia Ministry of Energy, Mines and Petroleum Resources, Geological Fieldwork, 1987, Paper 1988-1, p. 169-180.
- Ferri, F. and Melville, D.M. (1989): Geology of the Germansen Landing area, British Columbia; British Columbia Ministry of Energy, Mines and Petroleum Resources, Geological Fieldwork, 1988, Paper 1989-1, p. 209-220.
- Ferri, F., Dudka, S., Rees, C. J. and Meldrum, D.G. (1993a): Geology of Aiken Lake and Osilinka River Areas, Northern Quesnel Trough, B.C. (94C/2, 3, 5, 6 & 12); *in* Geological

- Fieldwork 1992, Grant, B. and Newell, J. M., Editors, B.C. Ministry of Energy, Mines and Petroleum Resources, Paper 1993-1, pages 109-134.
- Ferri, F., Dudka, S., Rees, C. J. and Meldrum, D.G. (1993b): Preliminary Geology and Geochemistry of the Aiken Lake and Osilinka River Areas, B.C. Ministry of Energy, Mines and Petroleum Resources, Open File 1993-2.
- Gabrielse, H., Monger, J.W.H., Wheeler, J. O., and Yorath, C.J. (1991): Part A. Morphogeological belts, tectonic assemblages, and terranes; in Chapter 2 of Geology of the Cordilleran Orogen in Canada, H. Gabrielse and C. J. Yorath (ed.); Geological Survey of Canada, Geology of Canada, no. 4, p. 15-28 (also Geological Society of America, The Geology of North America, v. G-2).
- Gabrielse, H. and Yorath C.J. (1991): Tectonic synthesis, Chapter 18 in Geology of the Cordilleran Orogen in Canada, H. Gabrielse and C. J. Yorath (ed.); Geological Survey of Canada, Geology of Canada, no. 4, p. 677-705 (also Geological Society of America, The Geology of North America, v. G-2).
- Geoscience BC (2009): QUEST Project - Geology; Geoscience BC, Map 2009-4-1, scale 1:500,000.
- Geoscience BC (2009): QUEST Project - Magnetics - Total Field; Geoscience BC, Map 2009-4-4, scale 1:500,000.
- Geoscience BC (2009): QUEST Project - Gravity - Bouguer Corrected; Geoscience BC, Map 2009-4-7, scale 1:500,000.
- Geoscience BC (2010): QUEST South Project - Magnetics – Total Field; Geoscience BC, Map 2010-7-4, scale 1:500 000 (Draft).
- Geoscience BC (2010): QUEST South Project - Gravity - Bouguer Corrected; Geoscience BC, Map 2010-7-7, scale 1:500,000 (Draft).
- Goodfellow, W. D. (2007): A Synthesis of Major Deposit Types, District Metallogeny, the Evolution of Geological Provinces & Exploration Methods, Geological Association of Canada, Special publication No. 5. CD-ROM (Digital maps).
- Gottardi, G. and Galli, D. (1985): Natural Zeolites. Springer-Verlag, Berlin, 409 pp

- Greenwood, H.J., Woodsworth, G.J., Read, P.B., Ghent, E.D., and Evenchick, C.A. (1991): Metamorphism, Chapter 16 in *Geology of the Cordillera Orogen in Canada*, H. Gabrielse and C. J. Yorath (ed.); Geological Survey of Canada, *Geology of Canada*, no. 4, p. 533-570 (also, Geological Society of America, *The Geology of North America*, v. G-2).
- Greig C.J. (1989): *Geology and geochronometry of the Eagle plutonic complex, Coquihalla area, southwestern British Columbia*; unpublished M.Sc. thesis, University of British Columbia, Vancouver, B.C. 423 p.
- Hammer, P.T.C., and Clowes, R.M. (2007): Lithosphere-scale structures across the Alaskan and Canadian Cordillera: Comparisons and tectonic implications. *In* *Whence the Mountains? Inquiries into the Evolution of Orogenic Systems: A Volume in Honor of Raymond A. Price*. Edited by J.W. Sears, T.A. Harms, and C.A. Evenchick. Geological Society of America, Special Paper 433, pp. 99–116.
- Hawkesworth, C. J., Gallagher, K., Hergt, J. M., McDermott, F. (1992): Trace element fractionation processes in the generation of island arc basalts. *Philosophical Transactions, The Royal Society of London*, vol. 342, no. 1663, 179-191.
- Hawkesworth, C. J., Gallagher, K., Hergt, J. M., McDermott, F. (1993): Mantle and slab contributions in arc magmas. *Annual Reviews Inc. Earth Planet. Sci.* 1993. 21: 175-204.
- Hirose, K. (1997): Partial melt compositions of carbonated peridotite at 3 GPa and role of CO₂ in alkali-basalt magma generation, *Geophysical Research Letters*, vol 24, p. 2837-2840.
- Holliday, J.R., and Cooke, D.R. (2007): Advances in geologic models and exploration methods for copper ± gold porphyry deposits, in Milkereit, B., ed., *Proceedings of Exploration 07: Fifth Decennial International Conference on Mineral Exploration: Toronto, Prospectors and Developers Association of Canada*, p. 791-809.
- Hunt, C.P., Moskowitz, B. M., Banerjee, S. K. (1995): Magnetic properties of rocks and minerals; *in* *Rock Physics and Phase Relations: A Handbook of Physical Constants*, T. J Ahrens. (ed.), AGU Reference Shelf 3, American Geophysical Union, p. 189–204.
- Irving, E., (1970): The Mid-Atlantic Ridge at 45° N. XIV. Oxidation and magnetic properties of basalt; review and discussion, *Canadian Journal of Earth Sciences*, 7, p. 1528-1538.

- Irving, E., Emslie, R.F., and Yole, R.W. (1980): New paleomagnetic evidence for displaced terranes in B.C.; Geological Association of Canada, Special Paper 20, p. 441-456.
- Irving, E. and Wynne, P. J. (1991): Paleomagnetism: review and tectonic implications, Chapter 3 *in* Geology of the Cordillera Orogen in Canada, H. Gabrielse and C. J. Yorath (ed.); Geological Survey of Canada, Geology of Canada, no. 4, p. 61-86 (also Geological Society of America, The Geology of North America, v. G-2).
- Jackson, M. L. (2008): Evolution of the Northeast Zone Breccia Body, Mount Polley Mine, British Columbia: Unpublished M.Sc. thesis, University of British Columbia, 238 p.
- Jago, C. P. (2008): Metal- and alteration-zoning, and hydrothermal flow paths at the moderately-tilted, silica-saturated Mt. Milligan Cu-Au alkalic porphyry deposit: Unpublished M.Sc. thesis, University of British Columbia, 227 p.
- Jensen, E. P., and Barton, M. D. (2000): Chapter 8 Gold Deposits Related to Alkaline Magmatism in Hagemann, S. G., and Brown, P. E., eds., Gold in 2000, Reviews in Economic Geology, 13: Chelsea, MI, Society of Economic Geologists Inc., p. 279-314.
- Johnston, S. T., and Borel, G. D., (2007): The odyssey of the Cache Creek terrane, Canadian Cordillera: Implications for accretionary orogens, tectonic setting of Panthalassa, the Pacific superwell, and break-up of Pangea: Earth and Planetary Science Letters, v. 253, p. 415-428.
- Kirkham, R.V., and Sinclair, W.D. (1995): Porphyry copper, gold, molybdenum, tungsten, tin, silver, in Eckstrand, O.R., Sinclair, W.D., and Thorpe, R.I., eds., Geology of Canadian Mineral Deposit Types: Geological Survey of Canada, Geology of Canada, no. 8, p. 421-446.
- Klein, C. & Hurlbut, C. S. Jr, (1993): Manual of Mineralogy, 21st edition. New York, Chichester, Brisbane, Toronto, Singapore: John Wiley ' Sons, Inc., 681 pp.
- Kroll, T., Müller, D., Seifert, T., Herzig, P.M. and Schneider, A. (2002): Petrology and geochemistry of the shoshonite-hosted Skouries porphyry Cu-Au deposit, Chalkidike, Greece. *Miner Deposita* 37:137–144.
- Kushiro, I. (1960): Si-Al relations in clinopyroxenes from igneous rocks; *American Journal of Science*, v. 258, p. 548–554.

- Lang, J.R., (1992): Mount Milligan Geochemistry: MDRU Porphyry Cu-Au Project, Year 1, Section 7, p. 2-49.
- Lang, J. R., Lueck, B., Mortensen, J. K., Russell, J. K., Stanely, C. R., and Thompson, J. F. H. (1995a): Triassic-Jurassic silica-undersaturated and silica-saturated alkalic intrusions in the Cordillera of British Columbia: Implications for arc magmatism: *Geology*, v. 23, p. 451-454.
- Lang, J. R., Stanley, C. R., and Thompson, J. F. H. (1995b): Porphyry Copper-Gold Deposits Related to Alkalic Igneous Rocks in the Triassic-Jurassic Arc terranes of British Columbia, in Pierce, F. W., and Bolm, J. G., eds., *Porphyry Copper Deposits of the American Cordillera*, Arizona Geological Society, Digest 20 p. 219-236.
- LeBas, M.J. (1962): The role of aluminum in igneous clinopyroxenes with relation to their parentage; *American Journal of Science*, v. 260, p. 267–288.
- Lefebure, D.V. (1976): *Geology of the Nicola Group in the Fairweather Hills, British Columbia*; M.Sc. thesis, Queen's University, Kingston, Ontario, 179 p.
- Logan, J.M. and Bath, A.B. (2006): Geochemistry of Nicola Group basalt from the central Quesnel trough at the latitude of Mount Polley (NTS 093A/5, 6, 11, 12), central British Columbia; *in Geological Fieldwork*, BC Ministry of Energy and Mines, Paper 2006-1, p. 83–98,
<http://www.empr.gov.bc.ca/Mining/Geoscience/PublicationsCatalogue/Fieldwork/Documents/2005/Paper09.pdf> [November 2011].
- Logan, J. M., Bath, A., Mihalynuk, M. G. and Rees, C. J. (2007): Regional Geology of the Mount Polley Area, scale 1:50.000, Central British Columbia, Geoscience map 2007-1.
- Logan, J.M., Schiarizza, P., Struik, L.C., Barnett, C., Nelson, J.L., Kowalczyk, P., Ferri, F., Mihalynuk, M.G., Thomas, M.D., Gammon, P., Lett, R., Jackaman, W. and Ferbey, T. (2010): Bedrock Geology of the QUEST map area, central British Columbia; British Columbia Geological Survey, Geoscience Map 2010-1, Geoscience BC Report 2010-5 and Geological Survey of Canada, Open File 6476.
- Logan, J.M., Mihalynuk, M.G., Friedman, R.M. and Creaser, R.A. (2011): Age constraints of mineralization at the Brenda and Woodjam Cu-Mo+/-Au porphyry deposits - an Early Jurassic calcalkaline event, south-central British Columbia. *in Geological Fieldwork 2010*,

BC Ministry of Energy and Mines, Paper 2011-1, p. 129–144.
<http://www.fjordlandex.com/Research/2010Fieldwork.pdf> [November 2011].

Massey, N.W.D., MacIntyre, D.G., Desjardins, P.J., and Cooney, R.T., (2005): Geology of British Columbia, BC Ministry of Energy, Mines and Petroleum Resources, Geoscience Map 2005-3, (3 sheets), scale 1:1 000 000.

Massey, N.W.D, MacIntyre, D.G., Desjardins, P.J. and Cooney, R.T. (2005): Digital Geology, Map of British Columbia: Whole Province; B.C. Ministry of Energy and Mines, Geofile 2005-1.

McMillan, W. J., and Panteleyev, A. (1995): Porphyry copper deposits of the Canadian Cordillera, in Pierce, F. W., and Bolm, J. G., eds., *Bootprints along the Cordillera; Porphyry copper deposits from Alaska to Chile*, 20. Porphyry copper deposits of the American Cordillera: Tucson, AZ, United States, Arizona Geological Society, p. 203-218.

Meade, H.D. (1977): Petrology and metal occurrences of the Takla Group and Hogem and Germansen batholiths, north central British Columbia; unpublished Ph.D. thesis, University of British Columbia, Vancouver, B.C., 355 p.

Melling, D.R., Watkinson, D.H., Fox, P.E., and Cameron, R.S. (1990): Carbonatization and propylitic alteration of fragmental basaltic rocks, Quesnel River gold deposit, Central British Columbia, *Mineralium Deposita*, 25, Suppl., 115-124, Gold '89 in Europe.

Mernagh, T.P. and Mieziotis, Y. (2008): A Review of the Geochemical Processes Controlling the Distribution of Thorium in the Earth's Crust and Australia's Thorium Resources. *Geoscience Australia Record* 2008/05, 48 p.

Micko, J. (2010): The geology and genesis of the Central Zone alkalic copper-gold porphyry deposit, Galore Creek District, northwestern British Columbia, Canada: Unpublished PhD thesis, University of British Columbia, 359 p.

Milliford, J.C. (1984): Geology of the Apex Mountain Group, north and east of the Similkameen River, south-central British Columbia; M.Sc. thesis, University of British Columbia, Vancouver, 108 p.

Mihalynuk M., Nelson J., and Diakow J. (1994): Cache Creek terrane entrapment: Oroclinal paradox within the Canadian Cordillera. *Tectonics*, Vol. 13, No.3, pp.575-595.

- Mitchinson, D. (2010): Relating geology to geophysics for known porphyry deposits in the Quest project area, SEG conference 2010, Keystone, Colorado, USA.
- Monger, J.W.H., Souther, J.G. and Gabrielse, H. (1972): Evolution of the Canadian Cordillera - a plate tectonic model; *American Journal of Science*, v. 272, p. 557–602.
- Monger, J. W. H. (1975): Upper Paleozoic rocks of the Atlin terrane, northwestern British Columbia and south-central Yukon; *Geological Survey of Canada, Paper 74-47*, 63 p.
- Monger, J. W. H. (1977b): Upper Paleozoic rocks of the western Canadian Cordillera and their bearing on Cordilleran evolution; *Canadian Journal of Earth Science*, v. 14, p. 1832-1859.
- Monger, J.W.H., Price, R.A. and Tempelman-Kluit, D.J. (1982): Tectonic accretion and the origin of the two major metamorphic and plutonic belts in the Canadian Cordillera. *Geology*, v. 10, p. 70-75.
- Moore, T. E. (1992): The Arctic Alaska superterrane, in Bradley, D.C., and Dusel-Bacon, C., eds., *Geologic studies in Alaska by the U.S. Geological Survey, 1991: U.S. Geological Survey Bulletin 2041*, p. 238-244.
- Moore, J.M. (2000): Nicola Horst, southern British Columbia: window into the pre-Triassic margin of North America?; *Geological Survey of Canada, Current Research 2000-A16*, 6 p.
- Moore, J.M. and Pettipas, A. (1990): Nicola Lake region geology and mineral deposits; *British Columbia Ministry of Energy, Mines and Petroleum Resources, Open File 1990-29 Part A*, p. 1-13.
- Morimoto, N., Fabries, J., Ferguson, A.K., Ginzburg, I.V., Ross, M., Seifert, F.A., Zussman, J., Aoki, K. and Gottardi, G. (1988): Nomenclature of pyroxenes; *American Mineralogist*, v. 173, p. 1123–1133. http://www.minsocam.org/ammin/AM73/AM73_1123.pdf [November 2011].
- Mortensen, J. K., Ghosh, D. K., and Ferri, F. (1995): U-Pb geochronology of intrusive rocks associated with copper-gold porphyry deposits in the Canadian Cordillera, in Schroter, T. G., ed., *Porphyry Deposits of the Northwestern Cordillera of North America, CIM Special Volume 46: Sainte-Anne-de-Bellevue, Quebec, Harpell's Press Cooperative*, p. 142-158, paper 7.

- Mortensen, J.K., Lucas, K., Monger, J.W.H. and Cordey, F. (2011): Geological investigations of the basement of the Quesnel terrane in southern British Columbia (NTS 082E, F, L, 092H, I): Progress Report; *in* Geoscience BC Summary of Activities 2010, Report 2011-1, p. 133–142.
- Mortimer, N. (1987): The Nicola Group: Late Triassic and Early Jurassic subduction-related volcanism in British Columbia; *Canadian Journal of Earth Sciences*, v. 24, p. 2521–2536.
- Morton, R.L. (1976): Alkalic Volcanism and Copper Deposits of the Horsefly Area, Central British Columbia; unpublished Ph.D. thesis, *Carleton University*, 196 p.
- Nelson J. and Mihalynuk M. (1993): Cache Creek ocean: Closure or enclosure? *Geology*, V. 21, p. 173-176.
- Nelson, J.L. and Bellefontaine, K.A. (1996): The geology and mineral deposits of north-central Quesnellia; Tezzeron Lake to Discovery Creek, central British Columbia; BC Ministry of Energy and Mines, Bulletin 99, 100 p.
http://www.empr.gov.bc.ca/Mining/Geoscience/PublicationsCatalogue/BulletinInformation/BulletinsAfter1940/Documents/Bulletin_099.pdf [November 2011].
- Nelson, J., and Colpron, M., (2007): Tectonics and metallogeny of the British Columbia, Yukon and Alaskan Cordillera, 1.8 Ga to the present, *in* Goodfellow, W.D., ed., *Mineral Deposits of Canada: A Synthesis of Major Deposit-Types, District Metallogeny, the Evolution of Geological Provinces, and Exploration Methods*: Geological Association of Canada, Mineral Deposits Division, Special Publication No. 5, 755-791 p.
- Nixon, G.T., Hammack, J.L., Ash, C.A., Cabri, L.J., Case, G., Connelly, J.N., Heaman, L.M., Laflamme, J.H.G., Nuttall, C., Paterson, W.P.E. and Wong, R.H. (1997): Geology and Platinum-Group-Element Mineralization of Alaskan-Type Ultramafic-Mafic Complexes in British Columbia Geological Survey of British Columbia, Bulletin 93, 141 p.
- Nixon, G., Cabri, L., LaFlamme, G., Sylvester, P. and Tubrett, M. (2004): Platinum Group Elements in Alkaline Cu-Au Porphyry, Ministry of Energy and Mines, Geofile 2004-6. Poster.
- Nokleberg, W. J., Bundtzen, T. K., Eremin, R. A., Ratkin, V. V., Dawson, K. M., Shpikerman, V. I., Goryachev, N. A., Byalobzhesky, S. G., Frolov, Y. F., Khanchuk, A. I., Koch, R. D., Monger, J.W.H., Pozdeev, A. I., Rozenblum, I. S., Rodionov, S. M., Parfenov, L. M.,

- Scotese, C. R. and Sidorov, A. A. (2005): Metallogensis and Tectonics of the Russian Far East, Alaska, and the Canadian Cordillera, U.S. Geological Survey, Professional paper 1697, 397 pp.
- Norris, J. (2012): Evolution of Alteration and Mineralization at the Red Chris Cu-Au Porphyry Deposit East Zone, Northwestern British Columbia, Canada: Unpublished M.Sc. thesis, University of British Columbia, 194 p.
- Ogg, J.G., Ogg, G. and Gradstein F.M. (2008): The Concise Geologic Time scale. Cambridge University Press, 177 p.
- Panteleyev, A., Bailey, D.G., Bloodgood, M.A. and Hancock, K.D. (1996): Geology and mineral deposits of the Quesnel River–Horsefly map area, central Quesnel trough, British Columbia; BC Ministry of Forest, Mines and Lands, Bulletin 97, 157 p.
http://www.em.gov.bc.ca/Mining/Geoscience/PublicationsCatalogue/BulletinInformation/BulletinsAfter1940/Documents/Bulletin_097.pdf [January 2012].
- Pass, H. (2010): Breccia-hosted chemical and mineralogical zonation patterns of the Northeast Zone, Mt. Polley Cu-Ag-Au alkalic porphyry deposit, British Columbia, Canada: Unpublished Ph.D. thesis, University of Tasmania, 276 p.
- Peatfield, G. R. (1978): Geologic history and metallogeny of the “Boundary District”, southern British Columbia and Northern Washington; Ph.D. thesis, Queen’s University, Kingston, Ontario, 247 p.
- Peters, C. and Dekkers, M.J. (2003): Selected room temperature magnetic parameters as a function of mineralogy, concentration and grain size; Physics and Chemistry of the Earth, v. 28, no. 16–19, p. 659–667.
- Pineau, F., Javoy M. and Bottinga, Y. (1976): $^{13}\text{C}/^{12}\text{C}$ ratios of rocks and inclusions in popping rocks of the Mid-Atlantic Ridge and their bearing on the problem of isotopic composition of deep-seated carbon, Earth and Planetary Science Letters. Vol. 29, p. 413-421.
- Plank, T., Lanmuir, C.H. (1988): An evaluation of the global variations in the major element chemistry of arc basalts. Earth Planet. Sci Lett. 90: 349-70.
- Piccoli, P.M. and Candela, P.A. (1994): Estimation of aqueous HCl and Cl concentrations in felsic systems. Lithos, 46: 591-604.

- Pouchou, J.L. and Pichoir, F. (1985): “PAP” $\phi(\rho Z)$ procedure for improved quantitative microanalysis; *in* Microbeam Analysis -1985, J.T. Armstrong (ed.), San Francisco Press, p. 104-106.
- Peters, C. and Dekkers, M.J. (2003): Selected room temperature magnetic parameters as a function of mineralogy, concentration and grain size; *Physics and Chemistry of the Earth*, v. 28, no. 16–19, p. 659–667.
- Plank, T., Lanmuir, C.H. (1988): An evaluation of the global variations in the major element chemistry of arc basalts. *Earth Planet. Sci Lett.* 90: 349-70.
- Piccoli, P.M. and Candela, P.A. (1994): Estimation of aqueous HCl and Cl concentrations in felsic systems. *Lithos*, 46: 591-604.
- Pouchou, J.L. and Pichoir, F. (1985): “PAP” $\phi(\rho Z)$ procedure for improved quantitative microanalysis; *in* Microbeam Analysis -1985, J.T. Armstrong (ed.), San Francisco Press, p. 104-106.
- Preto, V. A. (1972): Geology of Copper Mountain, British Columbia; BC Ministry of Energy, Mines and Petroleum Resources, Bulletin 59, 87 p.
- Preto, V. A. (1977): The Nicola Group: Mesozoic volcanism related to rifting in southern British Columbia. In *Volcanic regimes in Canada*. Edited by W. R. A. Baragar, L. C. Coleman, and J. M. Hall. Geological Association of Canada, Special Paper 16, 39-57 p.
- Preto, V.A. (1979): Geology of the Nicola Group between Merritt and Princeton; BC Ministry of Energy and Mines, Bulletin 69, 90 p.
http://www.em.gov.bc.ca/Mining/Geoscience/PublicationsCatalogue/BulletinInformation/BulletinsAfter1940/Documents/Bulletin_069.pdf [November 2011].
- Preto, V.A., Nixon, G.T. and Macdonald, E.A.M. (2004): Alkaline Cu-Au Porphyry Systems in British Columbia: Copper Mountain; BC Ministry of Energy and Mines, Geoscience Map 2004-3.
- Raudsepp, M. (1995): Recent advances in the electron-probe micro-analysis of minerals for the light elements. *The Canadian Mineralogist*, 33: 203-218.

- Read, P.B., Woodsworth, G.J., Greenwood, H.J., Ghent, E.D. and Evenchick, C.A. (1991): Metamorphic Map of the Canadian Cordillera, Geological Survey of Canada, Map 1714A, scale 1:2,000,000.
- Rollinson, H.R. (1993): Using Geochemical Data: Evaluation, Presentation, Interpretation. Longmans. Essex, UK. 352 pp.
- Roux, J., and Hamilton, D. L. (1976): Primary igneous analcite an experimental study. *Journal of Petrology*, 17: 244 -257 p.
- Schau, M.P. (1968): Geology of the Upper Triassic Nicola Group in south central British Columbia; Ph.D. thesis, University of British Columbia, Vancouver, 211 p.
- Schiarizza, P., Bligh, J., Bluemel, B. and Tait, D. (2008): Geology of the Timothy Lake Area (NTS 092P/14); BC Ministry of Energy and Mines, Open File, 2008-5, 1:50 000 scale, <http://www.empr.gov.bc.ca/Mining/Geoscience/PublicationsCatalogue/OpenFiles/2008/Pages/2008-5.aspx> [November 2011].
- Schiarizza, P., Bell, K., Bayliss, S. (2009): Geology and Mineral Occurrences of the Murphy Lake Area, South – Central British Columbia (NTS 093A/03): British Columbia Geological Survey, Geological Fieldwork 2008, Paper 2009-1.
http://www.empr.gov.bc.ca/Mining/Geoscience/PublicationsCatalogue/Fieldwork/Documents/15_Schiarizza_2008.pdf [February 2012].
- Schiarizza, P. (2009): Stratigraphic and Plutonic Framework for Copper, Gold and Molybdenum, Thuya Creek - Woodjam Creek, South-Central BC, Presentation.
http://www.empr.gov.bc.ca/Mining/Geoscience/PublicationsCatalogue/OpenFiles/2009/Documents/2009-12/Schiarizza_WoodjamCreekArea_Nov09.pdf
- Schidlowski, M. (1988): A 3800-million-year isotopic record of life from carbon in sedimentary rocks. *Nature*, v 333, n 6171, p 313-318.
- Seedorff, E., Dilles, J.H., Proffett, J.M., Jr., Einaudi, M.T., Zurcher, L., Stavast, W.J.A., Johnson, D. and Barton, M.D. (2005): Porphyry deposits: characteristics and origin of hypogene features; *Economic Geology*, 100th Anniversary Volume, p. 251–298.

- Schroeter, T. G. (1995): Porphyry Deposits of the Northwestern Cordillera of North America, CIM Special Volume 46: Quebec, Canada, Harpell's Press Cooperative, p. 888.
- Shannon, K. R. (1982): Cache Creek Group and contiguous rocks, near Cache Creek, B.C.; unpublished M.Sc. thesis, University of British Columbia, Vancouver, B.C., 72p.
- Sillitoe, R.H. (1980): Types of porphyry molybdenum deposits: Mining Magazine, v. 142, p. 550-551, 553.
- Sillitoe, R. H. (2010): Porphyry Copper Systems: Economic Geology, v. 105, p. 3-41.
- Sinclair, A.J. and White, W.H. (1968): Age of mineralization and post-ore hydrothermal alteration at Copper Mountain, BC; Canadian Institute of Mining, Metallurgy and Petroleum Bulletin, Volume 61, Number 673, 633–636 p.
- Sinclair, W.D. (2007): Porphyry deposits, in Goodfellow, W.D., ed., Mineral Deposits of Canada: A Synthesis of Major Deposit-Types, District Metallogeny, the Evolution of Geological Provinces, and Exploration Methods: Geological Association of Canada, Mineral Deposits Division, Special Publication No. 5, p. 223-243.
- Smith, R. B. (1979): Geology of the Harper Ranch Group (Carboniferous-Permian) and Nicola Group (upper Triassic) northeast of Kamloops, British Columbia; unpublished M.Sc. thesis, University of British Columbia, Vancouver, B.C., 225 p.
- Stakes, D. S. and O'Neil, J. R. (1982): Mineralogy and stable isotope geochemistry of hydrothermally altered oceanic rocks. Earth and Planetary Science Letters, Volume 57, Issue 2, p. 285–304.
- Staudigel, H., Muehlenbachs, K., Richardson, S., and Hart, S. R. (1981): Agents of low temperature ocean crust alteration: Contributions to Mineralogy and Petrology, v. 77, p. 150-157.
- Staudigel, H. and Hart S.R. (1983): Alteration of basaltic glass: Mechanism and significance to the oceanic crust - seawater budget. Geochimica et Cosmochimica Acta, vol. 47, p. 337-350.
- Stormer, J.C. Jr, Pierson, M.L. and Tacker, R.C. (1993): Variation in F and Cl X-ray intensity due to anisotropic diffusion in apatite during electron microprobe analysis. American Mineralogist, 78: 641-648.

- Taylor, R. W. (1964): Phase equilibria in the system FeO-Fe₂O₃-TiO₂ at 1300°C; *American Mineralogist*, v. 49, no. 7–8, p. 1016–1030.
- Taylor, H.P., Frechen, J. and Degens, E.T. (1967): Oxygen carbon isotope studies of carbonatites from the Laachersee district, West Germany and Alnö district, Sweden; *Geochimica et Cosmochimica Acta*, v. 31, p. 407–430.
- Thompson, J., Lang, J. and Stanley, C. (2001): Platinum group elements in alkaline porphyry deposits, British Columbia. *Exploration and Mining in British Columbia – 2001*, Ministry of Energy, Mines and Petroleum Resources, p. 57-64.
- Titley, S. R., and Beane, R. E. (1981): Porphyry Copper Deposits; Part 1. Geologic Settings, Petrology, and Tectogenesis, in Skinner, B. J., ed., 75th Anniversary Volume: El Paso, Society of Economic Geologists, p. 214-234.
- Tosdal, R., Cooke, D., Simpson, K., Bissig, T., Bath, A., Byrne, K., Jackson, M., Jago, P., Micko, J., Pass, H. and Chamberlain, C. (2008): Alkalic porphyry Cu-Au deposits: developing an Integrated Exploration Model. MDRU-CODES: Shallow and deep-level alkalic deposits: porphyry module, Final Report (Executive Summary).
- Tosdal, R., Mortensen, J., Harris, A., Bissig, T. and Hart, C. (2009): Construction of an alkalic porphyry Au-Cu province in British Columbia: Triassic and Early Jurassic magmatism, amalgamation, and accretion of offshore island arcs to North America: In Glen, R., and Martin, C., (eds.) *International Conference on Island Arc – Continent collisions: The Macquarie Arc Conference*, Orange, Australia, April, 2009, Geological Society of Australia Abstracts No 92, 146 p.
- Travers, W. B. (1982): Possible large-scale overthrusting near Ashcroft, British Columbia: Implications for petroleum prospecting; *Bulletin of Canadian Petroleum Geology*, v.30, no. 1, p. 1-8.
- Vaca, S., Bissig, T., Mitchinson, D.E., Barker, S. and Hart, C.J.R. (2011): Variability in the basaltic rocks hosting copper-gold porphyry mineralization in the Quesnel terrane, south-central British Columbia (NTS 092, 093): geochemistry, stable isotopes and physical properties; in *Geoscience BC Summary of Activities 2010*, Geoscience BC, Report 2011-1, p. 123–132.

Vaca, S., Bissig, T., Raudsepp, M. and Hart, C.J.R. (2012): Chemical variations of pyroxene and Fe-Ti-oxide crystals in basalts hosting Cu-Au porphyry mineralization in the Quesnel terrane, interior British Columbia (NTS 092H, I, P, 093A, J, N); in Geoscience BC Summary of Activities 2011, Geoscience BC, Report 2012-1, p. 69–78.

Veizer, J., Alab, D., Azmy, K., Bruckschen, P., Buhl, D., Bruhn, F., Cardena, G., Diener, A., Ebner, S., Godderis, Y., Jasper, T., Korte, C., Pawellek, F., Podlaha, O., and Strauss, H. (1999): $^{87}\text{Sr}/^{86}\text{Sr}$, ^{13}C and ^{18}O evolution of Phanerozoic seawater. *Chemical Geology*; v. 161, p. 59-88.

von Breyman, M.T., and Berner, U. (1991): Isotopic characterization of secondary carbonates from Sulu and Celebes sea basalts: contrasting scenarios of basalt-seawater interaction. In Silver, E.A., Rangin, C., von Breyman, M.T., et al., *Proc. ODP, Sci. Results*, 124: College Station, TX (Ocean Drilling Program), 233–237 p.

Wernicke, B. and Klepacki, D. (1988): Escape hypothesis for the Stikine block. *Geology*, v. 16, p. 461-464.

Winter, J.D. (2010): *Principles of Igneous and Metamorphic Petrology*. Second edition, Prentice Hall. 702 pp.

Wolfe, R. C. (2001): *Geology of the Didipio Region and Paragenesis of the Dinkidi Cu-Au Porphyry Deposit*: Unpublished PhD thesis, University of Tasmania, 201 p.

Woodsworth, G.J., Anderson, R.G. and Armstrong, R.L., 1991, *Plutonic Regimes: Chapter 15 of Geology of the Canadian Orogen in Canada*, H. Gabrielse and C.J. Yorath (ed.), Geological Survey of Canada, *Geology of Canada*, no. 4, p. 493-531 (also Geological Society of America, *The Geology of North America*, v. G-2).

<http://www.lithoprobe.ca/media/poster/panels/2.asp>

http://www.litho.ucalgary.ca/atlas/snorcle/snorcle_menu.html

http://www.stratigraphy.org/ics%20chart/09_2010/StratChart2010.pdf

APPENDIX A.

Table A1. List of samples showing the amounts of the most important phenocryst phases and the occurrence of Fe-Ti oxides and hematite within the basalts. All of the samples contain (5 – 10 %) of epidote, chlorite, calcite and clays as alteration minerals. Rocks with (*) in the sample ID show aphanitic texture. For these, the mineral amount of those samples represent the content within the whole rock.

Sample ID	UTM NAD83 zone 10		Location	Main phenocryst phases			Fe-Ti Oxide (%)	Hem ¹	MS (x10 ⁻³ SI units)	ρ_s (g/cm ³)
	East	North		Cpx (%)	Plag (%)	Anl (%)				
PSV001	588953	5830055	Mount Polley-LTNav	15	10	10	<1	x	1.41	-
PSV002	588966	5830062	Mount Polley-LTNav	30	14	12	1	x	21.5	2.65
PSV003	589059	5830056	Mount Polley-LTNav	30	15	-	1	-	41.9	2.728
PSV007	589328	5825476	Mount Polley-LTNpt	10	50	-	1-2	-	70.1	2.78
PSV009	588497	5820559	Mount Polley-LTNpv	25	35	-	1-2	-	70	2.83
PSV010	588388	5820571	Mount Polley-LTNpv	7	35	-	1-2	-	43.60	2.92
PSV011	588311	5820396	Mount Polley-LTNpv	15	30	-	1-2	-	40.5	2.86
PSV012	594951	5830341	Mount Polley-LTNpv	7	10	-	1-2	-	44	2.83
PSV016	597756	5826139	Mount Polley-LTNpv	25	4	-	1	x	23.7	2.84
PSV017	597925	5822708	Mount Polley-LTNpv	30	3	7	<1	x	1.16	-
PSV022	591325	5814986	Mount Polley-LTNpv	25	10	-	-	-	74.9	2.97
PSV026	593744	5822273	Mount Polley-LTNav	35	25	-	2-3	-	86.1	2.91
PSV028	588392	5825520	Mount Polley-LTNpt	20	30	-	2-3	-	111	2.87
PSV036	594651	5825485	Mount Polley-LTNav	12	-	2	-	x	23.4	2.72
PSV039	596426	5822502	Mount Polley-LTNav	20	15	30	1-2	x	60.9	2.68

Sample ID	UTM NAD83 zone 10		Location	Main phenocryst phases			Fe-Ti Oxide (%)	Hem ¹	MS (x10 ⁻³ SI units)	ρ _s (g/cm ³)
	East	North		Cpx (%)	Plag (%)	Anl (%)				
PSV046*	585818	5820707	Mount Polley-LTNpv	10	60	-	2 - 3	-	50.80	2.84
PSV047	585888	5821553	Mount Polley-LTNpv	20	-	-	1	x	14.20	2.88
PSV049	581416	5825988	Mount Polley-LTNav	8	5	-	-	x	25.70	-
MTB019	433638	6110081	Mount Milligan	25	30	-	~1	-	20.50	-
MTB021	432956	6110076	Mount Milligan	10	-	-	<1	-	0.52	-
MTB026	433314	6106210	Mount Milligan	20	10	-	<1	-	0.55	-
MTB027	433436	6106319	Mount Milligan	18	10	-	<1	-	14.00	2.87
MTB029	433445	6106319	Mount Milligan	15	20	-	<1	-	0.43	-
MTB030	433079	6105548	Mount Milligan	7	-	-	<1	-	0.59	2.83
MTB031	433079	6105548	Mount Milligan	27	10	-	<1	-	0.40	2.89
MTB032	433037	6105484	Mount Milligan	12	-	-	<1	-	0.68	3.00
MTB034	432316	6109336	Mount Milligan	15	20	-	<1	-	0.48	-
MTB041	432997	6109336	Mount Milligan	18	10	-	~1	-	38.8	-
MTB091	435471	6099107	Mount Milligan	18	7	-	<1	-	0.96	2.96
CMSV202	682230	5471334	Copper Mountain	15	20	-	<1	-	0.60	2.88
CMSV203	681762	5461207	Copper Mountain	30	-	-	<1	-	1.20	2.99
WTB083	610749	5786160	Woodjam	12	20	-	~1	x	0.96	2.92
WTB084*	610757	5786160	Woodjam	10	80	-	~2	x	1.02	2.89
WTB085	611019	5786299	Woodjam	20	30	-	~1	x	1.55	2.91
WTB086	610972	5786570	Woodjam	10	20	-	<1	x	0.58	2.88
WTB087	610940	5786703	Woodjam		30	-	<1	x	0.20	2.72
LTB067	617760	5755186	Lac la Hache	35	25	-	2	x	40.00	2.91

Sample ID	UTM NAD83 zone 10		Location	Main phenocryst phases			Fe-Ti Oxide (%)	Hem ¹	MS (x10 ⁻³ SI units)	ρ _s (g/cm ³)
	East	North		Cpx (%)	Plag (%)	Anl (%)				
LTB068	617760	5755186	Lac la Hache	17	25	-	~1	x	1.62	2.86
LTB071	605473	5773358	Lac la Hache	20	30	-	1-2	-	52.20	2.94
LTB072	605976	5772606	Lac la Hache	20	30	-	~1	-	25.40	2.96
LTB073	606030	5773254	Lac la Hache	33	13	-	1 - 2	-	83.50	2.98
LTB080	617706	5754892	Lac la Hache	10	30	-	~1	x	51.90	-
LTB081	617696	5754906	Lac la Hache	15	-	-	~1	x	0.59	-
BTB051	670097	5712526	Bridge Lake	37	5	-	<1	-	1.29	-
BTB053	671988	5713072	Bridge Lake	18	10	-	<1	-	0.61	2.95
BTB056	686663	5711042	Bridge Lake	15	5	-	~1	-	52.10	2.97
BTB057	689454	5714531	Bridge Lake	18	5	-	<1	-	0.52	3.05
BTB061	658595	5766692	Bridge Lake	13	-	-	<1	-	1.12	3.01
BTB062	664065	5761057	Bridge Lake	25	5	-	<1	-	1.07	-
BTB063	664065	5761057	Bridge Lake	30	-	-	<1	-	1.85	3.00
BTB077	663949	5763692	Bridge Lake	35	-	-	~1	-	44.50	2.96
SSV127	675079	5522407	South of Merritt	25	-	-	~3	x	10.50	2.96
SSV128	676083	5521435	South of Merritt	30	-	10	~1	x	0.97	2.98
SSV129	675831	5521742	South of Merritt	25	-	-	<1	x	1.40	3.03
SSV133	673013	5533483	South of Merritt	10	7	-	<1	x	0.40	2.86
SSV134	672750	5533373	South of Merritt	7	7	-	~1	x	30.00	2.89
SSV135	672482	5533925	South of Merritt	8	12	-	~1	x	5.50	2.88
SSV137	677670	5520099	South of Merritt	30	-	-	1-2	-	63.10	2.99

Cpx = clinopyroxene; Plag = plagioclase; Anl = analcime; Hem= hematite; MS= magnetic susceptibility; * = rock with aphanitic texture; ¹ = within the matrix and patches; ρ_s= density of sample.

APPENDIX B.

Rock samples were analysed at the ALS laboratory, Vancouver, BC, Canada. Using the analytical package code **ME-MS81d**, this is a combination of whole rock package by method ME-ICP06, plus rare earth and trace elements from method ME-MS81. Additionally, ferrous iron was measured on selected samples using the Fe-VOL05 package. All geochemical procedures were obtained from <http://www.alsglobal.com/>

ME-ICP06 package: Analysis of major oxides by Inductively Coupled Plasma - Atomic Emission Spectroscopy (ICP-AES).

Sample Decomposition: Lithium Metaborate/Lithium Tetraborate ($\text{LiBO}_2/\text{Li}_2\text{B}_4\text{O}_7$) Fusion* (FUS-LI01).

Analytical Method: A prepared sample (0.20g) is added to lithium metaborate/lithium tetraborate flux (0.90g), mixed well and fused in a furnace at 1000°C. The resulting melt is then cooled and dissolved in 100 mL of 4% nitric acid/2% hydrochloric acid. This solution is then analyzed by ICP-AES and the results are corrected for spectral inter-element interferences. Oxide concentration is calculated from the determined elemental concentration and the result is reported in that format.

Table B1. Major elements package ME-ICP06, indicating lower and upper limits.

Element	Symbol	Units	Lower Limit	Upper Limit
Aluminum	Al_2O_3	%	0.01	100
Barium	BaO	%	0.01	100
Calcium	CaO	%	0.01	100
Chromium	Cr_2O_3	%	0.01	100
Iron	Fe_2O_3	%	0.01	100
Magnesium	MgO	%	0.01	100
Manganese	MnO	%	0.01	100
Phosphorus	P_2O_5	%	0.01	100
Potassium	K_2O	%	0.01	100
Silicon	SiO_2	%	0.01	100
Sodium	Na_2O	%	0.01	100

ME-MS81 package: Analysis of trace elements by Inductively Coupled Plasma - Mass Spectroscopy (ICP - MS).

Sample Decomposition: Lithium Metaborate Fusion (FUS-LI01).

Analytical Method: A prepared sample (0.200g) is added to lithium metaborate flux (0.90 g), mixed well and fused in a furnace at 1000°C. The resulting melt is then cooled and dissolved in 100 mL of 4% HNO₃ / 2% HCl solution. This solution is then analyzed by inductively coupled plasma - mass spectrometry.

Table B2. Trace elements package ME-MS81, indicating lower and upper limits.

Element	Symbol	Units	Lower Limit	Upper Limit
Silver*	Ag	ppm	1	1000
Barium	Ba	ppm	0.5	10000
Cerium	Ce	ppm	0.5	10000
Cobalt*	Co	ppm	0.5	10000
Chromium	Cr	ppm	10	10000
Cesium	Cs	ppm	0.01	10000
Copper*	Cu	ppm	5	10000
Dysprosium	Dy	ppm	0.05	1000
Erbium	Er	ppm	0.03	1000
Europium	Eu	ppm	0.03	1000
Gallium	Ga	ppm	0.1	1000
Gadolinium	Gd	ppm	0.05	1000
Hafnium	Hf	ppm	0.2	10000
Holmium	Ho	ppm	0.01	1000
Lanthanum	La	ppm	0.5	10000
Lutetium	Lu	ppm	0.01	1000
Molybdenum*	Mo	ppm	2	10000
Niobium	Nb	ppm	0.2	10000
Neodymium	Nd	ppm	0.1	10000

Element	Symbol	Units	Lower Limit	Upper Limit
Nickel*	Ni	ppm	5	10000
Lead*	Pb	ppm	5	10000
Praseodymium	Pr	ppm	0.03	1000
Rubidium	Rb	ppm	0.2	10000
Samarium	Sm	ppm	0.03	1000
Tin	Sn	ppm	1	10000
Strontium	Sr	ppm	0.1	10000
Tantalum	Ta	ppm	0.1	10000
Terbium	Tb	ppm	0.01	1000
Thorium	Th	ppm	0.05	1000
Thallium	Tl	ppm	0.5	1000
Thulium	Tm	ppm	0.01	1000
Uranium	U	ppm	0.05	1000
Vanadium	V	ppm	5	10000
Tungsten	W	ppm	1	10000
Yttrium	Y	ppm	0.5	10000
Ytterbium	Yb	ppm	0.03	1000
Zinc*	Zn	ppm	5	10000
Zirconium	Zr	ppm	2	10000

***Note:** Some base metal oxides and sulfides may not be completely decomposed by the lithium borate fusion. Results for Ag, Co, Cu, Mo, Ni, Pb, and Zn will not likely be quantitative by this method.

Fe-VOL05 package: Analysis of ferrous Fe by Titration.

Sample Decomposition: Sulphuric- Hydrofluoric Acid Digestion.

Analytical Method: Titration.

Table B3. Ferrous iron package Fe-VOL05, indicating lower and upper limits.

Analyte	Units	Lower Limit	Upper Limit
FeO	%	0.01	100

Table B4. Whole rock geochemistry in rock samples collected in different localities along the Nicola Group.

Sample ID	Mount Polley-LTNpv									Mount Polley-LTNav			
	PSV 009	PSV 010	PSV 011	PSV 012	PSV 016	PSV 017	PSV 022	PSV 046	PSV 047	PSV 001	PSV 002	PSV 003	PSV 026
SiO ₂	48.70	47.40	48.20	47.20	47.70	46.70	48.00	46.80	44.50	43.80	48.70	45.00	46.70
TiO ₂	0.74	0.72	0.83	0.61	0.52	0.52	0.62	0.91	0.79	0.59	0.50	0.65	0.86
Al ₂ O ₃	14.75	14.95	15.25	16.65	12.60	10.55	13.50	16.15	13.40	10.00	15.25	14.60	14.05
Fe ₂ O ₃	10.85	10.65	11.75	9.41	9.86	10.75	10.80	12.25	10.85	11.40	8.60	9.84	13.10
MnO	0.19	0.19	0.21	0.15	0.17	0.18	0.17	0.20	0.18	0.21	0.16	0.26	0.23
MgO	6.10	5.36	5.01	5.33	8.96	10.05	7.61	5.74	7.52	9.82	4.80	4.60	6.30
CaO	8.26	9.87	8.06	10.75	10.55	11.15	11.55	9.20	9.91	12.10	7.86	9.76	10.40
Na ₂ O	3.25	4.72	4.04	3.53	2.03	2.41	1.86	3.05	2.29	3.00	5.79	4.09	3.26
K ₂ O	3.61	0.97	2.01	0.66	3.16	2.69	3.42	1.99	3.59	1.66	1.58	2.91	1.47
P ₂ O ₅	0.59	0.58	0.50	0.32	0.28	0.41	0.34	0.31	0.47	0.63	0.63	0.58	0.82
Cr ₂ O ₃	0.02	0.01	<0.01	0.01	0.05	0.06	0.04	0.01	0.03	0.07	0.02	0.01	0.01
SrO	0.11	0.10	0.09	0.06	0.06	0.08	0.11	0.13	0.07	0.04	0.11	0.05	0.11
BaO	0.11	0.01	0.08	0.02	0.09	0.11	0.09	0.21	0.06	0.08	0.10	0.11	0.10
LOI	2.15	2.56	2.19	4.62	3.67	4.47	2.36	2.94	6.11	6.48	5.37	6.73	2.08
Total	99.40	98.10	98.20	99.30	99.70	100.00	100.50	99.90	99.80	99.90	99.50	99.20	99.50
FeOvol05	4.98	-	-	-	3.94	1.62	4.92	-	-	-	2.03	3.74	5.37
Fe ²⁺	3.87	-	-	-	3.06	1.26	3.82	-	-	-	1.58	2.91	4.17
Fe ³⁺	3.72	-	-	-	3.83	6.26	3.73	-	-	-	4.44	3.98	4.99
<i>Trace elements</i>													
Rb	70.00	28.90	33.70	12.20	59.90	44.00	61.90	25.20	61.20	44.40	36.00	44.60	57.40
Cs	12.00	1.47	1.34	0.26	2.06	0.66	1.32	0.25	2.18	0.75	2.45	1.01	1.50
Ba	966.00	73.60	720.00	182.50	789.00	842.00	789.00	1725.00	517.00	683.00	986.00	851.00	822.00
Sn	1.00	1.00	1.00	1.00	1.00	1.00	1.00	1.00	1.00	1.00	1.00	1.00	1.00
Sr	916.00	842.00	706.00	482.00	519.00	598.00	915.00	1045.00	535.00	594.00	1160.00	568.00	920.00
La	13.80	14.40	11.80	6.00	5.90	9.40	6.70	7.50	11.50	10.80	15.60	13.10	22.30

Table B4. continued

Sample ID	Mount Polley-LTNpv							Mount Polley-LTNav					
	PSV 009	PSV 010	PSV 011	PSV 012	PSV 016	PSV 017	PSV 022	PSV 046	PSV 047	PSV 001	PSV 002	PSV 003	PSV 026
Ce	27.10	28.00	23.90	13.00	12.20	16.70	13.70	15.80	23.40	21.40	26.90	24.10	43.40
Pr	3.54	3.60	3.22	1.90	1.71	2.11	1.87	2.21	3.06	2.89	3.27	2.96	5.50
Nd	14.60	14.50	13.60	8.50	7.70	8.70	8.40	9.70	13.00	11.30	12.40	11.50	22.00
Sm	3.38	3.31	3.41	2.41	2.09	2.06	2.14	2.58	3.22	2.83	2.70	2.56	4.61
Eu	1.08	1.14	1.14	0.87	0.73	0.68	0.80	0.96	1.06	0.80	0.88	0.78	1.41
Gd	3.43	3.47	3.50	2.61	2.24	2.23	2.43	2.98	3.32	2.70	2.68	2.69	4.55
Tb	0.54	0.54	0.57	0.45	0.37	0.35	0.41	0.50	0.54	0.44	0.42	0.42	0.66
Dy	3.17	3.17	3.50	2.94	2.39	2.00	2.57	3.23	3.34	2.52	2.47	2.47	3.66
Tm	0.26	0.27	0.30	0.27	0.19	0.15	0.22	0.28	0.27	0.18	0.23	0.20	0.28
Yb	1.71	1.66	1.83	1.75	1.32	1.07	1.43	1.87	1.75	1.10	1.35	1.37	1.77
Lu	0.26	0.25	0.28	0.27	0.20	0.15	0.23	0.28	0.27	0.15	0.21	0.20	0.28
Zr	57.00	56.00	57.00	50.00	38.00	31.00	36.00	48.00	56.00	40.00	50.00	48.00	63.00
Hf	1.80	1.80	1.90	1.60	1.20	1.00	1.20	1.60	1.80	1.30	1.40	1.40	2.10
Th	1.96	1.95	1.45	0.78	0.78	1.37	0.80	1.07	1.46	1.43	2.26	2.10	3.13
Ho	0.64	0.62	0.69	0.60	0.46	0.39	0.53	0.68	0.67	0.45	0.49	0.50	0.70
Er	1.88	1.81	2.06	1.80	1.41	1.16	1.58	2.02	1.94	1.33	1.47	1.50	2.03
Nb	2.70	2.70	2.40	1.40	1.20	1.30	1.40	1.90	2.20	1.80	2.90	2.20	3.90
Ta	0.20	0.20	0.20	0.10	0.10	0.10	0.10	0.10	0.10	0.10	0.20	0.10	0.20
U	0.94	1.00	0.76	0.77	0.43	0.55	0.41	0.72	0.73	0.55	1.58	1.48	1.45
Y	17.30	17.10	19.00	16.60	12.80	10.80	14.10	17.90	17.80	12.70	13.70	13.70	19.30
Ni	31.00	21.00	28.00	36.00	91.00	65.00	95.00	23.00	43.00	78.00	29.00	11.00	20.00
Co	34.70	34.70	41.90	33.20	38.50	42.00	41.40	39.50	39.40	46.50	28.40	32.70	39.80
Cr	110.00	60.00	40.00	100.00	340.00	380.00	310.00	40.00	190.00	480.00	120.00	20.00	70.00
Cu	122.00	17.00	49.00	126.00	64.00	67.00	122.00	196.00	122.00	63.00	69.00	156.00	362.00
Zn	92.00	94.00	103.00	91.00	85.00	78.00	88.00	102.00	98.00	85.00	88.00	90.00	128.00
V	275.00	263.00	305.00	222.00	272.00	218.00	279.00	328.00	287.00	247.00	223.00	237.00	367.00
Ga	14.60	16.50	16.40	18.10	13.50	11.40	14.50	16.40	17.20	12.10	14.10	15.20	16.40

Table B4. continued

Mount Polley-LTNav				Mount Polley-LTNpt		Mount Milligan							
Sample ID	PSV 036	PSV 039	PSV 049	PSV 007	PSV 028	MTB 019	MTB 021	MTB 026	MTB 027	MTB 029	MTB 030	MTB 031	MTB 032
SiO ₂	38.90	47.50	43.00	49.10	45.60	49.40	47.60	51.80	46.40	51.10	47.60	47.30	48.30
TiO ₂	0.78	0.53	0.62	0.89	0.89	1.16	0.70	0.81	0.65	0.82	0.64	0.75	0.71
Al ₂ O ₃	11.65	16.20	10.95	16.15	13.75	11.80	15.40	16.15	13.50	16.40	15.40	13.35	12.90
Fe ₂ O ₃	10.35	8.77	10.45	10.10	11.90	9.36	9.02	9.95	9.92	9.53	9.11	9.67	10.25
MnO	0.33	0.18	0.20	0.22	0.20	0.22	0.19	0.18	0.18	0.16	0.21	0.16	0.16
MgO	4.33	5.82	5.63	4.11	6.77	6.36	6.06	4.42	9.85	4.75	8.40	10.45	9.26
CaO	15.25	7.86	13.35	7.69	11.15	8.63	8.72	6.59	9.25	7.69	8.62	9.13	9.17
Na ₂ O	2.45	6.42	1.50	3.82	3.20	2.58	3.14	4.63	1.64	3.09	2.56	2.61	2.30
K ₂ O	4.03	0.71	5.22	3.01	1.28	0.89	1.86	2.49	3.55	3.37	2.49	1.65	2.45
P ₂ O ₅	0.61	0.67	0.54	0.30	0.21	0.28	0.18	0.42	0.50	0.45	0.34	0.26	0.25
Cr ₂ O ₃	0.01	0.02	0.03	<0.01	0.01	0.03	0.01	0.01	0.05	0.02	0.03	0.07	0.05
SrO	0.10	0.09	0.06	0.12	0.07	0.03	0.06	0.05	0.12	0.06	0.05	0.04	0.04
BaO	0.09	0.10	0.11	0.25	0.15	0.02	0.12	0.11	0.13	0.11	0.10	0.05	0.08
LOI	11.10	5.20	8.70	4.04	5.06	9.56	7.06	2.65	4.31	2.80	3.80	4.28	4.60
Total	100.00	100.00	100.50	99.80	100.00	100.50	100.00	100.50	100.00	100.50	99.40	99.80	100.50
FeOvol05	-	3.66	2.66	-	5.11	-	-	-	5.86	-	6.84	7.19	7.32
Fe ²⁺	-	2.84	2.07	-	3.97	-	-	-	4.55	-	5.32	5.59	5.69
Fe ³⁺	-	3.29	5.24	-	4.35	-	-	-	2.38	-	1.05	1.17	1.48
<i>Trace elements</i>													
Rb	55.10	20.30	83.40	50.10	20.00	24.80	29.50	39.40	78.50	65.10	49.70	30.90	40.70
Cs	0.39	5.23	0.43	3.33	0.59	1.02	0.70	0.44	2.93	0.80	1.18	1.14	1.50
Ba	740.00	855.00	937.00	2130.00	1255.00	138.50	1065.00	1000.00	1135.00	995.00	904.00	422.00	738.00
Sn	1.00	1.00	1.00	1.00	1.00	1.00	1.00	1.00	1.00	1.00	1.00	1.00	1.00
Sr	805.00	753.00	530.00	944.00	586.00	279.00	437.00	405.00	911.00	450.00	458.00	330.00	362.00
La	13.80	16.20	12.80	8.00	4.80	7.70	6.20	10.90	11.50	10.90	4.70	4.50	4.00

Table B4. continued

Mount Polley-LTNav				Mount Polley-LTNpt		Mount Milligan							
Sample ID	PSV 036	PSV 039	PSV 049	PSV 007	PSV 028	MTB 019	MTB 021	MTB 026	MTB 027	MTB 029	MTB 030	MTB 031	MTB 032
Ce	27.90	28.00	26.00	17.30	11.10	17.70	12.70	20.30	21.70	21.30	10.30	10.20	8.90
Pr	3.65	3.33	3.44	2.51	1.72	2.62	1.81	2.75	2.81	2.81	1.56	1.55	1.37
Nd	14.70	12.70	13.90	11.20	8.30	12.30	7.80	11.30	11.50	11.70	7.00	7.10	6.40
Sm	3.21	2.71	3.04	3.14	2.56	3.79	2.22	2.87	2.82	2.93	2.09	2.27	1.99
Eu	1.06	0.86	0.92	1.09	0.93	1.27	0.77	0.89	0.89	0.88	0.75	0.77	0.66
Gd	3.30	2.85	3.08	3.58	3.13	4.35	2.35	3.18	2.82	3.10	2.35	2.39	2.24
Tb	0.50	0.42	0.44	0.63	0.57	0.77	0.41	0.51	0.45	0.51	0.41	0.43	0.39
Dy	2.87	2.46	2.53	4.17	3.55	4.86	2.45	3.02	2.49	3.03	2.49	2.66	2.44
Tm	0.22	0.22	0.21	0.38	0.30	0.46	0.21	0.28	0.22	0.28	0.23	0.24	0.22
Yb	1.39	1.42	1.28	2.58	1.99	2.93	1.41	1.74	1.30	1.86	1.44	1.48	1.42
Lu	0.21	0.21	0.20	0.39	0.29	0.43	0.22	0.27	0.20	0.30	0.21	0.23	0.22
Zr	46.00	52.00	41.00	71.00	45.00	104.00	41.00	75.00	47.00	82.00	44.00	51.00	42.00
Hf	1.40	1.40	1.40	2.20	1.60	2.90	1.30	2.20	1.40	2.30	1.30	1.50	1.20
Th	1.49	2.39	1.50	1.10	0.57	0.99	0.97	2.29	2.35	2.94	0.72	0.59	0.57
Ho	0.55	0.49	0.49	0.88	0.73	1.07	0.52	0.64	0.50	0.65	0.55	0.58	0.53
Er	1.62	1.50	1.45	2.64	2.15	3.11	1.49	1.87	1.42	1.91	1.52	1.63	1.49
Nb	2.70	3.00	1.90	2.10	1.20	3.80	2.40	6.10	5.40	6.50	2.00	2.30	1.90
Ta	0.20	0.20	0.10	0.10	0.10	0.30	0.10	0.40	0.30	0.40	0.10	0.20	0.10
U	0.80	1.79	0.75	0.60	0.33	0.60	0.49	1.21	1.12	1.42	0.43	0.34	0.36
Y	15.50	14.00	13.90	23.90	19.50	28.20	14.10	17.40	13.60	17.80	14.60	15.30	14.10
Ni	17.00	38.00	31.00	10.00	25.00	30.00	38.00	27.00	153.00	45.00	85.00	173.00	96.00
Co	33.40	29.70	34.80	29.60	38.80	28.40	29.50	31.70	42.60	28.10	39.80	44.40	44.00
Cr	60.00	120.00	210.00	10.00	40.00	220.00	90.00	70.00	360.00	120.00	230.00	450.00	320.00
Cu	107.00	293.00	71.00	135.00	63.00	61.00	108.00	177.00	144.00	126.00	87.00	93.00	93.00
Zn	90.00	104.00	83.00	129.00	91.00	146.00	130.00	123.00	87.00	101.00	109.00	77.00	91.00
V	210.00	215.00	229.00	275.00	354.00	247.00	240.00	245.00	240.00	260.00	222.00	249.00	224.00
Ga	13.80	14.90	11.70	16.20	14.90	15.20	15.20	16.10	14.80	17.60	15.40	13.30	13.40

Table B4. continued

Mount Milligan				Woodjack					Copper Mountain		Lac La Hache		
Sample ID	MTB 034	MTB 041	MTB 091	WTB 083	WTB 084	WTB 085	WTB 086	WTB 087	CMSV 202	CMSV 203	LTB 067	LTB 068	LTB 071
SiO ₂	48.70	48.90	48.70	51.40	51.40	49.90	50.80	55.10	50.40	47.90	44.00	44.10	48.20
TiO ₂	0.90	0.90	0.72	0.71	0.69	0.71	0.68	0.63	0.52	0.71	0.85	0.88	0.61
Al ₂ O ₃	15.25	15.05	13.15	15.75	18.50	15.55	15.10	20.10	16.90	11.30	14.55	16.10	13.25
Fe ₂ O ₃	9.95	11.40	10.35	9.82	9.18	9.66	9.26	6.13	10.40	10.95	11.90	12.50	10.65
MnO	0.18	0.13	0.18	0.13	0.12	0.14	0.12	0.03	0.26	0.19	0.25	0.26	0.19
MgO	5.75	6.78	6.08	5.00	3.86	6.84	6.81	2.22	5.24	9.22	6.10	5.12	8.87
CaO	9.46	8.31	11.60	8.86	7.77	7.01	7.78	4.36	7.87	11.85	9.80	9.85	10.30
Na ₂ O	2.83	3.27	3.75	4.17	4.36	3.46	3.08	5.14	2.92	3.14	2.40	2.89	2.04
K ₂ O	2.59	1.87	0.81	1.49	2.21	3.13	3.00	3.72	2.83	0.87	2.75	2.88	2.71
P ₂ O ₅	0.34	0.32	0.31	0.51	0.41	0.46	0.44	0.53	0.38	0.31	0.52	0.53	0.36
Cr ₂ O ₃	0.01	0.01	0.02	0.01	<0.01	0.03	0.03	0.01	<0.01	0.05	<0.01	<0.01	0.04
SrO	0.09	0.08	0.03	0.12	0.12	0.12	0.08	0.11	0.06	0.04	0.11	0.09	0.09
BaO	0.17	0.12	0.04	0.11	0.11	0.16	0.16	0.19	0.14	0.02	0.07	0.08	0.07
LOI	3.60	2.70	2.59	0.90	0.70	1.10	1.80	1.91	3.01	3.68	6.55	4.61	2.61
Total	99.80	99.80	98.30	99.00	99.40	98.30	99.10	100.00	101.00	100.00	99.90	99.90	100.00
FeOvol05	-	-	7.20	1.46	1.02	1.20	1.71	0.76	7.75	7.12	3.25	2.41	5.87
Fe ²⁺	-	-	5.60	1.13	0.79	0.93	1.33	0.59	6.02	5.53	2.53	1.87	4.56
Fe ³⁺	-	-	1.64	5.73	5.63	5.82	5.15	3.70	1.25	2.12	5.80	6.87	2.89
<i>Trace elements</i>													
Rb	58.90	43.00	16.40	22.00	64.80	49.30	61.30	64.90	56.00	42.00	39.90	48.50	47.80
Cs	0.84	1.03	0.77	1.07	2.97	3.50	2.21	1.22	5.34	6.59	0.71	0.86	1.69
Ba	1530.00	1075.00	346.00	1040.00	1060.00	1545.00	1540.00	1695.00	1285.00	219.00	636.00	639.00	589.00
Sn	1.00	1.00	1.00	1.00	1.00	1.00	1.00	1.00	1.00	1.00	1.00	1.00	1.00
Sr	757.00	630.00	317.00	1080.00	1070.00	1110.00	765.00	917.00	505.00	350.00	880.00	725.00	746.00
La	9.70	9.40	8.60	12.70	10.90	10.40	11.20	5.10	10.20	6.40	7.80	7.90	6.20

Table B4. continued

Mount Milligan				Woodjack					Copper Mountain		Lac la Hache		
Sample ID	MTB 034	MTB 041	MTB 091	WTB 083	WTB 084	WTB 085	WTB 086	WTB 087	CMSV 202	CMSV 203	LTB 067	LTB 068	LTB 071
Ce	19.80	18.80	17.60	26.60	23.30	22.10	23.80	10.30	20.30	14.20	16.30	16.60	12.60
Pr	2.74	2.71	2.31	3.41	3.09	2.92	3.08	1.50	2.63	1.97	2.26	2.36	1.74
Nd	11.70	11.80	10.00	14.40	13.40	12.60	12.90	6.90	10.90	9.10	10.40	10.90	8.00
Sm	3.00	3.06	2.54	3.61	3.29	3.30	3.28	2.11	2.79	2.49	2.87	2.82	2.08
Eu	1.04	1.06	0.85	1.10	1.03	0.94	1.00	0.68	0.80	0.79	1.02	0.99	0.81
Gd	3.32	3.33	2.71	3.25	2.98	2.94	2.86	2.10	2.50	2.56	3.23	3.23	2.39
Tb	0.53	0.55	0.47	0.51	0.51	0.49	0.51	0.38	0.45	0.42	0.54	0.56	0.42
Dy	3.18	3.30	2.67	2.84	2.87	2.62	2.91	2.10	2.55	2.46	2.99	3.15	2.38
Tm	0.29	0.30	0.25	0.25	0.26	0.23	0.28	0.21	0.24	0.23	0.26	0.27	0.21
Yb	1.79	1.75	1.55	1.56	1.63	1.50	1.74	1.29	1.45	1.38	1.63	1.70	1.38
Lu	0.28	0.28	0.25	0.24	0.27	0.24	0.29	0.22	0.25	0.23	0.27	0.26	0.22
Zr	64.00	54.00	52.00	64.00	67.00	60.00	98.00	81.00	44.00	47.00	50.00	50.00	38.00
Hf	1.80	1.70	1.70	2.00	1.90	1.90	2.70	2.70	1.50	1.50	1.60	1.60	1.30
Th	1.50	1.35	1.60	1.77	1.40	1.57	2.44	2.65	1.89	0.87	0.94	0.97	0.87
Ho	0.67	0.69	0.57	0.58	0.59	0.54	0.62	0.44	0.55	0.52	0.66	0.69	0.53
Er	1.92	1.95	1.75	1.70	1.76	1.59	1.85	1.40	1.67	1.56	1.81	1.87	1.41
Nb	4.90	3.30	4.00	2.80	2.40	2.60	3.00	3.60	1.50	1.60	2.00	2.00	1.40
Ta	0.30	0.20	0.20	0.20	0.10	0.10	0.20	0.20	0.10	0.10	0.10	0.10	0.10
U	0.82	0.57	1.10	1.13	0.84	0.80	1.31	1.13	0.99	0.42	0.68	0.83	0.48
Y	18.50	18.80	16.00	17.00	18.10	16.00	17.40	13.00	15.50	15.20	16.80	17.10	13.20
Ni	38.00	35.00	37.00	29.00	11.00	73.00	90.00	56.00	15.00	116.00	12.00	9.00	70.00
Co	30.30	23.10	34.00	19.00	17.00	27.00	25.00	9.00	29.00	41.00	37.30	35.40	38.60
Cr	100.00	60.00	160.00	80.00	10.00	220.00	240.00	50.00	30.00	380.00	20.00	20.00	280.00
Cu	74.00	169.00	154.00	4.00	4.00	5.00	1.00	1.00	49.00	190.00	<5	8.00	127.00
Zn	70.00	53.00	91.00	38.00	26.00	83.00	46.00	59.00	91.00	86.00	109.00	122.00	83.00
V	281.00	353.00	284.00	336.00	307.00	300.00	284.00	224.00	266.00	260.00	345.00	327.00	253.00
Ga	16.80	17.60	16.10	17.00	18.80	16.40	17.50	15.00	15.50	13.80	16.60	15.60	13.30

Table B4. continued

Lac la Hache					Bridge Lake								South of Merritt
Sample ID	LTB 072	LTB 073	LTB 080	LTB 081	BTB 051	BTB 053	BTB 056	BTB 057	BTB 061	BTB 062	BTB 063	BTB 077	SSV 127
SiO ₂	48.00	48.50	46.00	45.90	47.90	52.00	47.50	48.00	49.30	48.90	49.00	46.10	48.10
TiO ₂	0.60	0.64	0.86	0.85	0.66	0.62	0.53	0.60	0.64	0.62	0.63	0.65	0.65
Al ₂ O ₃	12.55	13.00	15.60	15.15	11.50	12.95	11.35	13.10	12.05	10.25	13.00	11.30	12.00
Fe ₂ O ₃	11.00	11.10	11.80	11.50	11.10	8.22	11.75	10.80	12.20	10.65	10.35	10.55	10.55
MnO	0.20	0.18	0.21	0.24	0.19	0.16	0.17	0.19	0.20	0.16	0.18	0.16	0.17
MgO	7.60	7.49	6.95	5.87	9.16	7.22	9.45	6.68	6.82	10.15	10.15	9.08	9.98
CaO	12.40	10.60	8.50	9.05	13.65	10.65	9.89	13.95	12.40	12.85	10.20	10.75	9.98
Na ₂ O	2.48	1.74	3.33	4.23	2.84	3.96	2.04	1.37	2.84	2.47	2.47	2.31	2.02
K ₂ O	2.57	3.02	1.37	1.42	1.02	1.08	2.79	2.67	1.79	1.40	1.93	2.12	3.71
P ₂ O ₅	0.35	0.42	0.46	0.46	0.46	0.25	0.35	0.30	0.36	0.29	0.37	0.31	0.39
Cr ₂ O ₃	0.05	0.02	<0.01	<0.01	0.04	0.05	0.06	0.03	0.02	0.07	0.05	0.05	0.05
SrO	0.07	0.11	0.10	0.11	0.06	0.04	0.04	0.12	0.11	0.04	0.05	0.08	0.06
BaO	0.06	0.08	0.05	0.06	0.05	0.04	0.10	0.12	0.08	0.07	0.05	0.12	0.07
LOI	2.15	1.34	5.10	4.20	2.05	3.47	3.73	2.28	1.06	2.69	1.68	4.22	3.69
Total	100.00	98.20	100.50	99.00	100.50	100.50	99.80	100.00	99.90	100.50	100.00	97.80	101.50
FeOvol05	-	5.42	-	4.00	7.42	6.56	6.56	6.55	-	8.45	-	-	2.47
Fe ²⁺	-	4.21	-	3.11	5.77	5.10	5.10	5.09	-	6.57	-	-	1.92
Fe ³⁺	-	3.55	-	4.93	2.00	0.65	3.12	2.46	-	0.88	-	-	5.46
<i>Trace elements</i>													
Rb	45.60	49.50	30.60	31.20	20.40	16.20	57.30	45.70	41.80	37.80	31.90	43.20	87.60
Cs	0.60	1.00	4.10	2.79	2.69	1.51	1.03	1.30	2.55	1.00	0.31	0.94	3.70
Ba	467.00	666.00	462.00	534.00	380.00	370.00	799.00	970.00	706.00	549.00	413.00	1215.00	666.00
Sn	1.00	1.00	1.00	1.00	1.00	1.00	1.00	1.00	1.00	1.00	1.00	1.00	1.00
Sr	566.00	876.00	940.00	969.00	488.00	368.00	338.00	1000.00	920.00	359.00	361.00	708.00	514.00
La	5.90	8.50	8.70	8.40	8.90	4.50	6.90	8.50	10.20	5.20	5.50	7.80	6.50

Table B4. continued

Lac la Hache					Bridge Lake									South of Merritt
Sample ID	LTB 072	LTB 073	LTB 080	LTB 081	BTB 051	BTB 053	BTB 056	BTB 057	BTB 061	BTB 062	BTB 063	BTB 077	SSV 127	
Ce	12.40	16.80	18.50	18.00	18.20	10.00	14.50	17.20	21.30	11.70	11.30	16.80	13.50	
Pr	1.69	2.28	2.54	2.51	2.45	1.52	1.98	2.30	2.90	1.66	1.65	2.28	1.98	
Nd	7.80	10.30	11.40	11.20	10.20	6.90	8.70	10.20	12.60	8.20	7.40	10.40	9.00	
Sm	2.04	2.33	3.08	3.11	2.54	2.09	2.27	2.67	3.19	2.13	2.08	2.90	2.47	
Eu	0.74	0.82	0.97	1.00	0.84	0.64	0.68	0.93	1.02	0.83	0.80	0.87	0.77	
Gd	2.38	2.70	3.15	3.23	2.66	2.31	2.44	2.84	3.11	2.45	2.37	2.75	2.52	
Tb	0.42	0.45	0.55	0.54	0.43	0.40	0.38	0.47	0.47	0.40	0.43	0.45	0.40	
Dy	2.31	2.44	3.27	3.29	2.60	2.64	2.37	2.75	2.74	2.31	2.36	2.43	2.46	
Tm	0.22	0.23	0.29	0.29	0.22	0.23	0.19	0.21	0.21	0.19	0.20	0.22	0.21	
Yb	1.33	1.33	1.75	1.75	1.39	1.59	1.22	1.42	1.39	1.19	1.28	1.26	1.39	
Lu	0.22	0.22	0.28	0.28	0.21	0.24	0.19	0.22	0.21	0.19	0.22	0.20	0.21	
Zr	35.00	37.00	53.00	50.00	43.00	40.00	32.00	41.00	34.00	36.00	34.00	42.00	49.00	
Hf	1.10	1.20	1.80	1.70	1.50	1.30	1.00	1.30	1.20	1.10	1.10	1.30	1.50	
Th	0.79	1.14	0.97	0.90	0.90	0.59	1.58	1.38	2.05	0.77	1.56	1.49	0.84	
Ho	0.51	0.53	0.68	0.69	0.53	0.54	0.45	0.53	0.53	0.48	0.51	0.49	0.49	
Er	1.45	1.50	1.99	2.05	1.53	1.65	1.35	1.59	1.50	1.34	1.38	1.47	1.34	
Nb	1.30	1.50	2.40	2.30	1.80	1.40	1.10	1.90	1.50	2.00	1.90	3.30	1.70	
Ta	0.10	0.10	0.10	0.10	0.10	0.10	0.10	0.10	0.10	0.10	0.10	0.20	0.10	
U	0.48	0.59	0.63	0.60	0.42	0.39	0.66	0.69	0.82	0.42	0.74	0.69	0.47	
Y	13.00	13.50	20.10	19.40	14.10	14.80	12.60	14.50	14.20	11.90	13.10	14.50	14.80	
Ni	72.00	38.00	10.00	10.00	54.00	60.00	103.00	36.00	35.00	159.00	131.00	124.00	74.00	
Co	40.10	37.10	34.00	32.00	44.20	31.00	49.00	39.50	41.70	49.60	40.40	37.00	36.00	
Cr	300.00	130.00	20.00	20.00	270.00	320.00	430.00	180.00	110.00	480.00	350.00	330.00	340.00	
Cu	86.00	134.00	12.00	97.00	161.00	120.00	64.00	156.00	116.00	155.00	126.00	9.00	83.00	
Zn	58.00	91.00	94.00	113.00	88.00	82.00	98.00	86.00	93.00	73.00	73.00	76.00	82.00	
V	242.00	272.00	391.00	371.00	285.00	263.00	240.00	256.00	280.00	230.00	260.00	275.00	265.00	
Ga	12.40	13.20	16.60	16.10	14.60	12.90	12.70	14.30	13.60	11.70	13.00	13.80	12.40	

Table B4. continued

South of Merritt						
Sample ID	SSV 128	SSV 129	SSV 133	SSV 134	SSV 135	SSV 137
SiO ₂	47.70	46.10	48.10	49.50	49.30	48.40
TiO ₂	0.55	0.52	0.80	0.81	0.89	0.85
Al ₂ O ₃	10.95	10.15	15.15	15.45	16.15	12.85
Fe ₂ O ₃	11.25	10.80	9.46	9.94	9.73	11.75
MnO	0.18	0.17	0.14	0.18	0.17	0.19
MgO	10.25	11.10	6.79	6.73	6.24	8.46
CaO	11.75	11.55	7.31	8.75	7.13	10.30
Na ₂ O	3.21	2.65	2.66	3.32	2.38	3.50
K ₂ O	1.35	1.47	3.68	2.21	4.25	0.92
P ₂ O ₅	0.52	0.45	0.49	0.48	0.47	0.32
Cr ₂ O ₃	0.06	0.07	0.02	0.02	0.01	0.03
SrO	0.08	0.09	0.08	0.09	0.10	0.04
BaO	0.10	0.09	0.25	0.18	0.32	0.08
LOI	3.19	2.39	3.19	2.00	2.81	3.12
Total	101.00	97.60	98.10	99.70	100.00	101.00
FeOvol05	1.65	1.90	1.46	2.86	2.16	5.78
Fe ²⁺	1.28	1.48	1.13	2.22	1.68	4.49
Fe ³⁺	6.59	6.08	5.48	4.73	5.13	3.73
<i>Trace elements</i>						
Rb	22.70	29.50	105.50	47.00	118.50	14.30
Cs	2.31	1.31	2.58	2.67	3.20	0.34
Ba	962.00	921.00	2460.00	1645.00	3080.00	716.00
Sn	1.00	1.00	1.00	1.00	1.00	1.00
Sr	680.00	777.00	730.00	748.00	835.00	348.00
La	7.70	6.70	11.70	11.60	11.20	5.60

Table B4. continued

South of Merritt						
Sample ID	SSV 128	SSV 129	SSV 133	SSV 134	SSV 135	SSV 137
Ce	15.50	13.30	23.30	23.30	23.80	12.50
Pr	2.21	1.97	3.18	3.22	3.25	1.95
Nd	10.00	8.70	13.60	14.00	14.30	9.40
Sm	2.65	2.24	3.23	3.38	3.62	2.74
Eu	0.75	0.72	0.97	0.99	1.08	0.91
Gd	2.46	2.25	3.13	3.17	3.50	2.95
Tb	0.35	0.32	0.46	0.48	0.53	0.48
Dy	2.09	1.99	2.89	2.95	3.30	2.99
Tm	0.16	0.16	0.25	0.26	0.28	0.25
Yb	1.15	1.16	1.70	1.74	1.92	1.65
Lu	0.17	0.17	0.27	0.26	0.28	0.26
Zr	33.00	30.00	63.00	70.00	60.00	46.00
Hf	1.20	1.10	1.90	2.20	1.90	1.50
Th	1.16	0.98	2.36	2.27	1.69	0.64
Ho	0.40	0.39	0.60	0.58	0.67	0.61
Er	1.07	1.03	1.62	1.59	1.84	1.64
Nb	1.00	1.00	3.50	3.50	3.30	1.70
Ta	<0.1	0.10	0.20	0.20	0.20	0.10
U	0.38	0.49	1.18	1.08	0.63	0.33
Y	12.60	12.10	17.70	18.10	19.70	18.30
Ni	80.00	99.00	46.00	56.00	43.00	48.00
Co	41.00	45.00	26.00	27.00	29.00	38.00
Cr	410.00	520.00	130.00	150.00	90.00	210.00
Cu	535.00	103.00	10.00	369.00	31.00	52.00
Zn	77.00	76.00	67.00	98.00	93.00	91.00
V	278.00	324.00	335.00	383.00	335.00	335.00
Ga	11.70	11.40	15.60	16.80	16.90	14.30

Table B5. Quality assurance/Quality control (QA/QC) of whole rock and trace elements chemistry. Comparison of standards used in this thesis with a compilation of results using the same standard (BAS-1) and the same geochemical methods and laboratory (ALS).

Analyte	Unit	Standards Analyzed at ALS-Minerals, Vancouver, BC, Canada in this thesis										Compiled standard geochemistry from MDRU data base				
		BAS-1-1	BAS-1-2	BSA1-A	BAS1-B	BAS1-C	BAS1-D	BAS1-W	BAS1-X	BAS1-Y	BAS1-Z	Number of data	Average	Median	Max	Min
SiO2	%	52.60	52.80	53.10	53.10	53.00	53.30	52.60	53.80	54.00	52.50	10	52.86	52.94	53.60	51.83
Al2O3	%	15.30	15.40	15.20	15.40	15.15	15.10	15.25	15.55	15.50	15.35	10	15.37	15.38	15.61	15.10
Fe2O3	%	10.80	10.90	10.65	10.80	10.80	10.75	10.80	11.10	10.90	11.00	10	10.81	10.76	11.11	10.60
CaO	%	7.93	8.00	8.10	8.23	8.08	8.17	7.98	8.19	8.16	8.14	10	8.05	8.10	8.21	7.84
MgO	%	7.07	7.11	7.10	7.20	6.99	7.17	7.01	7.17	7.13	6.91	10	7.29	7.33	7.49	6.91
Na2O	%	3.32	3.32	3.19	3.23	3.23	3.18	3.20	3.28	3.26	3.13	10	3.20	3.17	3.36	3.04
K2O	%	0.52	0.53	0.54	0.54	0.53	0.52	0.54	0.55	0.52	0.52	10	0.55	0.54	0.62	0.51
Cr2O3	%	0.03	0.03	0.03	0.03	0.03	0.03	0.03	0.03	0.03	0.03	10	0.03	0.03	0.03	0.03
TiO2	%	1.32	1.33	1.26	1.28	1.32	1.26	1.28	1.31	1.30	1.28	10	1.29	1.28	1.36	1.22
MnO	%	0.15	0.15	0.14	0.14	0.15	0.14	0.14	0.14	0.14	0.14	10	0.14	0.14	0.15	0.13
P2O5	%	0.18	0.21	0.22	0.21	0.24	0.21	0.21	0.21	0.22	0.20	10	0.21	0.21	0.26	0.15
SrO	%	0.06	0.06	0.04	0.05	0.06	0.06	0.05	0.05	0.06	0.06	10	0.05	0.05	0.05	0.05
BaO	%	0.02	0.02	0.02	0.02	0.02	0.02	0.02	0.02	0.02	0.02	10	0.02	0.02	0.02	0.02
LOI	%	0.48	0.30	0.00	-0.30	0.19	0.10	0.20	0.20	0.40	-0.10	10	0.20	0.20	0.20	0.20
Total	%	99.80	100.00	99.60	99.90	99.80	100.00	99.30	101.50	101.50	99.20	10	99.84	99.92	100.80	98.21
Ba	ppm	171.00	175.00	174.00	177.00	167.00	162.00	180.00	187.00	180.50	179.00	10	176.40	178.00	187.00	167.00
Ce	ppm	19.60	19.80	20.60	20.60	19.70	17.60	20.80	21.70	19.60	21.30	10	20.55	20.25	22.00	19.50
Co	ppm	44.70	45.10	45.30	45.80	43.20	43.00	38.40	41.20	45.50	44.40	10	60.76	47.00	180.00	44.00
Cr	ppm	210.00	210.00	210.00	210.00	200.00	200.00	190.00	210.00	220.00	230.00	10	229.44	222.00	260.00	215.00
Cs	ppm	0.11	0.12	0.09	0.10	0.09	0.09	0.09	0.09	0.11	0.11	10	4.60	0.11	45.00	0.09
Cu	ppm	59.00	59.00	58.00	59.00	55.00	53.00	65.00	60.00	59.00	60.00	10	85.21	61.00	275.00	3.10
Dy	ppm	2.94	2.90	3.06	3.21	2.95	2.92	2.94	3.10	2.92	3.24	10	2.90	3.05	3.20	1.60
Er	ppm	1.58	1.53	1.64	1.67	1.57	1.47	1.57	1.73	1.36	1.66	10	1.49	1.50	1.66	1.10
Eu	ppm	1.13	1.19	1.19	1.20	1.16	1.13	1.22	1.24	1.19	1.28	10	1.22	1.24	1.30	1.10
Ga	ppm	18.30	18.70	19.30	19.20	18.20	17.80	18.30	18.70	18.90	19.20	10	19.09	19.00	20.40	18.00
Gd	ppm	3.33	3.33	3.40	3.38	3.30	3.14	3.16	3.39	3.26	3.60	10	3.50	3.40	3.80	3.28

Analyte	Unit	BAS-1-1	BAS-1-2	BSA1-A	BAS1-B	BAS1-C	BAS1-D	BAS1-W	BAS1-X	BAS1-Y	BAS1-Z	Number of data	Average	Median	Max	Min
Hf	ppm	2.30	2.20	2.30	2.40	2.20	2.10	2.20	2.70	2.30	2.30	10	2.30	2.30	3.00	2.00
Ho	ppm	0.57	0.59	0.57	0.58	0.55	0.57	0.55	0.61	0.52	0.61	10	0.61	0.60	0.64	0.60
La	ppm	8.80	9.00	9.10	9.00	8.60	7.60	9.00	9.30	9.00	9.60	10	9.17	8.85	11.00	8.50
Lu	ppm	0.19	0.19	0.19	0.20	0.19	0.19	0.20	0.20	0.18	0.21	10	0.19	0.20	0.23	0.10
Nb	ppm	7.10	7.30	7.10	6.90	6.60	6.40	7.20	7.50	7.00	7.00	10	7.52	7.65	8.00	6.90
Nd	ppm	12.10	12.20	12.50	12.60	12.00	11.40	12.50	13.40	12.50	13.20	10	13.15	13.00	13.50	13.00
Ni	ppm	177.00	178.00	172.00	173.00	166.00	153.00	160.00	148.00	146.00	147.00	10	176.80	174.00	191.00	160.00
Pr	ppm	2.80	2.80	2.85	2.86	2.76	2.40	2.80	2.97	2.82	2.91	10	2.87	2.90	3.00	2.70
Rb	ppm	6.20	6.30	6.00	6.30	5.90	5.70	6.50	6.80	6.90	7.20	10	6.72	6.65	7.60	5.60
Sm	ppm	3.32	3.27	3.24	3.35	3.18	2.92	3.39	3.58	3.21	3.48	10	3.39	3.46	3.52	3.10
Sn	ppm	1.00	1.00	1.00	1.00	1.00	1.00	1.00	1.00	1.00	1.00	10	1.02	1.00	1.10	1.00
Sr	ppm	452.00	455.00	450.00	452.00	431.00	434.00	454.00	475.00	476.00	500.00	10	458.00	452.50	502.00	404.00
Ta	ppm	0.40	0.40	0.40	0.40	0.40	0.40	0.40	0.40	0.40	0.40	10	0.51	0.50	0.70	0.47
Tb	ppm	0.52	0.51	0.53	0.55	0.51	0.54	0.55	0.58	0.49	0.53	10	0.54	0.53	0.58	0.50
Th	ppm	0.81	0.82	0.87	0.84	0.81	0.87	0.89	0.89	0.82	0.84	10	0.88	0.83	1.00	0.80
Tm	ppm	0.23	0.24	0.22	0.21	0.20	0.21	0.21	0.23	0.19	0.21	10	0.21	0.21	0.23	0.20
U	ppm	0.30	0.31	0.29	0.29	0.27	0.29	0.29	0.31	0.28	0.31	10	0.32	0.32	0.32	0.31
V	ppm	152.00	152.00	151.00	150.00	145.00	140.00	140.00	168.00	160.00	162.00	10	170.60	164.50	200.00	154.00
Y	ppm	15.20	14.90	15.50	15.50	14.80	14.00	15.40	16.60	15.30	17.20	10	13.12	15.75	17.00	1.40
Yb	ppm	1.31	1.29	1.34	1.35	1.28	1.19	1.34	1.39	1.29	1.45	10	19.87	1.40	107.00	1.20
Zn	ppm	106.00	109.00	106.00	107.00	102.00	91.00	104.00	95.00	92.00	94.00	10	88.33	104.00	120.00	14.30
Zr	ppm	87.00	86.00	83.00	82.00	79.00	80.00	79.00	92.00	81.00	86.00	10	86.29	86.95	91.00	79.50

Table B6. Electron microprobe analyses of clinopyroxene from different localities along the Nicola Group.

Location		Mount Polley - LTNpv unit															
Sample ID		PSV009											PSV016				
Spot ID	A-1_R	A-2_I	A-3_I	A-4_C	A-5_I	B-10_C	B-11_I	B-12_R	B-6_R	B-7_I	B-8_C	B-9_C	A-1_R	A-2_I	A-3_I	A-4_C	A-5_I
SiO ₂	49.09	49.87	49.92	50.14	50.49	49.91	50.88	49.63	50.17	49.51	48.71	49.80	50.39	51.03	51.88	51.10	48.36
TiO ₂	0.67	0.82	0.73	0.64	0.55	0.79	0.61	1.19	0.57	0.66	0.84	0.70	0.45	0.24	0.25	0.39	0.68
Al ₂ O ₃	5.05	4.03	3.79	3.60	3.55	4.04	3.00	4.72	3.63	4.08	4.71	3.84	2.96	2.56	1.98	2.86	5.28
FeO(t)	8.06	8.41	8.18	8.77	8.39	8.64	8.81	8.83	8.63	8.90	9.81	8.99	8.74	5.59	8.21	7.73	7.81
MnO	0.20	0.28	0.27	0.26	0.28	0.32	0.25	0.15	0.23	0.24	0.27	0.30	0.28	0.07	0.38	0.27	0.20
MgO	13.90	13.27	13.69	13.41	13.69	13.29	13.92	13.06	13.75	13.65	12.98	13.54	14.50	15.77	15.29	15.81	13.84
CaO	22.72	22.25	22.59	22.39	22.35	22.12	21.96	21.70	21.97	21.78	21.67	22.06	21.92	22.78	21.22	20.92	21.87
Na ₂ O	0.34	0.59	0.54	0.56	0.53	0.45	0.45	0.67	0.44	0.45	0.51	0.43	0.34	0.20	0.38	0.36	0.34
NiO	0.00	0.00	0.00	0.02	0.01	0.03	0.00	0.00	0.04	0.00	0.00	0.00	0.00	0.01	0.03	0.05	0.00
Cr ₂ O ₃	0.03	0.01	0.02	0.02	0.00	0.01	0.05	0.04	0.00	0.00	0.00	0.00	0.03	0.36	0.05	0.14	0.00
Total	100.06	99.53	99.72	99.82	99.85	99.60	99.93	99.98	99.43	99.27	99.49	99.66	99.61	98.61	99.67	99.63	98.38
Cation calculation based in 6 O																	
Si	1.82	1.86	1.86	1.87	1.88	1.86	1.89	1.84	1.87	1.85	1.82	1.86	1.87	1.90	1.92	1.89	1.82
Ti	0.02	0.02	0.02	0.02	0.02	0.02	0.02	0.03	0.02	0.02	0.02	0.02	0.01	0.01	0.01	0.01	0.02
Al ^(IV)	0.19	0.14	0.15	0.14	0.13	0.14	0.11	0.16	0.13	0.15	0.18	0.14	0.13	0.10	0.08	0.11	0.18
Al ^(VI)	0.04	0.04	0.02	0.02	0.03	0.04	0.02	0.05	0.03	0.03	0.03	0.03	0.00	0.01	0.01	0.01	0.05
Fe ³⁺ (IV)	0.00	0.00	0.00	0.00	0.00	0.00	0.00	0.00	0.00	0.00	0.00	0.00	0.00	0.00	0.00	0.00	0.00
Fe ³⁺ (VI)	0.14	0.10	0.12	0.12	0.10	0.08	0.08	0.09	0.10	0.12	0.14	0.11	0.12	0.08	0.08	0.10	0.12
Fe ²⁺	0.11	0.16	0.13	0.16	0.16	0.19	0.19	0.19	0.17	0.16	0.17	0.17	0.15	0.09	0.18	0.14	0.12
Mn	0.01	0.01	0.01	0.01	0.01	0.01	0.01	0.01	0.01	0.01	0.01	0.01	0.01	0.00	0.01	0.01	0.01
Mg	0.77	0.74	0.76	0.74	0.76	0.74	0.77	0.72	0.77	0.76	0.72	0.75	0.80	0.87	0.85	0.87	0.78
Ca	0.90	0.89	0.90	0.89	0.89	0.89	0.87	0.86	0.88	0.87	0.87	0.88	0.87	0.91	0.84	0.83	0.88
Na	0.02	0.04	0.04	0.04	0.04	0.03	0.03	0.05	0.03	0.03	0.04	0.03	0.03	0.02	0.03	0.03	0.03
Ni	0.00	0.00	0.00	0.00	0.00	0.00	0.00	0.00	0.00	0.00	0.00	0.00	0.00	0.00	0.00	0.00	0.00
Cr	0.00	0.00	0.00	0.00	0.00	0.00	0.00	0.00	0.00	0.00	0.00	0.00	0.00	0.01	0.00	0.00	0.00
Mg#	87.18	81.99	85.14	82.58	82.75	79.92	80.29	79.32	81.51	82.32	80.90	81.52	84.24	90.62	82.79	86.28	86.19

Mg# = 100*Mg/(Mg+Fe²⁺) ; C= Core; I= Interior; R= Rim

Table B6. (continued)

Location		Mount Polley – LTNpv unit															
Sample ID		PSV016													PSV017		
Spot ID	A-6_I	A-7_R	A-8_C	B-9_R	B-10_I	B-11_I	B-12_I	B-13_I	B-14_C	B-15_C	B-16_I	B-17_I	B-18_I	B-19_R	1_R	2_I	3_I
SiO ₂	47.87	47.94	51.05	48.96	48.96	48.13	48.95	48.58	52.00	49.94	49.08	49.09	49.44	47.81	48.73	49.73	48.44
TiO ₂	0.62	0.83	0.33	0.71	0.75	0.74	0.41	0.77	0.21	0.44	0.61	0.62	0.69	0.69	0.56	0.45	0.61
Al ₂ O ₃	5.96	5.01	3.04	4.39	4.39	4.51	4.94	5.01	1.95	4.06	4.75	4.59	4.16	5.54	5.18	4.01	5.06
FeO(t)	7.90	9.31	8.30	9.17	8.79	8.77	7.37	8.17	5.33	7.47	8.59	8.33	8.89	8.41	7.67	6.90	7.80
MnO	0.15	0.26	0.32	0.18	0.22	0.21	0.16	0.19	0.12	0.14	0.17	0.23	0.19	0.17	0.17	0.21	0.17
MgO	13.42	13.19	14.80	13.58	13.47	13.34	14.29	14.08	16.17	14.50	13.85	13.98	14.16	13.50	13.89	14.71	13.89
CaO	22.25	21.96	21.54	22.12	22.07	22.14	22.26	22.18	23.46	22.20	21.54	22.09	21.93	22.43	22.61	22.65	22.79
Na ₂ O	0.35	0.45	0.38	0.40	0.41	0.34	0.37	0.38	0.26	0.54	0.36	0.37	0.40	0.36	0.41	0.39	0.38
NiO	0.05	0.04	0.00	0.00	0.00	0.02	0.00	0.02	0.00	0.05	0.00	0.05	0.00	0.00	0.03	0.03	0.00
Cr ₂ O ₃	0.15	0.02	0.00	0.05	0.02	0.00	0.08	0.12	0.15	0.16	0.12	0.07	0.00	0.05	0.07	0.00	0.01
Total	98.73	99.00	99.78	99.56	99.08	98.21	98.84	99.50	99.66	99.50	99.07	99.42	99.87	98.96	99.32	99.08	99.15
Cation calculation based in 6 O																	
Si	1.79	1.80	1.89	1.83	1.83	1.82	1.82	1.81	1.91	1.85	1.84	1.83	1.83	1.79	1.81	1.85	1.80
Ti	0.02	0.02	0.01	0.02	0.02	0.02	0.01	0.02	0.01	0.01	0.02	0.02	0.02	0.02	0.02	0.01	0.02
Al ^(IV)	0.21	0.20	0.11	0.17	0.17	0.18	0.18	0.20	0.08	0.15	0.17	0.17	0.17	0.21	0.19	0.15	0.20
Al ^(VI)	0.06	0.02	0.02	0.02	0.03	0.02	0.04	0.02	0.00	0.03	0.04	0.03	0.02	0.03	0.04	0.02	0.03
Fe ³⁺ (IV)	0.00	0.00	0.00	0.00	0.00	0.00	0.00	0.00	0.01	0.00	0.00	0.00	0.00	0.00	0.00	0.00	0.00
Fe ³⁺ (VI)	0.14	0.17	0.09	0.14	0.12	0.14	0.14	0.15	0.09	0.13	0.11	0.13	0.14	0.17	0.15	0.13	0.16
Fe ²⁺	0.11	0.13	0.16	0.14	0.15	0.13	0.09	0.10	0.07	0.10	0.16	0.13	0.14	0.10	0.09	0.08	0.08
Mn	0.01	0.01	0.01	0.01	0.01	0.01	0.01	0.01	0.00	0.00	0.01	0.01	0.01	0.01	0.01	0.01	0.01
Mg	0.75	0.74	0.82	0.76	0.75	0.75	0.79	0.78	0.89	0.80	0.77	0.78	0.78	0.75	0.77	0.81	0.77
Ca	0.89	0.88	0.86	0.88	0.89	0.90	0.89	0.88	0.92	0.88	0.86	0.88	0.87	0.90	0.90	0.90	0.91
Na	0.03	0.03	0.03	0.03	0.03	0.03	0.03	0.03	0.02	0.04	0.03	0.03	0.03	0.03	0.03	0.03	0.03
Ni	0.00	0.00	0.00	0.00	0.00	0.00	0.00	0.00	0.00	0.00	0.00	0.00	0.00	0.00	0.00	0.00	0.00
Cr	0.00	0.00	0.00	0.00	0.00	0.00	0.00	0.00	0.00	0.01	0.00	0.00	0.00	0.00	0.00	0.00	0.00
Mg#	87.13	85.44	83.38	84.09	83.28	84.88	89.40	88.41	93.12	89.18	82.82	86.01	85.31	88.46	89.34	90.98	90.52

Table B6. (continued)

Location	Mount Polley-LTNpv								Mount Polley-LTNav								
Sample ID	PSV017								PSV002								
Spot ID	4_I	5_I	6_I	7_C	8_C	9_I	10_I	11_R	1_R	2_I	3_I	4_I	5_I	6_C	7_I	8_I	9_R
SiO ₂	48.36	48.07	48.03	51.06	53.22	48.79	49.15	49.86	50.35	48.66	48.73	47.39	47.54	47.44	47.88	48.96	49.51
TiO ₂	0.65	0.64	0.64	0.34	0.12	0.54	0.53	0.45	0.44	0.67	0.62	0.69	0.61	0.78	0.80	0.63	0.70
Al ₂ O ₃	5.18	5.30	5.43	2.80	1.39	4.94	4.49	3.82	3.82	4.86	4.32	5.86	5.26	5.80	5.81	4.60	5.11
FeO(t)	7.97	7.90	8.01	5.47	3.49	7.79	7.18	6.98	6.88	7.95	7.64	8.19	8.36	8.16	8.27	7.99	8.05
MnO	0.16	0.18	0.13	0.12	0.12	0.19	0.15	0.25	0.23	0.26	0.26	0.20	0.22	0.22	0.24	0.29	0.25
MgO	13.90	13.64	13.75	15.55	17.35	14.21	14.45	14.33	14.16	13.34	13.43	12.97	13.25	12.94	12.87	13.42	13.21
CaO	22.79	22.70	22.87	22.85	23.31	22.85	22.85	22.64	22.77	22.61	22.75	22.82	22.68	22.94	22.96	22.79	22.69
Na ₂ O	0.39	0.31	0.41	0.36	0.22	0.35	0.38	0.41	0.48	0.61	0.55	0.54	0.41	0.58	0.60	0.55	0.59
NiO	0.01	0.02	0.00	0.01	0.00	0.03	0.00	0.03	0.00	0.00	0.00	0.00	0.00	0.00	0.00	0.00	0.01
Cr ₂ O ₃	0.05	0.02	0.00	0.66	0.52	0.07	0.01	0.02	0.01	0.00	0.04	0.04	0.07	0.00	0.00	0.01	0.00
Total	99.45	98.78	99.26	99.23	99.74	99.75	99.19	98.80	99.14	98.95	98.35	98.70	98.40	98.86	99.42	99.25	100.11
Cation calculation based in 6 O																	
Si	1.80	1.80	1.79	1.89	1.94	1.81	1.83	1.86	1.87	1.82	1.83	1.78	1.79	1.78	1.78	1.83	1.83
Ti	0.02	0.02	0.02	0.01	0.00	0.02	0.02	0.01	0.01	0.02	0.02	0.02	0.02	0.02	0.02	0.02	0.02
Al ^(IV)	0.20	0.20	0.21	0.11	0.06	0.20	0.18	0.14	0.13	0.18	0.17	0.22	0.21	0.22	0.22	0.18	0.17
Al ^(VI)	0.02	0.03	0.03	0.01	0.00	0.02	0.02	0.03	0.04	0.03	0.02	0.04	0.02	0.03	0.04	0.03	0.05
Fe ³⁺ (IV)	0.00	0.00	0.00	0.00	0.00	0.00	0.00	0.00	0.00	0.00	0.00	0.00	0.00	0.00	0.00	0.00	0.00
Fe ³⁺ (VI)	0.17	0.15	0.18	0.09	0.05	0.17	0.15	0.12	0.10	0.16	0.15	0.19	0.18	0.19	0.18	0.15	0.12
Fe ²⁺	0.08	0.09	0.07	0.08	0.06	0.07	0.07	0.10	0.12	0.09	0.09	0.07	0.08	0.06	0.08	0.10	0.13
Mn	0.01	0.01	0.00	0.00	0.00	0.01	0.01	0.01	0.01	0.01	0.01	0.01	0.01	0.01	0.01	0.01	0.01
Mg	0.77	0.76	0.76	0.86	0.94	0.78	0.80	0.80	0.79	0.74	0.75	0.73	0.74	0.72	0.72	0.75	0.73
Ca	0.91	0.91	0.91	0.91	0.91	0.91	0.91	0.91	0.91	0.91	0.92	0.92	0.91	0.92	0.92	0.91	0.90
Na	0.03	0.02	0.03	0.03	0.02	0.03	0.03	0.03	0.03	0.04	0.04	0.04	0.03	0.04	0.04	0.04	0.04
Ni	0.00	0.00	0.00	0.00	0.00	0.00	0.00	0.00	0.00	0.00	0.00	0.00	0.00	0.00	0.00	0.00	0.00
Cr	0.00	0.00	0.00	0.02	0.02	0.00	0.00	0.00	0.00	0.00	0.00	0.00	0.00	0.00	0.00	0.00	0.00
Mg#	90.96	88.97	91.77	91.61	94.40	91.44	91.80	88.65	87.08	88.90	89.08	91.20	90.14	91.82	89.85	88.36	84.79

Table B6. (continued)

Location			Mount Polley – LTNav unit														
Sample ID	PSV002		PSV003														
Spot ID	10_I	11_I	A-1_R	A-2_I	A-3_I	A-4_C	A-5_C	A-6_I	A-7_I	A-8_I	A-9_R	B-10_R	B-11_I	B-12_I	B-13_C	B-14_C	B-15_I
SiO ₂	48.97	48.95	49.82	49.22	49.70	49.77	48.11	48.38	47.98	48.58	47.84	47.93	47.96	47.79	48.94	48.63	48.50
TiO ₂	0.60	0.61	0.58	0.64	0.58	0.52	0.70	0.70	0.83	0.68	0.80	0.72	0.74	0.67	0.77	0.71	0.72
Al ₂ O ₃	4.59	4.97	4.17	4.28	4.07	3.91	5.42	5.42	5.64	5.21	5.57	5.45	4.78	4.87	4.86	5.35	4.82
FeO(t)	7.97	7.89	8.20	8.09	7.74	7.77	8.37	8.59	8.82	8.67	8.44	8.71	8.35	8.31	8.39	8.44	8.07
MnO	0.20	0.16	0.21	0.30	0.24	0.27	0.21	0.28	0.22	0.28	0.30	0.24	0.29	0.26	0.24	0.29	0.30
MgO	13.45	13.54	13.56	13.55	13.89	13.75	13.18	13.01	12.69	13.00	12.82	12.54	13.06	12.89	13.14	13.00	13.37
CaO	22.43	23.28	22.62	22.42	22.61	22.80	22.39	22.31	22.38	22.58	22.06	22.22	22.59	22.27	22.28	22.33	22.49
Na ₂ O	0.57	0.41	0.53	0.44	0.41	0.50	0.47	0.45	0.46	0.49	0.47	0.53	0.46	0.48	0.52	0.50	0.46
NiO	0.01	0.01	0.01	0.00	0.00	0.00	0.01	0.03	0.00	0.03	0.00	0.02	0.00	0.00	0.00	0.03	0.05
Cr ₂ O ₃	0.00	0.02	0.00	0.00	0.00	0.00	0.01	0.03	0.00	0.00	0.00	0.01	0.00	0.00	0.00	0.00	0.03
Total	98.78	99.83	99.70	98.94	99.23	99.29	98.88	99.19	99.02	99.52	98.29	98.36	98.21	97.54	99.13	99.28	98.82
Cation calculation based in 6 O																	
Si	1.83	1.81	1.85	1.84	1.85	1.85	1.80	1.81	1.80	1.81	1.81	1.81	1.81	1.82	1.83	1.82	1.82
Ti	0.02	0.02	0.02	0.02	0.02	0.02	0.02	0.02	0.02	0.02	0.02	0.02	0.02	0.02	0.02	0.02	0.02
Al ^(IV)	0.17	0.19	0.15	0.16	0.15	0.15	0.20	0.19	0.20	0.19	0.19	0.19	0.19	0.18	0.17	0.18	0.18
Al ^(VI)	0.04	0.03	0.03	0.03	0.03	0.03	0.04	0.05	0.05	0.04	0.05	0.05	0.02	0.04	0.05	0.05	0.03
Fe ^{3+ (IV)}	0.00	0.00	0.00	0.00	0.00	0.00	0.00	0.00	0.00	0.00	0.00	0.00	0.00	0.00	0.00	0.00	0.00
Fe ^{3+ (VI)}	0.14	0.15	0.12	0.12	0.11	0.13	0.15	0.13	0.14	0.15	0.13	0.14	0.16	0.15	0.12	0.13	0.14
Fe ²⁺	0.11	0.10	0.13	0.13	0.13	0.11	0.11	0.14	0.14	0.13	0.14	0.14	0.11	0.12	0.14	0.14	0.11
Mn	0.01	0.01	0.01	0.01	0.01	0.01	0.01	0.01	0.01	0.01	0.01	0.01	0.01	0.01	0.01	0.01	0.01
Mg	0.75	0.75	0.75	0.76	0.77	0.76	0.74	0.73	0.71	0.72	0.72	0.71	0.74	0.73	0.73	0.72	0.75
Ca	0.90	0.92	0.90	0.90	0.90	0.91	0.90	0.89	0.90	0.90	0.89	0.90	0.91	0.91	0.89	0.89	0.90
Na	0.04	0.03	0.04	0.03	0.03	0.04	0.03	0.03	0.03	0.04	0.04	0.04	0.03	0.04	0.04	0.04	0.03
Ni	0.00	0.00	0.00	0.00	0.00	0.00	0.00	0.00	0.00	0.00	0.00	0.00	0.00	0.00	0.00	0.00	0.00
Cr	0.00	0.00	0.00	0.00	0.00	0.00	0.00	0.00	0.00	0.00	0.00	0.00	0.00	0.00	0.00	0.00	0.00
Mg#	87.07	88.77	85.03	85.11	85.81	87.05	86.78	84.30	83.50	85.25	84.09	83.46	87.30	85.99	83.55	84.08	87.23

Table B6. (continued)

Location		Mount Polley-LTNav															
Sample ID	PSV003	PSV026												PSV039			
Spot ID	B-16_R	A-1_I	A-2_R	A-3_I	A-4_I	A-5_I	A-6_C	A-7_C	B-10_R	B-11_I	B-12_C	B-13_I	B-14_R	1_R	2_I	3_I	4_I
SiO ₂	48.02	47.40	46.96	46.59	53.58	53.34	53.65	53.43	48.07	49.39	47.74	47.99	48.04	49.81	51.44	51.89	49.36
TiO ₂	0.81	0.72	0.84	0.86	0.14	0.18	0.11	0.15	0.83	0.60	0.73	0.66	0.76	0.59	0.33	0.24	0.58
Al ₂ O ₃	5.38	6.24	6.29	6.67	0.92	1.01	0.84	0.95	5.73	4.17	5.70	5.38	5.69	4.34	2.73	2.16	4.33
FeO(t)	8.67	8.06	8.53	8.18	2.51	2.97	2.79	2.89	8.06	6.95	7.96	8.20	8.13	7.65	5.50	5.23	7.56
MnO	0.19	0.17	0.18	0.18	0.05	0.06	0.10	0.03	0.21	0.13	0.18	0.23	0.21	0.28	0.17	0.17	0.30
MgO	12.72	13.02	12.77	12.71	17.74	17.37	17.55	17.49	12.72	14.01	13.27	13.29	12.91	13.69	15.57	16.21	13.54
CaO	22.11	22.74	22.85	22.81	24.23	23.89	23.97	24.30	22.96	23.44	22.66	22.75	22.64	22.41	22.94	22.98	22.65
Na ₂ O	0.53	0.44	0.42	0.43	0.18	0.20	0.23	0.17	0.44	0.33	0.45	0.45	0.48	0.62	0.42	0.40	0.56
NiO	0.00	0.04	0.04	0.00	0.02	0.00	0.03	0.03	0.00	0.03	0.03	0.02	0.00	0.00	0.00	0.00	0.04
Cr ₂ O ₃	0.00	0.00	0.04	0.00	0.44	0.19	0.27	0.18	0.00	0.40	0.09	0.03	0.00	0.03	0.18	0.25	0.02
Total	98.43	98.83	98.92	98.44	99.81	99.20	99.55	99.63	99.01	99.46	98.81	99.01	98.86	99.42	99.28	99.53	98.95
Cation calculation based in 6 O																	
Si	1.81	1.77	1.76	1.75	1.95	1.95	1.96	1.95	1.80	1.84	1.79	1.79	1.80	1.85	1.90	1.91	1.84
Ti	0.02	0.02	0.02	0.02	0.00	0.01	0.00	0.00	0.02	0.02	0.02	0.02	0.02	0.02	0.01	0.01	0.02
Al ^(IV)	0.19	0.23	0.24	0.25	0.04	0.04	0.04	0.04	0.20	0.17	0.21	0.21	0.20	0.15	0.10	0.09	0.16
Al ^(VI)	0.05	0.05	0.04	0.05	0.00	0.00	0.00	0.00	0.05	0.02	0.04	0.03	0.05	0.04	0.02	0.00	0.04
Fe ³⁺ (IV)	0.00	0.00	0.00	0.00	0.01	0.00	0.01	0.01	0.00	0.00	0.00	0.00	0.00	0.00	0.00	0.00	0.00
Fe ³⁺ (VI)	0.13	0.17	0.18	0.18	0.05	0.05	0.05	0.05	0.13	0.13	0.16	0.17	0.14	0.12	0.09	0.10	0.13
Fe ²⁺	0.14	0.09	0.08	0.08	0.02	0.04	0.03	0.03	0.12	0.09	0.09	0.09	0.12	0.12	0.08	0.06	0.11
Mn	0.01	0.01	0.01	0.01	0.00	0.00	0.00	0.00	0.01	0.00	0.01	0.01	0.01	0.01	0.01	0.01	0.01
Mg	0.72	0.73	0.71	0.71	0.96	0.95	0.95	0.95	0.71	0.78	0.74	0.74	0.72	0.76	0.86	0.89	0.75
Ca	0.89	0.91	0.92	0.92	0.94	0.94	0.94	0.95	0.92	0.93	0.91	0.91	0.91	0.89	0.91	0.90	0.91
Na	0.04	0.03	0.03	0.03	0.01	0.01	0.02	0.01	0.03	0.02	0.03	0.03	0.04	0.05	0.03	0.03	0.04
Ni	0.00	0.00	0.00	0.00	0.00	0.00	0.00	0.00	0.00	0.00	0.00	0.00	0.00	0.00	0.00	0.00	0.00
Cr	0.00	0.00	0.00	0.00	0.01	0.01	0.01	0.01	0.00	0.01	0.00	0.00	0.00	0.00	0.01	0.01	0.00
Mg#	83.49	89.53	89.43	90.32	98.12	95.73	96.74	97.32	85.32	89.62	89.58	89.40	86.20	86.56	91.64	93.85	87.50

Table B6. (continued)

Location	Mount Polley – LTNav unit												Mount Polley – LTNpt unit				
Sample ID	PSV039												PSV007				
Spot ID	5_I	6_I	7_C	8_C	9_I	10_I	11_R	12_I	13_R	14_C	15_I	16_R	A-1_C	A-2_I	A-3_I	A-4_R	B-5_I
SiO ₂	49.49	49.58	53.05	51.61	49.56	48.56	49.63	47.82	47.60	47.34	48.31	48.49	52.76	51.94	51.67	51.43	53.59
TiO ₂	0.61	0.66	0.18	0.31	0.60	0.63	0.56	0.86	0.79	0.81	0.80	0.64	0.35	0.39	0.40	0.44	0.11
Al ₂ O ₃	4.33	4.57	2.20	2.39	4.44	5.33	4.50	5.76	5.82	6.21	5.59	5.49	1.67	2.05	1.89	2.38	0.98
FeO(t)	7.58	7.85	4.81	5.30	7.56	7.76	7.66	8.23	8.35	8.08	8.08	7.61	7.72	8.36	8.63	8.20	2.67
MnO	0.22	0.29	0.15	0.09	0.27	0.24	0.22	0.24	0.22	0.20	0.26	0.20	0.46	0.52	0.52	0.53	0.07
MgO	13.47	13.28	15.98	15.69	13.52	13.06	13.28	12.70	12.54	13.01	12.83	13.22	15.40	15.48	15.11	15.16	17.56
CaO	22.39	22.52	22.04	23.58	22.57	22.62	22.63	22.46	22.27	22.58	22.38	22.83	21.45	21.20	21.04	21.55	23.92
Na ₂ O	0.67	0.63	0.34	0.28	0.62	0.65	0.62	0.59	0.71	0.54	0.67	0.49	0.35	0.32	0.46	0.45	0.16
NiO	0.00	0.00	0.01	0.01	0.00	0.02	0.00	0.02	0.03	0.02	0.01	0.05	0.00	0.00	0.00	0.04	0.05
Cr ₂ O ₃	0.04	0.00	0.11	0.09	0.01	0.01	0.02	0.00	0.03	0.00	0.00	0.16	0.00	0.02	0.00	0.00	0.46
Total	98.79	99.38	98.86	99.36	99.13	98.88	99.13	98.68	98.36	98.79	98.94	99.19	100.16	100.28	99.71	100.17	99.58
Cation calculation based in 6 O																	
Si	1.85	1.85	1.96	1.90	1.85	1.82	1.85	1.80	1.79	1.77	1.81	1.81	1.95	1.92	1.92	1.90	1.96
Ti	0.02	0.02	0.01	0.01	0.02	0.02	0.02	0.02	0.02	0.02	0.02	0.02	0.01	0.01	0.01	0.01	0.00
Al ^(IV)	0.15	0.15	0.04	0.10	0.15	0.18	0.15	0.20	0.21	0.23	0.19	0.19	0.05	0.09	0.08	0.10	0.04
Al ^(VI)	0.04	0.05	0.06	0.01	0.04	0.05	0.05	0.05	0.05	0.05	0.05	0.05	0.02	0.00	0.00	0.00	0.00
Fe ^{3+ (IV)}	0.00	0.00	0.00	0.00	0.00	0.00	0.00	0.00	0.00	0.00	0.00	0.00	0.00	0.00	0.00	0.00	0.00
Fe ^{3+ (VI)}	0.12	0.12	0.00	0.09	0.12	0.15	0.11	0.15	0.16	0.17	0.14	0.14	0.04	0.08	0.09	0.11	0.04
Fe ²⁺	0.12	0.13	0.15	0.07	0.11	0.10	0.13	0.11	0.10	0.08	0.11	0.10	0.20	0.18	0.17	0.14	0.04
Mn	0.01	0.01	0.01	0.00	0.01	0.01	0.01	0.01	0.01	0.01	0.01	0.01	0.01	0.02	0.02	0.02	0.00
Mg	0.75	0.74	0.88	0.86	0.75	0.73	0.74	0.71	0.70	0.73	0.72	0.74	0.85	0.85	0.84	0.83	0.96
Ca	0.90	0.90	0.87	0.93	0.90	0.91	0.91	0.90	0.90	0.91	0.90	0.91	0.85	0.84	0.84	0.85	0.94
Na	0.05	0.05	0.02	0.02	0.05	0.05	0.05	0.04	0.05	0.04	0.05	0.04	0.03	0.02	0.03	0.03	0.01
Ni	0.00	0.00	0.00	0.00	0.00	0.00	0.00	0.00	0.00	0.00	0.00	0.00	0.00	0.00	0.00	0.00	0.00
Cr	0.00	0.00	0.00	0.00	0.00	0.00	0.00	0.00	0.00	0.00	0.00	0.01	0.00	0.00	0.00	0.00	0.01
Mg#	86.60	85.05	85.56	92.07	86.82	88.26	85.30	86.42	87.39	90.23	86.56	88.02	81.09	82.93	82.80	85.43	95.83

Table B6. (continued)

Location						Mount Polley-LTNpt												Mount Milligan
Sample ID		PSV007				PSV028											MBT031	
Spot ID	B-6_I	B-7_I	B-8_C	B-9_I	B-10_R	1_R	2_I	3_I	4_I	5_I	6_C	7_I	8_C	9_R	10_I	11_I	A-1_R	
SiO ₂	52.87	53.69	53.07	53.86	53.61	50.14	50.67	49.69	50.34	48.65	50.50	50.17	49.16	49.14	48.91	47.39	48.62	
TiO ₂	0.11	0.16	0.14	0.11	0.09	0.57	0.48	0.51	0.52	0.57	0.43	0.53	0.62	0.70	0.85	0.94	0.97	
Al ₂ O ₃	0.94	0.95	0.96	0.98	1.02	3.28	3.23	3.88	3.23	4.51	2.94	2.83	3.76	4.02	4.59	6.44	4.76	
FeO(t)	2.91	2.84	2.68	2.70	2.87	8.66	8.69	8.96	8.69	8.34	8.72	8.52	8.68	8.29	9.21	9.09	8.30	
MnO	0.13	0.06	0.06	0.05	0.07	0.32	0.28	0.36	0.32	0.24	0.35	0.32	0.29	0.28	0.28	0.25	0.15	
MgO	17.30	17.66	17.65	17.60	17.49	14.25	14.34	13.75	14.26	13.68	14.30	14.38	13.65	13.67	13.37	12.63	13.60	
CaO	23.90	24.14	24.03	24.02	24.30	21.32	21.44	21.17	21.32	21.95	21.04	21.92	22.12	21.77	21.61	21.73	22.18	
Na ₂ O	0.20	0.21	0.15	0.16	0.21	0.45	0.38	0.49	0.42	0.38	0.42	0.38	0.37	0.39	0.42	0.50	0.29	
NiO	0.00	0.00	0.00	0.06	0.01	0.04	0.02	0.00	0.06	0.04	0.00	0.00	0.00	0.00	0.04	0.05	0.00	
Cr ₂ O ₃	0.52	0.50	0.55	0.59	0.59	0.00	0.00	0.00	0.02	0.00	0.00	0.00	0.00	0.02	0.00	0.02	0.13	
Total	98.90	100.22	99.28	100.12	100.24	99.03	99.53	98.82	99.17	98.36	98.69	99.06	98.65	98.29	99.27	99.05	99.02	
Cation calculation based in 6 O																		
Si	1.94	1.95	1.94	1.96	1.94	1.88	1.89	1.87	1.88	1.83	1.90	1.88	1.85	1.85	1.83	1.78	1.82	
Ti	0.00	0.00	0.00	0.00	0.00	0.02	0.01	0.01	0.02	0.02	0.01	0.02	0.02	0.02	0.02	0.03	0.03	
Al ^(IV)	0.04	0.04	0.04	0.04	0.04	0.12	0.11	0.14	0.12	0.17	0.10	0.12	0.15	0.15	0.17	0.22	0.18	
Al ^(VI)	0.00	0.00	0.00	0.00	0.00	0.02	0.03	0.04	0.02	0.03	0.03	0.00	0.02	0.03	0.03	0.06	0.03	
Fe ^{3+ (IV)}	0.02	0.01	0.02	0.00	0.01	0.00	0.00	0.00	0.00	0.00	0.00	0.00	0.00	0.00	0.00	0.00	0.00	
Fe ^{3+ (VI)}	0.05	0.05	0.05	0.03	0.05	0.10	0.09	0.11	0.10	0.13	0.08	0.12	0.13	0.10	0.12	0.14	0.11	
Fe ²⁺	0.02	0.03	0.02	0.05	0.03	0.17	0.18	0.18	0.18	0.13	0.19	0.15	0.15	0.16	0.17	0.14	0.15	
Mn	0.00	0.00	0.00	0.00	0.00	0.01	0.01	0.01	0.01	0.01	0.01	0.01	0.01	0.01	0.01	0.01	0.01	
Mg	0.95	0.95	0.96	0.95	0.95	0.80	0.80	0.77	0.79	0.77	0.80	0.80	0.77	0.77	0.75	0.71	0.76	
Ca	0.94	0.94	0.94	0.93	0.94	0.85	0.86	0.85	0.85	0.89	0.85	0.88	0.89	0.88	0.87	0.87	0.89	
Na	0.01	0.02	0.01	0.01	0.01	0.03	0.03	0.04	0.03	0.03	0.03	0.03	0.03	0.03	0.03	0.04	0.02	
Ni	0.00	0.00	0.00	0.00	0.00	0.00	0.00	0.00	0.00	0.00	0.00	0.00	0.00	0.00	0.00	0.00	0.00	
Cr	0.02	0.01	0.02	0.02	0.02	0.00	0.00	0.00	0.00	0.00	0.00	0.00	0.00	0.00	0.00	0.00	0.00	
Mg#	97.50	97.22	98.11	95.42	97.35	82.66	81.22	81.47	81.89	85.51	80.86	84.66	83.92	82.85	81.35	83.18	83.38	

Table B6. (continued)

Location	Mount Milligan											Woodjam			
Sample ID	MBT031											WTB085			
Spot ID	A-2_I	A-3_C	A-4_C	A-5_I	A-6_R	A-7_R	B-8_I	B-9_I	B-10_I	B-11_R	B-12_C	1_R	2_C	3_R	4_I
SiO ₂	50.92	50.92	51.12	50.34	48.21	50.79	51.10	50.85	50.85	48.52	49.68	52.14	53.72	54.05	53.81
TiO ₂	0.61	0.54	0.52	0.60	1.03	0.61	0.56	0.55	0.57	1.03	0.75	0.24	0.04	0.08	0.04
Al ₂ O ₃	3.10	3.38	3.48	3.87	5.82	3.01	3.25	3.29	3.54	5.60	4.89	1.67	0.70	1.06	0.72
FeO(t)	7.36	7.01	6.36	6.42	8.63	7.60	7.28	7.15	6.93	8.63	6.71	3.72	2.51	2.83	2.65
MnO	0.14	0.20	0.13	0.09	0.20	0.16	0.19	0.19	0.22	0.15	0.16	0.50	0.56	0.52	0.68
MgO	14.69	15.05	15.44	14.96	13.30	14.95	14.87	15.09	14.58	13.69	14.15	15.90	16.69	18.06	17.16
CaO	22.02	21.94	22.02	22.43	21.77	21.99	22.13	21.59	22.25	21.30	22.22	23.62	24.30	21.53	22.47
Na ₂ O	0.23	0.35	0.21	0.25	0.33	0.25	0.32	0.26	0.27	0.34	0.28	0.47	0.29	0.32	0.37
NiO	0.02	0.02	0.01	0.01	0.00	0.01	0.02	0.02	0.01	0.04	0.00	0.06	0.00	0.04	0.03
Cr ₂ O ₃	0.14	0.19	0.27	0.33	0.04	0.16	0.13	0.03	0.27	0.18	0.36	0.09	0.00	0.02	0.06
Total	99.23	99.62	99.56	99.31	99.32	99.52	99.85	99.03	99.49	99.48	99.20	98.40	98.80	98.51	97.99
Cation calculation based in 6 O															
Si	1.90	1.88	1.89	1.87	1.80	1.89	1.89	1.89	1.89	1.81	1.85	1.93	1.98	1.99	1.99
Ti	0.02	0.02	0.02	0.02	0.03	0.02	0.02	0.02	0.02	0.03	0.02	0.01	0.00	0.00	0.00
Al ^(IV)	0.10	0.12	0.11	0.13	0.20	0.11	0.11	0.11	0.11	0.19	0.15	0.07	0.02	0.01	0.01
Al ^(VI)	0.03	0.03	0.04	0.04	0.06	0.02	0.03	0.04	0.04	0.06	0.06	0.01	0.01	0.03	0.03
Fe ^{3+ (IV)}	0.00	0.00	0.00	0.00	0.00	0.00	0.00	0.00	0.00	0.00	0.00	0.00	0.00	0.00	0.00
Fe ^{3+ (VI)}	0.05	0.08	0.05	0.07	0.11	0.08	0.07	0.06	0.05	0.10	0.06	0.08	0.03	0.00	0.00
Fe ²⁺	0.18	0.14	0.15	0.13	0.17	0.16	0.16	0.17	0.17	0.17	0.15	0.04	0.05	0.09	0.08
Mn	0.00	0.01	0.00	0.00	0.01	0.01	0.01	0.01	0.01	0.01	0.01	0.02	0.02	0.02	0.02
Mg	0.82	0.83	0.85	0.83	0.74	0.83	0.82	0.84	0.81	0.76	0.79	0.88	0.92	0.99	0.95
Ca	0.88	0.87	0.87	0.89	0.87	0.88	0.88	0.86	0.89	0.85	0.89	0.94	0.96	0.85	0.89
Na	0.02	0.03	0.02	0.02	0.02	0.02	0.02	0.02	0.02	0.03	0.02	0.03	0.02	0.02	0.03
Ni	0.00	0.00	0.00	0.00	0.00	0.00	0.00	0.00	0.00	0.00	0.00	0.00	0.00	0.00	0.00
Cr	0.00	0.01	0.01	0.01	0.00	0.01	0.00	0.00	0.01	0.01	0.01	0.00	0.00	0.00	0.00
Mg#	81.85	85.40	85.33	86.78	81.82	83.81	84.04	83.56	82.92	81.70	83.59	95.81	95.27	91.93	92.24

Table B6. (continued)

Location		Copper Mountain							Lac la Hache							
Sample ID		CMSV203							LTB067							
Spot ID	1_R	2_I	3_I	4_I	5_C	6_I	7_I	8_C	1_R	2_R	3_I	4_C	5_C	6_I	7_I	
SiO ₂	48.67	47.31	50.12	49.18	49.46	49.80	49.61	49.29	48.15	49.06	49.93	49.23	48.53	49.29	49.27	
TiO ₂	0.73	0.75	0.50	0.64	0.83	0.53	0.60	0.55	1.00	0.48	0.62	0.68	0.86	0.55	0.56	
Al ₂ O ₃	5.14	5.27	3.47	4.05	3.85	3.42	3.82	3.65	5.34	4.33	3.82	4.10	4.84	4.44	4.38	
FeO(t)	7.67	7.98	6.78	7.35	6.64	7.01	7.26	7.22	8.78	7.09	8.17	8.38	8.57	7.36	7.67	
MnO	0.17	0.17	0.15	0.24	0.21	0.24	0.23	0.20	0.24	0.15	0.24	0.25	0.25	0.15	0.18	
MgO	14.06	13.84	15.31	14.79	15.09	15.11	14.63	15.06	12.58	14.27	13.43	13.54	12.69	13.98	13.90	
CaO	22.28	22.33	22.28	21.91	21.96	21.75	21.94	21.76	22.06	22.78	22.14	22.03	22.30	23.12	22.26	
Na ₂ O	0.36	0.39	0.35	0.41	0.56	0.40	0.37	0.41	0.41	0.26	0.46	0.42	0.42	0.26	0.31	
NiO	0.00	0.00	0.05	0.01	0.04	0.02	0.02	0.01	0.01	0.01	0.06	0.00	0.01	0.00	0.00	
Cr ₂ O ₃	0.01	0.06	0.02	0.04	0.05	0.04	0.00	0.07	0.04	0.00	0.00	0.00	0.00	0.08	0.01	
Total	99.10	98.09	99.03	98.62	98.69	98.32	98.49	98.21	98.61	98.44	98.86	98.63	98.47	99.24	98.53	
Cation calculation based in 6 oxygen																
Si	1.81	1.78	1.86	1.84	1.84	1.86	1.86	1.85	1.82	1.84	1.87	1.85	1.83	1.84	1.85	
Ti	0.02	0.02	0.01	0.02	0.02	0.02	0.02	0.02	0.03	0.01	0.02	0.02	0.02	0.02	0.02	
Al ^(IV)	0.19	0.22	0.14	0.16	0.16	0.14	0.14	0.15	0.18	0.16	0.13	0.15	0.17	0.16	0.15	
Al ^(VI)	0.04	0.01	0.01	0.01	0.01	0.01	0.03	0.01	0.06	0.03	0.04	0.03	0.05	0.03	0.04	
Fe ³⁺ (IV)	0.00	0.00	0.00	0.00	0.00	0.00	0.00	0.00	0.00	0.00	0.00	0.00	0.00	0.00	0.00	
Fe ³⁺ (VI)	0.13	0.19	0.13	0.14	0.14	0.12	0.11	0.14	0.10	0.13	0.08	0.11	0.10	0.12	0.10	
Fe ²⁺	0.11	0.06	0.08	0.09	0.06	0.10	0.12	0.08	0.18	0.10	0.17	0.16	0.17	0.11	0.14	
Mn	0.01	0.01	0.01	0.01	0.01	0.01	0.01	0.01	0.01	0.01	0.01	0.01	0.01	0.01	0.01	
Mg	0.78	0.78	0.85	0.82	0.84	0.84	0.82	0.84	0.71	0.80	0.75	0.76	0.71	0.78	0.78	
Ca	0.89	0.90	0.89	0.88	0.88	0.87	0.88	0.87	0.89	0.91	0.89	0.89	0.90	0.92	0.90	
Na	0.03	0.03	0.03	0.03	0.04	0.03	0.03	0.03	0.03	0.02	0.03	0.03	0.03	0.02	0.02	
Ni	0.00	0.00	0.00	0.00	0.00	0.00	0.00	0.00	0.00	0.00	0.00	0.00	0.00	0.00	0.00	
Cr	0.00	0.00	0.00	0.00	0.00	0.00	0.00	0.00	0.00	0.00	0.00	0.00	0.00	0.00	0.00	
Mg#	88.07	92.57	90.96	90.42	93.03	89.63	87.60	91.13	79.91	89.12	81.27	83.02	80.73	87.58	84.57	

Table B6. (continued)

Location		Lac la Hache								Bridge Lake						
Sample ID	LTB067	LTB073								BTB051						
Spot ID	8_R	1_R	2_I	3_I	4_C	5_C	6_I	7_I	8_C	A-1_R	A-2_I	A-3_C	A-4_C	A-5_I	A-6_R	
SiO ₂	49.91	49.81	50.12	48.93	48.76	49.03	48.94	49.87	48.78	48.16	48.58	48.99	48.73	49.25	48.46	
TiO ₂	0.65	0.46	0.37	0.64	0.70	0.51	0.58	0.51	0.63	0.77	0.75	0.70	0.75	0.59	0.84	
Al ₂ O ₃	3.76	3.76	3.31	4.61	4.62	4.26	4.33	3.90	4.41	5.40	5.23	4.95	5.36	4.40	5.56	
FeO(t)	8.50	7.71	7.17	8.13	8.19	7.73	7.67	7.61	8.15	8.95	8.73	8.44	8.90	8.31	8.91	
MnO	0.29	0.22	0.23	0.20	0.26	0.21	0.20	0.19	0.21	0.28	0.22	0.24	0.23	0.21	0.18	
MgO	13.53	14.67	15.08	14.10	13.91	14.20	14.26	14.40	13.97	12.84	13.33	13.53	12.99	13.88	12.80	
CaO	21.93	21.98	22.00	21.93	21.79	22.01	21.96	21.73	21.93	22.54	22.22	22.56	22.17	22.26	22.28	
Na ₂ O	0.42	0.30	0.37	0.42	0.50	0.41	0.44	0.46	0.39	0.42	0.41	0.36	0.42	0.40	0.36	
NiO	0.00	0.01	0.00	0.00	0.00	0.02	0.03	0.00	0.00	0.05	0.00	0.02	0.00	0.00	0.00	
Cr ₂ O ₃	0.04	0.00	0.10	0.05	0.01	0.01	0.08	0.00	0.03	0.03	0.13	0.00	0.03	0.04	0.05	
Total	99.03	98.92	98.74	99.02	98.73	98.40	98.49	98.67	98.51	99.45	99.60	99.79	99.58	99.35	99.44	
Cation calculation based in 6 O																
Si	1.87	1.86	1.87	1.83	1.83	1.84	1.83	1.86	1.83	1.80	1.81	1.82	1.82	1.84	1.81	
Ti	0.02	0.01	0.01	0.02	0.02	0.01	0.02	0.01	0.02	0.02	0.02	0.02	0.02	0.02	0.02	
Al ^(IV)	0.13	0.14	0.13	0.17	0.18	0.16	0.17	0.14	0.17	0.20	0.19	0.18	0.18	0.17	0.19	
Al ^(VI)	0.04	0.02	0.01	0.03	0.03	0.03	0.03	0.04	0.03	0.04	0.04	0.04	0.05	0.03	0.06	
Fe ³⁺ (IV)	0.00	0.00	0.00	0.00	0.00	0.00	0.00	0.00	0.00	0.00	0.00	0.00	0.00	0.00	0.00	
Fe ³⁺ (VI)	0.09	0.12	0.12	0.14	0.14	0.13	0.14	0.11	0.14	0.15	0.13	0.13	0.12	0.13	0.11	
Fe ²⁺	0.18	0.13	0.10	0.12	0.12	0.11	0.10	0.13	0.12	0.13	0.14	0.13	0.16	0.13	0.17	
Mn	0.01	0.01	0.01	0.01	0.01	0.01	0.01	0.01	0.01	0.01	0.01	0.01	0.01	0.01	0.01	
Mg	0.76	0.82	0.84	0.79	0.78	0.79	0.80	0.80	0.78	0.72	0.74	0.75	0.72	0.77	0.71	
Ca	0.88	0.88	0.88	0.88	0.87	0.88	0.88	0.87	0.88	0.90	0.89	0.90	0.89	0.89	0.89	
Na	0.03	0.02	0.03	0.03	0.04	0.03	0.03	0.03	0.03	0.03	0.03	0.03	0.03	0.03	0.03	
Ni	0.00	0.00	0.00	0.00	0.00	0.00	0.00	0.00	0.00	0.00	0.00	0.00	0.00	0.00	0.00	
Cr	0.00	0.00	0.00	0.00	0.00	0.00	0.00	0.00	0.00	0.00	0.00	0.00	0.00	0.00	0.00	
Mg#	80.63	86.66	89.21	87.20	87.08	88.02	88.66	85.77	86.59	84.45	84.27	85.03	81.63	85.87	80.63	

Table B6. (continued)

Location	Bridge Lake							South of Merritt						
Sample ID	BTB051							SSV128						
Spot ID	B-7_R	B-8_I	B-9_C	B-10_R	B-11_I	B-12_I	B-13_R	1_R	2_I	3_C	4_C	5_I	6_I	7_R
SiO ₂	47.78	53.32	53.40	47.73	53.26	53.65	48.62	48.39	47.65	47.94	48.62	48.21	48.26	48.51
TiO ₂	0.85	0.14	0.13	0.86	0.17	0.14	0.73	0.62	0.65	0.62	0.58	0.65	0.62	0.63
Al ₂ O ₃	6.03	1.21	1.06	6.21	1.22	1.27	5.34	5.04	4.98	5.17	4.30	5.29	4.99	4.88
FeO(t)	8.66	3.25	2.81	8.68	3.18	3.41	8.61	7.38	7.21	7.31	6.90	7.89	7.53	7.18
MnO	0.18	0.04	0.05	0.18	0.06	0.08	0.21	0.22	0.16	0.12	0.15	0.18	0.16	0.19
MgO	12.76	17.28	17.26	12.35	17.02	17.25	12.87	14.04	13.94	13.74	14.25	13.80	13.85	13.93
CaO	22.50	23.97	24.34	22.56	23.92	23.70	22.57	22.75	22.58	22.92	23.03	22.67	22.56	22.89
Na ₂ O	0.40	0.17	0.13	0.49	0.18	0.17	0.43	0.47	0.45	0.48	0.41	0.44	0.40	0.45
NiO	0.04	0.00	0.02	0.02	0.00	0.03	0.05	0.01	0.00	0.00	0.01	0.00	0.07	0.00
Cr ₂ O ₃	0.00	0.36	0.38	0.00	0.28	0.34	0.00	0.00	0.03	0.03	0.03	0.04	0.08	0.03
Total	99.20	99.74	99.59	99.07	99.29	100.04	99.43	98.92	97.65	98.33	98.27	99.18	98.52	98.68
Cation calculation based in 6 O														
Si	1.79	1.95	1.95	1.79	1.95	1.95	1.82	1.80	1.80	1.80	1.82	1.80	1.81	1.81
Ti	0.02	0.00	0.00	0.02	0.01	0.00	0.02	0.02	0.02	0.02	0.02	0.02	0.02	0.02
Al ^(IV)	0.21	0.05	0.05	0.21	0.05	0.05	0.18	0.20	0.20	0.20	0.18	0.21	0.19	0.19
Al ^(VI)	0.06	0.00	0.00	0.07	0.01	0.01	0.05	0.02	0.02	0.03	0.01	0.03	0.03	0.03
Fe ^{3+ (IV)}	0.00	0.00	0.00	0.00	0.00	0.00	0.00	0.00	0.00	0.00	0.00	0.00	0.00	0.00
Fe ^{3+ (VI)}	0.14	0.05	0.04	0.13	0.04	0.03	0.12	0.17	0.18	0.18	0.16	0.17	0.16	0.16
Fe ²⁺	0.13	0.05	0.04	0.14	0.06	0.07	0.15	0.06	0.05	0.05	0.05	0.07	0.08	0.07
Mn	0.01	0.00	0.00	0.01	0.00	0.00	0.01	0.01	0.01	0.00	0.01	0.01	0.01	0.01
Mg	0.71	0.94	0.94	0.69	0.93	0.94	0.72	0.78	0.78	0.77	0.80	0.77	0.77	0.78
Ca	0.90	0.94	0.95	0.91	0.94	0.92	0.90	0.91	0.91	0.92	0.92	0.90	0.91	0.92
Na	0.03	0.01	0.01	0.04	0.01	0.01	0.03	0.03	0.03	0.04	0.03	0.03	0.03	0.03
Ni	0.00	0.00	0.00	0.00	0.00	0.00	0.00	0.00	0.00	0.00	0.00	0.00	0.00	0.00
Cr	0.00	0.01	0.01	0.00	0.01	0.01	0.00	0.00	0.00	0.00	0.00	0.00	0.00	0.00
Mg#	84.17	95.16	95.79	83.19	93.91	93.09	83.06	93.13	94.09	93.55	93.74	91.31	90.54	92.05

Table B7. Electron microprobe analyses of Fe-Ti oxide inclusions in clinopyroxene from different localities along the Nicola Group.

Location		Mount Polley – LTNpv unit											
Sample ID		PSV009				PSV016							PSV017
Spot ID	A-1	A-2	B1-3	B2-4	A1-1	A1-2	A2-3	B1-4	B1-5	B2-6	B3-7	1	
SiO ₂	0.01	0.01	0.06	0.12	0.08	0.11	0.11	0.42	0.09	0.08	0.23	0.09	
TiO ₂	1.99	1.87	0.74	2.31	4.87	4.75	5.77	4.04	4.44	3.61	4.33	0.41	
Al ₂ O ₃	0.73	0.78	0.47	1.10	5.68	5.76	4.40	2.59	8.37	7.09	8.28	13.04	
Cr ₂ O ₃	0.17	0.14	0.10	0.14	0.18	0.13	0.17	0.61	0.60	7.89	2.40	0.87	
V ₂ O ₃	0.25	0.25	0.67	0.30	0.27	0.32	0.37	0.00	0.37	0.12	0.38	0.19	
FeO	88.74	88.76	91.78	89.61	77.05	77.68	77.32	84.16	75.27	72.48	73.67	72.22	
MnO	0.24	0.09	0.17	0.61	0.47	0.44	0.49	0.58	0.96	2.66	0.85	0.43	
MgO	0.11	0.11	0.11	0.15	3.46	3.83	2.84	0.21	2.97	0.47	2.78	8.73	
CaO	0.21	0.22	0.15	0.07	0.04	0.07	0.10	0.34	0.15	0.10	0.18	0.24	
NiO	0.01	0.06	0.00	0.05	0.13	0.11	0.05	0.18	0.11	0.13	0.02	0.13	
Total	92.46	92.29	94.25	94.46	92.23	93.19	91.62	93.15	93.33	94.64	93.12	96.35	
Cation calculation based in 32 O													
Si	0.00	0.00	0.02	0.04	0.02	0.03	0.03	0.13	0.03	0.02	0.07	0.02	
Ti	0.46	0.44	0.17	0.53	1.09	1.05	1.31	0.93	0.97	0.80	0.95	0.08	
Al	0.27	0.29	0.17	0.39	1.99	1.99	1.57	0.93	2.87	2.46	2.85	4.07	
Cr	0.04	0.03	0.02	0.03	0.04	0.03	0.04	0.15	0.14	1.84	0.55	0.18	
V	0.06	0.06	0.16	0.07	0.06	0.08	0.09	0.00	0.09	0.03	0.09	0.04	
Fe ³⁺	14.70	14.74	15.27	14.38	11.69	11.75	11.62	12.81	10.91	10.03	10.47	11.50	
Fe ²⁺	8.28	8.28	8.05	8.30	7.42	7.25	7.90	8.66	7.40	7.89	7.54	4.47	
Mn	0.06	0.02	0.04	0.16	0.12	0.11	0.13	0.15	0.24	0.66	0.21	0.10	
Mg	0.05	0.05	0.05	0.07	1.53	1.67	1.28	0.10	1.29	0.21	1.21	3.44	
Ca	0.07	0.07	0.05	0.02	0.01	0.02	0.03	0.11	0.05	0.03	0.06	0.07	
Ni	0.00	0.02	0.00	0.01	0.03	0.03	0.01	0.04	0.03	0.03	0.01	0.03	

Table B7. (continued)

Location	Mount Polley - LTNpv unit		Mount Polley – LTNpv unit									
Sample ID	PSV017		PSV002									
Spot ID	2	3	A1-1	A1-2	A1-3	A2-4	A2-5	A2-6	A2-7	A3-8	A3-9	A3-10
SiO ₂	2.83	0.13	1.94	2.59	1.62	8.34	10.70	6.40	10.82	5.71	5.42	4.53
TiO ₂	8.13	0.46	0.77	1.56	0.84	8.69	0.03	6.90	0.06	3.96	3.97	2.65
Al ₂ O ₃	1.63	5.85	0.41	0.55	0.40	1.21	3.98	1.25	4.02	2.13	2.01	1.63
Cr ₂ O ₃	0.43	0.84	0.32	0.35	0.34	0.08	0.11	0.19	0.09	0.32	0.31	0.28
V ₂ O ₃	0.00	0.19	0.00	0.00	0.00	0.00	0.02	0.05	0.02	0.00	0.00	0.00
FeO	72.89	80.52	86.01	84.37	87.40	66.28	66.86	69.44	65.41	76.34	76.47	80.73
MnO	0.04	0.50	0.24	0.18	0.25	0.25	0.16	0.49	0.20	2.03	2.04	1.45
MgO	7.59	5.69	0.19	0.23	0.14	0.63	8.07	1.16	8.33	0.49	1.22	0.95
CaO	2.97	0.19	0.59	1.14	0.33	6.83	0.51	4.72	0.46	0.11	0.12	0.11
NiO	0.00	0.14	0.01	0.01	0.00	0.01	0.02	0.06	0.00	0.06	0.07	0.00
Total	96.50	94.51	90.49	90.98	91.32	92.32	90.46	90.66	89.42	91.14	91.63	92.34
Cation calculation based in 32 O												
Si	0.78	0.04	0.61	0.81	0.51	2.49	3.05	1.96	3.11	1.76	1.65	1.38
Ti	1.69	0.10	0.18	0.37	0.20	1.95	0.01	1.59	0.01	0.92	0.91	0.61
Al	0.53	1.95	0.15	0.20	0.15	0.43	1.34	0.45	1.36	0.77	0.72	0.58
Cr	0.09	0.19	0.08	0.09	0.08	0.02	0.03	0.05	0.02	0.08	0.08	0.07
V	0.00	0.04	0.00	0.00	0.00	0.00	0.01	0.01	0.01	0.00	0.00	0.00
Fe ³⁺	10.42	13.55	14.18	13.37	14.36	6.66	8.52	8.41	8.37	9.80	10.08	11.38
Fe ²⁺	6.45	5.52	8.44	8.64	8.46	9.91	7.43	9.33	7.36	9.87	9.43	9.14
Mn	0.01	0.12	0.06	0.05	0.07	0.06	0.04	0.13	0.05	0.53	0.53	0.37
Mg	3.13	2.40	0.09	0.11	0.07	0.28	3.43	0.53	3.57	0.23	0.56	0.43
Ca	0.88	0.06	0.20	0.38	0.11	2.19	0.16	1.55	0.14	0.04	0.04	0.04
Ni	0.00	0.03	0.00	0.00	0.00	0.00	0.01	0.02	0.00	0.02	0.02	0.00

Table B7. (continued)

Location		Mount Polley – LTNav unit										
Sample ID		PSV003						PSV026				
Spot ID	A1-1	A2-2	B1-3	B1-4	B2-5	B2-6	B2-7	A1-1	A2-2	B1-3	B1-4	B2-5
SiO ₂	4.29	0.14	1.63	2.08	6.16	4.28	4.26	3.61	1.10	3.25	1.09	1.34
TiO ₂	5.76	4.75	0.12	0.33	0.45	0.46	0.76	8.64	1.58	3.00	0.64	0.96
Al ₂ O ₃	2.42	7.81	0.28	0.33	3.39	2.50	2.11	0.66	3.27	0.68	0.16	0.15
Cr ₂ O ₃	0.00	0.00	0.01	0.01	0.06	0.00	0.03	0.28	0.40	0.07	0.06	0.28
V ₂ O ₃	0.00	0.18	0.06	0.06	0.21	0.23	0.21	0.00	0.22	0.16	0.32	0.35
FeO	74.21	76.14	89.19	84.96	77.89	82.38	82.16	72.83	83.21	82.85	88.82	89.10
MnO	0.63	0.56	0.09	0.11	0.23	0.24	0.18	2.51	0.06	0.17	0.28	0.11
MgO	0.85	4.55	0.10	0.15	4.82	3.29	2.52	0.26	4.32	0.44	0.27	0.13
CaO	2.67	0.24	0.37	0.63	0.22	0.19	0.22	3.08	0.57	2.43	0.84	1.00
NiO	0.05	0.00	0.00	0.04	0.04	0.00	0.00	0.03	0.00	0.02	0.02	0.05
Total	90.89	94.36	91.86	88.71	93.46	93.57	92.45	91.91	94.74	93.09	92.51	93.48
Cation calculation based in 32 O												
Si	1.32	0.04	0.51	0.67	1.77	1.25	1.27	1.11	0.32	0.99	0.34	0.41
Ti	1.33	1.02	0.03	0.08	0.10	0.10	0.17	2.00	0.34	0.68	0.15	0.22
Al	0.88	2.62	0.10	0.13	1.15	0.86	0.74	0.24	1.11	0.24	0.06	0.05
Cr	0.00	0.00	0.00	0.00	0.01	0.00	0.01	0.07	0.09	0.02	0.02	0.07
V	0.00	0.04	0.02	0.02	0.05	0.05	0.05	0.00	0.05	0.04	0.08	0.09
Fe ³⁺	9.84	11.22	14.81	14.36	11.05	12.37	12.31	9.46	13.43	12.36	14.88	14.53
Fe ²⁺	9.20	6.92	8.34	8.42	7.67	7.80	8.21	9.32	6.61	8.63	8.01	8.20
Mn	0.16	0.14	0.02	0.03	0.06	0.06	0.05	0.66	0.02	0.04	0.07	0.03
Mg	0.39	1.93	0.05	0.07	2.07	1.44	1.12	0.12	1.86	0.20	0.12	0.06
Ca	0.88	0.07	0.12	0.22	0.07	0.06	0.07	1.02	0.18	0.79	0.28	0.33
Ni	0.01	0.00	0.00	0.01	0.01	0.00	0.00	0.01	0.00	0.01	0.01	0.01

Table B7. (continued)

Location		Mount Polley – LTNav unit				Mount Polley – LTNpt unit								
Sample ID		PSV039				PSV007	PSV007	PSV007	PSV007	PSV007	PSV007	PSV007	PSV007	PSV007
Spot ID	A1-1	A1-2	A2-3	A2-4	A1-1	A1-2	A2-3	A2-4	A2-5	B1-6	B2-7	B3-8		
SiO ₂	3.80	4.16	4.17	0.54	1.88	3.10	1.35	0.17	2.52	3.09	0.05	0.73		
TiO ₂	2.72	2.71	2.45	3.71	63.79	15.20	5.41	61.24	5.62	2.62	1.54	1.52		
Al ₂ O ₃	1.07	1.23	1.28	1.75	0.30	1.29	0.94	0.00	0.88	1.95	1.57	1.65		
Cr ₂ O ₃	0.31	0.34	0.36	0.25	0.00	0.00	0.11	0.02	0.08	0.76	0.67	0.70		
V ₂ O ₃	0.00	0.00	0.00	0.00	0.00	0.00	0.11	0.00	0.10	0.34	0.48	0.39		
FeO	80.92	81.20	79.61	83.03	19.32	66.64	80.27	26.91	78.73	80.26	87.30	85.65		
MnO	0.15	0.11	0.09	0.50	4.20	2.96	2.03	0.56	1.71	0.28	0.45	0.28		
MgO	0.49	0.48	0.66	0.41	2.11	0.14	0.15	2.35	0.17	0.29	0.35	0.38		
CaO	2.53	2.54	2.35	0.72	1.73	2.97	1.24	0.51	2.25	1.90	0.24	0.49		
NiO	0.03	0.00	0.03	0.05	0.00	0.00	0.05	0.01	0.00	0.02	0.00	0.00		
Total	92.03	92.77	91.00	90.96	93.32	92.30	91.64	91.78	92.06	91.52	92.66	91.78		
Cation calculation based in 32 O														
Si	1.16	1.26	1.28	0.17	0.60	0.96	0.42	0.06	0.78	0.95	0.02	0.23		
Ti	0.63	0.62	0.57	0.87	15.37	3.53	1.27	15.09	1.30	0.61	0.36	0.35		
Al	0.39	0.44	0.46	0.64	0.11	0.47	0.35	0.00	0.32	0.71	0.57	0.60		
Cr	0.08	0.08	0.09	0.06	0.00	0.00	0.03	0.01	0.02	0.19	0.16	0.17		
V	0.00	0.00	0.00	0.00	0.00	0.00	0.03	0.00	0.03	0.08	0.12	0.10		
Fe ³⁺	11.97	11.73	11.75	13.22	0.00	6.55	12.23	0.00	11.48	11.91	14.41	13.97		
Fe ²⁺	8.69	8.81	8.74	8.46	5.18	10.67	8.66	7.37	8.81	8.72	8.02	8.17		
Mn	0.04	0.03	0.02	0.13	1.14	0.78	0.54	0.16	0.45	0.07	0.12	0.07		
Mg	0.22	0.22	0.30	0.19	1.01	0.06	0.07	1.15	0.08	0.13	0.16	0.18		
Ca	0.83	0.82	0.78	0.24	0.59	0.98	0.41	0.18	0.74	0.63	0.08	0.16		
Ni	0.01	0.00	0.01	0.01	0.00	0.00	0.01	0.00	0.00	0.01	0.00	0.00		

Table B7. (continued)

Location		Mount Polley – LTNpt unit							Mount Milligan		Woodjam	
Sample ID	PSV007	PSV028	PSV028	PSV028	PSV028	PSV028	PSV028	PSV028	MTB031	MTB031	WTB085	WTB085
Spot ID	B4-9	A1-1	A1-2	A2-3	A2-4	A2-5	A2-6	A2-9	1	2	1	2
SiO ₂	2.12	6.89	7.58	0.01	0.58	7.47	0.03	0.63	0.85	0.50	0.50	0.82
TiO ₂	0.06	6.88	7.41	0.36	0.20	3.98	0.14	0.35	1.28	1.90	2.49	3.07
Al ₂ O ₃	1.17	1.05	1.38	0.28	0.51	3.36	0.34	0.52	10.14	10.75	0.56	0.84
Cr ₂ O ₃	0.53	0.04	0.03	0.01	0.02	0.09	0.02	0.08	22.43	22.50	0.59	0.61
V ₂ O ₃	0.44	0.00	0.00	0.52	0.52	0.22	0.54	0.51	0.34	0.33	0.01	0.01
FeO	84.35	70.56	67.82	91.34	90.81	70.01	91.88	89.84	54.52	54.55	85.80	84.10
MnO	0.13	0.25	0.23	0.08	0.08	0.34	0.10	0.01	1.36	1.43	0.05	0.10
MgO	0.76	0.08	0.09	0.09	0.33	2.53	0.10	0.19	0.51	0.30	0.15	0.17
CaO	0.86	5.83	6.17	0.11	0.09	2.28	0.06	0.19	0.28	0.21	0.15	0.27
NiO	0.07	0.03	0.03	0.02	0.02	0.05	0.03	0.00	0.04	0.07	0.04	0.09
Total	90.49	91.62	90.73	92.82	93.15	90.32	93.23	92.33	91.73	92.53	90.33	90.09
Cation calculation based in 32 O												
Si	0.66	2.10	2.32	0.00	0.18	2.25	0.01	0.20	0.26	0.15	0.16	0.26
Ti	0.01	1.57	1.70	0.08	0.05	0.90	0.03	0.08	0.29	0.43	0.59	0.73
Al	0.43	0.38	0.50	0.10	0.18	1.19	0.12	0.19	3.60	3.79	0.21	0.32
Cr	0.13	0.01	0.01	0.00	0.01	0.02	0.01	0.02	5.35	5.32	0.15	0.15
V	0.11	0.00	0.00	0.13	0.13	0.05	0.13	0.13	0.08	0.08	0.00	0.00
Fe ³⁺	13.98	8.28	7.45	15.59	15.24	8.44	15.66	15.11	5.88	5.66	14.14	13.55
Fe ²⁺	7.98	9.66	9.89	7.98	8.02	9.18	7.94	8.12	7.87	8.00	8.61	8.77
Mn	0.03	0.06	0.06	0.02	0.02	0.09	0.03	0.00	0.35	0.36	0.01	0.03
Mg	0.35	0.04	0.04	0.04	0.15	1.14	0.05	0.09	0.23	0.13	0.07	0.08
Ca	0.29	1.90	2.02	0.04	0.03	0.74	0.02	0.06	0.09	0.07	0.05	0.09
Ni	0.02	0.01	0.01	0.01	0.01	0.01	0.01	0.00	0.01	0.02	0.01	0.02

Table B7. (continued)

Location	Woodjam				Copper Mountain			Lac la Hache				
Sample ID	WTB085				CMSV203			LLTB067			LTB073	
Spot ID	3	4	5	6	1	2	3	2	3	4	1	2
SiO ₂	0.27	0.68	0.05	1.38	0.13	0.09	0.09	1.21	7.00	0.28	0.07	0.14
TiO ₂	2.27	2.53	1.30	1.34	3.01	3.31	1.90	8.06	2.86	5.66	2.66	3.66
Al ₂ O ₃	0.35	0.45	0.15	0.82	7.93	7.72	9.07	1.13	2.02	0.53	7.41	5.64
Cr ₂ O ₃	0.59	0.52	0.05	0.08	0.56	0.49	2.86	0.03	0.07	0.04	0.47	0.31
V ₂ O ₃	0.01	0.02	0.25	0.39	0.11	0.12	0.04	0.00	0.00	0.00	0.24	0.11
FeO	86.08	84.88	87.67	84.00	75.06	75.14	71.86	77.78	73.98	84.96	79.33	81.57
MnO	0.06	0.09	0.07	0.06	0.36	0.39	0.63	0.19	0.17	0.35	0.42	0.14
MgO	0.24	0.12	0.11	0.21	6.49	6.39	6.87	0.18	1.84	0.09	1.93	1.17
CaO	0.07	0.14	0.05	0.83	0.32	0.33	0.11	0.39	2.34	0.28	0.14	0.12
NiO	0.00	0.09	0.00	0.03	0.02	0.11	0.17	0.00	0.00	0.06	0.04	0.12
Total	89.95	89.51	89.70	89.14	93.99	94.09	93.60	88.96	90.28	92.25	92.72	93.00
Cation calculation based in 32 O												
Si	0.09	0.22	0.02	0.44	0.04	0.02	0.03	0.39	2.13	0.09	0.02	0.04
Ti	0.54	0.61	0.31	0.32	0.64	0.70	0.40	1.95	0.65	1.33	0.59	0.83
Al	0.13	0.17	0.06	0.31	2.63	2.56	3.00	0.43	0.73	0.20	2.58	1.99
Cr	0.15	0.13	0.01	0.02	0.13	0.11	0.63	0.01	0.02	0.01	0.11	0.07
V	0.00	0.00	0.06	0.10	0.02	0.03	0.01	0.00	0.00	0.00	0.06	0.03
Fe ³⁺	14.46	14.04	15.21	14.05	11.88	11.85	11.51	10.88	9.69	12.97	12.02	12.18
Fe ²⁺	8.48	8.68	8.24	8.35	5.77	5.83	5.34	10.07	9.15	9.17	7.60	8.24
Mn	0.02	0.02	0.02	0.02	0.09	0.09	0.15	0.05	0.04	0.09	0.11	0.04
Mg	0.11	0.06	0.05	0.10	2.72	2.68	2.87	0.09	0.83	0.04	0.85	0.52
Ca	0.02	0.05	0.02	0.28	0.10	0.10	0.03	0.13	0.76	0.09	0.05	0.04
Ni	0.00	0.02	0.00	0.01	0.01	0.02	0.04	0.00	0.00	0.02	0.01	0.03

Table B7. (continued)

Location	Lac la Hache				Bridge Lake		South of Merritt			
Sample ID	LTB073				BTB051		SSV128			
Spot ID	3	4	5	6	1	2	1	2	3	4
SiO ₂	0.56	0.43	0.47	0.57	0.15	4.63	0.11	0.04	0.73	0.87
TiO ₂	2.10	2.75	3.73	3.64	0.12	4.01	2.78	4.74	2.02	2.00
Al ₂ O ₃	3.02	4.97	2.63	4.22	1.35	0.78	1.94	1.93	0.40	0.38
Cr ₂ O ₃	0.52	0.49	0.26	0.25	13.16	5.22	0.49	0.43	0.66	0.50
V ₂ O ₃	0.14	0.12	0.02	0.11	0.42	0.03	0.20	0.00	0.00	0.00
FeO	85.17	82.67	82.68	81.97	75.52	72.59	84.53	80.91	85.31	84.70
MnO	0.09	0.12	0.77	0.51	0.58	0.42	0.02	0.09	0.21	0.21
MgO	0.27	0.29	0.14	0.42	0.10	0.39	0.51	1.07	0.24	0.22
CaO	0.11	0.09	0.15	0.09	0.64	3.64	0.03	0.05	0.21	0.20
NiO	0.03	0.08	0.00	0.04	0.05	0.09	0.02	0.04	0.04	0.03
Total	92.00	92.01	90.85	91.84	92.10	91.78	90.63	89.31	89.81	89.10
Cation calculation based in 32 O										
Si	0.17	0.13	0.15	0.18	0.05	1.42	0.04	0.01	0.23	0.28
Ti	0.49	0.63	0.88	0.84	0.03	0.92	0.66	1.13	0.48	0.48
Al	1.09	1.79	0.97	1.52	0.49	0.28	0.72	0.72	0.15	0.15
Cr	0.13	0.12	0.07	0.06	3.24	1.26	0.12	0.11	0.17	0.13
V	0.03	0.03	0.01	0.03	0.11	0.01	0.05	0.00	0.00	0.00
Fe ³⁺	13.44	12.54	12.92	12.36	12.01	9.76	13.73	12.88	14.25	14.21
Fe ²⁺	8.46	8.55	8.70	8.65	7.65	8.84	8.43	8.59	8.47	8.53
Mn	0.02	0.03	0.20	0.13	0.15	0.11	0.01	0.03	0.06	0.06
Mg	0.12	0.13	0.07	0.19	0.05	0.18	0.24	0.50	0.11	0.10
Ca	0.04	0.03	0.05	0.03	0.22	1.19	0.01	0.02	0.07	0.07
Ni	0.01	0.02	0.00	0.01	0.01	0.02	0.01	0.01	0.01	0.01

Table B8. Electron microprobe analyses of apatite inclusions in clinopyroxene from different rocks units within the Mount Polley area.

Location	Mount Polley LTNpv unit		Mount Polley – LTNav unit							
Sample ID	PSV016		PSV002							
Spot ID	1	2	1	2	3	4	5	6	7	8
CaO	55.17	54.66	55.72	54.91	55.60	54.92	55.09	54.88	53.96	54.33
P ₂ O ₅	40.38	42.22	41.83	42.92	41.96	42.60	42.68	42.53	40.49	42.75
SO ₃	ND	ND	ND	ND	ND	ND	ND	ND	ND	ND
Cl	1.08	1.17	0.28	0.25	0.26	0.28	0.27	0.28	0.23	0.26
F	1.30	1.40	2.64	2.66	2.86	2.65	2.80	2.83	2.83	2.91
Total	97.93	99.45	100.48	100.73	100.68	100.44	100.83	100.53	97.52	100.24
Anion calculation based in 26 (O, OH, Cl, F)										
Ca	10.210	9.866	9.882	9.651	9.810	9.692	9.672	9.660	9.833	9.560
P	5.905	6.022	5.862	5.960	5.851	5.940	5.921	5.916	5.831	5.944
Cl	0.316	0.335	0.080	0.068	0.072	0.078	0.076	0.078	0.067	0.071
F	0.710	0.745	1.383	1.380	1.491	1.379	1.450	1.473	1.523	1.509
OH	0.974	0.921	0.537	0.552	0.437	0.543	0.474	0.449	0.409	0.420

ND = Not detectable.

APPENDIX C

Table C1. $\delta^{13}\text{C}_{\text{PDB}}$ (‰) and $\delta^{18}\text{O}_{\text{SMOW}}$ (‰) isotopic compositions of carbonates within basalts from different arc segments along the Nicola Group.

Sample ID	Location	$\delta^{13}\text{C}_{\text{PDB}}$ (‰)	$\delta^{18}\text{O}_{\text{SMOW}}$ (‰)	Sample ID	Location	$\delta^{13}\text{C}_{\text{PDB}}$ (‰)	$\delta^{18}\text{O}_{\text{SMOW}}$ (‰)
PSV001	Mount Polley	1.54	19.24	MTB030	Mount Milligan	-16.11	19.35
PSV002	Mount Polley	0.48	17.99	MTB091	Mount Milligan	-6.40	13.50
PSV003	Mount Polley	1.68	20.52	LTB68	Lac la Hache	-1.67	15.05
PSV007	Mount Polley	-2.43	17.34	LTB072	Lac la Hache	-3.93	12.29
PSV010	Mount Polley	-5.61	15.12	LTB080	Lac la Hache	-2.26	17.26
PSV011	Mount Polley	-4.63	17.41	LTB081	Lac la Hache	-2.03	14.73
PSV012	Mount Polley	-0.98	19.24	BTB051	Bridge Lake	-9.57	10.59
PSV017	Mount Polley	0.40	17.64	BTB053	Bridge Lake	-15.40	8.33
PSV022	Mount Polley	0.82	14.39	BTB056	Bridge Lake	-7.77	11.51
PSV028	Mount Polley	-0.96	18.11	BTB077	Bridge Lake	-6.94	14.22
PSV036	Mount Polley	2.20	18.67	SSV128	South of Merritt	-2.69	15.45
MTB017	Mount Milligan	-8.85	11.08	SSV129	South of Merritt	-5.65	15.60
MTB019	Mount Milligan	-7.83	13.89	SSV133	South of Merritt	-0.48	14.19
MTB020	Mount Milligan	-9.19	12.85	SSV137	South of Merritt	-3.58	5.12

APPENDIX D

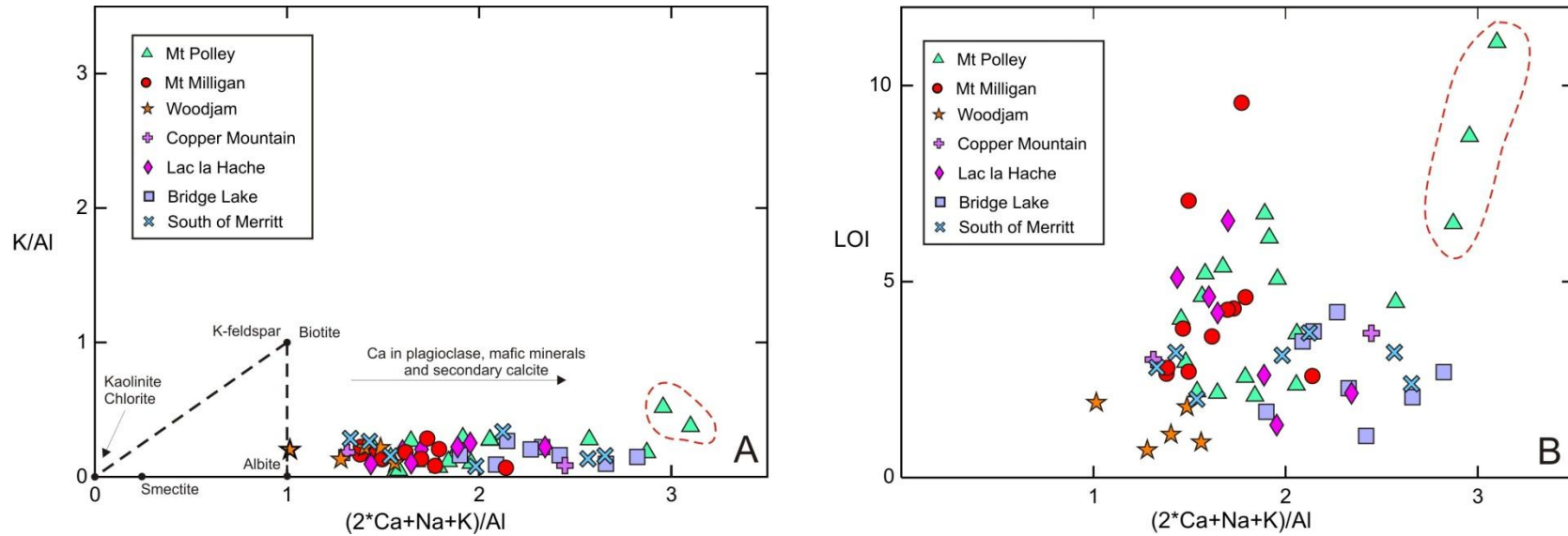


Figure D1. Molar element ratio plots documenting the level of Ca, K, and Na mobility in the Nicola Group rocks. A) The basaltic to andesitic rocks all plot to the right of the albite-K-feldspar-kaolinite triangle in the diagram. The most primitive rocks (e.g. Bridge Lake) plot to the right, reflecting their high anorthite content, whereas the andesitic rocks of Woodjam plot furthest to the left. Note that with the possible exception of two Mount Polley samples (PSV036 and PSV049 from the LTNav unit, red-dashed line) no addition of K is evident. B) Loss on Ignition (LOI) versus $(2 \cdot \text{Ca} + \text{Na} + \text{K}) / \text{Al}$. There is no correlation of LOI with Ca-Na-K content in the rock, again with the possible exception of samples PSV001, PSV036 and PSV049 from the LTNav unit (red-dashed line). The spread of LOI in the sample set is interpreted as the effect of variable amounts of secondary carbonate formation and hydration of the rock during seafloor alteration or low grade metamorphism but secondary carbonate formed with Ca already present in the rock and did not require addition of Ca to the rock.